

**IDENTIFICATION OF *BCL-XL* INDUCED
MICRORNAS INVOLVED IN THE APOPTOTIC PROPERTIES OF
HUMAN LUNG ADENOCARCINOMA CELLS, A549.**

NORAHAYU BINTI OTHMAN

**FACULTY OF SCIENCE
UNIVERSITY OF MALAYA
KUALA LUMPUR**

2012

**IDENTIFICATION OF *BCL-XL* INDUCED
MICRORNAS INVOLVED IN THE APOPTOTIC
PROPERTIES OF HUMAN LUNG ADENOCARCINOMA
CELLS, A549**

NORAHAYU BINTI OTHMAN

**DISSERTATION SUBMITTED IN FULFILLMENT OF
THE REQUIREMENTS FOR THE DEGREE OF MASTER
OF SCIENCE**

**INSTITUTE OF BIOLOGICAL SCIENCES
FACULTY OF SCIENCE
UNIVERSITY OF MALAYA
KUALA LUMPUR**

2012

UNIVERSITI MALAYA

ORIGINAL LITERARY WORK DECLARATION

Name of Candidate: NORAHA YU BINTI OTHMAN (I.C/Passport No: 850517-10-5472)

Registration/Matric No: SGR090129

Name of Degree: MASTER OF SCIENCE

Title of Project Paper/Research Report/Dissertation/Thesis ("this Work"): IDENTIFICATION OF *BCL-XL* INDUCED MICRORNAS INVOLVED IN THE APOPTOTIC PROPERTIES OF HUMAN LUNG ADENOCARCINOMA CELLS, A549.

Field of Study: MOLECULAR ONCOLOGY

I do solemnly and sincerely declare that:

- (1) I am the sole author/writer of this Work;
- (2) This Work is original;
- (3) Any use of any work in which copyright exists was done by way of fair dealing and for permitted purposes and any excerpt or extract from, or reference to or reproduction of any copyright work has been disclosed expressly and sufficiently and the title of the Work and its authorship have been acknowledged in this Work;
- (4) I do not have any actual knowledge nor do I ought reasonably to know that the making of this work constitutes an infringement of any copyright work;
- (5) I hereby assign all and every rights in the copyright to this Work to the University of Malaya ("UM"), who henceforth shall be owner of the copyright in this Work and that any reproduction or use in any form or by any means whatsoever is prohibited without the written consent of UM having been first had and obtained;
- (6) I am fully aware that if in the course of making this Work I have infringed any copyright whether intentionally or otherwise, I may be subject to legal action or any other action as may be determined by UM.



Candidate's Signature

Date: 16 . 8 . 12

Subscribed and solemnly declared before,



Witness's Signature

Name:

Designation:

Noor Hasima Bt. Nagoor PhD
Associate Professor
Division of Genetics & Molecular Biology
Institute of Biological Sciences
Faculty of Science
University of Malaya
50603 Kuala Lumpur, Malaysia

Date: 16 . 8 . 12

ABSTRACT

Bcl-xL is an anti-apoptotic protein that is frequently found to be overexpressed in lung adenocarcinoma leading to an inhibition of apoptosis and associated with poor prognosis of this disease. Recently, the roles of microRNAs (miRNAs) in regulating apoptosis and cell survival during tumorigenesis have become evident, with cancer cells showing perturbed expression of various miRNAs. In this project, we utilized miRNA microarrays to determine if miRNA dysregulation in *bcl-xL* silenced A549 lung adenocarcinoma cells could be involved in apoptotic behavior. Data from qRT-PCR and Western blotting indicated that a siRNA-based transfection induced a decrease of *bcl-xL* expression in A549 cells at both the gene and protein level, resulting in a decrease in cell viability. MiRNA microarray revealed that a total of 10 miRNAs were found to be significantly differentially expressed between *bcl-xL* silenced A549 cells and non-transfected cells. qRT-PCR validation of the miRNA microarray results indicated that there was a strong positive correlation between the two sets of data. Bioinformatics analysis demonstrated that the differentially expressed miRNAs were found to be involved in several signaling pathways, primarily the PI3K/AKT, intrinsic and extrinsic, WNT, TGF- β , and the MAPK pathway. Based on this, a hypothetical pathway illustrating the interactions between these miRNAs with their specific targets were generated describing the effects of *bcl-xL* silencing on initiation of apoptosis in A549 cells. In conclusion, this study demonstrated that *bcl-xL* silencing in A549 lung adenocarcinoma cells leads to the occurrence of apoptosis through the dysregulation of specific miRNAs. With further studies carried out to determine the true targets and functions of these miRNAs, our study provided a platform for antisense treatment whereby miRNA expression can be exploited to increase the apoptotic properties in lung adenocarcinoma cells.

ABSTRAK

Bcl-xL merupakan protein anti-apoptosis yang kerap didapati dalam sel-sel adenokarsinoma peparu yang menyebabkan perencatan apoptosis serta prognosis tidak baik. MicroRNAs (miRNAs) telah dilaporkan untuk memainkan peranan dalam pengawalan apoptosis dalam tumorigenesis, dan sel-sel kanser berkeupayaan untuk memanipulasi miRNAs untuk mengawal selia penghidupan sel dalam oncogenesis. Dalam projek ini, kami menggunakan miRNA microarray untuk menentukan peranan yang dimainkan oleh miRNAs dalam aspek apoptosis sel-sel adenokarsinoma peparu, A549, sebagai tindak balas terhadap pendiaman *bcl-xL*. Data daripada qRT-PCR dan pemblotan Western menunjukkan bahawa transfeksi dengan siRNA mengurangkan ekspresi *bcl-xL* dalam sel-sel A549 ditahap gen dan protein. MiRNA microarray mendedahkan bahawa sejumlah 10 miRNAs yang diekspreskan berlainan signifikan antara sel-sel A549 di mana *bcl-xL*-nya didiamkan dan sel-sel A549 yang tidak ditransfect. Keputusan miRNA microarray disahkan dengan qRT-PCR dan ia menunjukkan korelasi positif yang kukuh antara dua set data ini. Analisis bioinformatik menunjukkan bahawa miRNAs yang diekspreskan berlainan didapati terlibat dalam beberapa laluan; terutamanya laluan PI3K/AKT, intrinsik dan ekstrinsik, WNT, TGF- β , dan MAPK. Satu laluan hipotetikal telah dibentuk untuk menerangkan interaksi antara miRNAs dengan sasaran gen mereka. Laluan hipotetikal ini menggambarkan kesan mendiamkan ekspresi *bcl-xL* ke atas apoptosis di dalam sel-sel A549. Kesimpulannya, kajian ini telah menunjukkan bahawa pendiaman ekspresi *bcl-xL* dalam sel-sel adenokarsinoma peparu membawa kepada kejadian apoptosis melalui perancatan pengawal aturan miRNAs. Kajian kami telah menyediakan dataran untuk rawatan antisense, dimana ekspresi miRNA boleh dieksploitasikan untuk meningkatkan apoptosis dalam sel-sel adenokarsinoma peparu.

ACKNOWLEDGEMENTS

The completion of this project would not have been possible without the support of many people, who in one way or another has contributed and extended valuable assistance in the preparation and completion of this study. First and foremost, I would like to thank my project supervisor, Assoc. Prof. Dr. Noor Hasima Nagoor, without whom the completion of this project would not be possible. I am grateful for her invaluable knowledge, and continuous guidance and support throughout the duration of my project. I would also like to extend my gratitude to my co-supervisor, Prof. Dr. Jennifer Ann Harikrishna, for all of the advice and insights she has shared.

I am indebted to all Cancer Research lab members, who have made their support and encouragement available in a number of ways. I owe my deepest gratitude to you all for the countless brainstorming sessions and discussions we had, which enabled me to develop a greater understanding of the subject. I would also like to acknowledge the Cancer Research Initiative Foundation (CARIF) for their generous provision of the cancer cell line used in this study, as well as Research Instruments Sdn. Bhd. for helping me in my microarray global miRNA expression work.

This study was funded by University Malaya through the Postgraduate Research Grant (PPP) (PS295/2010A and PV058/2011B) and the University of Malaya Research Grant (UMRG) (RG037-10BIO). I would like to thank them for their utmost generosity in terms of financing this project.

Finally I would like to express my love and gratitude to my beloved family and friends for their patience and endless support throughout the duration of my studies. Most importantly, I would like to thank God, for all His blessings and for giving me the strength to keep pushing forward. Thank you.

TABLE OF CONTENTS

	Page No.
Abstract	ii
Abstrak	iii
Acknowledgements	iv
Table of Contents	v
List of Figures	xiii
List of Tables	xix
List of Abbreviations	xxii
Chapter 1: Introduction	1
1.1 Study Objectives	3
Chapter 2: Literature Review	4
2.1 Cancer	4
2.1.1 Hallmarks of Cancer	5
2.1.2 Cancer Statistics	8
2.2 Lung Cancer	10
2.2.1 Lung Cancer Subtypes	11
2.2.2 Etiology of Lung Cancer	12

2.2.3	Epidemiology of Lung Cancer	14
2.2.4	Pathogenesis of Cancer	15
2.2.5	Lung Adenocarcinoma Cell Line (A549)	18
2.3	Apoptosis	18
2.3.1	Extrinsic Pathway of Apoptosis	19
2.3.2	Intrinsic Pathway of Apoptosis	20
2.3.3	Bcl-2 Family Members	21
2.3.4	Bcl-2 Expression in Cancer	23
2.3.5	Bcl-xL Overexpression in Lung Cancer	24
2.3.6	Phosphatidylinositol-3-Kinase (PI3K)/ Akt Pathway	24
2.3.7	Wingless-Type MMTV Integration Site Family (WNT) Pathway	27
2.3.8	Transforming Growth Factor (TGF- β) Signaling Pathway	30
2.3.9	Mitogen-Activated Protein Kinase (MAPK) Signaling Pathway	32
2.3.9.1	ERK1/2 Cascade	33
2.3.9.2	JNK/SAPK Cascade	34
2.3.9.3	p38 Cascade	36
2.4	MicroRNA (miRNA)	37
2.4.1	MiRNA Biogenesis	38
2.4.2	MiRNA and Cancer	40
2.4.3	MiRNA as Oncogenes and Tumor Suppressors	42
2.5	MiRNA and Apoptosis	43
2.5.1	Pro-apoptotic miRNAs	43
2.5.2	Anti-apoptotic miRNAs	45

2.6	MiRNA in Cancer Diagnosis and Treatment	46
2.6.1	MiRNA Signatures in Cancer Diagnosis	46
2.6.2	MiRNA as Target for Cancer Treatment	47
Chapter 3:	Materials and Methods	51
3.1	Cancer Cell Lines	51
3.1.1	Cell Lines and Culture Conditions	51
3.1.2	Subculturing Cell Line Monolayers: Harvesting a Cell Monolayer	51
3.1.3	Cell Counting	52
3.2	Short Interfering RNA (siRNA) Transfection	53
3.2.1	Stealth RNAi™ siRNA Duplex Oligonucleotides (Invitrogen, USA)	53
3.2.2	Transfection of siRNA	54
3.3	RNA Isolation Using TRIzol-Reagent (Invitrogen, USA)	55
3.3.1	Homogenization	55
3.3.2	Phase Separation	55
3.3.3	RNA Precipitation	56
3.3.4	RNA Wash	56
3.3.5	Re-Dissolving the RNA	56
3.4	Quantitation of RNA	57
3.5	Agarose Gel Electrophoresis	57
3.5.1	Detection of RNA Bands	58
3.6	Protein Isolation Using NE-PER Nuclear and Cytoplasmic Extraction Kit (Pierce, USA)	59
3.7	Bradford Assay Protein Quantification	60

3.8	Quantitative Reverse Transcription Polymerase Chain Reaction (qRT-PCR)	61
3.9	Sodium Dodecyl Sulphate Polyacrylamide Gel Electrophoresis (SDS-PAGE)	63
3.9.1	Sample Preparation	64
3.9.2	Sample Loading and Running the Gel	65
3.10	Western Blotting	66
3.10.1	Protein Transfer	66
3.10.2	Visualization of Proteins on Membrane Using Ponceau S Stain (Sigma, USA)	67
3.10.3	Blocking the Membrane	67
3.10.4	Incubation With Primary Antibody	68
3.10.5	Incubation With Secondary Antibody	68
3.10.6	Exposure of Membrane to Electrochemiluminescence (ECL)	69
3.11	3-(4,5-dimethylthiazol-2-yl)-2,5-diphenyltetrazolium bromide (MTT) Cell Viability Assay	70
3.12	BioAnalyzer Quantification of Total RNA	71
3.12.1	Setting Up Chip Priming Station	71
3.12.2	Preparing the Gel	71
3.12.3	Preparing the Gel-Dye Mix	71
3.12.4	Loading the Gel-Dye Mix	72
3.12.5	Loading the Agilent RNA Nano Marker	72
3.12.6	Loading the Ladder and Samples	72
3.13	MiRNA Microarray – Global miRNA Expression	73
3.13.1	Poly (A) Tailing	73

3.13.2	FlashTag Biotin HSR Ligation	74
3.13.3	Hybridization of Affymetrix Arrays	74
3.13.4	Washing and Staining	75
3.14	ELOSA QC Assay	77
3.14.1	Washing and Blocking for ELOSA	77
3.14.2	Sample Hybridization	78
3.14.3	SA-HRP Binding	79
3.14.4	Signal Development	79
3.15	MiRNA Microarray Analysis	79
3.16	MiRNA Microarray Validation	80
3.16.1	TaqMan® MicroRNA Assays	81
3.17	Bioinformatics Analyses of miRNA Gene Targets	83
3.18	Statistical Analysis	83
Chapter 4:	Results	84
4.1	Selection Process of siRNA 1, 2 & 3	84
4.1.1	siRNA Silencing Of <i>Bcl-xL</i>	84
4.1.1.1	siRNA Targets on <i>Bcl-xL</i> mRNA	84
4.1.1.2	siRNA Transfection Efficiency in A549 cells	85
4.1.2	RNA Extraction	88
4.1.2.1	RNA Quantification Via Spectrophotometry	88
	Readings	
4.1.2.2	Agarose Gel Electrophoresis	89
4.1.3	Protein Extraction	90
4.1.3.1	Bradford Assay Protein Quantification	90

4.1.4	Quantitative Real-Time Reverse Transcribe PCR (qRT-PCR)	91
4.1.4.1	Determination of PCR Amplification Efficiencies	91
4.1.4.2	Evaluation <i>Bcl-xL</i> Gene Expression	92
4.1.5	Western blot	94
4.2	A549 Transfection With siRNA 1	97
4.2.1	<i>Bcl-xL</i> Silencing Using siRNA 1	97
4.2.1.1	siRNA Transfection Efficiency in A459 cells	97
4.2.2	RNA Extraction	99
4.2.2.1	RNA Quantification Via NanoDrop	99
4.2.2.2	Agarose Gel Electrophoresis	100
4.2.2.3	Quality Check Of Extracted Total RNA Using Agilent 2100 BioAnalyzer	100
4.2.3	Protein Extraction	102
4.2.3.1	Bradford Assay Protein Quantification	102
4.2.4	Quantitative Real-Time Reverse Transcribe PCR (qRT-PCR)	103
4.2.4.1	Determination of PCR Amplification Efficiencies	103
4.2.4.2	Evaluation of <i>Bcl-xL</i> Gene Expression	104
4.2.5	Western Blot	106
4.3	MTT Cell Viability Assay	108
4.4	MiRNA Microarray	109
4.4.1	MiRNA Microarray Analysis	109

4.4.2	MiRNA Microarray Validation	112
4.4.2.1	Quantitative Real-Time Reverse Transcribe PCR (qRT-PCR)	112
4.4.3	MiRNA Putative Target	114
4.4.3.1	Hypothetical Pathway Analysis	120
Chapter 5: Discussion		122
5.1	Transient siRNA Based <i>Bcl-xL</i> Silencing in Lung Adenocarcinoma Cells (A549)	122
5.1.1	siRNA Transfection in A549 Cells	123
5.2	MiRNAs Dysregulated in Response to <i>Bcl-xL</i> Silencing	125
5.2.1	MiRNA Microarray Analysis	126
5.2.2	qRT-PCR Validation	128
5.3	Hypothetical Pathway Analysis	129
5.3.1	PI3K/AKT Pathway	130
5.3.2	Intrinsic and Extrinsic Pathway	133
5.3.3	WNT Pathway	135
5.3.4	TGF- β Pathway	137
5.3.5	MAPK Pathway	139
5.4	Future Prospects	141
Chapter 6: Conclusion		143
References		144

Appendices	164
Appendix 1: Solutions and Formulations	164
Appendix 2: Molecular Markers	169
Appendix 3: siRNA Binding Site	172
Appendix 4: siRNA Transfection Efficiency	173
Appendix 5: qRT-PCR Melting Curve Analysis	179
Appendix 6: qRT-PCR Quantification Data	183

LIST OF FIGURES

	Page No.
Figure 2.1 The hallmarks of cancer.	4
Figure 2.2 Worldwide incidence and mortality of cancers in males and females combined, in 2008.	9
Figure 2.3 Malaysian population's incidence and mortality of cancers in males and females combined, in 2008.	10
Figure 2.4 Scheme depicting intrinsic and extrinsic pathways of apoptosis.	21
Figure 2.5 PI3K Signaling.	27
Figure 2.6 Canonical Wnt/ β -catenin signaling pathway.	29
Figure 2.7 TGF- β signaling pathway.	32
Figure 2.8 The current model for the biogenesis and post-transcriptional suppression of microRNAs.	40
Figure 2.9 Oncogenic MiRNAs can be blocked through the use of antisense oligonucleotides, miRNA.	49
Figure 4.1 Determination of transfection efficiency in non-transfected A549 cells	86
(A) Phase-contrast image of non-transfected A549 cells.	86
(B) Fluorescent image of non-transfected A549 cells.	86
(C) Merged image of non-transfected A549 cells.	86

Figure 4.2	Determination of transfection efficiency in siRNA 1 transfected A549 cells	86
	(A) Phase-contrast image of siRNA 1 A549 cells transfected with BLOCK-iT™ Alexa Fluor® Red Fluorescent Oligo.	86
	(B) Fluorescent image of siRNA 1 A549 cells transfected with BLOCK-iT™ Alexa Fluor® Red Fluorescent Oligo.	86
	(C) Merged image of siRNA 1 A549 cells transfected with of BLOCK-iT™ Alexa Fluor® Red Fluorescent Oligo.	86
Figure 4.3	Determination of transfection efficiency in siRNA 2 transfected A549 cells.	87
	(A) Phase-contrast image of siRNA 2 A549 cells transfected with BLOCK-iT™ Alexa Fluor® Red Fluorescent Oligo.	87
	(B) Fluorescent image of siRNA 2 A549 cells transfected with BLOCK-iT™ Alexa Fluor® Red Fluorescent Oligo.	87
	(C) Merged image of siRNA 2 A549 cells transfected with of BLOCK-iT™ Alexa Fluor® Red Fluorescent Oligo.	87
Figure 4.4	Determination of transfection efficiency in siRNA 3 transfected A549 cells.	87
	(A) Phase-contrast image of siRNA 3 A549 cells transfected with BLOCK-iT™ Alexa Fluor® Red Fluorescent Oligo.	87
	(B) Fluorescent image of siRNA 3 A549 cells transfected with BLOCK-iT™ Alexa Fluor® Red Fluorescent Oligo.	87
	(C) Merged image of siRNA 3 A549 cells transfected with BLOCK-iT™ Alexa Fluor® Red Fluorescent Oligo.	87

Figure 4.5	Agarose gel electrophoresis image for the total RNA extraction of siRNA 1, 2, and 3 transfected and non-transfected A549 cells.	89
Figure 4.6	Standard curve generated for <i>bcl-xL</i> standards had an efficiency of 2.10.	91
Figure 4.7	Standard curve generated for <i>β-actin</i> standards had an efficiency of 2.06.	92
Figure 4.8	Quantitative real-time RT-PCR analysis of <i>bcl-xL</i> expression in siRNA-transfected and non-transfected A549 cells.	93
Figure 4.9	Indication of significantly decreased Bcl-xL (30-kDa) protein levels in A549 cells transfected with siRNA 1.	95
Figure 4.10	Densitometry analysis of the Western blots using the ImageJ Analyst software.	96
Figure 4.11	Determination of transfection efficiency in siRNA 1 biological replicate 1 transfected A549 cells.	98
	(A) Phase-contrast image of siRNA 1 biological replicate 1 A549 cells transfected with BLOCK-iT™ Alexa Fluor® Red Fluorescent Oligo.	98
	(B) Fluorescent image of siRNA 1 biological replicate 1 A549 cells transfected with BLOCK-iT™ Alexa Fluor® Red Fluorescent Oligo.	98
	(C) Merged image of siRNA 1 biological replicate 1 A549 cells transfected with BLOCK-iT™ Alexa Fluor® Red Fluorescent Oligo had a transfection efficiency of 81.2% \pm 3.57%.	98

Figure 4.12	Determination of transfection efficiency in siRNA 1 biological replicate 2 transfected A549 cells.	98
(A)	Phase-contrast image of siRNA 1 biological replicate 2 A549 cells transfected with BLOCK-iT TM Alexa Fluor [®] Red Fluorescent Oligo.	98
(B)	Fluorescent image of siRNA 1 biological replicate 2 A549 cells transfected with BLOCK-iT TM Alexa Fluor [®] Red Fluorescent Oligo.	98
(C)	Merged image of siRNA 1 biological replicate 2 A549 cells transfected with BLOCK-iT TM Alexa Fluor [®] Red Fluorescent Oligo had a transfection efficiency of 79.0% \pm 4.17%.	98
Figure 4.13	Determination of transfection efficiency in siRNA 1 biological replicate 3 transfected A549 cells.	99
(A)	Phase-contrast image of siRNA 1 biological replicate 3 A549 cells transfected with BLOCK-iT TM Alexa Fluor [®] Red Fluorescent Oligo.	99
(B)	Fluorescent image of siRNA 1 biological replicate 3 A549 cells transfected with BLOCK-iT TM Alexa Fluor [®] Red Fluorescent Oligo.	99
(C)	Merged image of siRNA 1 biological replicate 3 A549 cells transfected with BLOCK-iT TM Alexa Fluor [®] Red Fluorescent Oligo had a transfection efficiency of 81.2% \pm 3.7%.	99
Figure 4.14	Agarose gel electrophoresis image for the total RNA extraction of siRNA 1 transfected and non-transfected A549 cells.	100

Figure 4.15	Total RNA Nano Agilent BioAnalyzer gel image of total RNA triplicate samples extracted from siRNA 1 transfected and non-transfected A549 cells.	101
Figure 4.16	Standard curve generated for <i>bcl-xL</i> standards had an efficiency of 1.93.	103
Figure 4.17	Standard curve generated for <i>β-actin</i> standards had an efficiency of 2.04.	104
Figure 4.18	Quantitative teal-time RT-PCR analysis for <i>bcl-xL</i> expression in siRNA-transfected and non-transfected A549 cells.	105
Figure 4.19	Indication of significantly decreased Bcl-xL (30-kDa) protein levels in A549 cells transfected with siRNA 1.	106
Figure 4.20	Densitometry analysis of the Western blots using the ImageJ Analyst software.	107
Figure 4.21	Comparison of total viable cell count on NP-69 normal cell control and A549 lung adenocarcinoma cells after siRNA transfection over 48 hours.	108
Figure 4.22	Hierarchical clustering heat map of 10 differentially expressed miRNAs in siRNA-transfected A549 cells versus non-transfected A549 cells.	111
Figure 4.23	Quantitative real-time RT-PCR validation of five representative miRNAs.	113
Figure 4.24	Pearson correlation scatter plot between two variables, miRNA microarray fold-change and qRT-PCR fold-change, produced a correlation coefficient value of $r = 0.950$ with an $r^2 = 0.903$, indicating a strong positive association between both sets of data.	114

Figure 4.25	Hypothetical pathway model illustrating the effects the five selected miRNAs play on apoptosis as well as cell proliferation and angiogenesis in <i>bcl-xL</i> silenced A549 cells.	121
Figure 5.1	Hypothetical pathway model illustrating miRNA targets in the PI3K/Akt pathway.	130
Figure 5.2	Hypothetical pathway model illustrating miRNA targets in the intrinsic and extrinsic apoptotic pathway	133
Figure 5.3	Hypothetical pathway model illustrating miRNA targets in the WNT pathway.	135
Figure 5.4	Hypothetical pathway model illustrating miRNA targets in the TGF- β pathway.	137
Figure 5.5	Hypothetical pathway model illustrating miRNA targets in the MAPK pathway.	139

LIST OF TABLES

	Page No.
Table 2.1 Functional categories of the Bcl-2 family of proteins.	23
Table 3.1 Stealth RNAi™ siRNA Duplex Oligonucleotides used for transfection.	53
Table 3.2 Oligonucleotides used for qRT-PCR	61
Table 3.3 Kit components used to prepare cDNA samples.	62
Table 3.4 Kit components used to prepare qPCR samples.	62
Table 3.5 Real-time PCR instrument conditions.	63
Table 3.6 Reagents for preparation of 4.0% stacking gel and 12.0% resolving gel for SDS-PAGE.	64
Table 3.7 Components used to prepare Poly (A) tail.	73
Table 3.8 Components used to prepare array hybridization cocktail.	75
Table 3.9 Components of GeneChip Hybridization, Wash & Stain Kit.	76
Table 3.10 Fluidic station protocol summary for the staining of each Affymetrix GeneChip® miRNA Arrays.	77
Table 3.11 Components used to prepare for ELOSA sample hybridization	78
Table 3.12 Components used to prepare negative and positive controls for ELOSA sample hybridization	78
Table 3.13 TaqMan® MicroRNA Assays used for qRT-PCR.	81
Table 3.14 Kit components used to prepare RT master mix.	81
Table 3.15 Thermal cycler conditions for cDNA synthesis.	82
Table 3.16 Components used to prepare qPCR master mix.	82
Table 3.17 Real-time PCR instrument conditions for qPCR.	83

Table 4.1	Hybridization sites of the Stealth RNAi™ siRNA Duplex Oligonucleotides on the <i>bcl-xL</i> mRNA.	84
Table 4.2	Spectrophotometric quantification of total RNA extracted from siRNA-transfected and non-transfected A549 cells.	88
Table 4.3	Spectrophotometric quantification of protein using Bradford Assay.	90
Table 4.4	Fold-change in <i>bcl-xL</i> gene expression in siRNA-transfected A549 cells as compared to non-transfected A549 cells	93
Table 4.5	Percentage of <i>Bcl-xL</i> gene knockdown in siRNA-transfected A549 cells as compared to non-transfected A549 cells.	94
Table 4.6	Densitometry analysis of the Western blots was carried out using the ImageJ Analyst software.	96
Table 4.7	Spectrophotometric quantification of total RNA extracted from siRNA 1 transfected and non-transfected cells.	99
Table 4.8	RNA integrity number (RIN value) was determined using the Agilent 2100 BioAnalyzer.	102
Table 4.9	Spectrophotometric quantification of protein using Bradford Assay.	102
Table 4.10	Fold-change in <i>bcl-xL</i> gene expression in siRNA-transfected A549 cells as compared to non-transfected A549 cells	105
Table 4.11	Percentage of <i>Bcl-xL</i> gene knockdown in siRNA-transfected A549 cells as compared to non-transfected A549 cells.	106
Table 4.12	Densitometry analysis of the Western blots was carried out using the ImageJ Analyst software.	107

Table 4.13	Table comparing total cell viability levels (%) as obtained from MTT assays at 12 hours, 24 hours and 48 hours in NP-69 and A549 cell lines.	109
Table 4.14	List of differentially expressed miRNAs filtered with at least a 1.5-fold change in expression and $p \leq 0.05$ using the GeneSpring and Partek Genomics Suite Software.	112
Table 4.15	Fold-change of miRNA expression in siRNA-transfected A549 cells as compared to non-transfected A549 cells.	113
Table 4.16	Summary of miRNA apoptosis-, proliferation- and angiogenesis-related putative gene targets.	115

LIST OF ABBREVIATIONS

°C	Degrees Celsius
μ	Micro
μg/ml	Micrograms per Milliliter
μl	Microliter
μM	Micromolar
%	Percentage
®	Registered
(v/v)	Volume per Volume
(w/v)	Weight per Volume
3'UTR	Three Prime Untranslated Region
A549	Human Lung Adenocarcinoma Cell Line
A-Raf	V-raf Murine Sarcoma 3611 Viral Oncogene Homolog
AAV	Adenovirus-Associated Vector
ABCG2	ATP-Binding Cassette, Subfamily G, Member 2
Abl	Abelson
Akt	Protein kinase B
ALT	Alternative Lengthening of the Telomeres
AMO	Anti-miRNA Oligonucleotide
ANOVA	Analysis of Variance
AP-1	Activator Protein 1
Apaf	Apoptotic Protease-Activating Factor 1
APC	Adenomatous Polyposis Coli
APS	Ammonium Persulfate
ASK1	Apoptosis Signal-Regulating Kinase 1
ASK2	Apoptosis Signal-Regulating Kinase 2
ATF2	Activating Transcription Factor 2
ATF3	Activating Transcription Factor 3
ATP	Adenosine Triphosphate
B-CLL	B-cell Chronic Lymphocytic Leukemia
B-Raf	V-raf Murine Sarcoma Viral Oncogene Homolog B1
Bad	Bcl-2-Associated Death Promoter
Bak	Bcl-2-Antagonist Killer
Bax	Bcl-2-Associated X Protein
Bcl-2	B-Cell Lymphocyte 2
Bcl-B	B-Cell Lymphocyte 10
Bcl-w	B-Cell Lymphocyte W
Bcl-x _L	B-Cell Lymphocyte x _L
BCR	Breakpoint Cluster Region
BCRP	Breast Cancer Resistance Protein
Bfl-1	Bcl-2-Related Protein A1
BH	Bcl-2 Homology
BH1	B-Cell Lymphocyte 2 Homology Domain 1
BH2	B-Cell Lymphocyte 2 Homology Domain 2
BH3	B-Cell Lymphocyte 2 Homology Domain 3
BH4	B-Cell Lymphocyte 2 Homology Domain 4
Bid	BH3 Interacting-Domain Death Agonist
Bik	B-Cell Lymphocyte 2-Interacting Killer
Bim	B-Cell Lymphocyte 11

BLAST	Basic Local Alignment Search Tool
Bmf	B-Cell Lymphocyte 2-Modifying Factor
BMP	Bone Morphogenetic Proteins
Bok	B-Cell Lymphocyte 2-Related Ovarian Killer Protein
bp	Base Pairs
BSA	Bovine Serum Albumin
CAM	Cell Adhesion Molecule
CARIF	Cancer Research Initiative Foundation
Caspase	Cysteine Aspartate Protease
CDC42	Cell Division Control Protein 42 Homolog
CDK	Cyclin-Dependent Kinase
CDKI	Cyclin-Dependent Kinase inhibitor
CDK4	Cyclin-Dependent Kinase 4
CDK6	Cyclin-Dependent Kinase 6
cDNA	Complementary Deoxyribonucleic Acid
CEL	Affymetrix Cell Intensity File
CER I	Cytoplasmic Extraction Reagent I
CER II	Cytoplasmic Extraction Reagents II
c-Fos	FBJ Murine Osteosarcoma Viral Oncogene Homolog
c-Jun	Jun Proto-Oncogene
c-Myc	V-myc Myelocytomatosis Viral Oncogene Homolog
CO ₂	Carbon Dioxide
Co-Smad	Common-Mediated Smad
COX-2	InducibleCyclooxygenase-2
CpG	-Cytosine-Phosphate-Guanine-
DAVID	Database for Annotation, Visualization and Integrated Discovery
DGCR8	Di-George Syndrome Critical Region Gene 8
DISC	Death Inducing Signal Complex
DLK	Delta-Like Protein 1
DMEM	Dulbecco's Modified Eagles Medium
DMSO	Dimethyl Sulfoxide
DNA	Deoxyribonucleic Acid
DTT	Dithiothreitol
Dvl	Dishevelled
E2F	E2 Transcription Factor
E2F1	E2 Transcription Factor 1
E2F3	E2 Transcription Factor 3
EDTA	Ethylenediaminetetraacetic Acid
EGF	Epidermal Growth Factor
EGFR	Epidermal Growth Factor Receptor
ELK-1	E Twenty-Six (ETS)-Like Transcription Factor 1
ELOSA	Enzyme Linked Oligosorbent Assay
ERBB	Epidermal Growth Factor Receptor Family
ERBB1	Epidermal Growth Factor Receptor
ERBB2	Epidermal Growth Factor Receptor Family 2
ERK	Extracellular Signal-Regulated Kinase
ERK1	Extracellular Signal-Regulated Kinase 1
ERK1	Extracellular Signal-Regulated Kinase 2
EtBr	Ethidium Bromide
ETS1	V-ets Erythroblastosis Virus E26 Oncogene Homolog
ETS2	V-ets Erythroblastosis Virus E26 Oncogene Homolog 2
FADD	Fas-Associated Death Domains

FasL	F29 Associated Surface Antigen Ligand
FasR	F29 Associated Surface Antigen Receptor
FBS	Foetal Bovine Serum
FKHR	Forkhead Transcription Factor
Fzd	Frizzled
G ₀	Gap Zero Phase
G ₁	Gap One pPase
G ₁ /S	G ₁ /S Phase Transition
G ₂ /M	G ₂ /M Phase Transition
GADD45	Growth Arrest and DNA Damage
GEF	Guanine Nucleotide Exchange Factors
GS	Guanidine Specificity
GSK3 β	Glycogen Synthase-Kinase-3-Beta
HGFR	Hepatocyte Growth Factor Receptor
HODXD10	Homeobox D10
HRAS	v-Ha-ras Harvey Rat Sarcoma Riral Oncogene Homolog
Hrk	Harakiri, Bcl-2 Interacting Protein
HRP	Horse Radish Peroxidase
IAP	Inhibitor of Apoptosis
I κ B	Inhibitor of Nuclear Factor Kappa B
IKK	I κ B kinase
JAK	Janus Kinase
JNK	c-Jun N-Terminal Kinases
kDa	Kilodalton
KRAS	v-Ki-Ras2 Kirsten Rat Sarcoma Viral Oncogene Homolog
LEF	Lymphoid enhancer factor
LOH	Loss of Heterozygosity
LRP	Lipoprotein Receptor Related Protein
LZK	Leucine Zipper Kinase
mA	Milliampere
MAP	Mitogen-Activated Protein
MAPK	Mitogen-Activated Protein Kinase
MAP2K	Mitogen-Activated Protein Kinase Kinase
MAP3K	Mitogen-Activated Protein Kinase Kinase Kinase
MAP4K	Mitogen-Activated Protein Kinase Kinase Kinase Kinase
MAPKAPK	Mitogen-Activated Protein Kinase-Activated Protein Kinase
Mcl-1	Myeloid Cell Leukemia Sequence 1
Mdm2	Murin Double Minute Protein 2
MEKK	MAP kinase kinase kinase
Met	Hepatocyte Growth Factor Receptor
mg	Milligrams
mg/ml	Milligrams per Milliliter
MiRNA	MicroRNA
ml	Milliliter
mM	Millimolar
mm	Millimeter
mm ³	Millimeter cube
MLK1	Mixed Lineage Protein Kinase
MLK2	Mixed Lineage Protein Kinase 2
MLK3	Mixed Lineage Protein Kinase 3
MMP	Matrix Metalloproteinases
MMP2	Matrix Metallopeptidase 2

MMP3	Matrix Metallopeptidase 3
MMP7	Matrix Metallopeptidase 7
MMP9	Matrix Metallopeptidase 9
MnCl ₂	Manganese Chloride
mRNA	Messenger RNA
MTT	3-(4,5-dimethylthiazol-2-yl)-2,5-Diphenyltetrazolium Bromide
NCBI	National Center for Biotechnology Information
NER	Nuclear Extraction Reagent
NFAT	Nuclear Factor of Activated T Cells
NFκB	Nuclear factor kappa-light-chain-enhancer of activated B
ng	Nanogram
ng/μl	Nanogram per Microliter
nm	Nanometer
Noxa	Phorbol-12-Myristate-13-Acetate-Induced Protein
NRAS	Neuroblastoma RAS Viral (v-ras) Oncogene Homolog
NSCLC	Non-Small Cell Lung Cancer
OD	Optical Density
OSCC	Oral Squamous Cell Carcinoma
<i>P</i>	<i>p</i> -value of Data Statistical Significance
PAGE	Polyacrylamide Gel Electrophoresis
PAK2	p21 Protein Activated Kinase 2
PAP	Phosphatidic Acid Phosphatase
PBS	Phosphate Buffer Saline
PDCD4	Programmed Cell Death 4
PDGF	Platelet-Derived Growth Factor
PDGFR	Platelet-Derived Growth Factor Receptor
PDK1	3-Phosphoinositide-Dependent Protein Kinase-1
pH	Potential Hydrogen
PH	Plekstrin Homology
PI3K	Phosphatidylinositol 3-Kinase
PIP ₂	Phosphatidylinositol 4,5-Bisphosphate
PIP ₃	Phosphatidylinositol (3,4,5)-Triphosphate
PKB	Protein Kinase B
pRb	Phosphorylated Retinoblastoma Protein
Pre-miRNA	Precursor miRNA
Pri-miRNA	Primary miRNA
PtdIns	Phosphatidylinositols
PTEN	Phosphatase and Tensin Homolog
Puma	p53 Upregulated Modulator of Apoptosis
qRT-PCR	Quantitative Reverse Transcription Polymerase Chain Reaction
R-Smads	Receptor Activated Smads
Rac1	Ras-Related C3 Botulinum Toxin Substrate 1
Ras	Rat Sarcoma
Raf-1	V-Raf-1 Murine Leukemia Viral Oncogene Homolog 1
Rb	Retinoblastoma Protein
RER+	Replication Error Repair
RhoC	Ras Homolog Gene Family, Member C
RIN	RNA Integrity Number
RISC	RNA-Induced Silencing Complex
RMA	Robust Multichip Average
RNA	Ribonucleic Acid
RPM	Revolutions per Minute

RPMI 1640	Roswell Park Memorial Institute 1640
rRNA	Ribosomal RNA
RT	Reverse Transcription
RTK	Receptor Tyrosine Kinases
RT-PCR	Reverse Transcription Polymerase Chain Reaction
SA-HRP	Streptavidin-Horse Radish Peroxidase
SAPK	Stress-Activated Protein Kinases
SCC	Squamous Cell Carcinoma
SCLC	Small-Cell Lung Cancer
±SD	Mean Standard deviation
SDS	Sodium Dodecyl Sulphate
siRNA	Small Interfering RNA
Sos	Son of Sevenless
STAT3	Signal Transducer and Activator of Transcription 3
STAT5	Signal Transducer and Activator of Transcription 5
TAK1	Transforming Growth Factor-Beta Activated Kinase 1
TBE	Tris/Borate/EDTA
TBS	Tris-Buffered Saline
TBST	Tris-Buffered Saline Tween20
TCF	T-Cell Factor
TEMED	Tetramethylethylenediamine
TGF-β	Transforming Growth Factor Beta
TGF-β2	Transforming Growth Factor Beta 2
TGF-β3	Transforming Growth Factor Beta 3
TGFBR 1	Transforming Growth Factor Beta Receptor Type 1
TGFBR 2	Transforming Growth Factor Beta Receptor Type 2
TGS	Tris/Glycine/SDS
™	Trademark
TMB	3,3',5,5'-Tetramethylbenzidine
TNF	Tumor Necrosis Factor
TNF-α	Tumor Necrosis Factor Alpha
TNFR	Tumor Necrosis Factor Receptor
TRAF	TNF Associated Factors
TRAIL	TNF-Related Apoptosis Inducing Ligand
TRBP	Transactivating Response DNA Binding Protein
Tris-HCl	Tris-Hydrochloride
TSG	Tumor Suppressor Gene
TWIST1	Twist Homolog 1
UV	Ultraviolet
V	Volts
VEGF	Vascular Endothelial Growth Factor
VEGFR	Vascular Endothelial Growth Factor Receptor
Wnt	Wingless-Type MMTV Integration Site Family
Wnt1	Wingless-Type MMTV Integration Site Family, Member 1
Wnt2	Wingless-Type MMTV Integration Site Family, Member 2
Wnt7a	Wingless-Type MMTV Integration Site Family, Member 7A

CHAPTER 1: INTRODUCTION

Lung cancer remains a major health problem worldwide. In 2008, lung cancer was the most commonly diagnosed cancer as well as the leading cause of cancer deaths in males worldwide (Jemal *et al.*, 2011). Among females, lung cancer was the fourth most commonly diagnosed cancer and the second leading cause of cancer death (Jemal *et al.*, 2011). 13% (1.6 million) of the total cases and 18% (14 million) of the deaths in 2008 was caused by lung cancer (Jemal *et al.*, 2011). In Malaysia, lung cancer accounts for 10.2% of all cancer deaths, making it the most common cancer followed by colon and then breast cancer (Zainal and Nor Saleha, 2011) with adenocarcinoma being the most common cell type (Liam *et al.*, 2006).

In contrast to normal cells, cancer cells have the ability to disrupt the balance between pro- and anti-apoptotic factors to promote cell survival under the conditions of environmental stress. In terms of molecular events occurring in tumors, evasion of apoptosis is an important hallmark of tumor progression. Members of the evolutionarily conserved B-cell lymphocyte 2 (Bcl-2 family) are thought to be the central regulators of apoptosis. The expression level of Bcl-2 differs for different cell types, however high levels and aberrant patterns of Bcl-2 expression have been reported in a wide variety of human cancers (Hockenberry *et al.*, 1991). Elevation of Bcl-2 protein expression contributes not only to the development of cancer but also to resistance against a wide variety of anti-cancer agents (Miyashita and Reed, 1993; Fisher *et al.*, 1993; Tang *et al.*, 1994). However, studies conducted on non-small cell lung cancer (NSCLC), which accounts for the majority of lung cancer cases (Liam *et al.*, 2006), have shown that the expression of Bcl-2 is either very low or even absent (Daniel and Smith, 2004). Instead, the expression of B-cell lymphocyte xL (*bcl-xL*), the other major prototype of the anti-apoptotic *Bcl-2* gene, is shown to be over-expressed in NSCLC (Soini *et al.*, 1999).

Over-expression of Bcl-xL inhibits apoptosis in NSCLC and has been coupled with poor prognosis of this disease (Soini *et al.*, 1999).

Over-expression of Bcl-xL has been shown to counteract the pro-apoptotic functions of Bcl-2-associated X protein (Bax) and Bcl-2-associated death promoter (Bad) by preventing their translocation from the cytosol to the mitochondria. This inhibits apoptosis by maintaining the permeabilization status or stabilization of the outer mitochondrial membrane, which subsequently prevents cytochrome c release and pro-caspase-9 activation (Gottlieb *et al.*, 2000).

MicroRNAs (miRNAs) are small non-coding RNA of about 19-23 nucleotides long that regulate gene expression post-transcriptionally, by either inhibiting mRNA translation or by inducing mRNA degradation (Bartel, 2004). These regulatory elements play a role in a wide range of biological processes including cell proliferation (Hayashita *et al.*, 2005), differentiation (Shivdasani, 2006) and apoptosis (Mott, 2007). Therefore a disturbed miRNA function or altered miRNA expression may disorganize cellular processes and eventually cause or contribute to disease, including cancer (Weimer, 2007).

MiRNAs are critical apoptosis regulators in tumorigenesis, and cancer cells are able to manipulate miRNAs to regulate cell survival in oncogenesis. For example, miR-133 acts as a regulator of survival in cardiac cells by repressing caspase-9 expression at both protein and mRNA levels (Xu *et al.*, 2007), while the miR-17-92 cluster, which is amplified in B-cell lymphomas, is capable of inhibiting apoptosis by negatively regulating the tumor suppressor phosphatase and tensin homolog (PTEN) and the pro-apoptotic protein B-cell lymphocyte 11 (Bim) (Xiao *et al.*, 2008).

While many miRNAs have been identified to be dysregulated in cancers, their specific functions remain unclear due to the nonspecific binding properties of each individual miRNA. As the miRNA field continues to evolve and develop it is important to gain a better understanding of miRNA biogenesis and function, as it will certainly affect the development of miRNA-based therapies. Therefore, this study describes the siRNA-based silencing of the anti-apoptotic *bcl-xL* gene, followed by the establishment of a global miRNA expression profile through the comparison between silenced and non-silenced cells. It is hypothesized that *bcl-xL* silencing in A549 cells would result in different miRNA expression patterns which could potentially be used for antisense gene therapeutic applications in NSCLC.

1.1 Study Objectives

- i. To investigate the apoptotic effects of *bcl-xL* silencing in A549 cells.
- ii. To observe the global miRNA expression profile in *bcl-xL* silenced A549 cells.
- iii. To predict and identify the target genes of selected miRNAs dysregulated in *bcl-xL* silenced A549 cells.
- iv. To identify the potential role(s) of the dysregulated miRNAs in various signaling pathways in *bcl-xL* silenced A549 cells.

CHAPTER 2: LITERATURE REVIEW

2.1 Cancer

Cancer is a genetic disease that occurs when various mutations take place in specific genes. These mutations may enhance the effects of normal genes that control cell growth, survival and spread, while the genes that suppress these effects may be inhibited. Dysregulated gene expressions leads to a number of important changes in the fundamental biological processes within cancer cells, termed the hallmarks of cancer (Hannahan & Weinberg, 2011). The “hallmarks of cancer” are traits that are acquired by cancer cells to enable them to become tumorigenic and ultimately malignant. These hallmarks of cancer include growth factor independence, insensitivity to anti-growth signals, avoidance of apoptosis, sustained angiogenesis, cellular immortalization, and tissue invasion and metastasis (Hannahan & Weinberg, 2011).

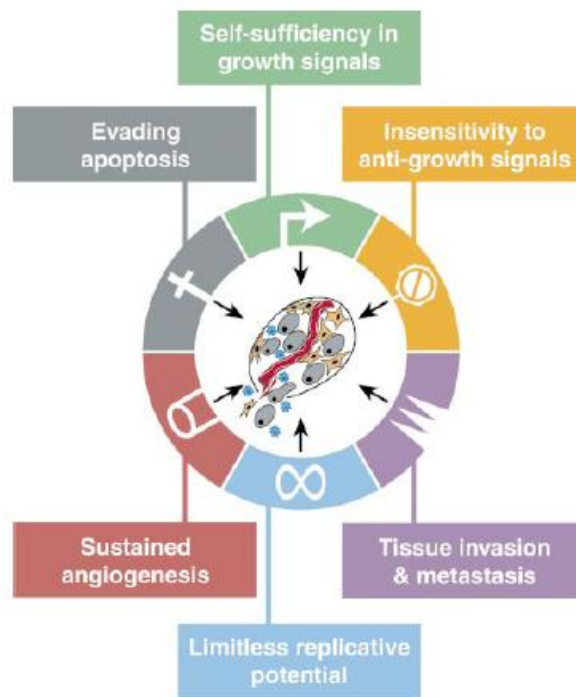


Figure 2.1: The hallmarks of cancer (Figure adapted from Hanahan & Weinberg, 2000).

2.1.1 Hallmarks of Cancer

Growth factor independence: Independence of growth factors allows the cells to have sustained signaling in pathways that control essential biological functions such as growth, apoptosis, angiogenesis, invasion and DNA damage repair (Harrington, 2007). Cancer cells use three main strategies to attain self-sufficiency in growth factors. The first strategy is to produce and release growth factors that stimulate their own receptors (autocrine signaling) and those of neighboring cells (paracrine signaling). Secondly, they can alter the number, structure or function of the growth factor receptors on their surface, thus making them more likely to send a growth signal to the nucleus. Thirdly, cancer cells can deregulate signaling pathways downstream of the growth factor receptor, making them permanently turned on (Hanahan & Weinberg, 2011; Harrington, 2007).

Insensitivity to anti-growth signals: Anti-growth signals function by forcing the cells into quiescence (G_0 stage of the cycle) or by inducing terminal differentiation so that the cells are unable to enter the cell cycle (Hanahan & Weinberg, 2011). Ligands mediate anti-growth signaling and these pathways are involved in controlling the cell cycle clock. Their effects are mediated through various proteins, which include retinoblastoma protein (Rb), cyclins, cyclin-dependant kinase (CDK) and their inhibitors (CDKI) (Hannon and Beach, 1994;). Dysregulation of the anti-growth signaling pathways play a role in aiding the cancer cells to progress through the cell cycle.

Avoidance of apoptosis: The balance between anti-apoptotic and pro-apoptotic signals are continually assessed in normal cells. In normal cells, DNA damage will lead to cell cycle arrest while the potential for repair is evaluated. If the amount of damage surpasses the ability of the cells to repair, the balance of the anti- and pro-apoptotic signals will tip and the cell undergo apoptosis (Harrington, 2007). Dysregulation of normal apoptotic pathway signaling is common in cancer (Ker *et al.*, 1972). Due to their ability to ignore signals that are sent through the extrinsic pathway, cancer cells are able to avoid apoptosis. Also, cancer cells have the ability to re-set the balance of intracellular pro- and anti-apoptotic molecules in favor of inhibition of apoptosis (Hannahan and Weinberg, 2011; Harrington, 2007).

Sustained angiogenesis: A good source of blood supply is essential to the survival and growth of cancer cells. Cancer cells can grow to 60-100µm by obtaining a supply of oxygen and nutrients through direct diffusion (Hannahan and Weinberg, 2011). However, beyond this size the tumor must obtain its own dedicated blood supply (Bouck *et al.*, 1996; Hanahan and Folkman, 1996). By overthrowing the balance between pro- and anti-angiogenic factors, cancer cells can acquire the ability to grow a new blood supply. For example, this can be carried out through up-regulation of the production of pro-angiogenic proteins such as vascular endothelial growth factor (VEGF) and downregulation of the production of anti-angiogenic proteins such as thrombospondin-1 (Bull *et al.*, 1994).

Cellular immortalization: Malignant cells can acquire immortality through the maintenance of the length of their telomeres. In contrast, normal cells can only undergo a finite number of cell division before they enter a period of permanent growth arrest, due to their inability to replicate their telomeres fully at each division (Hanahan and Weinberg, 2011). Cancer cells do this through either the up-regulation of the enzyme telomerase or by a mechanism called alternative lengthening of the telomeres (ALTs) (Harrington, 2007).

Invasion and metastasis: Dissemination of cancer cells into the circulation involves various biological processes. At the local site, the cells must first undergo detachment from their immediate neighbors and stroma (Hannahan and Weinberg, 2011). Cohesion to the primary tumor mass is mediated by active homotypic cell adhesion molecules (CAMs) (Aplin *et al.*, 1998). Downregulation of the cadherin family of cell surface receptors results in the loss of tissue integrity and is responsible for the breakdown of tissue architecture and allows for the escape of individual cells (Hart, 2004). Once the cancer cells have penetrated into the blood of lymphatic vessels, they must survive in the circulation until they arrive at the metastatic site. At its destination, they will adhere to the endothelium of blood cells and extravasate from the vessel. At this site, the cancer cells will begin to proliferate and set about constructing a new blood supply (Hannahan & Weinberg, 2011).

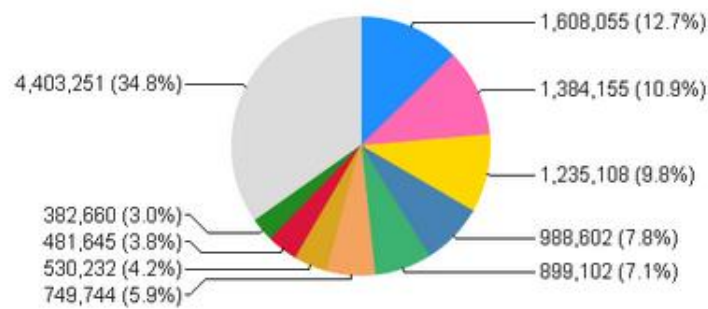
2.1.2 Cancer Statistics

Cancer is a major burden of disease worldwide. Yearly, tens of millions of people are diagnosed with cancer, and eventually more than half of the patients would die from it. Worldwide, cancer ranks as the second most common cause of death following cardiovascular diseases (Ma & Yu, 2006). However due to the vast improvement in the treatment and prevention of cardiovascular diseases, cancer has or will become the number one killer in the world (Ma & Yu, 2006).

GLOBOCAN, a Windows based software, provides access to a global cancer incidence and mortality rates data (International Agency for Research on Cancer, 2008). Based on the GLOBOCAN database, there were about 12,662,600 new cancer cases in the world in 2008. Of these, 52.3% were male and 47.7% were female (International Agency for Research on Cancer, 2008). For males and females combined, the most common cancer site worldwide was lung. The second most common site was breast, followed by colon. For women, the number one cancer site was breast followed by colon and cervix. Among men, the three most common cancer sites were lung, prostate and colon (Jemal *et al.*, 2011). In Malaysia, for males and females combined, the most common cancer site, for the year 2008, was lung followed by colon and then breast (International Agency for Research on Cancer, 2008).

The number of deaths caused by cancer worldwide in 2008 was 7,564,800 among which 4,219,600 were males and 3,345,200 were females. Lung cancer led to the most cancer deaths in the world. The second on the list was breast followed by colorectum. Similarly, in Malaysia, lung cancer led to the most cancer deaths in the country. This was followed by colon cancer and then breast cancer (International Agency for Research on Cancer, 2008).

Incidence



Mortality

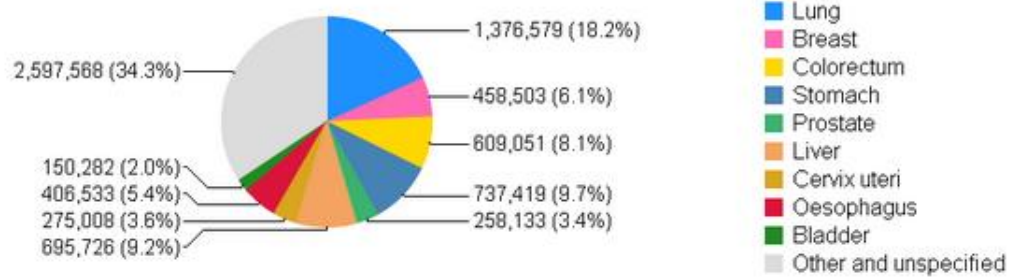
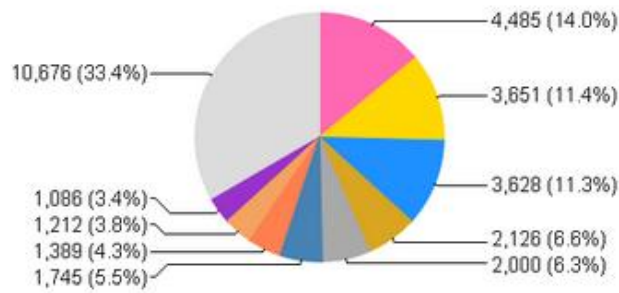


Figure 2.2: Worldwide incidence and mortality of cancers in males and females combined, in 2008 (Figure adapted from International Agency for Research on Cancer, 2008).

Incidence



Mortality

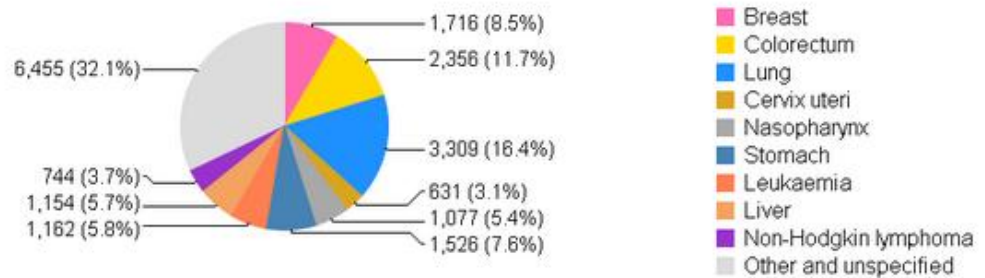


Figure 2.3: Malaysian population's incidence and mortality of cancers in males and females combined, in 2008 (Figure adapted from International Agency for Research on Cancer, 2008).

2.2 Lung Cancer

Lung cancer is a disease that is associated with the uncontrolled cell growth in tissues of the lung (Collins *et al.*, 2007). The vast majority of primary lung cancers are carcinomas, which are derived from epithelial cells (The Merck Manuals Online Medical Library, 2009). Lung cancer can be characterized into two main groups based upon the size and appearance of malignant cells: small cell lung cancer (SCLC) and non-small cell lung cancer (NSCLC) (The Merck Manuals Online Medical Library,

2009). NSCLC includes squamous cell carcinoma, adenocarcinoma, large-cell undifferentiated carcinoma, as well as some rare subtypes such as adenosquamous cell carcinoma, coepidermoid carcinoma, and adenoid cystic carcinoma (The Merck Manuals Online Medical Library, 2009).

2.2.1 Lung Cancer Subtypes

SCLC accounts for 20% of lung cancer and it is highly aggressive and is most strongly associated with smoking (The Merck Manuals Online Medical Library, 2009). SCLC usually grows in the submucosa of the airways. It is rapidly growing and about 60% of patients have widespread metastatic disease at the time of diagnosis cancers (The Merck Manuals Online Medical Library, 2009).

NSCLC has a more variable clinical behavior and depends on histologic type. About 40% of patients have metastatic disease outside of the chest at the time of diagnosis. NSCLC accounts for approximately 75-80% of all lung cancers (The Merck Manuals Online Medical Library, 2009). Lung adenocarcinoma normally begins in the tissues near the outer parts of the lungs and is usually present for a long time prior to the onset of symptoms. Lung adenocarcinoma is the most common form of lung cancer found in women, and is largely associated with non-smokers. As lung adenocarcinoma occurs in the outer parts of the lung, common symptoms of this type of cancer include chronic cough and coughing up of blood (The Merck Manuals Online Medical Library, 2009).

Squamous cell cancer of the lung occurs in about a quarter of all lung cancer patients and is normally located near the central bronchus. Squamous cell carcinomas are strongly linked with smoking. However, the incidence of this type of cancer has decreased since filtered cigarettes have become available and the smoke is inhaled more

deeply into the lungs, the region where adenocarcinoma begins (The Merck Manuals Online Medical Library, 2009). Squamous cell lung cancer is less aggressive and grows more slowly. Due to the location of this type of cancer, it is often found earlier than other forms of lung cancer (The Merck Manuals Online Medical Library, 2009).

Large cell carcinoma is the least common form of NSCLC, occurring in 10-15% of patients, and can start in any part of the lung (The Merck Manuals Online Medical Library, 2009). This type of carcinoma occurs in the outer regions of the lungs and tends to grow and spread quickly (The Merck Manuals Online Medical Library, 2009). Because large cell carcinomas are often found in the outer regions of the lungs, they can cause fluid to develop in the space between the tissues that line the lung, invading into the chest wall. This can cause pain in the chest or side, which worsens with a deep breath (The Merck Manuals Online Medical Library, 2009).

2.2.2 Etiology of Lung Cancer

There are numerous risk factors for lung cancer, and these risk factors can be grouped into two broad categories: factors that are inherent to the individual (intrinsic factors) and factors that are extraneous to the individual (extrinsic or environmental factors). The former category includes intrinsic features such as genetic susceptibility, family history of cancer, sex, race, age and previous respiratory diseases, while the latter category includes extrinsic aspects such as tobacco use, diet, occupation and environmental pollution (Ruano-Ravina *et al.*, 2003).

The most important environmental carcinogen that has been linked to lung cancer is tobacco smoke (Miller, 2005). Tobacco was used for many centuries prior to the modern epidemic of lung cancer. However, tobacco products only become more widely and intensively used with the development of machines for the commercial

production of cigarettes in the late nineteenth century (Miller, 2005). As early as the 1920s, tobacco smoke was suspected to cause lung cancer, when physicians began to see an increase in the number of patients with lung cancer, and discovered that nearly all were cigarette smokers (Witschi, 2001). Today, the most important cause of lung cancer is still cigarette smoking, which accounts for 85% of lung cancer cases (Hecht, 1999). Due to the complexity of tobacco smoke, the mechanism by which it causes lung cancer is still unknown. Among the many components of tobacco smoke, there have been about 55 carcinogens that have been closely linked to lung tumors in laboratory animals or humans and are therefore likely to be involved in lung cancer induction (Hecht, 1999).

The risk of cancer differs by age, smoking intensity and smoking duration. However, about 15% of people who develop lung cancer have never smoked. Studies have reported that lung cancer patients who have never smoked have genetic mutations in the epidermal growth factor gene (EGF) (Miller, 2005).

Various other environmental carcinogens include pollution from motor vehicle exhaust fumes, heating systems, power stations and other industrial emissions, such as asbestos, radiation, arsenic chromates, nickel, chloromethyl ethers, mustard gas or coke-oven emissions (Ruano-Ravina *et al*, 2003; The Merck Manuals Online Medical Library, 2009). The respiratory epithelial becomes neoplastic only after prolonged exposure to cancer-promoting agents and accumulation of multiple genetic mutations. Mutations in genes that stimulate cell growth may cause abnormalities in growth factor receptor signaling inhibit apoptosis and contributes to the proliferation of abnormal cells. In addition, mutations that inhibit the tumor suppressor genes can also lead to cancer (The Merck Manuals Online Medical Library, 2009).

In terms of intrinsic factors, the highest incidence of lung cancer occurs at around 65 years of age (Ruano-Ravina *et al.*, 2003). This finding allows for a strong link to be made between lung cancer and tobacco use, as it takes into account the required induction time for the habit of smoking to exert its effects (Ruano-Ravina *et al.*, 2003). Studies have shown that incidence of lung cancer declines after the age of 80 years. This can be due to two possible reasons: a lower prevalence of smoking habit amongst the older age group; or a bias of survival effect due to the fact that people who reach such ages are in some way genetically resistant to certain risk factors (Parkin *et al.*, 1996).

2.2.3 Epidemiology of lung cancer

In 2008, lung cancer was the most commonly diagnosed cancer as well as the leading cause of cancer deaths in males worldwide. Among females, lung cancer was the fourth most commonly diagnosed cancer and the second leading cause of cancer death (Jemal *et al.*, 2011). 13% (1.6 million) of the total cases and 18% (14 million) of the deaths in 2008 was caused by lung cancer. The highest lung cancer incidence rates in males occurs in Eastern and Southern Europe, North America, Micronesia and Polynesia, and Eastern Asia, while the rates in sub-Saharan Africa are low (Jemal *et al.*, 2011). On the other hand, for females, the highest lung cancer incidence rates are found in North America, Northern Europe, and Australia/New Zealand (Jemal *et al.*, 2011). The differences in lung cancer rates and trends that are observed across countries or between males and females within each country are largely due to the differences in the stage and degree of the tobacco epidemic. Smoking accounts for 80% of the worldwide lung cancer burden in males and 50% of the lung cancer burden in females (Jemal *et al.*, 2011).

In Malaysia lung cancer is the leading cause of cancer deaths, accounting for 19.8% of all cancer deaths. Lung cancer accounts for 13.8% of all cancers in males and 3.8% of all cancers in females (National Cancer Registry, 2008). In a study conducted by Liam *et al.*, a comparison was made between patients with lung cancer diagnosed at the University of Malaya Medical Centre, Kuala Lumpur, Malaysia, from October 1991 to September 1999, with another group of lung cancer patients diagnosed at the same hospital during an earlier period of 1967-1976 (Liam *et al.*, 2006; Menon & Saw, 1979). This study was conducted to determine whether there had been a change in the distribution of lung cancer types. It was found that in the recent period, the percentage of patients with adenocarcinoma had increased significantly to 34.2% from 25.2%, while that of the large cell carcinoma had decreased to 3.3% from 11.9% (Liam *et al.*, 2006). The percentage of patients with squamous cell carcinoma (SCC) and SCLC remained stable. In the period of 1967-1976, SCC was the predominant cell type in men, while adenocarcinoma was the main cell type in women. In the period of 1991-1999, it was found that adenocarcinoma was the most common cell type in both men and women (Liam *et al.*, 2006).

2.2.4 Pathogenesis of Lung Cancer

Lung cancer is the end result of a multi-step carcinogenesis, that is, in most cases driven by the genetic and epigenetic damage that is caused by prolonged exposure to tobacco smoke carcinogens (Fong *et al.*, 1999). There are two levels of genetic instability that can be seen in human cancers: the chromosomal level, which includes large-scale losses and gains, and the nucleotide level, which includes single or several base changes (Fong *et al.*, 1999). In lung cancer, many numeric chromosome abnormalities (aneuploidy) and structural cytogenetic abnormalities, which include

deletions and nonreciprocal translocations, occur. The chromosomal instability that leads to aneuploidy is strongly associated with the loss of function of a mitotic checkpoint (Fong *et al.*, 1999). However, how exactly this loss occurs in lung cancer is not known.

There are at least three classes of cellular genes involved in cancers: proto-oncogenes, tumor suppressor genes (TSGs), and DNA repair genes (Fong *et al.*, 1999). Studies have shown alterations in simple repeat sequences in lung cancer. The phenotype that is seen in lung cancers appears to be different from the typical replication error repair (RER+) phenotype that is seen in tumors with mutations in DNA mismatch repair genes. This instability affects a small proportion of markers, which causes a single “shift” of individual allelic bands, and is thus referred to as “microsatellite alteration” (Fong *et al.*, 1999). These microsatellite alteration frequencies have been reported in around 35% of SCLCs and 22% of NSCLCs (Sekido *et al.*, 1998), and have been reported to be associated with reduced survival and advanced tumor stage (Rosell *et al.*, 1997).

There are various specific molecular alterations that occur in lung cancer. For example, NSCLC demonstrate abnormalities of the neuregulin receptors ERBB2 (human epidermal growth factor receptor 2) and ERBB1 (epidermal growth factor receptor), which are a family of transmembrane receptor tyrosine kinases (Weiner *et al.*, 1990). Upon ligand binding, the ERBB receptors homodimerize or heterodimerize, thereby inducing intrinsic kinase activities which in turn initiate intracellular signal transduction cascades including the mitogen-activated protein (MAP) kinase pathway (Weiner *et al.*, 1990; Rachwal *et al.*, 1995). High levels of ERBB2 levels have been associated with the multiple drug resistance phenotype and increased metastatic potential (Yu *et al.*, 1994). The ERBB1 regulates epithelial proliferation and differentiation, and studies have shown ERBB1 to be activated in lung cancer cells

(Tateishi *et al.*, 1990; Damstrup *et al.*, 1992). Activated ERBB1 has been shown to be related to tumor stage and differentiation.

The *RAS* proto-oncogene family (*KRAS*, *HRAS*, and *NRAS*) has also been shown to be altered in lung cancer. The *RAS* proto-oncogene family encodes for plasma membrane proteins and is activated in some lung cancers by point mutations. Mutations in *RAS* expression will result in inappropriate prolonged signaling for cell division (Fong *et al.*, 1999). The most frequently activated *RAS* gene in lung cancers is *KRAS*, and this usually occurs by mutations at codon 12 and occasionally codons 13 and 61. Mutations of *KRAS* affect approximately 20-30% of lung adenocarcinomas and 15-20% of all NSCLC, but rarely SCLCs (Richardson and Johnson, 1993).

A tumor suppressor gene that has been shown to be altered in lung cancer is p53. When challenged with ultraviolet radiation and carcinogens, DNA damage occurs, p53 expression is increased and it acts as a sequence-specific transcription factor regulating downstream genes including *p21*, *MDM2*, *GADD45*, and *Bax*, thereby helping to regulate the G₁/S cell cycle transition, G₂/M DNA damage checkpoint, and apoptosis (Fong *et al.*, 1999). Therefore, a dysfunction of p53 will allow for inappropriate survival of genetically damaged cells, thus leading to accumulation of multiple mutations and the subsequent evolution of a cancer cell (Fong *et al.*, 1999). In lung cancer, p53 plays an integral role. Its chromosome 17p13 locus is frequently hemizygotously deleted, and mutational inactivation of the remaining allele occurs in 75% or more of SCLCs and about 50% of NSCLCs (Greenblatt *et al.*, 1994).

There are many other molecular alterations that occur in lung cancer. The potential of molecular epidemiology is increasingly recognized as it allows for the identification of individual genetic susceptibility factors to lung cancer as well as the identification of individuals at the highest risk for development of lung cancer (Fong *et al.*, 1999).

2.2.5 Lung Adenocarcinoma Cell Line (A549)

The A549 lung adenocarcinoma cell line was first initiated in 1972 by Giard *et al.*, and is derived from type II alveolar epithelial cells from a 58-year-old Caucasian male (Giard *et al.*, 1972). This male presented with a brief history of chest pain, blood-streaked productive cough and loss of weight. When X-rays and tomography were carried out, a mass lesion in the right lower lobe of the lung was observed. Histologic examination showed the alveoli lined with epithelial carcinoma cells in clumps and acini (Lieber *et al.*, 1976).

When examined by electron microscopy at both the early and late passage levels, A549 cells contain multilamellar cytoplasmic inclusion bodies that are characteristic of those found in type II alveolar epithelial cells of the lung (Lieber *et al.*, 1976). At the early and late passage levels, A549 cells synthesize lecithin with a high percentage of disaturated fatty acids utilizing the cytidine diphosphocholine pathway (Lieber *et al.*, 1976).

A549 cell line is maintained as a monolayer culture in culture flasks in Dulbecco's Modified Eagles medium (DMEM) with 10% heat-inactivated fetal bovine serum (FBS). The culture is incubated in 37°C with high relative humidity (95%), stable temperature (37°C) with controlled CO₂ levels (5.0%).

2.3 Apoptosis

Apoptosis plays an important role during development and in the maintenance of multicellular organisms through the removal of damaged, aged or autoimmune cells (Sorenson, 2004). Apoptosis allows for organisms to control cell number and tissue size, thus protecting itself from cells that threaten homeostasis (Hengartner, 2000).

Dysregulation of apoptosis contributes to half of all human diseases. Excessive apoptosis occurs in various neurodegenerative disorders including Alzheimer's, Parkinson's, autoimmune disorders, heart disease, as well as infectious diseases (Singh & Anand, 1994). Apoptosis dysregulation can also lead to abnormal accumulation of cells thus contributing to tumor growth. There are many ways by which cell death via apoptosis can be induced; including growth factor deprivation, cytokine interactions, cell-cell interactions, irradiation, glucocorticoids or treatment with various cytotoxic agents (Cohen *et al.*, 1992).

2.3.1 Extrinsic Pathway of Apoptosis

The extrinsic pathway, also known as the death receptor pathway, is initiated by cell surface-expressed death receptors of the tumor necrosis factor (TNF) family. Once activated, for example by Fas ligands, the receptors oligomerize and recruit intracellular adaptor proteins, the Fas-associated death domains (FADD), to form scaffolding complexes (Strasser *et al.*, 2009).

The complexes recruit members of the caspase family of cell death protease, most commonly caspase-8. Caspase-8 will in turn be cleaved leading to the formation of an active enzyme, comprising of p20 and p10 heterotetramer (Engel and Henshall, 2009). This activated initiator caspase will then cleave downstream effector caspases, such as caspase-3. Caspase-3 in turn cleaves a large number of intracellular substrates (Taylor *et al.*, 2008).

Most of the morphological changes that occur in cells undergoing apoptosis are caused by caspases (Alnemri *et al.*, 2000). As caspases bring about the most visible changes that characterize apoptotic death, caspases are thought to be the central executioners of the apoptotic pathway (Hengartner, 2000). Caspases selectively cleave a

restricted set of target proteins, usually at one or more positions in the primary sequence (Hengartner, 2000). Cleavage of specific substrates by caspase explains several of the characteristic features of apoptosis, such as the cleavage of the nuclear lamins that are required for nuclear shrinking and budding (Buendia *et al.*, 1999; Rao *et al.*, 1996). Also, cleavage of the cytoskeletal proteins such as fodrin and gelsolin cause loss of the overall cell shape. Lastly, cleavage of PAK2, a member of the p21-activated kinase family, by caspases mediates active blebbing, which is observed in apoptotic cells (Hengartner, 2000).

2.3.2 Intrinsic Pathway of Apoptosis

The intrinsic pathway, commonly known as the mitochondrial pathway, is activated in response to disturbances within the cell, which may include DNA damage, endoplasmic reticulum stress, calcium overload, and withdrawal of survival factors (Engel and Henshall, 2009). Cytochrome c will be released into the cytosol, as a result of this activation. Cytochrome c then binds to the apoptotic protease-activating factor 1 (APAF1) and pro-caspase-9, leading to the assembly of a heptamere protein ring called an apoptosome. This apoptosome catalyzes the activation of caspase-9, an initiator caspase, which in turn activates effector caspases that cleave multiple cellular proteins (Singh, 2007). The central regulators of this mitochondrial pathway are the Bcl-2 family of proteins.

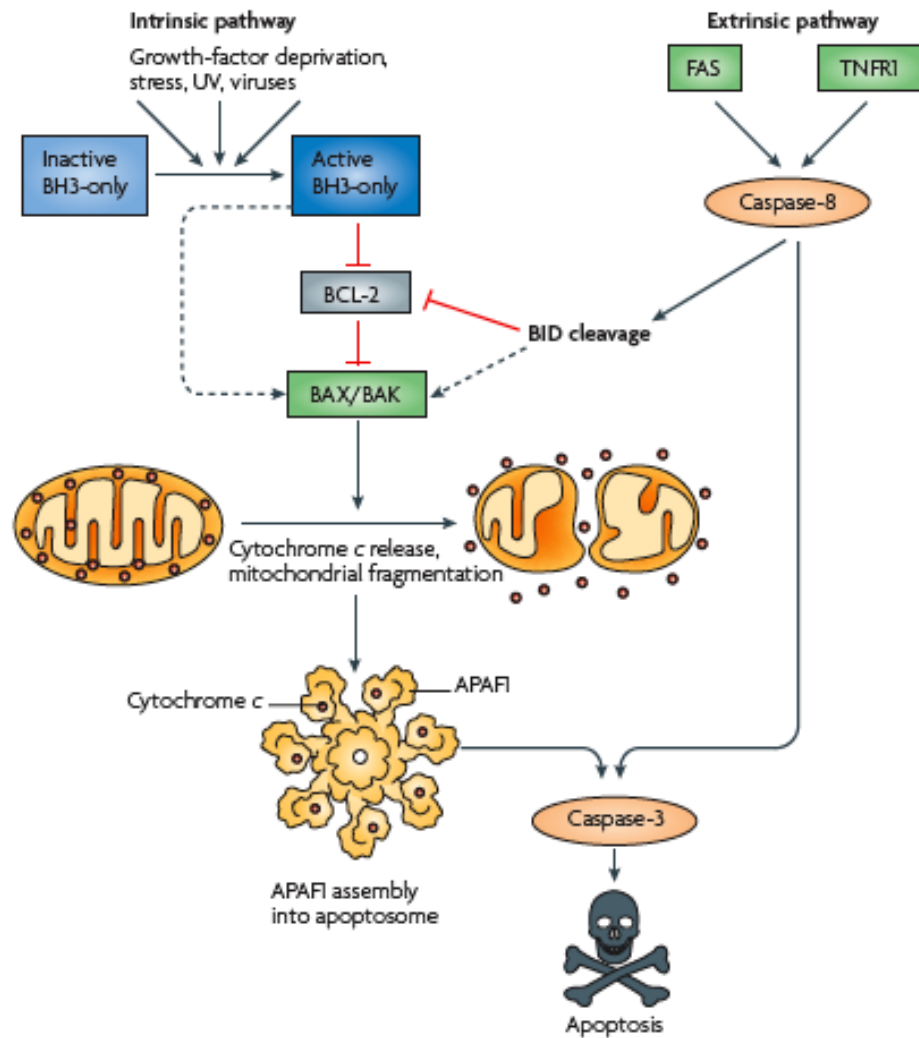


Figure 2.4: Scheme depicting intrinsic and extrinsic pathways of apoptosis. (Figure adapted from Youle and Strasser, 2008).

2.3.3 Bcl-2 Family Members

The B-cell lymphoma-2 (Bcl-2) gene was first discovered at the t(14;18) chromosome translocation breakpoint in follicular lymphomas where the transcription of the gene was excessively driven by the immunoglobulin heavy chain promoter and enhancer of chromosome 14 (Tsujimoto *et al.*, 1985; Bakshi *et al.*, 1985; Cleary *et al.*, 1986). Additionally homologs of Bcl-2 were later discovered. Members of the Bcl-2 gene family encode proteins that function to either promote or inhibit apoptosis.

The Bcl-2 protein contains four conserved domains (BH1, BH2, BH3 and BH4) that can be found in the other family members. The members can be categorized into three functional groups, as found in Table 2.1. The first group is made up of the anti-apoptotic proteins, which generally contain all four BH domains, and are responsible for protecting the cells from apoptotic stimuli (Dewson *et al.*, 2010). The second comprises of the BH3-only proteins. The sequence homology of this group with other members of the family is restricted to the BH3 domain. The BH3-only proteins are activated in response to various cellular stresses to initiate apoptosis, such as DNA damage, growth factor deprivation and endoplasmic reticulum stress. The third group also contains all four BH domains, however they are pro-apoptotic. Activation of this group of proteins is downstream to BH3-only proteins and thus they are ultimately responsible for the death of the cell (Dewson *et al.*, 2010).

The pro-apoptotic proteins Bax and Bcl-2-antagonist killer (Bak) can induce cell death via mitochondrial membrane permeabilization. The activation of Bax/Bak occurs in response to DNA damage and is facilitated by the translocation of Bax/Bak from the cytoplasm to the mitochondria. This will induce the oligomerization of Bax/Bak and the oligomer will then be inserted into the mitochondrial outer membrane for the release of cytochrome c, which then activates caspases to induce cell death (Green and Kroemer, 2004; Khosravi-Far and Esposti, 2004; Debatin, 2004).

The pro-apoptotic BH3-only proteins function by activating the multidomain proapoptotic Bax/Bak either through direct binding or by indirectly binding to the anti-apoptotic proteins (Engel and Henshall, 2009). The anti-apoptotic proteins function to sequester the activation of the pro-apoptotic proteins and thereby binding of pro-apoptotic proteins will antagonize the activity of the anti-apoptotic proteins thus favoring cell destruction (Engel and Henshall, 2009). Therefore, the concentration, or

balance of expression, of the various members of the family is largely responsible for cellular apoptotic homeostasis (Daniel and Smith, 2004).

Table 2.1: Functional categories of the Bcl-2 family of proteins

Anti-apoptotic proteins	BH-3 only proteins	Pro-apoptotic proteins
	Bid	
Bcl-2	Bim	
Bcl-xL	Puma	Bax
Mcl-1	Noxa	Bak
Bcl-w	Bad	Bok/Mtc
Bfl-1	Bmf	
Bcl-B	Hrk	
	Bik	

(Table adapted from Daniel and Smith, 2004).

2.3.4 Bcl-2 Expression in Cancer

The expression level of Bcl-2 differs for different cell types, however high levels and aberrant patterns of Bcl-2 expression have been reported in a wide variety of human cancers. The elevation of Bcl-2 protein expression contributes not only to the development of cancer but also to resistance against a wide variety of anti-cancer agents (Baffy *et al.*, 1993; Miyashita and Reed, 1993; Walton *et al.*, 1993; Kamesaki *et al.*, 1993; Fisher *et al.*, 1993; Tang *et al.*, 1994). However, studies have shown that in NSCLC the expression of Bcl-2 is either very low or even absent (Daniel and Smith, 2004). Instead, the expression of *bcl-xL*, the other major prototype of the anti-apoptotic *bcl-2* gene, is shown to be over-expressed. Over-expression of Bcl-xL protein inhibits apoptosis in NSCLC and has been coupled with poor prognosis of this disease (Soini *et al.*, 1999).

2.3.5 Bcl-xL Overexpression in Lung Cancer

Over-expression of Bcl-xL can counteract the pro-apoptotic functions of Bax and Bad. Bcl-xL can prevent the translocation of Bax from the cytosol to the mitochondria thus inhibiting apoptosis by maintaining the permeabilization status or stabilization of the outer mitochondrial membrane. Such stabilization of the membrane prevents cytochrome c release and resulting pro-caspase-9 activation (Grad *et al.*, 2000; Groeger *et al.*, 2004; Gottlieb *et al.*, 2000). Bad is a BH3-only, pro-apoptotic Bcl-2 family member, and is a cytosolic protein in healthy cells. In the cytosol, Bad is normally phosphorylated at a number of serine residues. This will allow the phosphorylated Bad to be sequestered by the cytosolic scaffold protein 14-3-3. An apoptotic signal that triggers Bad dephosphorylation will then result in the binding of the phosphorylated Bad to Bcl-xL and the inactivation of Bcl-xL's pro-survival function (Zha *et al.*, 1996). However, when Bcl-xL is present in large quantities it will have a higher affinity for Bad than 14-3-3, thus sequestering Bad to the mitochondria, leaving the excess of uncomplexed Bcl-xL to perform its pro-survival function (Cheng *et al.*, 2001; Jeong *et al.*, 2004). As research has shown that the Bcl-xL gene is an anti-apoptotic gene that is over-expressed in lung adenocarcinoma cancer, this project will concentrate upon how this gene effects the expression of microRNAs.

2.3.6 Phosphatidylinositol 3-Kinase (PI3K)/AKT Pathway

The PI3K/AKT pathway is a crucial regulator of mammalian cell survival and proliferation (Vivanco and Sawyers, 2002). P13K catalyzes the phosphorylation of inositol-containing lipids, known as phosphatidylinositols (PtdIns). Activation of PI3K leads to the generation of PtdIns(4,5)P₂ (PIP₂), which is converted to PtdIns(3,4,5)P₃

(PIP₃). The PIP₃ will then act as a ligand to recruit plekstrin homology (PH) domain containing proteins to the inner surface of the cell membrane (Vivanco and Sawyers, 2002).

One target of PIP₃ is the serine/threonine kinase Akt, the cellular homologue of the retroviral oncogene v-Akt, also known as protein kinase B (PKB) (Vivanco and Sawyers, 2002; Datta *et al.*, 1997). At the membrane, another PH-domain containing serine/threonine kinase named 3-phosphoinositide-dependent protein kinase-1 (PDK1) will phosphorylate Akt on threonine-308 (Thr-308). Phosphorylation at Thr-308 and direct binding by PIP₃ is necessary for the activation of Akt (Vivanco and Sawyers, 2002).

Akt signaling plays an important role in various processes that are critical to tumorigenesis including inhibition of apoptosis, aberrant cell proliferation, promotion of angiogenesis and tumor cell invasiveness (Testa and Bellacosa, 2001). Various studies have shown that aberrant expression of Akt plays an important role in human malignancy. Akt has been demonstrated to be amplified and overexpressed in various tumor types, including ovarian, breast, prostate, pancreatic, and human gastric cancer (Bellacosa *et al.*, 1995; Cheng *et al.*, 1998; Staal, 1987). In lung cancer Akt has been suggested to contribute to resistance to chemotherapy, radiation and tyrosine kinase inhibitors through mediation of survival signals that guard the cells from undergoing apoptosis (Brognard *et al.*, 2001; Hill and Hemmings, 2002; Janmaat *et al.*, 2003).

Akt promotes survival through various mechanisms as Akt directly phosphorylates several components of the cell-death machinery. For example, Akt can phosphorylate Bad, a pro-apoptotic member of the Bcl-2 family of proteins (Datta *et al.*, 1997). Bad promotes cell death through the formation of a non-functional heterodimer with the anti-apoptotic protein Bcl-xL. Phosphorylation of Bad by Akt would prevent interaction of Bad with Bcl-xL and promote its association with 14-3-3 proteins in the

cytosol instead. Thus Akt inhibits apoptosis by reinstating Bcl-xL's anti-apoptotic function and preventing cytochrome c release from the mitochondria (Vivanco and Sawyers, 2002; Zhou *et al.*, 2001). Similarly, Akt phosphorylates the pro-death protease, caspase-9, thus inhibiting its catalytic activity (Cardone *et al.*, 1998).

Akt is also able to influence the activity of the pro-apoptotic tumor suppressor p53 (Vivanco and Sawyers, 2002). Mdm2 is an oncoprotein that promotes cell survival and cell cycle progression through the inhibition p53. However, regulation of p53 can only occur once Mdm2 enters the nucleus. Phosphorylation by Akt on serine-166 and serine-186 is necessary for the translocation of Mdm2 from the cytoplasm into the nucleus. Once Mdm2 is in the nucleus, p53 will be targeted for degradation by the proteasome through its E3 ubiquitin ligase activity (Mayo and Donner, 2001).

Akt also has the ability to influence survival through indirect effects on nuclear factor of light polypeptide gene enhancer in B cells (NFκB). The NFκB transcription factor complex can promote cell survival in response to various apoptotic stimuli (Vivanco and Sawyers, 2002). Akt carries out its positive effect by phosphorylation and activation of the inhibitor of kappa light polypeptide gene enhancer in B cells (IκB) kinases (IKK), a kinase that directly phosphorylates the NFκB inhibitor, thus leading to its ubiquitination and degradation. Degradation of IκB will allow for the release of NFκB from the cytoplasm into the nucleus, and activation of its target genes (Vivanco and Sawyers, 2002).

Akt plays a role in proliferation through signals to the cell machinery. The cell cycle is controlled by the organized action of CDK complexes and CDK inhibitors. Cyclin D1 levels are important in the G₁/S phase transition, and its levels are regulated at the transcriptional, post-transcriptional and post-translational level by various mechanisms (Vivanco and Sawyers, 2002). Akt prevents cyclin D1 degradation through its regulation of the activity of cyclin D1 kinase glycogen synthase-kinase-3β (GSK3β).

Akt directly phosphorylates GSK3 β thus inhibiting its kinase activity, thereby leading to cyclin D1 accumulation (Diehl *et al.*, 1998).

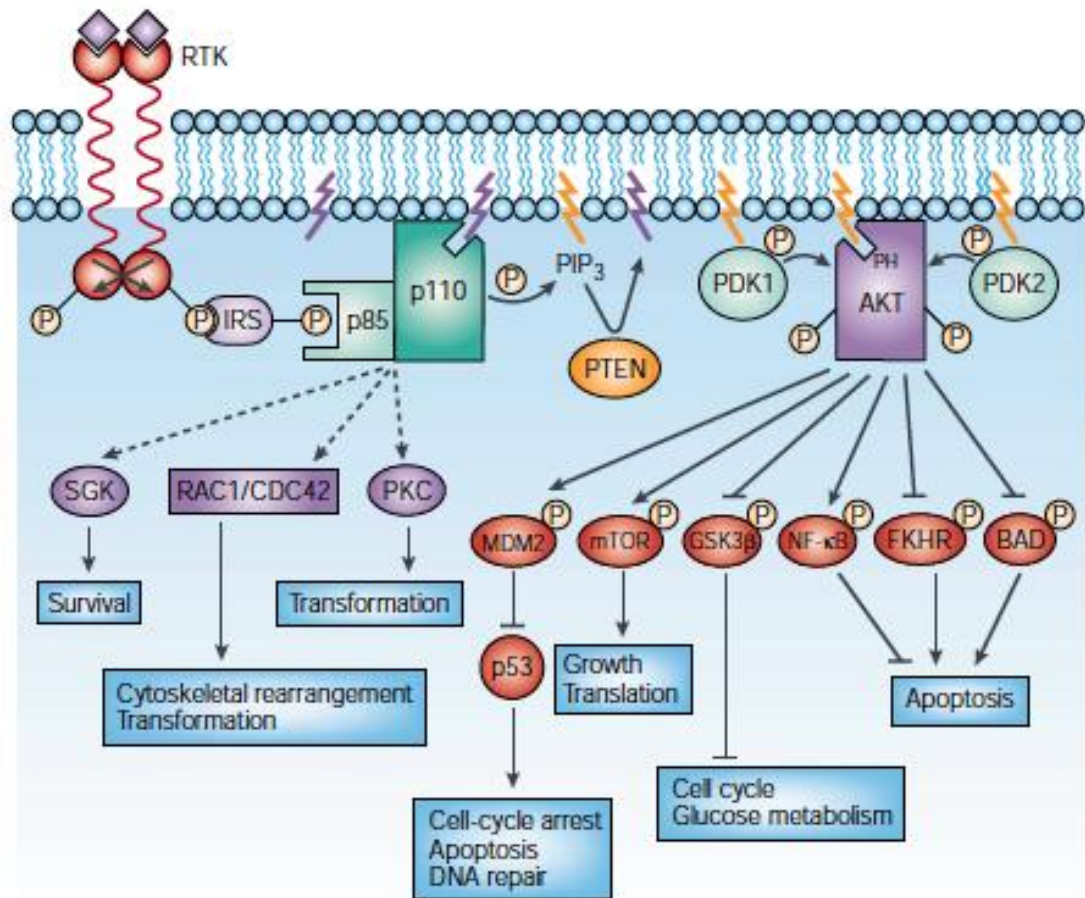


Figure 2.5: PI3K Signaling (Figure adapted from Vivanco and Sawyers, 2002).

2.3.7 Wingless-Type MMTV Integration Site Family (WNT) Pathway

The Wnt ligands are a family of secreted glycoproteins that have varying expression patterns and a variety of roles (Tennis *et al.*, 2007). These ligands play a role in the activation of signal transduction pathways and elicit changes in gene expression, cell behavior, adhesion and polarity (Mazieres *et al.*, 2005). Three pathways have been elucidated to demonstrate Wnt protein signaling. The pathway best understood, known as the canonical Wnt-catenin pathway, involves Wnt binding to two distinct families of

cell receptors: the Frizzled (Fzd) receptor family and the low density lipoprotein receptor related proteins (LRP) family (Mazieres *et al.*, 2005).

In the situation of an unstimulated canonical pathway, GSK3 β phosphorylates β -catenin in a complex that includes adenomatous polyposis coli (APC) and axin. Phosphorylation would cause β -catenin to be targeted for ubiquitin-mediated degradation, thereby decreasing levels of cytosolic β -catenin (Tennis *et al.*, 2007).

In active Wnt signaling, Wnt ligands are bound to the Fzd receptors complexed with LRP, which leads to the phosphorylation of Dishevelled (Dvl), a family of cytosolic transducer molecules (Noordermeer *et al.*, 1994). Activated Dvl inhibits the GSK3 β /APC/axin complex, which in turn prevents GSK3 β from phosphorylating β -catenin. Thus free β -catenin is stabilized and accumulates in the cytosol where it will be translocated into the cell nucleus forming an active transcription complex with T-cell factor (TCF) and lymphoid enhancer factor (LEF) (Tennis *et al.*, 2007; Mazieres *et al.*, 2005). Assembly of the transcription complex leads to target gene activation of various genes including matrix metalloproteinases (MMP2, MMP3, MMP7 and MMP9) (Tamamura *et al.*, 2005), cyclin D1 (Shtutman *et al.*, 1999; Tetsu and McCormick, 1999), Cox-2 (Longo *et al.*, 2002), c-myc (He *et al.*, 1998), c-jun, Fra-1 (Mann *et al.*, 1999), and VEGFR (Zhang *et al.*, 2001).

Studies have reported aberrant activation of the Wnt signaling pathway in various human cancers, including colorectal cancer, head and neck carcinoma, melanoma and leukemia (Mazieres *et al.*, 2005). To date, Wnt signaling has been reported to be occasionally involved in lung carcinogenesis (Sunaga *et al.*, 2001; Hommura *et al.*, 2002; Winn *et al.*, 2002). In lung cancer, the canonical Wnt signaling has been found to be excessively active. In studies of lung cancer cell lines and primary tumors, Wnt7a has been found to be frequently lost (Calvo *et al.*, 2000), while Wnt1 (He *et al.*, 2004) and Wnt2 (You *et al.*, 2004) have been reported to be overexpressed in

NSCLC cells. Cells with an overexpression of Wnt1 have been shown to be resistant to therapies that mediate apoptosis (Mazieres *et al.*, 2002). Furthermore, expression of Dvl has also been shown to be overexpressed in NSCLC tumors and cell lines, and is involved in lung carcinogenesis (Kazutsugu *et al.*, 2003).

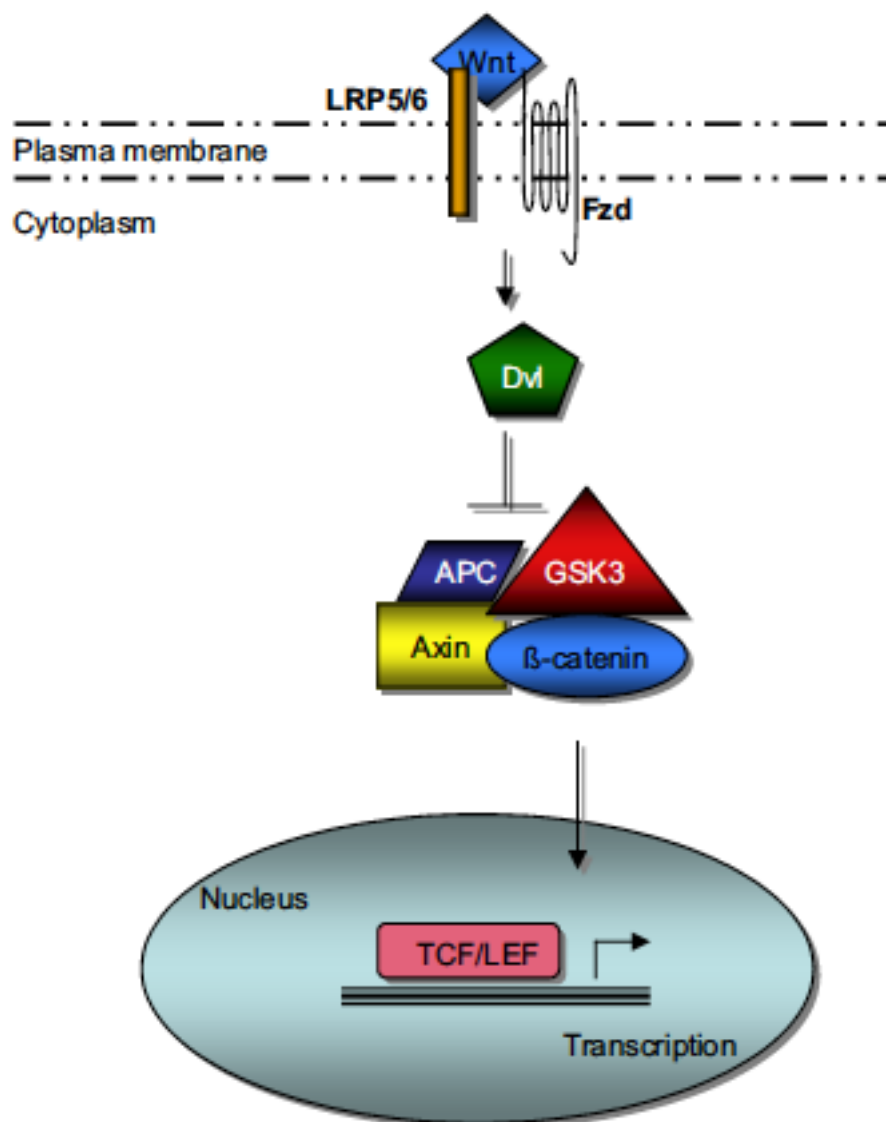


Figure 2.6: Canonical Wnt/β-catenin signaling pathway (Figure adapted from Tennis *et al.*, 2007).

2.3.8 Transforming Growth Factor (TGF- β) Signaling Pathway

TGF- β is part of a superfamily, which comprise of a large number of structurally related polypeptides, including TGF- β 2, TGF- β 3, Activins, Nodals and bone morphogenetic (BMP) proteins (Massagué, 1998). They are produced by a variety of cell types, and are capable of regulating numerous cellular processes including cell proliferation, lineage determination, differentiation, motility, adhesion and death (Massagué, 1998). The TGF- β family members are multifunctional, and their effects depend upon the responsiveness of the target cell (Massagué and Wotton, 2000).

TGF- β signaling is initiated when two different serine/threonine kinase transmembrane proteins, known as receptor I and II, are brought together by the TGF- β ligand (Massagué, 1998). The TGF- β ligand is a receptor assembly factor which complexes with receptor I, thus phosphorylating the guanine specificity (GS) region, resulting in the activation of receptor I. TGF- β receptor I is then recruited to the heteromeric complex of TGF- β receptor II (Massagué, 1998).

The TGF- β receptor I will phosphorylate the receptor activated Smads (R-Smads), which are comprised of Smad2 and 3 (Massagué and Wotton, 2000). Phosphorylation by the TGF- β receptor, initiates R-Smad activation and accumulation in the nucleus. Prior to translocation into the nucleus, the activated Smad2 and 3, binds with the common-mediated Smad (Co-Smad), Smad4 (Massagué and Wotton, 2000). The R-Smad and Co-Smad complex now move into the nucleus, and both participates in DNA binding and recruitment of transcriptional co-factors (Massagué and Wotton, 2000; Massagué, 1998) (Refer to Figure 2.7).

TGF- β negatively regulates cell proliferation through the induction of G₁ arrest, promotion of termination differentiation, or activation of cell death mechanisms (Alexandrow and Moses, 1995). For example p15 and p21, which are cyclin-dependent kinase inhibitors, are rapidly induced in response to TGF- β , which in turn mediates cell cycle arrest (Hannon and Beach, 1994). Also, inhibition of gene transcription can occur through the downregulation of c-myc and the Cdk-activating phosphatase cdc25A, thus resulting in antiproliferative effects (Iavarone and Massagué, 1997).

Studies have shown that alterations in TGF- β signaling have been associated with a variety of human diseases, including cancer (Jeon and Jen, 2010; Massagué and Wotton, 2000). It has been shown that the ligand along with downstream elements, including the receptors as well as the Smad proteins, are essential in suppressing primary tumorigenesis in many tissue types (Markowitz and Roberts, 1996).

Lung cancer has been shown to often overexpress TGF- β (Roberts and Wakefield, 2003). While most lung cancer cells secrete TGF- β , the malignant transformation that occurs in lung cancer leads to a loss of the tumor suppressor effects of TGF- β . The loss of this TGF- β response will in turn result in a loss of the inhibitory effects on proliferation, which has been associated with tumor development and progression in several cancers (Yanagisawa *et al.*, 1998; Kim *et al.*, 2000).

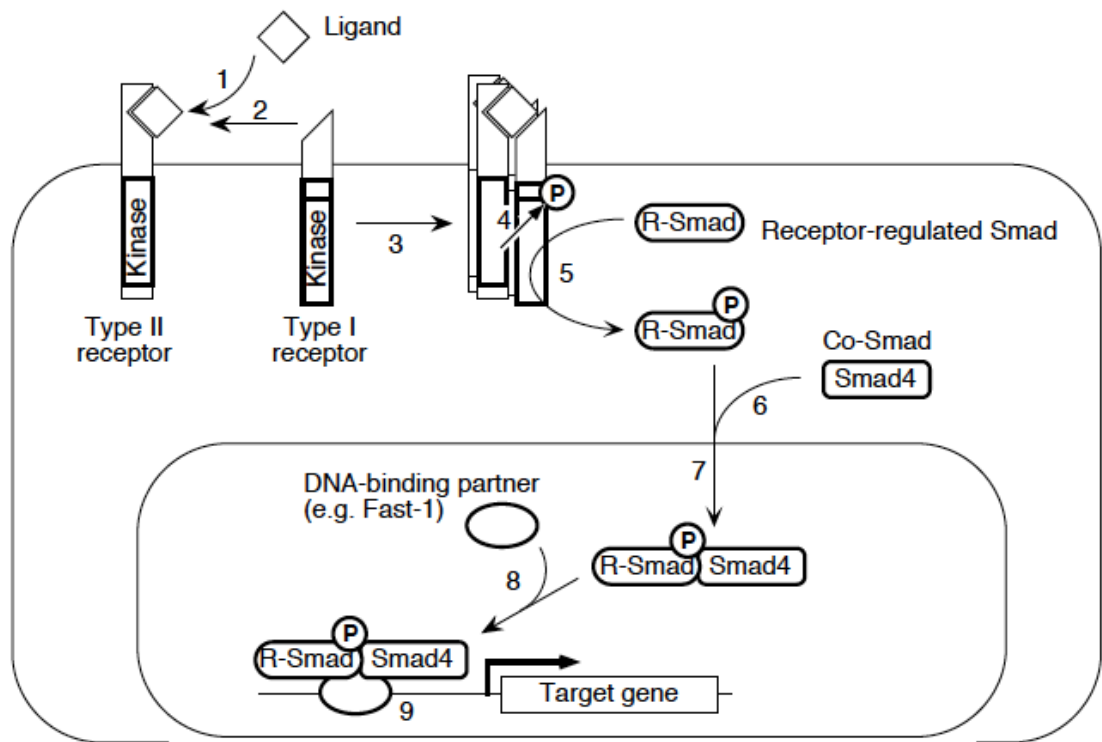


Figure 2.7: TGF- β Signaling pathway. (Figure adapted from Massague, 1998.)

2.3.9 Mitogen-Activated Protein Kinase (MAPK) Signaling Pathway

The mitogen-activated protein kinase (MAPK) cascades are intracellular signal transduction pathways that are triggered by various extracellular and intracellular stimuli, which include peptide growth factors, cytokines, hormones and diverse cellular stresses such as oxidative stress and endoplasmic reticulum stress (Kim and Choi, 2010). There are three well described pathways: the extracellular signal-regulated kinases 1 and 2 (ERK1/2), c-Jun N-terminal kinases/ stress-activated protein kinases (JNK/SAPK) and the p38 pathway (Raman *et al*, 2007). Each cascade is composed of three core components: a MAPK kinase kinase (MAP3K), a MAPK kinase (MAP2K), and a MAPK. Additional upstream MAP4K and downstream MAPKAPK components also exist (Plotnikov *et al.*, 2011). Within the cascade, one or more kinase component will phosphorylate and activate components in the next tier, eventually leading to the phosphorylation of the target regulatory molecules by the MAPK, thus initiating various

cellular processes (Raman *et al.*, 2007). The MAPK pathway regulates numerous essential cellular activities including growth, proliferation, differentiation, motility, stress response, survival and apoptosis (Lewis *et al.*, 1998). Aberrant MAPK signaling have been associated with the development of several human diseases including Alzheimer's disease (Wang and Liu, 2008; Perez *et al.*, 2008), Parkinson's disease (Levy *et al.*, 2009), amyotrophic lateral sclerosis (Bendotti, 2005), and many types of cancer (Dhillon, 2007; Boutros *et al.*, 2008; Schubbert *et al.*, 2007).

2.3.9.1 ERK 1/2 Cascade

The ERK cascade is the best characterized MAPK pathway, and it is composed of two genes, the ERK1 (p44) and ERK2 (p42), which are 83% identical (Chen *et al.*, 2001) and are likely functionally redundant although they may have different substrate specificities (Greenberg *et al.*, 2002). The signaling via the ERK cascade is initially activated by mitogenic stimuli such as peptide growth factors EGF or PDGF. The binding of the growth factors to its cell surface receptor tyrosine kinase, will lead to dimerization and autophosphorylation of the receptor (Mercer and D'Armiento, 2006). Phosphorylation of the intracellular domain of the receptor will activate guanine nucleotide exchange factors (GEFs) such as Son of Sevenless (Sos), which will facilitate the activation of GTPase Ras (Plotnikov, 2011). Ras-GTP will activate the MAP3K tier of the cascade, the Raf isoforms (A-Raf, B-Raf or Raf-1), leading to Raf-mediated phosphorylation of the dual-specificity MAP kinase kinase-1 and -2 (MEKs), MEK1/2 (Mercer and D'Armiento, 2006; Malumbres and Barbacid, 2003). MEK1/2 will in turn phosphorylate ERK1/2, thus transmitting ERK1/2 through the nuclear membrane pore allowing for the phosphorylation and activation of various transcription factors including TCF-member ELK-1 (Gille *et al.*, 1992), c-Fos (Murphy *et al.*, 1992),

p53 (Milne *et al.*, 1994), Ets1/2 (Yang *et al.*, 1996) and c-Jun (Morton *et al.*, 2003), all of which are important for the initiation and regulation of cell proliferation and oncogenic transformation (Shaul and Seger, 2007). Various studies have been conducted to analyze the ERK pathway and its role in tumorigenesis. Correlation between incidence of cancer and increased Ras activation, ERK1/2 activity, or binding of DNA by ERK1/2 transcription factor targets (Mercer and D'Armiento, 2006), have been made *in vitro* (Vincent *et al.*, 2004), animal (Sebolt-Leopold, 1999) and human (Han *et al.*, 2005) studies.

2.3.9.2 JNK/SAPK Cascade

The JNK-family of kinases was initially identified as protein kinases involved in the activation of the transcription factor c-Jun, in response to UV irradiation (Hibi *et al.*, 1993). They were also found to be mediators of intra- or extra-cellular stresses, thus giving them their other name, stress-activated protein kinase (SAPKs) cascade (Davis, 1994). Initial studies show that JNK can be activated by various stimuli including growth factors (Hibi *et al.*, 1993), cytokines (Westwick *et al.*, 1994), and stress factors (Cano *et al.*, 1994). Later studies indicated that inflammatory cytokines and many different cytotoxic as well as genotoxic reagents stimulate JNK, leading to the discovery of the critical role JNKs played in mediating apoptotic signaling (Sluss *et al.*, 1994; Cano and Mahadevan, 1995; Dai *et al.*, 1995).

Activated stress, or other, stimuli transmits their signal to small GTPases such as CDC42 and Rac1, which in turn activates the MAP3K level kinases either directly or through the MAP4Ks (Plotnikov *et al.*, 2011). The MAP3Ks can also, alternatively, be activated by interaction with adaptor proteins such as TRAF (Bradley and Pober, 2001). The MAP3Ks include members of the MEKK group (MEKK1-4), apoptosis signal-

regulating kinase group (ASK1 and ASK2), mixed lineage kinase (MLK1, MLK2, MLK3, DLK, and LZK), and transforming growth factor-beta activated kinase 1 (TAK1) (Davis, 2000). The kinases at the MAP3K tier will then transmit the signals further by phosphorylating the kinases of the MAPKK level, MEK4 (MKK4) and MEK7 (MKK7), which in turn activate the three components at the MAPK level (JNK1-3) (Davis, 2000).

Activated JNKs phosphorylate a large number of substrates, including transcription factors c-Jun, c-Myc ATF2, ATF3, p53, Elk-1 and nuclear factor of activated T cells (NFAT) (Raman *et al*, 2007; Johnson and Nakamura, 2007). These phosphorylated targets would further regulate the transcription of many genes, thus mediating cellular processes such as apoptosis (Dhanasekaran and Reddy, 2008), immunological effects (Rincon Davis, 2009), neuronal activity (Haeusgen *et al.*, 2009), insulin signaling (Haeusgen *et al.*, 2009) and more. For example, JNKs can activate apoptotic signaling through the up-regulation of pro-apoptotic genes, via activation of c-Jun. The phosphorylation of c-Jun will lead to the formation of AP-1, which is involved in the transcription of a wide range of proteins, including known pro-apoptotic proteins (Dhanasekaran and Reddy, 2008). The JNK-AP-1 pathway has been shown to be involved in the increased expression of pro-apoptotic genes such as TNF-alpha, Fas-L and BAK (Fan and Chambers, 2001).

2.3.9.3 p38 Cascade

The p38 cascade is also an SAPK pathway and shares many components with the other SAPK pathway, the JNK cascade (Kyriakis and Avruch, 2001). This cascade is primarily induced by stress related stimuli, however it can also be activated by various growth factors including insulin-like growth factor (IGF) (Cheng and Feldman, 1998), vascular endothelial growth factor (VEGF) (Rousseau *et al.*, 1997) and platelet-derived growth factor (PDGF) (Pyne and Pyne, 1997) and many more. Upon activation of the receptors by the stimuli, the signals will be transmitted via adaptor proteins, small GTPases, MAP4Ks and MAP3K, similar to those functioning in the JNK cascade (Plotnikov *et al.*, 2011). The MAP3K will in turn phosphorylate and activate the MAPKK components, which include the MKK3 and MKK6 (Whitmarsh and Davis, 2007). Activation of MKK3 and MKK6 would lead to signal transmission to the four isoforms at MAPK tier of the cascade, p38 α - δ (Plotnikov *et al.*, 2011). The p38s can additionally be mediated by autophosphorylation in a MAPKK-independent manner. This autophosphorylation is induced by stimulated interaction with adaptor proteins Tab1 (Ge *et al.*, 2002), or by interaction with lipidic phosphatidyl inositol analogues (Gills *et al.*, 2007). The signals are then finally transmitted, via p38s, or MAPKAPKs to target molecules, such as ATF-2, c-Fos, c-Myc, c-Jun, p53, and Elk-1, which are responsible for various processes that are stimulated and regulated by the cascade (Plotnikov *et al.*, 2011).

Studies have shown that the p38s play a central role in the regulation of immunological effects (Huang *et al.*, 2009), apoptosis (Sohn *et al.*, 2007), cell cycle checkpoint and even survival (Thornton and Rincon, 2009). Therefore a dysregulation of the cascade may have pathological manifestations (Plotnikov *et al.*, 2011). p38 has been shown to act as a tumor suppressor via the downregulation of Ras-dependent and

independent transformation, invasion and also by inducing apoptosis (Plotnikov *et al.*, 2011).

2.4 MicroRNA (miRNA)

In 1993, microRNAs (miRNAs) were first discovered in the worm *Caenorhabditis elegans* (*C. elegans*) by Ambros and colleagues. By identifying the *C. elegans* mutants that were disturbed in developmental timing, they discovered that a 22-nucleotide transcript of *lin-4* regulated developmental timing by acting as a negative regulator of the protein coding gene *lin-14* (Lee *et al.*, 1993; Wightman *et al.*, 1993). *Lin-4* showed a partial sequence complementarity to a sequence repeat in the 3'UTR of *lin-14*, which lead the authors to hypothesize that *lin-4* functions by interacting with these 3'UTR elements, thus inhibiting the translation of *lin-14*. Originally miRNAs were considered to be unique to nematodes, until it was found that the sequence and temporal expression pattern of another miRNA involved in developmental timing in *C. elegans*, *let-7*, was phylogenetically conserved in a wide variety of animals including humans (Pasquinelli *et al.*, 2000). This observation lead to the construction and characterization of several large-scale cDNA libraries enriched for small miRNAs, in turn leading to the identification of many additional miRNAs from plants, *C. elegans*, *Drosophila* and mammals (Lagos-Quintana *et al.*, 2001; Lagos-Quintana *et al.*, 2003).

MiRNAs are defined as small non-coding RNA of about 19-23 nucleotides long that regulates gene expression post-transcriptionally, by either inhibiting mRNA translation or by inducing mRNA degradation. MiRNAs play a role in a wide range of biological processes including cell proliferation, differentiation, apoptosis, developmental timing, fat metabolism, insulin secretion, stem cell maintenance, neuronal patterning, and hematopoietic differentiation (Ruan *et al.*, 2009; Weimer, 2007). MiRNAs are an integral part of the regulatory networks in cells, therefore a disturbed miRNA function or altered miRNA expression may disorganize cellular processes and eventually cause or contribute to disease (Weimer, 2007).

2.4.1 MiRNA Biogenesis

MiRNA genes can be found distributed across the genome as either single genes or as gene clusters. Gene clusters give rise to large polycistronic transcripts, from which the individual miRNAs are processed. Some miRNAs can be found in intergenic regions, but at least 50% are found in defined transcription units (in introns and exons) of both protein coding and non-coding transcripts and are therefore co-transcribed with the gene in which they reside (Kim and Nam, 2006; Rodriguez *et al.*, 2004; Weber, 2005).

MiRNAs are initially transcribed by RNA polymerase II, forming long primary miRNA (pri-miRNA), which contains a 5'CAP structure and are polyadenylated at their 3'end. These pri-miRNA can be up to several kilobases in length and contains one or more stem-loop or hairpin structures of about 70 nucleotides. These hairpin structures are recognized and cleaved in the nucleus by the 650 kDa microprocessor complex which consists of a dsRNA specific RNase III endonuclease Drosha and the dsRNA binding proteins, the Di-George syndrome critical region gene 8 (DGCR8) (Han *et al.*,

2004). The resulting precursor miRNA (pre-miRNA) which is a 60-100 nucleotide RNA hairpin intermediate with a two nucleotide 3' overhang, is then transported to the cytoplasm by the nuclear export factor Exportin-5 and its co-factor Ran-GTP. In the cytoplasm, the pre-miRNA is further cleaved by a second RNase endonuclease Dicer with its dsRNA binding partner, the immunodeficiency virus (HIV) transactivating response DNA binding protein (TRBP), resulting in a mature product of 19-24 imperfect nucleotide duplex (Lund *et al.*, 2004; Yi *et al.*, 2003).

The TRBP will then recruit the human agronaute protein hAgo2 to the Dicer complex, thus forming a minimal RNA-induced silencing complex (RISC). The core components of the RISC are members of the agronaute family of proteins, which contain the conserved RNA-binding domains: the PAZ domain, which binds to the single stranded 3' end of the miRNA, and the PIWI domain, which interacts with the 5' end of the miRNA guide strand (Filipowicz, 2005; Sontheimer, 2005).

The strand of the duplex, which has the weakest base-pairing at its 5' terminus, is selected as the guide strand. This guide strand will direct the RISC to the 3'UTR of the target mRNA on the basis of sequence complementarity between the guide miRNA and target mRNA (Matranga *et al.*, 2005; Rand *et al.*, 2005). The passenger strand will later be removed.

The mature miRNA can regulate their targets by direct cleavage of mRNA or by inhibition of protein synthesis, according to the degree of complementarities with their target 3'UTR. Target mRNA cleavage can only take place if the miRNA has a near perfect complementarity to its target sequence. Imperfect base-pairing cannot bring about mRNA cleavage but instead induces transcriptional silencing (Bartel, 2004).

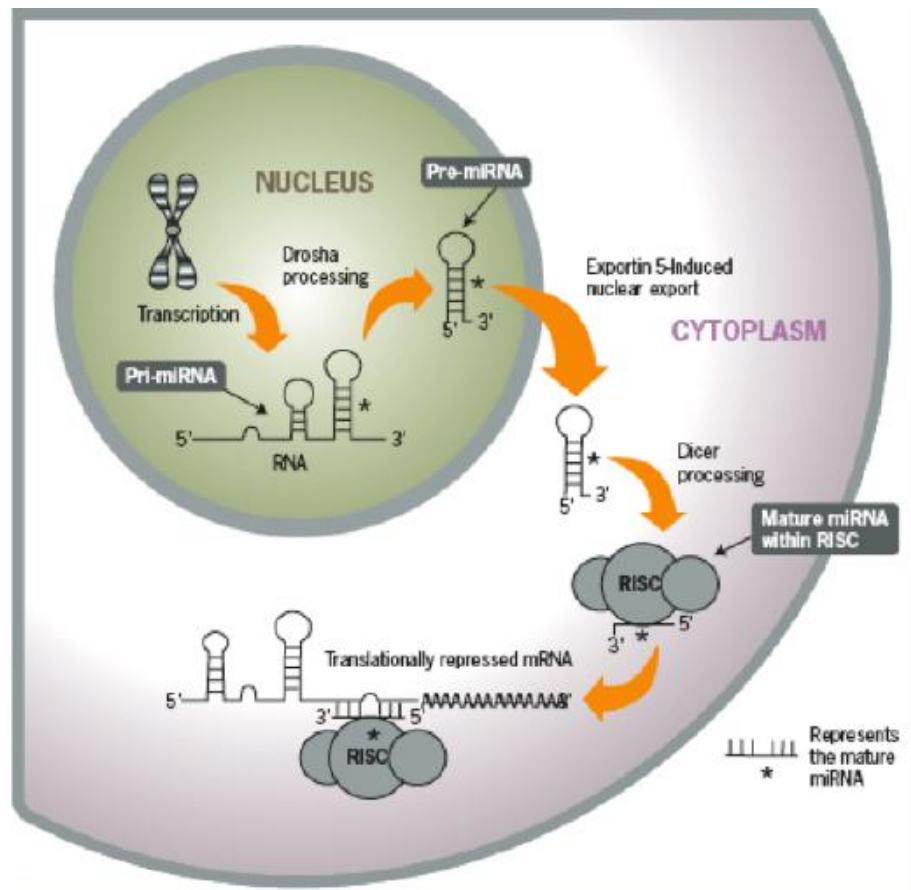


Figure 2.8: The current model for the biogenesis and post-transcriptional suppression of microRNAs (Figure adapted from Applied Biosystems, 2009).

2.4.2 MiRNA and Cancer

As mentioned previously, miRNAs play a key role in an assortment of biological processes including development, cell proliferation, differentiation and apoptosis. Therefore, an altered miRNA expression is likely to contribute to human disease including cancer. When human miRNAs were first discovered it was noticed that many miRNA genes reside in genomic regions that are involved in cancers, including minimal regions of loss of heterozygosity (LOH), minimal regions of amplification (minimal amplicons), or breakpoint cluster regions (Calin *et al.*, 2004). Overexpressed oncogenic miRNAs are located in amplified regions and the down-regulated suppressor miRNAs in deleted regions in cancer (Calin *et al.*, 2004).

The proof that chromosomal rearrangements are fundamental to the inducement of cancer, was an early report of a masked t(8;17) translocation that resulted in an aggressive B-cell leukemia by overexpressing *c-myc* oncogene by an unknown mechanism at the moment of identification (Calin *et al.*, 2004). Later it was discovered that *miR-143* was located at chromosome 17 breakpoint, and that the *c-myc* was rearranged under the control of the promoter of *miR-143* with consequent overexpression (Calin *et al.*, 2004).

Compared to normal tissues, malignant tumors and tumor cell lines have been found to have widespread deregulated miRNA expression (Sassen *et al.*, 2008). A global decrease in miRNA levels has been observed in human cancers, demonstrating that small RNAs may have an intrinsic function in tumor suppression (Sassen *et al.*, 2008). Lu and colleagues were the first to show that the expression levels of many miRNAs were significantly reduced in cancers compared to the corresponding normal tissues. The authors hypothesized that miRNAs can function to drive terminal differentiation and prevent cell division (Lu *et al.*, 2005). Cancer specific fingerprints have since been identified in various cancers including B-cell chronic lymphocytic leukemia (B-CLL), breast carcinoma, primary glioblastoma, hepatocellular carcinoma, papillary thyroid carcinoma, lung cancer, gastric carcinoma, colon carcinoma and endocrine pancreatic tumors (Calin *et al.*, 2004).

2.4.3 MiRNA As Oncogenes and Tumor Suppressors

MiRNAs can be either up-regulated or down-regulated in various human cancers. MiRNAs whose expressions are increased in tumors are considered as oncogenes (Zhang *et al.*, 2007). These oncogenic miRNAs, called oncomirs, promote the development of tumors by negatively inhibiting tumor suppressor genes and/or genes that control cell differentiation or apoptosis (Zhang *et al.*, 2007). MiRNAs overexpressed in human cancers may result from amplification, deregulation of a transcription factor or demethylation of CpG islands in the promoter regions of the gene (Croce, 2008).

An example of an oncomir is the *miR-17-92* cluster, which is a miRNA polycistron located at chromosome 13q31, a genomic locus that is amplified in lung cancer and other kinds of lymphomas including diffuse large B-cell lymphoma (Hayashita *et al.*, 2005; He *et al.*, 2005). In comparison to normal tissue the expression of *miR-17-92* is significantly increased in several cancer types. The *miR-17-92* cluster appears to enhance lung cancer cell growth (Hayashita *et al.*, 2005).

MiRNAs that are down-regulated are considered tumor suppressor genes. Tumor suppressor miRNAs usually prevent tumor development by negatively regulating oncogenes and/or genes that control cell differentiation or apoptosis (Zhang *et al.*, 2007). MiRNAs that act as tumor suppressors can be down-regulated as a result of deletions, epigenetic silencing, or loss of the expression of transcription factors (Ruan *et al.*, 2009).

Let-7 is an example of a tumor suppressor miRNA. Inappropriate expression of *let-7* results in oncogenic loss of differentiation. In *let-7* mutants, stem cells are unable to exit the cell cycle and terminally differentiate at the correct time, which is a hallmark of cancer (Reinhart *et al.*, 2000). *Let-7* is located at a chromosome region that is usually deleted in human cancer. *Let-7* is found to be poorly expressed in lung cancers, and the

reduced *let-7* expression has been shown to be significantly associated with shortened post-operative survival (Takamizawa *et al.*, 2004).

2.5 MiRNA and Apoptosis

In contrast to normal cells, cancer cells have the ability to disrupt the balance between pro- and anti-apoptotic factors to promote cell survival under the conditions of environmental stress. In terms of molecular events occurring in tumors, apoptosis is an important hallmark of tumor progression. MiRNAs are critical apoptosis regulator in tumorigenesis, and cancer cells are able to manipulate miRNAs to regulate cell survival in oncogenesis.

2.5.1 Pro-Apoptotic miRNAs

MiRNAs can participate in tumorigenesis by directly targeting anti-apoptotic genes.

miR-15 & miR-16: miR-15 and miR-16 are two examples of pro-apoptotic miRNAs, and they function by targeting and inhibiting the pro-survival molecule Bcl-2 to disrupt tumor development by promoting apoptosis through the mitochondrial pathway (Calin *et al.*, 2002). Deletions and translocations involving *miR-15a* and *miR-16-1* are located in a cluster at 13q14.3, and their downregulation can be found in B-cell CLL patients. Bcl2 overexpression by downregulation of *miR-15a* and *miR-16-1* seems to be the main regulatory mechanism involved in the pathogenesis of the major fraction of human B cell CLL (Cimmino *et al.*, 2005). Downregulation of miR-15a and miR-16-1 have also been reported in cases of diffuse large BCLs. Therefore it can be assumed that the

significance of this mechanism may be extended to other human malignancies.

miR-29: *miR-29* regulates myeloid cell leukemia-1 (Mcl-1) protein expression and induces apoptosis. Mcl-1 is an important multidomain anti-apoptotic protein of the Bcl-2 family, which contains the Bcl-2-homology domains BH1-3, and heterodimerizes with other Bcl-2 family members (Mott *et al.*, 2007). When *miR-29b* expression is increased, the cellular protein levels of Mcl-1 can be reduced, which in turn leads to an increase of BH3-only domain proteins Bim and Puma and sensitizes the cancer cells to tumor necrosis-factor-related apoptosis inducing ligand (TRAIL) cytotoxicity. This will activate the Bak/Bax dependent apoptotic cascade and death ligand-induced apoptosis (Mott *et al.*, 2007; Han *et al.*, 2006).

miR-34 family members: *miR-34a*, *miR-34b*, and *miR-34c*, members of the miR-34 family, are down-regulated in various human cancers. The expression of *miR-34* is associated with the expression of p53 and is strongly induced by genotoxic and oncogenic stress in a p53-dependent manner (He *et al.*, 2007). When *miR-34* expression is reduced, p53-mediated cell death is weakened, whereas an overexpressed expression of *miR-34* leads to apoptosis or cellular senescence through the direct repression of several target genes, such as Bcl-2, Cdk4 and hepatocyte growth factor receptor (Met), which promotes cell cycle arrest, apoptosis and senescence (He *et al.*, 2007).

2.5.2 Anti-apoptotic miRNAs

miR-133 and miR-24a: During initiation of the intrinsic pathway of apoptosis, cytochrome c is released from the mitochondrial intermembrane space after BAX and/or BAK oligomerisation forms a caspase-9 activating complex of apoptosome with APAF1 and pro-caspase 9. miR-133 and miR-24a have been shown to inhibit the expression of Caspase-9, thus leading to a block of the intrinsic pathway of apoptosis. MiR-133 acts as a regulator of survival in cardiac cells by repressing Caspase-9 expression at both the protein and mRNA levels (Xu *et al.*, 2007). miR-24 is capable of repressing apoptosis by directly inhibiting Caspase-9, and prevents apoptosis of the retina during eye morphogenesis of *Xenopus*, thus playing a pivotal role in controlling the eye size (Walker and Harland, 2009).

miR let-7a: miR let-7 inhibits the executioner caspase-3, thus antagonizing drug-induced apoptosis. Let-7 has been shown to play a role in modifying the sensitivity of cells to therapeutic drugs including duxorubicin, paclitaxel and interferon-gamma (Tsang and Kwok, 2008). A dysregulated expression of let-7 decreases the extent of drug induced apoptosis as well as apoptotic cell population.

miR-17-92 cluster: The miR-17-92 cluster has been reported to negatively regulate the expression of E2F1 and shift the E2F transcriptional balance away from the pro-apoptotic E2F1 and toward the proliferative E2F3 transcriptional network (Woods *et al.*, 2007). The miR-17-92 cluster is amplified in B cell lymphomas and shows an altered expression in many tumor types. This cluster is also capable of inhibiting apoptosis by negatively regulating the tumor suppressor PTEN and the pro-apoptotic protein Bim. Downregulation of Bim by the miR-17-92 cluster may contribute to this miRNAs

ability to increase the severity of disease progression (Xiao *et al.*, 2008).

miR-21: mir-21 expression is up regulated in human breast, colon, lung, pancreas, prostate and stomach cancers (Volinia *et al.*, 2006). Direct targets of miR-21 include PTEN, tropomyosin 1, and programmed cell death 4 (PDCD4). Up-regulation of miR-21 will reduce cell death and promotes angiogenesis and invasion of hepatocellular carcinoma (Loffler *et al.*, 2007). Overexpression of miR-21 provides a significant survival advantage to cancer cells.

2.6 MiRNA in Cancer Diagnosis and Treatment

2.6.1 MiRNA Signatures in Cancer Diagnosis

Through the use of transcriptional profiling, it has been found that the expression of miRNAs is highly standardized in specific tissues. Therefore, it has been suggested that these miRNA signatures can be used for the detection and classification of various cancers as well as to predict the severity of disease (Garzon *et al.*, 2010). These include chronic lymphocytic leukemia, chronic myelogenous leukemia, and prostate, testicular, lung, breast, ovarian, pancreatic, and gastric cancer (Tricoli and Jacobson, 2007). For example, in a study conducted by Yanaihara and colleagues, in 2006, it was found that the genome-wide expression profiling of miRNAs was significantly different among primary lung cancers and the corresponding non-cancerous lung tissues. The correlation between miRNA expression profiles and lung adenocarcinoma patient survival were also investigated and it was found that lung adenocarcinoma patients with either high hsa-mir-155 or reduced hsa-let-7a expression had a poorer survival than patients with low hsa-mir-155 or high hsa-let-7a-2 expression,

respectively (Yanaihara *et al.*, 2006). Furthermore, studies have shown that the miRNA signatures characterize the developmental origins of tumors more effectively than mRNA signatures, thus providing a more useful tool for diagnosis and prognosis of human cancer (Tricoli and Jacobson, 2007).

2.6.2 MiRNA as a Target For Cancer Treatment

Experimental studies have shown that targeting miRNA expression can modify cancer phenotypes, thus miRNAs have become targets of novel anticancer gene therapy. Targeting of miRNA is based on either selective inhibition of miRNA expression or binding or selective overexpression (Nana-Sinkan and Croce, 2011). Using miRNAs as therapeutic agents have become very appealing due to their ability to target multiple genes, thus making them extremely efficient in regulating distinct biological cell processes that are involved in normal and malignant cell homeostasis (Garzon *et al.*, 2010).

There are a number of different strategies for miRNA targeting. Direct strategies involve the use of oligonucleotides or virus-based constructs to either block the expression of an oncogenic miRNA or to substitute for the loss of expression of tumor suppressor miRNA (Garzon *et al.*, 2010). Some examples of direct strategies include anti-miRNA oligonucleotide (AMOs), antagomirs, miRNA sponges (Nana-Sinkan and Croce, 2011) and miR-masking antisense oligonucleotide technology (miR-mask) (Garzon *et al.*, 2010). AMOs are single-stranded molecules that form direct complementarity and thus inhibiting specific miRNA. Antagomirs are also single stranded molecules that form direct complementarity, thus inhibiting specific miRNAs. However they have been modified with a cholesterol conjugated 2'-O-methyl in order to maintain stability, thus minimizing degradation (Nana-Sinkan and Croce, 2011).

MiRNA sponges function by using multiple complementary 3'UTR mRNA sites for a specific miRNA. These sponges will competitively bind to miRNA, thus interfering with normal targeting of miRNA. The advantage of using miRNA sponges include its ability to target and inhibit a whole family of miRNAs as opposed to single miRNA targeting that occurs with antisense oligonucleotides (Nana-Sinkin and Croce, 2011). MiRNA-mask consist of single-stranded 2'-O-methyl-modified antisense oligonucleotides that are fully complementary to the predicted miRNA binding sites in the 3'UTR of the target mRNA. This will allow the miR-mask to cover up the miRNA-binding site, thus blocking the oncogenic miRNA deleterious functions at the target level, and activating the translation of target mRNA (Garzon *et al.*, 2010).

In a study conducted by Tuschl and colleagues, targeting of miR-122 in the mouse liver using an anti-miR-122 antagomir resulted in the complete degradation of miR-122 in a dose-dependent manner. These antagomirs were highly specific and long lasting, with little or no short-term toxicity (Tricoli and Jacobson, 2007). In another study, conducted by Blenkiron and Miska, the oncogenic miR-17-92 cluster was also successfully down-regulated, through the use of 2'-O-methyl oligoribonucleotides (2'-O-Me-RNA) antagomir in mouse tissues following intravenous injection *in vivo* (Blenkiron and Miska, 2007). These studies suggested that targeting of specific miRNAs for the purpose of attaining a therapeutic advantage might be possible through the use of antagomirs (Tricoli and Jacobson, 2007).

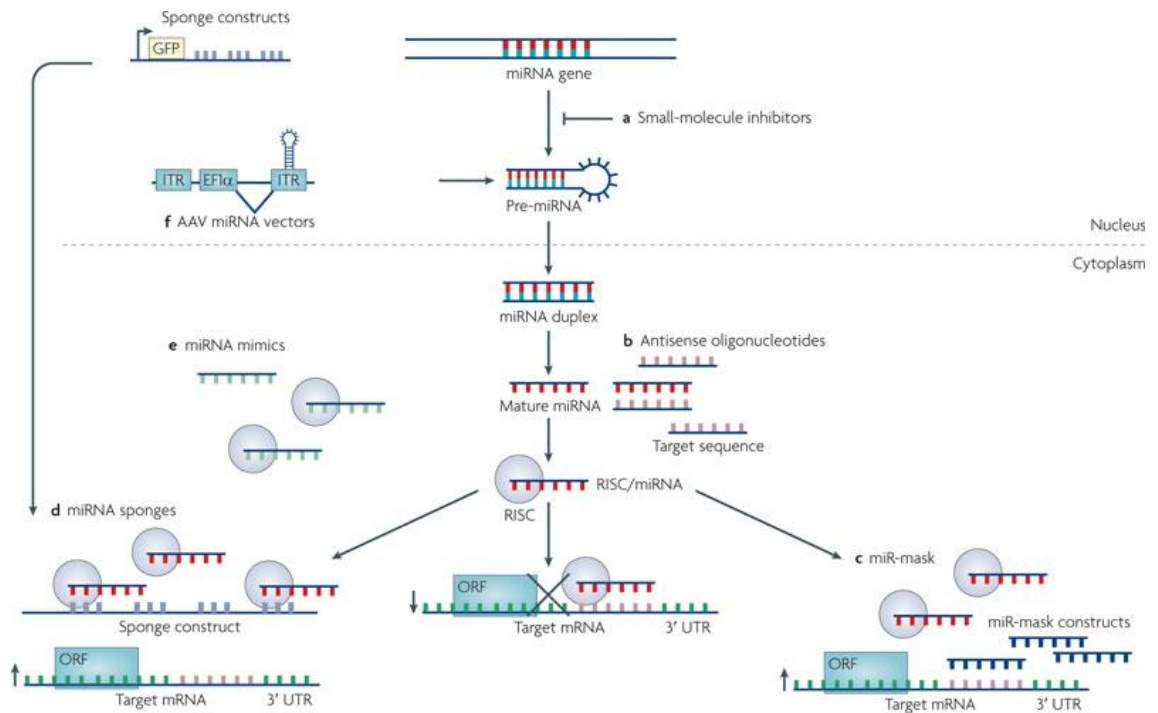


Figure 2.9: Oncogenic miRNAs can be blocked through the use of antisense oligonucleotides, miRNA (Figure adapted from Garzon *et al.*, 2010).

The expression of miRNAs that function as tumor-suppressors can be lost or down-regulated in cancer. This issue can be overcome through the introduction of synthetic oligonucleotides that are identical to the selected miRNA, known as miRNA mimics (Garzon *et al.*, 2010). Various studies have shown that synthetic miRNA mimics with tumor-suppressor functions in cancer cells induced cell death and as well as blocking proliferation (Bonci *et al.*, 2008; Akao *et al.*, 2006). For example, mimics of miR-15a in prostate cell lines induce apoptosis. These miRNA mimics are small, usually double stranded and are chemically modified, 2'-O-methyl with phosphorothioate modifications (Bonci *et al.*, 2008).

Another strategy that is utilized to increase the expression of tumor-suppressor miRNAs in cancer is the adenovirus-associated vectors (AAV). An advantage of these AAV is that they do not integrate into the genome and are eliminated efficiently with minimal toxicity. Also, AAV vectors have efficient transduction of target cells. In a

study conducted by Kota and colleagues, it was found that the expression of miR-26 was lost in human liver cancers, while expressed at high levels in normal tissue (Kota *et al.*, 2009). The decreased levels of miR-26 in liver cancer cells were shown to induce cell-cycle arrest. Kota and colleagues then cloned miR-26 into an AAV, and intravenous injection of this miRNA into liver cancer mouse models resulted in the suppression of tumorigenicity by inducing tumor apoptosis and repressing cell growth, without any signs of toxicity (Kota *et al.*, 2009). Many serotypes of AAV are available which allow for efficient targeting of many tissues of interest. Therefore through use of this technology, it would be possible to target cancers that arise from different tissues (Garzon *et al.*, 2010).

CHAPTER 3: MATERIALS AND METHODS

3.1 Cancer Cell Lines

3.1.1 Cell Lines and Culture Conditions

The human lung adenocarcinoma cell line (A549) and the normal human nasopharyngeal epithelial cell line (NP69) was obtained from Cancer Research Initiative Foundation (CARIF), Sime Darby Medical Centre, Malaysia. A549 cells were cultured in Roswell Park Memorial Institute 1640 (RPMI 1640) (Thermo Scientific Hyclone, USA) culture medium, supplemented with heat inactivated 10% (v/v) fetal bovine serum (FBS) (JR Scientific Inc. USA), while NP69 was cultured in keratinocyte serum-free medium (KSFM) (Gibco, USA) supplemented with $1 \times 2.5 \mu\text{g}$ recombinant epidermal growth factor (rEGF) (Gibco, USA) and $1 \times 2.5 \text{mg}$ bovine pituitary extract (Gibco, USA). Both cell lines were grown as a monolayer and maintained in a carbon dioxide (CO_2) incubator (Mettler, Germany) with high relative humidity (95.0%), stable temperature (37°C), controlled CO_2 levels (5.0%) and controlled pH (7.2-7.4).

3.1.2 Subculturing Cell Line Monolayers: Harvesting a Cell Monolayer

A549 was split every two to three days, or when 80-90% confluency was achieved on the culture flask surface. The spent culture medium was removed and discarded using a serological pipette. The cell monolayer was rinsed with sterile autoclaved $1 \times$ phosphate- buffered saline ($1 \times \text{PBS}$) to remove any residual serum that could inactivate trypsin activity. The PBS was removed and discarded using a serological pipette. 3ml of dissociating agent, 0.25% trypsin (Sigma-Aldrich, USA)

ethylenediaminetetraacetic acid (EDTA) (Gibco, USA), was added to the culture flask. The culture flask was incubated in 37°C in the CO₂ incubator for approximately 10 minutes to allow the cells in the culture flask to detach from the flask. The progress of cell detachment was checked every five minutes using an inverted fluorescence microscope (Nikon, Japan).

Once the cells were detached, equal volume of culture medium, supplemented with 10% (v/v) FBS, was added to the culture flask to inactivate trypsin activity. Any remaining cells were washed from the bottom of the culture flask and a quick check was done under the inverted microscope to look for single cells in the suspension. If mostly single cells were observed, more vigorous pipetting was performed on the suspension. All the suspension was then transferred to a labeled 15ml Falcon tube and the tube was centrifuged for 5 minutes at 1,200 RPM using the Eppendorf Centrifuge 5702 (Eppendorf, Germany). The supernatant in the tube was then discarded and the cell pellet was resuspended in fresh culture medium. The cell suspension was then collected for cell counting or divided into prepared culture flasks for routine maintenance of cell lines. For routine maintenance of cell lines, approximately 2ml of cell suspension was transferred to a new T-25cm² culture flask with 3 ml of new growth medium. The culture flask was then stored at 37°C in the 5.0% CO₂ incubator.

3.1.3 Cell Counting

A dye exclusion viability assay using a haemocytometer was used to determine the number of cells present in a specific population. The cell suspension was gently mixed and 20µl of the suspension was aliquoted into a 1.5ml microcentrifuge tube, and 20µl of 0.08% trypan blue stain (Sigma-Aldrich, USA) was then added to this aliquot and mixed well. The tube was left to stand for about 3 minutes. After 3 minutes, 10µl of

the mixture was removed and loaded on to a clean haemocytometer (Resistance, Germany) chamber to be counted. The counting was conducted under the inverted fluorescence microscope at 100× magnification. Dead cells appeared blue, while viable cells appeared as unstained bright spheres. The number of cells in each of the four square grid corners was counted and the average number of cells was obtained. Each square grid represents a 0.1mm³ or 10⁻⁴ml volume, and the concentration of cells was determined according to the following formula, with a dilution factor of two.

$$\text{Cell Concentration (cell/ml)} = \left(\frac{\text{Avg. Number of Cells Counted}}{\text{Volume Counted (ml)}} \right) \times \text{Dilution Factor}$$

From the concentration, the volume of suspension required for cell plating was calculated.

3.2 Short Interfering RNA (siRNA) Transfection

3.2.1 Stealth RNAi™ siRNA Duplex Oligonucleotides (Invitrogen, USA)

Table 3.1: Stealth RNAi™ siRNA Duplex Oligonucleotides used for transfection

Primer Name		Sequence	Length
BCL2L1-	Forward	(RNA) – UCA CUA AAC UGA CUC CAG CUG UAU C	25
HSS141361	Reverse	(RNA) – GAU ACA GCU GGA GUC AGU UUA GUG A	25
BCL2L1-	Forward	(RNA) – AUG GGU UGC CAU UGA UGG CAC UGG G	25
HSS141362	Reverse	(RNA) – CCC AGU GCC AUC AAU GGC AAC CCA U	25
BCL2L1-	Forward	(RNA) – AUC ACC UCC CGG GCA UCC AAA CUG C	25
HSS141363	Reverse	(RNA) – GCA GUU UGG AUG CCC GGG AGG UGA U	25

3.2.2 Transfection of siRNA

siRNA silencing of the *Bcl-xL* gene was performed using the Stealth RNAi™ siRNA Duplex Oligonucleotides (Table 3.1.), according to a modified version of the manufacturer's protocol. One day prior to transfection, 1.125×10^6 A549 cells were plated in 15ml of RPMI 1640 medium without antibiotics in a T-75cm² culture flask (Corning, USA). Cells were 60% confluent at the time of transfection. For each transfection sample, a Stealth RNAi™-Lipofectamine™ 2000 complex was prepared as follows: 10µl of 20µM of Stealth RNAi™ oligonucleotide was diluted in 1990µl of Opti-MEM® I Reduced Serum Medium (Invitrogen, USA) and mixed gently. 37.5µl of Lipofectamine™ 2000 Transfection Reagent (Invitrogen, USA) was diluted in 1875µl of Opti-MEM® I Reduced Serum Medium and mixed gently. Both solutions were left to incubate for 15 minutes at room temperature. After the 15 minute incubation, the diluted Stealth RNAi and the diluted Lipofectamine™ 2000 (total volume ≈4ml) was combined and mixed gently. The combined solution was incubated for 15 minutes at room temperature to allow complexes to form. The ≈4ml of Stealth RNAi™-Lipofectamine™ 2000 complexes was added to the 75cm² flask containing cells and growth medium. The flask was mixed gently by rocking back and forth. The cells were then incubated at 37°C in the humidified CO₂ incubator for 24 hours.

The same procedure was carried out with the Stealth RNAi™ siRNA Negative Control Low GC (Invitrogen, USA) and Stealth RNAi™ siRNA Negative Control High GC (Invitrogen, USA) as well as the BLOCK-iT™ Alexa Fluor® Red Fluorescent Oligo (Invitrogen, USA).

3.3 RNA isolation using TRIzol® Reagent (Invitrogen, USA)

3.3.1 Homogenization

The spent culture medium in the flask was removed and discarded using a serological pipette. The remaining cells were washed with sterile autoclaved 1×PBS to remove any remaining culture medium. The solution in the culture flask was removed and discarded. 5ml of dissociating agent 0.25% trypsin EDTA was added to the culture flask. The flask was then incubated at 37°C in the CO₂ incubator for approximately 10 minutes to allow the cells in the culture flask to detach. The progress of cell detachment was checked every five minutes using the inverted fluorescence microscope.

Once the cells were detached 5ml of RPMI 1640 culture medium was added to the flask. The suspension was then transferred from the culture flask to a labeled 15ml Falcon tube, and the tube was centrifuged for 10 minutes at 1200RPM. The supernatant in the tube was discarded and the pellet was resuspended in 1ml of TRIzol® reagent. The cell lysate was passed through a pipette several times.

3.3.2 Phase Separation

The homogenized sample was transferred to a 1.5ml microcentrifuge tube and incubated for 5 minutes at room temperature to allow for the complete dissociation of nucleoprotein complexes. 0.2ml of chloroform (J.T Baker, USA) was added and the caps capped securely. The tubes were shaken vigorously by hand for 15 seconds and incubated at room temperature for 3 minutes. The tubes were then centrifuged at 12,000×g for 10 minutes at 4°C in the Sorvall Legend Micro 17R (Thermo Scientific, USA) centrifuge. Following centrifugation, the mixture separated into a lower red,

phenol-chloroform phase, an interphase, and a colorless upper aqueous phase. RNA remains exclusively in the aqueous phase. The volume of the aqueous phase was about 60% of the volume of TRIzol-reagent used for homogenization.

3.3.3 RNA Precipitation

The aqueous phase was transferred to a fresh tube. The RNA was precipitated from the aqueous phase by mixing with 0.5ml of isopropanol (Merck, Germany). The samples were incubated at room temperature for 10 minutes and then centrifuged at 12,000×g for 10 minutes at 4°C.

3.3.4 RNA Wash

The supernatant was removed and the pellet washed once with 1ml of 75% ethanol (J.T Baker, USA). The sample was mixed by vortexing and then centrifuged at 7,500×g for 5 minutes at 4°C.

3.3.5 Re-Dissolving the RNA

After centrifugation, the supernatant was removed and the RNA pellet was air-dried for about 5 to 10 minutes. The RNA samples were then dissolved in nuclease-free water (Qiagen, Germany) by passing the solution a few times through a pipette tip, and incubating for 10 minutes in the water bath incubator (Mettler, Germany) at 58°C.

3.4 Quantitation of RNA

The concentration and purification of extracted RNA for transfected and non-transfected cells were analyzed using the NanoDrop 2000 (Thermo Scientific, USA). When the arm was open, 1µl of distilled water was pipetted directly on the pedestal and used as a blank for the NanoDrop. When the measurement was complete, the surfaces were wiped with a lint-free KimWipe before going on to the next sample. The RNA concentration, OD₂₆₀, OD₂₈₀, A_{260/280}, and A_{260/230} ratio of the samples were measured

3.5 Agarose Gel Electrophoresis

In the casting tray 1.0×10^{-2} g/ml gel solution was prepared. In other words 1% Low EEO Agarose (Amresco, USA) in 40.0ml 1×Tris/Borate/EDTA (TBE), prepared from 10X TBE liquid concentrate (Bio-Rad, USA), was measured and prepared using the Analytical Balance CP224S (Sartorius, Germany). The solution was heated in the microwave oven (Pensonic, Malaysia) at medium heat for 2 minutes. Meanwhile an attached 6 well 1.0mm gel comb was placed in the 5.5×12.0cm gel-casting tray (BayGene, China). After the agarose powder was dissolved completely, the mixture was cooled under running water before being poured into the prepared casting tray. When the gel was completely solidified, after approximately 30 minutes, the gel comb was carefully removed without damaging the gel's sample wells and the gel was placed in the gel buffer tank, BG-Submidi Submarine Unit (BayGene, China). 1×TBE electrophoresis buffer was then added into the tank until it covered the gel's surface to a depth of 1-2mm.

For RNA sample loading, 2 volumes of 2×RNA loading dye (Fermentas, Canada) was mixed with 2 volumes of RNA sample. This mixture was boiled for 10 minutes at 70°C using a water bath, and then cooled to room temperature. 3µl of RiboRuler™ High Range RNA Ladder (Fermentas, Canada), was also boiled for 10 minutes at 70°C. After boiling, 3µl of the RiboRuler™ High Range RNA Ladder was loaded into the well of the gel. 3µl of each RNA sample was also loaded into the gel. After all the RNA samples had been loaded, the lid was assembled onto the electrophoresis chamber correctly so that the RNA can be migrated towards the positive lead. The electric sources were provided by Power Supply-PowerPac (Bio-Rad, USA). The gel electrophoresis was run at 80.0 volts and 400.0 mA of free running current for approximately 60 minutes or until the dye front was 1.0-2.0cm from the bottom of the gel.

3.5.1 Detection of RNA Bands

The gel was stained for 15 minutes in 0.5µg/ml ethidium bromide (EtBr) (Sigma-Aldrich, USA) solution and de-stained for 10 minutes in distilled water to remove any residual staining solution. The gel was then visualized under UV transillumination and analyzed by the Imager Kit Digital, AlphaImager™ 2000 (Alpha Innotech, USA) at 320nm wavelength.

3.6 Protein Isolation Using NE-PER Nuclear and Cytoplasmic Extraction Kit (Pierce, USA)

The A549 cells were plated on a 75.0cm² culture flask and grown to 80% confluency. The confluency of the cells was assessed through use of an inverted microscope. Once the desired confluency was achieved, the spent culture medium in the flask was removed and discarded using a serological pipette. The remaining cells were washed with sterile autoclaved 1×PBS to remove any remaining culture medium. The solution in the culture flask was removed and discarded. 5 ml of dissociating agent 0.25% trypsin was added to the culture flask. The flask was then incubated in 37°C and 5% CO₂ incubator for approximately 10 minutes to allow the cells in the culture flask to detach. The progress of cell detachment was checked every five minutes using an inverted microscope.

Once the cells were detached, 5 mL of the RPMI-1640 culture medium was added to the flask. Any remaining cells were washed from the bottom of the culture flask and a quick check was conducted under the inverted microscope to ensure that the suspension was made up of single cells. If they are not mostly single cells, vigorous pipetting of the mixture was done on the suspension. The suspension was then transferred from the culture flask to a labeled 15 ml Falcon tube, and the tube was centrifuged for 10 minutes at 1500 RPM using a Centrifuge 502 (Eppendorf, USA).

NE-PER® Nuclear and Cytoplasmic Extraction Kit was used to extract the cytoplasmic protein from the whole cell lysate. The NE-PER® Nuclear and Cytoplasmic Extraction Kit contains three reagents, Cytoplasmic Extraction Reagent I (CER I), Cytoplasmic Extraction Reagents II (CER II) and Nuclear Extraction Reagent (NER). 1×Halt™ Protease (Thermo Scientific, USA) and 1×Phosphatase inhibitor cocktails (Thermo, USA) were freshly prepared and added to the CER I in 1:1000 dilution to

prevent proteolysis and dephosphorylation.

The supernatant in the tube was discarded and the pellet was resuspended in 200 μ l of ice cold CER I and vortexed vigorously for 15 seconds to fully resuspend the pellet. The tube was then incubated on ice for 10 minutes. 11 μ l of ice cold CER II was added to the tube and vortexed for 5 seconds. The tubes were incubated on ice for 1 minute and then vortexed again for 5 seconds. The tubes were then centrifuged at 16,000 \times g for 5 minutes and the supernatant, containing the cytoplasmic extract, was transferred to a new pre-chilled tube. The protein solution was used immediately for Western blotting, otherwise, the solubilized proteins was stored at -20°C and the heating, centrifugation steps performed at the time of use.

3.7 Bradford Assay Protein Quantification

The Quick Start Bradford Protein Assay Kit was used to determine the protein concentration of extracted protein samples. The Quick Start™ Bradford Dye Reagent (Bio-Rad, USA) was removed from the 4°C fridge and allowed to cool to room temperature. The Quick Start™ Bovine Serum Albumin (BSA) Standard Set (Bio-Rad, USA), containing seven known concentrations of BSA (2.000, 1.500, 1.000, 0.750, 0.500, 0.250, and 0.125 mg/ml) was used to create a standard curve. This allows for the determination of the unknown sample's concentration. Blank, standards and samples were diluted with a dilution factor of 100. 10.0 μ l of each BSA standards and protein samples were added into separate 10.0mm \times 10mm disposable cuvettes, followed by 990 μ l 1 \times dye reagent and mixed well. Blank sample was prepared using 10.0 μ l of distilled water and 990.0 μ l 1 \times dye reagent. The blank, standards and samples were incubated at least 5 minutes at room temperature.

The parameter of the spectrophotometer was set to 595nm wavelength. This instrument was zeroed by the blank sample. Absorbance of each standards and samples were then measured. A standard curve was created by plotting the 595nm values (y-axis) against the standard concentration in mg/ml (x-axis). After obtaining the samples concentration, samples were then normalized to the same concentration with distilled water. All samples were kept at -20.0°C freezer until further use.

3.8 Quantitative Reverse Transcription Polymerase Chain Reaction (qRT-PCR)

The oligonucleotides used for qRT-PCR was obtained from 1st Base, Singapore.

Table 3.2: Oligonucleotides used for qRT-PCR

Synthesis ID	Oligo Name	Sequence	Length
782265	Bcl-xL Forward	5' -CGT GGA AAG CGT AGA CAA GGA-3'	21
782266	Bcl-xL Reverse	5' -ATT CAG GTA AGT GGC CAT CCA A-3'	22
782267	β -Actin Forward	5' -AAG CCA CCC CAC TTC TCT CTA A-3'	22
782268	β -Actin Reverse	5' -ACC TCC CCT GTG TGG ACT TG-3'	20

First strand cDNA was synthesized for use in real-time quantitative RT-PCR, using the SuperScript III First-Strand Synthesis SuperMix (Invitrogen, USA). The following kit components were combined on ice. For multiple reactions, a master mix without RNA was prepared.

Table 3.3: Kit components used to prepare cDNA samples

Component	Volume
2× RT Reaction Mix	10µl
RT Enzyme Mix	2µl
RNA (up to 1µg)	χ µl
DEPC-treated water	to 20µl

The tube contents was gently mixed and incubated at 25 °C for 10 minutes. The tubes were then incubated at 50 °C for 30 minutes and the reaction then terminated at 85 °C at 5 minutes. The tubes were then chilled on ice and 1µl of *E. coli* RNase H was added and the tubes incubated at 37 °C for 20 minutes. The cDNA was then used in qPCR.

The Platinum SYBR Green qPCR SuperMix-UDG with ROX (Invitrogen, USA) was used to carry out qPCR. For each qPCR reaction the following components were added to a 0.2-ml microcentrifuge tube. The volumes for a single 50µl reaction are listed below. For multiple reactions, a master mix of common components was prepared and the appropriate volume added to each tube, and the unique reaction components (eg. template) was then added.

Table 3.4: Kit components used to prepare qPCR samples

Component	Volume
Platinum [®] SYBR [®] Green qPCR SuperMix-UDG with ROX	25µl
Forward primer, 10µM	1µl
Reverse primer, 10µM	1µl
Template (cDNA generated from 10pg to 1µg of total RNA)	≤ 10µl
DEPC-treated water	to 50µl

The reaction tubes were capped and gently mixed. The reactions were then placed into a preheated real-time instrument, the CFX96™ Real-Time PCR Detection System (Bio-Rad Laboratories, USA), and programmed as described below.

Table 3.5: Real-time PCR instrument conditions

50°C	for 2 minutes hold (UDG incubation)
90°C	for 2 minutes
40 cycles of:	95°C, 15 seconds
	60°C, 30 seconds
Melting curve analysis.	

3.9 Sodium Dodecyl Sulphate Polyacrylamide Gel Electrophoresis (SDS-PAGE)

The SDS-PAGE is a technique for separating proteins according to their molecular weight. The separation of protein molecules within a gel is determined by relative size of the pores formed within the gel. 12.0% resolving gel was used to separate proteins ranging from 14-70kDa. 4.0% stacking gel and 12.0% resolving gel was prepared by mixing the reagents listed in Table 2.4 together. Freshly prepared 10.0% (w/v) APS and TEMED were added last to the mixture to initiate gel polymerization. Bromophenol blue, an anionic small molecule, was added to the stacking gel and functioned as a tracking dye, which monitored the migration front of the proteins.

18.0cm×16.0cm, with 0.75mm thickness, glass plates (Bio-Rad, USA) were aligned and clipped to the casting tray (Bio-Rad, USA). The resolving gel was prepared and loaded until 75% of the glass plate was filled. The remaining resolving gel solution was kept in a tube rack as an indicator of complete gel polymerization, which usually takes approximately 45 minutes. Immediately after adding the resolving gel, 0.1% (v/v) SDS was added gently on top of the resolving gel to prevent oxidization and dehydration of the gel, which can slow down the polymerization process. After polymerization was complete, the 0.1% SDS solution was rinsed out by tilting the casting tray and blotting out the solution with Kim-wipe (Kimberly-Clark, Canada).

The desired volume of 10% APS was added into the stacking solution. The solution was mixed well and straight away added to the cast above the resolving gel. The stacking solution was ensured to completely fill 100% of the glass plate until it overflows. The 10-well gel comb, with a 0.75mm thickness, was inserted at an angle to prevent formation of air bubbles. The remaining stacking gel solution was kept in a tube rack as an indicator of complete gel polymerization (approximately 45 minutes).

Table 3.6: Reagents for preparation of 4.0% stacking gel and 12.0% resolving gel for SDS-PAGE

Reagents	Stacking Gel (4.0%)	Resolving gel (12.0%)
40.0% (w/v) Acrylamide (Promega, USA)	360µl	4320µl
2.0% (w/v) Bis-Acrylamide (Promega, USA)	195µl	2400µl
0.5M Tris HCl (pH6.8)	945µl	-
1.5M Tris HCl (pH 8.8)	-	3750µl
10.0% (w/v) SDS	37.5µl	150µl
Distilled H ₂ O	2175µl	4280µl
N,N,N',N' – Tetramethyl-ethylenediamine (TEMED) (Acros, USA)	3.8µl	7.5µl
10.0% (w/v) APS	18.8µl	75.0µl
Bromophenol Blue (Fisher Scientific, USA)	7.5µl	-
Total Volume	3.75ml	15.0ml

3.9.1 Sample Preparation

Antibodies typically recognize a small portion of the protein of interest (epitope), and this domain may reside within the three dimensional conformation of the protein. To enable access of the antibody to this portion it is necessary to denature the protein. Lane Marker Reducing Sample Buffer (5×) (Thermo Scientific, USA) contained dithiothreitol (DTT) as a reducing agent to reduce disulphide bridges within tertiary protein structures to produce primary protein structures. The sample buffer also contained SDS, which binds to the polypeptides to form complexes with fairly constant

negative charge to mass ratios. The electrophoretic migration rate through a gel is therefore determined only by the size of the complexes.

First, protein samples and the Lane Marker Reducing Sample Buffer (5×) was equilibrated to room temperature. One volume of sample buffer was mixed with four volumes of protein samples in a microcentrifuge tube. These mixtures were vortexed before and after boiling for 5 minutes at 95°C using a thermal cycler, and then cooled to room temperature.

3.9.2 Sample Loading and Running the Gel

The glass plates were transferred to the Mini PROTEAN Tetra System (Bio-Rad, USA) and placed in the holder facing each other. The space between the gels was filled fully with 1×Tris/Glycine/SDS (TGS) running buffer. The comb was gently removed and the wells were flushed with this buffer to allow the wells to form properly and to rinse off traces of unpolymerized gel. The tank was then filled with sufficient amount of buffer according to the number of gels being run. 5.0µl of Spectra Multicolor Broad Range Protein Ladder (Fermentas, Canada) was loaded into the first well followed by 5.0µl of Biotinylated Protein Ladder (Cell Signaling Technology, USA) (Protein ladder sizes are listed in Appendix 2. 15.0µl of protein samples pre-mixed with sample buffer was then added to subsequent wells. Gel was run at 110 volts until the sample front reached the resolving gel, followed by 120 volts until the end of the gel. Power supply was provided by the Power Pack (Bio-Rad, USA).

3.10 Western Blotting

3.10.1 Protein Transfer

The 2 μ m nitrocellulose membrane (Bio-Rad, USA) and the Extra Thick Blot Paper (Bio-Rad, USA) were cut to the same size as the gel or slightly larger than the gel. The membrane and filter papers were soaked in 1 \times TGS transfer buffer with 20.0% (v/v) methanol for 10 minutes. Once the SDS-PAGE finished running, the glass was removed from the tank carefully. The upper glass plate was removed using a plastic spatula. Using a delicate task wiper, the stacking gel was carefully torn away from the resolving gel. The glass plate was then inverted over the transfer buffer and then lifted so that the surface tension will peel the gel from the glass plate. The gel was soaked in transfer buffer for at least 10 minutes. The “transfer sandwich” was then placed in the Trans-Blot SD Semi-Dry Transfer Cell (Bio-Rad, USA). Each layer of the sandwich was rolled out to ensure no air bubbles were formed. The gels were then transferred at 50mA at 25 volts for 90 minutes using the MP-2AP Power Supply (Major Science, Taiwan).

Transfer sandwich:

Cathode (-)

Blot paper

PAGE gel

Nitrocellulose membrane

Blot paper

Anode (+)

3.10.2 Visualization of Proteins on Membrane Using Ponceau S Stain (Sigma, USA)

After transferring, the membrane was stained with 0.1% (w/v) Ponceau S Stain in 5.0% (v/v) to check the efficiency of proteins transferred. The membrane was soaked in Ponceau S staining solution for 5 minutes. After observation, the membrane was washed twice with aqueous solution with 5.0% (v/v) acetic acid (Merck, Germany) followed by washing twice with distilled water by shaking slowly on the Reciprocal Shaker MS-RC (Major Science, Taiwan) for 5 minutes each. After washing, membrane was continued to blocking step.

3.10.3 Blocking the Membrane

The membrane was blocked to prevent non-specific binding of the primary and secondary antibodies to the membrane. Two blocking buffers, blocking buffer A and blocking buffer B, were used for non-phosphorylated proteins and phosphorylated proteins respectively. Blocking buffer A consisted of consisted of 5.0% (w/v) non-fat skim milk powder (Merck, Germany), 0.05% (v/v) Tween 20 (Promega, USA) in 1×TBS, while blocking buffer B consisted of consisted of 5.0% Bovine Serum Albumin (BSA) (Calbiochem, USA), 0.05% Tween 20 and 1×TBS. The membrane was soaked in blocking buffer A or B for one and a half hours at room temperature under agitation.

3.10.4 Incubation With Primary Antibody

Equal amounts of cytoplasmic protein extracts were probed against two antibodies: Bcl-xL and β -actin. The Bcl-xL rabbit monoclonal antibody (Cell Signaling Technology, USA) and β -actin rabbit monoclonal antibody (Cell Signaling Technology, USA) was diluted in blocking buffer A and blocking buffer B, respectively, at a dilution of 1:1000. The blocked membrane was incubated in primary antibody at 4° overnight in a petri dish sealed with parafilm. The following day the membrane was incubated at room temperature for 3 hours with agitation. The membrane was then washed 3 times with 1×TBST buffer for 5 minutes each with agitation and then incubated with secondary antibody.

3.10.5 Incubation With Secondary Antibody

Anti-rabbit IgG HRP-linked antibody (Cell Signaling Technology, USA) and anti-biotin HRP-linked antibody (Cell Signaling Technology, USA) was added at a dilution of 1:1000 to blocking buffer B. The membrane was then incubated for 2 hours with agitation at room temperature. The membrane was then washed 3 times with 1×TBST buffer for 5 minutes each, with agitation, followed by a 1×TBS buffer wash for 5 minutes, with agitation. The membrane was then blotted dry with Kim-wipes.

3.10.6 Exposure of Membrane to Electrochemiluminescence (ECL)

SuperSignal West Pico Chemiluminescent Substrate (Thermo Scientific, USA) is a high-sensitivity substrate that reacts with horseradish peroxidase (HRP) conjugated to the secondary antibodies on the membrane by releasing chemiluminescence signal. This kit contained two solutions; the Enhance Solution (hydrogen peroxide) and the Stable Peroxide Solution. The working solution was prepared by mixing equal parts of the stable peroxide solution and enhancer solution. The membrane was incubated in the working solution for 5 minutes. The excess substrate on the membrane was blotted away and the membrane wrapped in cling wrap and carefully pressed to get rid of any air bubbles. The light emission was most intense during the first 5-30 minutes after substrate incubation and decreased with time. Therefore, to protect the membrane, it was placed in a Medical X-Ray Cassette (Kodak, USA) in order to prevent light exposure.

In the darkroom, a piece of General Purpose Green X-Ray film (Kodak, USA) was cut to the size of the membrane and carefully placed on top of the membrane inside the Medical X-Ray Cassette. The cassette was closed and the film was exposed to the chemiluminescence signal for 30 seconds. The exposure time was varied to achieve optimal results. The film was then washed in Kodak RP X-OMAT Developer and Replenisher (Kodak, USA) to allow the exposed areas of the film to become dark. After development, the film was washed with distilled water to remove excess chemical. The film was then placed in the Kodak RP X-OMAT Fixer and Replenisher (Kodak, USA). The film was subsequently washed with running tap water to remove fixing chemicals and allowed to completely dry. Film was then scanned with CanonScan LiDE600F Scanner (Canon, Vietnam) and the results analyzed.

3.11 MTT [3-(4,5-dimethylthiazol-2-yl)-2,5-diphenyltetrazolium bromide]

Cell Viability Assay

A549 cells were harvested by trypsinization and centrifugation, and then re-suspended with RPMI 1640 culture medium. Using a dye exclusion viability assay, viable A549 cells were counted and 1.0×10^4 A549 cells in 100 μ l of RPMI 1640 medium were plated in triplicates onto a 96 well microtiter plate. The plate was then incubated at 37°C overnight in a CO₂ incubator to allow for cell attachment to the well surface. Commencement of siRNA transfection was carried out at 100nM at various incubation periods (12 hrs, 24hrs and 48hrs). Wells containing Stealth RNAi™ siRNA Negative Control Low GC were used as negative controls and solvent controls using Opti-MEM® I Reduced Serum Medium and Lipofectamine™ 2000 Transfection Reagent were conducted to ensure that decrease in cell viability was not solvent induced. Wells containing cells at descending concentrations (10,000 cells, 5,000 cells, 2,500 cells, 1,250 cells and 0 cells) via a serial dilution was used to construct standard curves for quantification purposes. After incubation,

Following incubation, 20.0 μ l MTT reagent (5.0mg/ml) (Calbiochem, USA) was added to each well and incubated in the dark at 37°C for one hour. Periodically the cells were viewed under an inverted microscope for the presence of the purple formazon crystals at the bottom of each well. When the purple formazon crystals were clearly visible under the microscope, the media containing excessive MTT reagent was aspirated and 200 μ l of dimethyl sulfoxide (DMSO) (Merck, Germany) was added to dissolve the purple formazon precipitates. After a few minutes at room temperature, to allow for complete colour stabilization of the formazon compound, results were obtained using a microtiter plate reader (Tecan Sunrise®, Switzerland) at 570nm

absorbance wavelength and 650nm reference wavelength. The results were then quantified using the Magellan Version 6.3 (Tecan, Switzerland) software.

3.12 BioAnalyzer Quantification of Total RNA

The Agilent RNA 6000 Nano Kit (Agilent, Germany) was used with the Agilent 2100 BioAnalyzer (Agilent, Germany) to determine the RNA integrity number (RIN value).

3.12.1 Setting Up Chip Priming Station

The plastic cap of the syringe was removed and the syringe inserted into the clip. The syringe was slid into the hole of the lock adaptor and screwed tightly to the chip priming station.

3.12.2 Preparing the Gel



550µl of RNA 6000 Nano gel matrix was pipetted into a spin filter and centrifuged at 1500g for 10 minutes at room temperature. 65µl of the filtered gel was aliquoted into 0.5ml RNase-free microfuge tubes.

3.12.3 Preparing the Gel-Dye Mix


The RNA 6000 Nano dye concentrate was allowed to equilibrate to room temperature for 30 minutes. The dye was then vortexed for 10 seconds, spun down, and 1µl of the dye was added to the 65µl aliquot of filtered gel. The solution was vortexed

and the tube centrifuged at 13000g for 10 minutes at room temperature. The prepared gel-dye mix was used within one day.


3.12.4 Loading the Gel-Dye Mix

A new RNA 6000 Nano chip was placed on the chip priming station. 9.0µl of gel-dye mix was pipetted into the well marked . The plunger was positioned at 1ml and the chip priming station closed. The plunger was pressed until it was held by the clip. After 30 seconds the clip was released. After 5 seconds the plunger was pulled back to the 1ml position. The chip priming station was opened and 9.0µl of gel-dye mix was pipetted into the well marked . The remaining gel-dye mix was discarded.

3.12.5 Loading the Agilent RNA Nano Marker

5µl of RNA Nano marker was pipetted into all 12 sample wells and in the wells marked .

3.12.6 Loading the Ladder and Samples

1µl of prepared ladder was pipetted into the well marked . 1µl was pipetted into each of the sample wells. 1µl of RNA 6000 Nano marker was pipetted into each unused sample. The chip was placed horizontally in the adaptor of the IKA vortexer and vortexed for 1 minute at 2400rpm. The chip was then run in the Agilent 2100 bioanalyzer (Agilent, Germany) within 5 minutes.

3.13 MiRNA Microarray – Global miRNA Expression

The microRNA microarray analysis allowed for the examination of the global expression pattern of miRNAs in the transfected and non-transfected A549 cells, using the Affymetrix GeneChip®miRNA Arrays (Affymetrix, USA) with the FlashTag Biotin HSR RNA Labeling Kit (Genisphere, USA).

3.13.1 Poly (A) Tailing

The volume of RNA was adjusted to 8µl with nuclease-free water in a microcentrifuge tube, and transferred to ice. 2µl of RNA Spike Control Oligos (Affymetrix, USA) was added and the tube returned to ice. The ATP mix was diluted in 1mM Tris (Applied Biosystems, USA) at a dilution of 1:500. The following components were then added to the 10µl RNA/Spike Control Oligos, to make a final volume of 15µl. If at least 5 labeling reactions are run simultaneously, a master mix was prepared. 5µl of master mix was added to the 10µl RNA/Spike Control Oligos, for a volume of 15µl.

Table 3.7: Components used to prepare Poly (A) tail

Component	Volume (µl)
10× Reaction Buffer	1.5
25mM MnCl ₂	1.5
Diluted ATP mix	1.0
PAP Enzyme	1.0

3.13.2 FlashTag Biotin HSR Ligation

The FlashTag Biotin HSR RNA Labeling Kit (Genisphere, USA) contains the following components: 10× Reaction Buffer, 25mM MnCl₂, ATP Mix, PAP Enzyme, 5× FlashTag Biotin HSR Ligation Mix, T4 DNA Ligase, HSR Stop Solution, RNA Spike Control Oligos, ELOSA Spotting Oligos, ELOSA Positive Control, Nuclease-free water, and 27.5% Formamide.

The 15µl of tailed RNA was briefly centrifuged and placed on ice. 4µl of 5× FlashTag Biotin HSR Ligation Mix was added. 2µl of T4 DNA Ligase was then added. The mixture was gently mixed and centrifuged. The tubes were then incubated at 25°C for 30 minutes. The reaction was then stopped by adding 2.5µl of HSR Stop Solution. The 23.5µl of ligated sample was then mixed and centrifuged. 2µl of biotin-labeled sample was removed and ELOSA QC Assay was carried out. The remaining biotin-labeled sample may be stored on ice for up to 6 hours, or at -20°C for up to 2 weeks, prior to hybridization on Affymetrix GeneChip miRNA Arrays.

3.13.3 Hybridization of Affymetrix Arrays

The reagents in table 2.6 were first allowed to cool to room temperature. The 20× Eukaryotic Hybridization Controls (bioB, bioC, bioD, cre from the GeneChipEukaryotic Hybridization Control Kit (Affymetrix, USA)) was completely thawed and then heated for 5 minutes at 65°C. The following components were then added to the 21.5µl biotin-labeled sample in the order listed below, to prepare the array hybridization cocktail:

Table 3.8: Components used to prepare array hybridization cocktail

Component	Volume (μl)
Hybridization Mix (from GeneChip Hyb, Wash and Stain Kit)	50
Nuclease-free water	10
Deionized formamide, molecular biology grade	5
DMSO (from GeneChip Hyb, Wash and Stain Kit)	10
20 \times Eukaryotic Hybridization Controls	5
Control Oligonucleotide B2, 3nM (From GeneChip Eukaryotic Hyb Control Kit)	1.7

The resulting final volume was 103.2 μ l. The samples were then incubated at 99°C for 5 minutes and then 45°C for 5 minutes. 100 μ l of the sample was aspirated and injected into an array. The pipet tip was removed from the upper right septum of the array and both septa covered with 1/2" Tough-Spots to minimize evaporation and/or prevent leaks. The arrays were placed into the hybridization oven trays and loaded into the hybridization oven. The arrays were incubated at 48°C and 60rpm for 16 hours.

3.13.4 Washing and Staining

The GeneChip Hybridization, Wash & Stain Kit (Affymetrix, USA) was used for the washing and staining procedure. The GeneChip Hybridization, Wash & Stain Kit contains the components listed in table 3.9.

Table 3.9: Components of GeneChip Hybridization, Wash & Stain Kit

Component	Volume (mL)
Box 1 of 2	
Hybridization Module	
Pre-hybridization mix	6
2× Hybridization mix	4.5
DMSO	0.9
Nuclease-free water	4
Stain Module	
Stain cocktail 1	18
Stain cocktail 2	18
Array holding buffer	30
Nuclease-free water	4
Box 2 of 2	
Wash buffer A (3 bottles)	800mL/bottle
Wash buffer B (1 bottle)	600mL/bottle

After the 16 hours of hybridization, the arrays were removed from the oven and the Tough-Spots removed. The hybridization cocktail was extracted from each array and transferred to a new tube or well of a 96-well plate in order to save the hybridization cocktail. The hybridization cocktail was stored on ice during the procedure, or at -80°C for long-term storage. Each array was then filled completely with Array Holding Buffer, and the arrays allowed to equilibrate to room temperature before washing and staining.

The following vials were placed into sample holders on the fluidics station:

1. One amber vial containing 600µl Stain Cocktail 1 was placed in sample holder 1.
2. One clear vial containing 600µl Stain Cocktail 2 was placed in sample holder 2.
3. One clear vial containing 800µl Array Holding Buffer was placed in sample holder 3.

The arrays were then washed and stained with Fluidics Station 450 using fluidics script FS450_0003.

Table 3.10: Fluidic station protocol summary for the staining of each Affymetrix GeneChip® miRNA Arrays

Protocol	Description of Protocol
Post Hyb Wash #1	10 cycles of 2 mixes/cycle with Wash Buffer A at 25°C.
Post Hyb Wash #2	8 cycles of 15 mixes/cycle with Wash Buffer B at 50°C.
1 st stain	Probe array stained for 10 minutes with Stain Cocktail 1 (Vial position 1) at 25°C.
Post Stain Wash	10 cycles of 4 mixes/cycle with Wash Buffer A at 30°C.
2 nd stain	Probe array stained for 10 minutes with Stain Cocktail 2 (Vial position 2) at 25°C.
3 rd stain	Probe array stained for 10 minutes with Stain Cocktail 1 (Vial position 1) at 25°C.
Final Wash	15 cycles of 4 mixes/cycle with Wash Buffer A at 35°C.
Array Holding Buffer	Probe array filled with Array Holding Buffer (Vial position 3).

The arrays were checked for air bubbles. If air bubbles were observed, the arrays were filled manually with Array Holding Buffer. If no air bubbles were observed, both septa were covered with 3/8" Tough-Spots. The array glass surface was observed for dust and/or other particulates, and if necessary, the surface was carefully wiped with a clean lab wipe before scanning.

3.14 ELOSA QC Assay

3.14.1 Washing and Blocking for ELOSA

The following steps were completed prior to or during the FlashTag Labeling procedure. The ELOSA Spotting Oligos were removed by expelling the liquid into the sink. The wells were washed 2 times with 1×PBS, 0.02% Tween-20, and blot dry. 150µl

of 5% BSA in 1×PBS was added to each well. The wells were covered and incubated for 1 hour at room temperature.

3.14.2 Sample Hybridization

2.0µl of each biotin-labeled reaction was used in the ELOSA. The following components were added and gently vortexed until the dextran sulfate was in solution.

Table 3.11: Components used to prepare for ELOSA sample hybridization

Component	Volume (µl)
FlashTag Biotin-labeled RNA sample or negative control labeling reaction	2.0
5× SSC, 0.05% SDS, 0.005% BSA	48.0
25% Dextran sulfate	2.5

For the positive and negative control the following components were added and gently vortexed until the dextran sulfate was in solution. The mixture was then briefly centrifuged.

Table 3.12: Components used to prepare negative and positive controls for ELOSA sample hybridization

Positive Control		Negative Control	
Component	Volume (µl)	Component	Volume (µl)
ELOSA Positive Control	2.0	5× SSC, 0.05% SDS, 0.005% BSA	50
5× SSC, 0.05% SDS, 0.005% BSA	48.0	Dextran sulfate	2.5
25% Dextran sulfate	2.5		

The BSA blocking solution was then removed by expelling the liquid into a sink, and the wells blotted dry. 52.5µl of hybridization solution was then added to the designated wells. The wells were covered and incubated at room temperature for 1 hour.

3.14.3 SA-HRP Binding

SA-HRP was diluted in 5% BSA in 1×PBS at a dilution of 1:4000. The hybridization solution was removed from the wells by expelling the liquid into the sink. The wells were washed vigorously 3-4 times with 1×PBS, 0.02% Tween 20, and then blotted dry. 75µl of the diluted SA-HRP was then added to each well. The wells were covered and incubated for 30 minutes at room temperature.

3.14.4 Signal Development

The SA-HRP was removed from the wells by expelling the liquid into a sink. The wells were washed vigorously 3-4 times with 1×PBS, 0.02% Tween 20, and blotted dry. Any bubbles in the wells were removed with a forced air duster or equivalent device. 100µl of TMB Substrate was then added to the wells. The wells were covered and incubated at room temperature for 30 minutes in the dark (or covered with aluminum foil). A blue substrate color indicated a positive result and was used as qualitative results. After a successful ELOSA QC assay, Affymetrix GeneChip miRNA array procedure was carried out.

3.15 MiRNA Microarray Analysis

Statistical and gene expression analyses were carried out using the GeneSpring[®] GX (Agilent Technologies, USA) and Partek[®] Genomics Suite[™] (Partek Incorporated, USA) software. Following scanning of each array, a CEL file containing probe intensity readings and a library file specifying the location of each probe on the array was generated and input into the software. Microarray images were analyzed and the

average values of the replicate spots of each miRNA were background subtracted, normalized and subjected to further analysis. The microarray raw data were normalized using per chip median normalization method and the summarization algorithm Robust Multichip Average (RMA). The differentially expressed miRNAs were then filtered with p -value of <0.05 , using two-way ANOVA, and fold change thresholds, between siRNA-transfected and non-transfected samples, of more than 1.5.

3.16 MiRNA Microarray Validation

The microRNA microarray results were validated with qRT-PCR, using the TaqMan® MicroRNA Assays (Applied Biosystems, USA).

3.16.1 TaqMan® MicroRNA Assays

The primers used for qRT-PCR was obtained from Applied Biosystems, USA.

Table 3.13: TaqMan® MicroRNA Assays used for qRT-PCR.

Assay ID	Ascension Number	Assay Name
000480	MIMAT0000256	hsa-miR-181a
001998	MIMAT0003886	hsa-miR-769-5p
000554	MIMAT0000703	hsa-miR-361-5p
002874	MIMAT0005892	hsa-miR-1304-5p
001571	MIMAT0003276	hsa-miR-608
001093	-	U6

Reverse transcription was performed using the TaqMan® MicroRNA Reverse Transcription Kit (Applied Biosystems, USA) according to a modified version of the manufacturer's protocol. The components of the kit were first allowed to thaw on ice. The RT master mix was then prepared by combining the following components.

Table 3.14. Kit components used to prepare RT master mix

Component	Master mix volume per 10µl reaction*
100nM dNTPs (with dTTP)	0.10µl
MultiScribe™ Reverse Transcriptase, 50 U/µl	0.67µl
10× Reverse Transcription Buffer	1.00µl
RNase Inhibitor, 20 U/µl	0.13µl
Nuclease-free water	2.78µl
Total Volume	4.68µl

* Each 10µl RT reaction consists of 4.68µl master mix, 2.0µl of 5× RT primer, and 3.3µl RNA sample.

The components were mixed gently and centrifuged to bring solution to the bottom of the tube. The RT master mix was then placed on ice until the RNA reaction was prepared.

The 5× RT primer and RNA template was thawed on ice. The RT primer tubes were then vortexed to mix and then briefly centrifuged. For each 10µl RT reaction, the RT master mix was combined with 10ng of total RNA in the ratio of 4.68µl RT master mix : 3.3µl total RNA. The mixture was then mixed gently and gently centrifuged briefly to bring the solution to the bottom of the tube. 2.0µl of RT primer from each assay set was added to the corresponding RT reaction tube. The reaction tube was sealed and mixed gently, followed by a brief centrifugation. The reactions were incubated on ice for 5 minutes and then loaded into the thermal cycler, and run according to the following conditions:

Table 3.15: Thermal cycler conditions for cDNA synthesis

Time	Temperature
30 minutes	16°C
30 minutes	42°C
5 minutes	85°C
∞	4°C

Quantitative PCR (qPCR) amplification was then carried out. The following components were placed on ice and gently mixed. The volumes required, based upon the number of reactions and a reaction volume of 20µl, was calculated.

Table 3.16: Components used to prepare qPCR master mix

Component	Master mix volume per 10µl reaction
TaqMan [®] Fast Advanced PCR Master Mix	5.00µl
Nuclease-free water	3.84µl
TaqMan [®] MicroRNA Assay (20)	0.50µl
Product from RT reaction	0.67µl
Total Volume	10.01µl

The reaction components were combined in a microcentrifuge tube and gently mixed by inversion and then centrifugation. 10µl was transferred into low-profile microcentrifuge tubes and the tubes were sealed and briefly centrifuged. The reactions were then loaded into the real-time PCR instrument, and run according to the following conditions:

Table 3.17: Real-time PCR instrument conditions for qPCR.

Step	Optional AmpErase UNG Activity	Enzyme Activation	PCR	
	HOLD	HOLD	CYCLE (40 Cycles)	
			Denature	Anneal/Extend
Temperature	50°C	95°C	95°C	60°C
Time	2 minutes	10 minutes	15 seconds	60 seconds

3.17 Bioinformatic Analyses of MiRNA Gene Targets

An *in silico* approach was used to identify the putative miRNA targets by using TargetScan Human v5.2 (Lewis *et al*, 2005) (Whitehead Institute for Biomedical Research, USA), the database of conserved 3'UTR miRNA targets, found at <http://www.targetscan.org/>. Gene-annotation enrichment analyses of the predicted miRNA targets, with total context scores below 0, were then performed using the web tool Database for Annotation, Visualization and Integrated Discovery (DAVID) v6.7 (Huang *et al*, 2009) (SAIC-Frederick, Inc., USA) at <http://david.abcc.ncifcrf.gov/summary.jsp>, using default parameters.

3.18 Statistical Analysis

All experiments were performed in triplicate independent experiments. All data were presented as mean \pm standard deviation (SD). Student's t-test was used to determine the statistical significance of results, where a *p*-value of ≤ 0.05 was considered significant. Pearson's correlation coefficient (*r*) value was used to determine the association between miRNA microarray and qRT-PCR data.

CHAPTER 4: RESULTS

4.1 Selection Process of siRNA 1, 2 & 3

4.1.1 siRNA Silencing Of *Bcl-xL*

4.1.1.1 siRNA Targets on *Bcl-xL* mRNA

The expression of *Bcl-xL* in A549 cells was transiently silenced through the transfection of Stealth RNAi™ siRNA Duplex Oligonucleotides. Using a set of three siRNAs, the siRNAs were compared to determine which siRNA had the greatest silencing efficiency in A549 cells.

Table 4.1: Hybridization sites of the Stealth RNAi™ siRNA Duplex Oligonucleotides on *bcl-xL* mRNA.

	siRNA Sequences	Target Site on <i>Bcl-xL</i> (nucleotide number)
siRNA 1	(RNA) – UCACUAAACUGACUCCAGCUGUAUC	452...5' –TCACTAAACTGACTCCAGCTGTATC–3' ...428
siRNA 2	(RNA) – AUGGGUUGCCAUUGAUGGCACUGGC	532...5' –ATGGGTTGCCATTGATGGCACTGGG–3' ...508
siRNA 3	(RNA) – AUCACCUCCTCCGGGCAUCCAAACUGC	608...5' –ATCACCTCCCGGGCATCCAAACTGC–3' ...584

The *bcl-xL* gene sequence (ascension number NM_138578) was taken from the National Center for Biotechnology Information (NCBI) (http://www.ncbi.nlm.nih.gov/gene?term=NM_138578). The hybridization site of the siRNA oligonucleotides on *Bcl-xL* mRNA was determined using the Basic Local Alignment Search Tool (BLAST) search algorithm from the NCBI website (<http://blast.ncbi.nlm.nih.gov/Blast.cgi>). The sequence identity of all three siRNAs to the *Bcl-xL* mRNA was 100%.

4.1.1.2 siRNA Transfection Efficiency in A549 Cells

As the siRNA utilized do not fluoresce, A549 cells were transfected with BLOCK-iT Alexa Fluor Red Fluorescent Oligo to determine the transfection efficiency of the experimental siRNA (Figure 4.2, Figure 4.3, & Figure 4.4). BLOCK-iTTM Alexa Fluor[®] Red Fluorescent Oligo is a highly stable, fluorescein-labeled, non-targeted dsRNA compound that allows for visual monitoring of transfection efficiency. After 24 hours, transfection efficiency was assessed by visualizing uptake of BLOCK-iTTM Alexa Fluor[®] Red Fluorescent Oligo using fluorescence microscopy. This transfection control was carried out for each set of siRNA. The percentage of transfection efficiency shown is a representative of mean values from independent triplicate experiments with mean \pm S.D. The complete transfection efficiency data for each transfection condition are shown in Appendix 4.

As shown in Figures 4.2A-C, the siRNA 1 set of A549 cells transfected with 100nM of BLOCK-iTTM Alexa Fluor[®] Red Fluorescent Oligo showed a transfection efficiency of $87.1\% \pm 6.5\%$, while the transfection control for siRNA 2 and 3 had a transfection efficiency of $77.4\% \pm 10.9\%$ and $84.9\% \pm 3.7\%$, respectively. Cells that were not transfected with any siRNAs or BLOCK-iTTM Alexa Fluor[®] Red Fluorescent Oligo had a transfection efficiency of 0% (Figure. 4.1). All three siRNA sets had a

transfection efficiency of 70% or higher thus allowing for the experiment to proceed to determine which of the three siRNA sets had the greatest silencing efficiency.

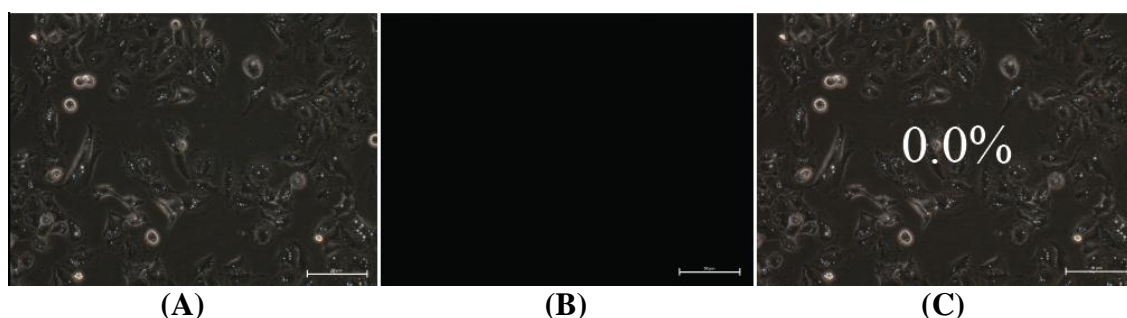


Figure 4.1: Determination of transfection efficiency in non-transfected A549 cells. (A) Phase-contrast image of non-transfected A549 cells. (B) Fluorescent image of non-transfected A549 cells. (C) Merged image of non-transfected A549 cells. Percentage of mean transfection efficiency is indicated, and image shown are representative of triplicates independent experiments.

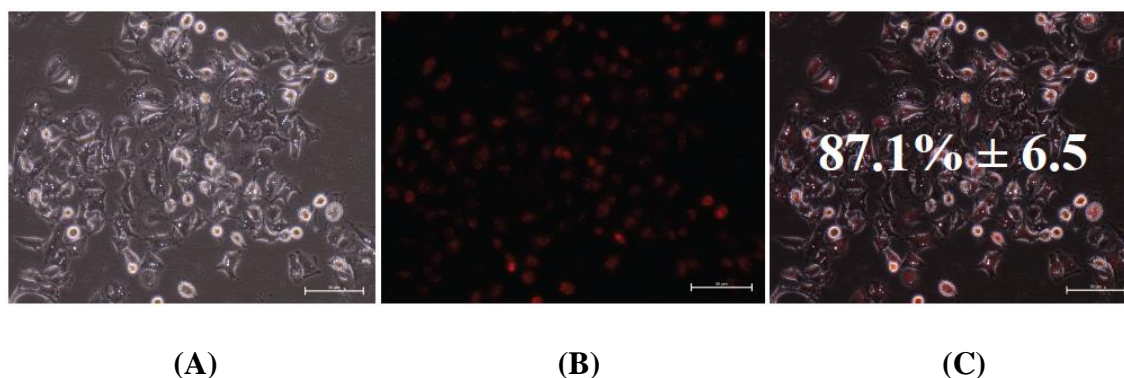


Figure 4.2: Determination of transfection efficiency in siRNA 1 transfected A549 cells. (A) Phase-contrast image of siRNA 1 A549 cells transfected with BLOCK-iT™ Alexa Fluor® Red Fluorescent Oligo. (B) Fluorescent image of siRNA 1 A549 cells transfected with BLOCK-iT™ Alexa Fluor® Red Fluorescent Oligo. (C) Merged image of siRNA 1 A549 cells transfected with BLOCK-iT™ Alexa Fluor® Red Fluorescent Oligo. Percentage of mean transfection efficiency is indicated, and image shown are representative of triplicates independent experiments.

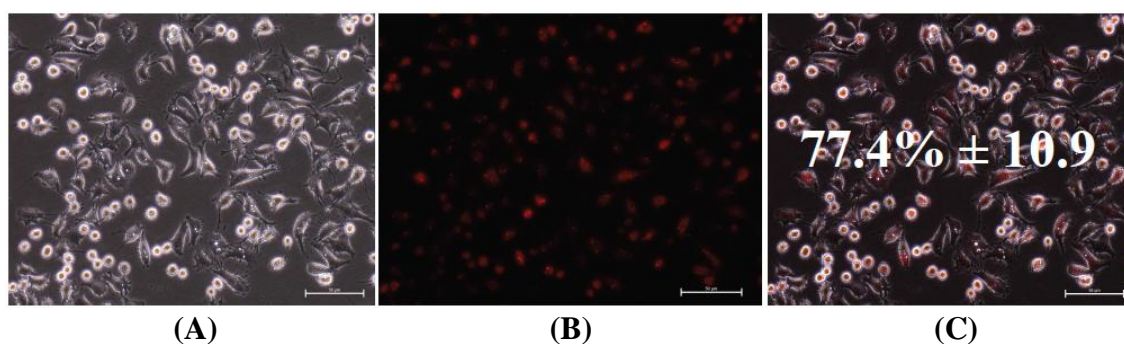


Figure 4.3: Determination of transfection efficiency in siRNA 2 transfected A549 cells.

(A) Phase-contrast image of siRNA 2 A549 cells transfected with BLOCK-iT™ Alexa Fluor® Red Fluorescent Oligo. (B) Fluorescent image of siRNA 2 A549 cells transfected with BLOCK-iT™ Alexa Fluor® Red Fluorescent Oligo. (C) Merged image of siRNA 2 A549 cells transfected with BLOCK-iT™ Alexa Fluor® Red Fluorescent Oligo. Percentage of mean transfection efficiency is indicated, and image shown are representative of triplicates independent experiments.

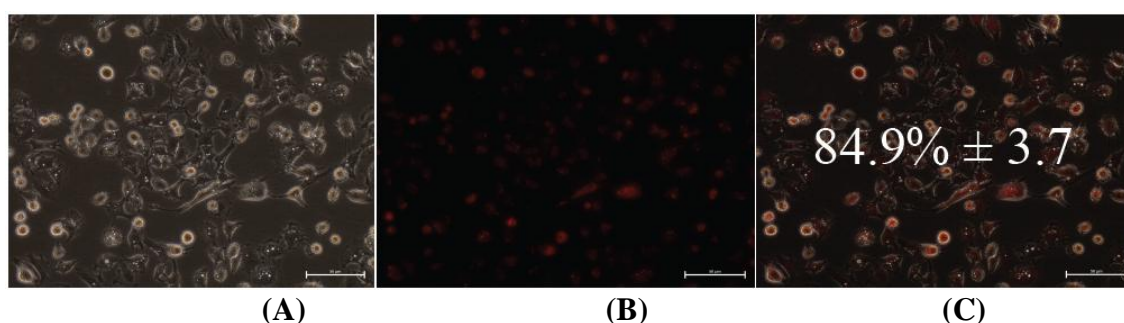


Figure 4.4: Determination of transfection efficiency in siRNA 3 transfected A549 cells.

(A) Phase-contrast image of siRNA 3 A549 cells transfected with BLOCK-iT™ Alexa Fluor® Red Fluorescent Oligo. (B) Fluorescent image of siRNA 3 A549 cells transfected with BLOCK-iT™ Alexa Fluor® Red Fluorescent Oligo. (C) Merged image of siRNA 3 A549 cells transfected with BLOCK-iT™ Alexa Fluor® Red Fluorescent Oligo. Percentage of mean transfection efficiency is indicated, and image shown are representative of triplicates independent experiments.

4.1.2 RNA Extraction

4.1.2.1 RNA Quantification Via Spectrophotometry Readings

Upon visual confirmation of siRNA uptake into A549 cells, total RNA was extracted from siRNA-transfected and non-transfected A549 cells to determine the silencing efficiency of each siRNA set. Spectrophotometric readings of the RNA sample were taken to determine the purity and RNA concentration of the samples. The ratio of the readings at 260nm and 280nm (A_{260}/A_{280}) was an estimation of the purity of RNA with respect to contaminants that absorb in the UV spectrum. When measuring RNA in a buffered solution (10nM Tris-HCl (pH 8.7.5)), pure RNA had an A_{260}/A_{280} ratio between 1.8-2.0. A ratio below 1.8 indicated samples contaminated with organic solvents. Based on Table 4.2, it can be seen that all RNA samples extracted from the A549 cells were pure RNA samples that did not contain any contaminants.

Table 4.2: Spectrophotometric quantification of total RNA extracted from siRNA-transfected and non-transfected A549 cells.

Sample	$\mu\text{g/ml}$	A_{260}/A_{280}	A_{260}	RNA Concentration ($\mu\text{g/ml}$)	Total RNA (μg)
siRNA 1	0.982	1.95	0.491	982	49.1
siRNA 2	0.860	1.94	0.430	860	43.0
siRNA 3	0.293	1.79	0.146	292	14.6
Hi GC NC [†]	0.763	1.65	0.382	794	39.7
Lo GC NC [‡]	0.843	1.80	0.422	844	42.2
NTC [†]	0.606	1.96	0.303	606	30.3

[†] Hi GC NC denotes cells transfected with high GC content negative controls

[‡] Lo GC NC denotes cells transfected with low GC content negative controls

NTC denotes non-transfected cells

4.1.2.2 Agarose Gel Electrophoresis

Agarose gel electrophoresis and ethidium bromide staining evaluated the integrity and size distribution of total RNA. Intact total RNA run on a denaturing gel had sharp, clear 28S and 18S ribosomal RNA (rRNA) bands. The 28S rRNA band was approximately twice as intense as the 18S rRNA band. This 2:1 ratio (28S: 18S) was a good indication that the RNA is completely intact. As the rRNA bands in Figure 4.5 have a 2:1 ratio, it was concluded that the RNA samples are intact and can be used for further downstream work.

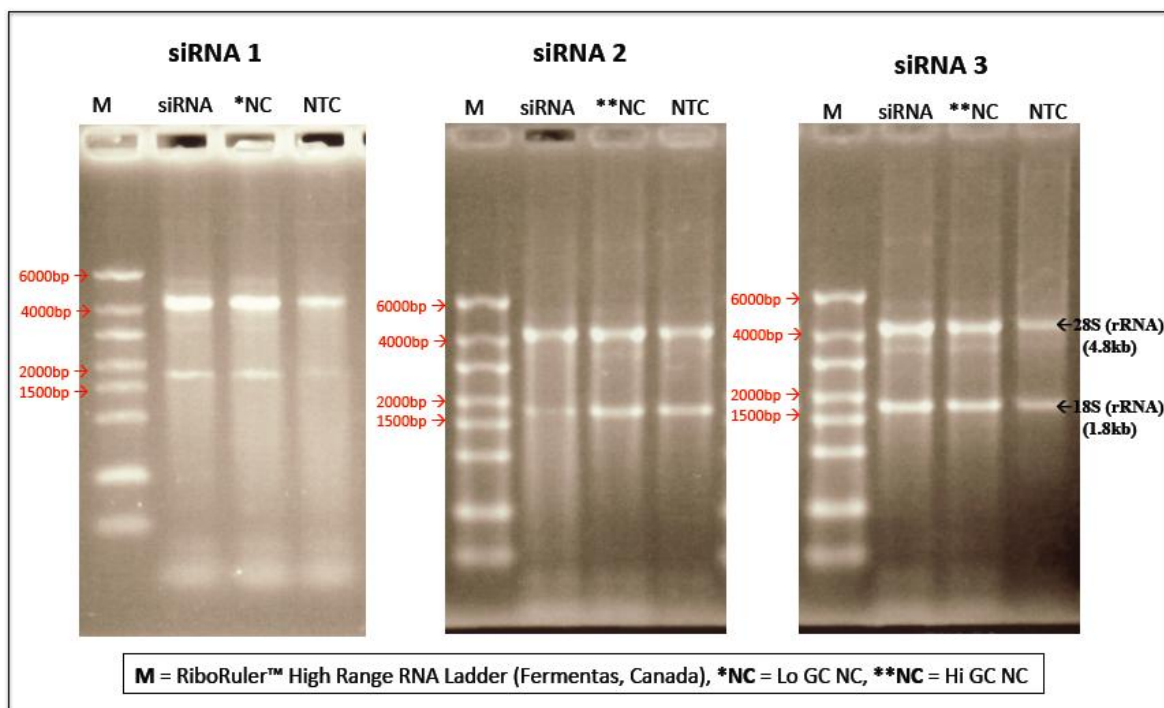


Figure 4.5: Agarose gel electrophoresis image for the total RNA extraction of siRNA 1, 2, and 3 transfected and non-transfected A549 cells.

4.1.3 Protein Extraction

4.1.3.1 Bradford Assay Protein Quantification

The Bradford protein assay is a spectroscopic analytical procedure used to measure the concentration of protein in a solution. This assay is based on an absorbance shift of the dye Coomassie Brilliant Blue G-250, in which under acidic conditions the red form of the dye is converted into its bluer form to bind to the protein being assayed. The binding of protein stabilizes the blue form of the Coomassie dye; thus the amount of the complex present in solution is a measure for the protein concentration, and can be estimated by the use of an absorbance reading.

The bound form of the dye has an absorption spectrum held at 595nm. The increase in absorbance at 595nm is proportional to the amount of bound dye, and thus to the amount of protein (concentration) present in the sample.

Table 4.3: Spectrophotometric quantification of protein using Bradford Assay.

siRNA	Sample	µg/mL	A ₅₉₅
1	siRNA	1827.5	0.892
	Lo GC NC [‡]	1532.7	0.755
	NTC [†]	1314.3	0.653
2	siRNA	2419.5	1.167
	Hi GC NC [†]	2310.5	1.116
	NTC [†]	2114.2	1.025
3	siRNA	2070.5	1.005
	Hi GC NC [†]	202.51	0.984
	NTC [†]	1626.3	0.798

[†] Hi GC NC denotes cells transfected with high GC content negative controls

[‡] Lo GC NC denotes cells transfected with low GC content negative controls

NTC denotes non-transfected cells

4.1.4 Quantitative Real-Time Reverse Transcribe PCR (qRT-PCR)

4.1.4.1 Determination of PCR Amplification Efficiencies

To determine the silencing efficiency of siRNA, quantitative real-time RT-PCR (qRT-PCR) was performed to allow for the evaluation of the *bcl-xL* expression in siRNA-transfected and non-transfected A549 cells. Real-time PCR amplification efficiencies and linearity was first determined through the generation of standard curves. The real-time PCR efficiencies were calculated from the given slopes generated by the Bio-Rad CFX Manager™ Software v1.6 (Bio-Rad Laboratories, USA). The corresponding real-time PCR efficiency (E) of one cycle in the exponential phase was calculated according to the equation: $E = 10^{-1/\text{slope}}$. Figure 4.6 indicated that the real-time PCR efficiency for *bcl-xL* primers was 110.0%, while β -actin had an efficiency of 106.3% (Figure 4.7).

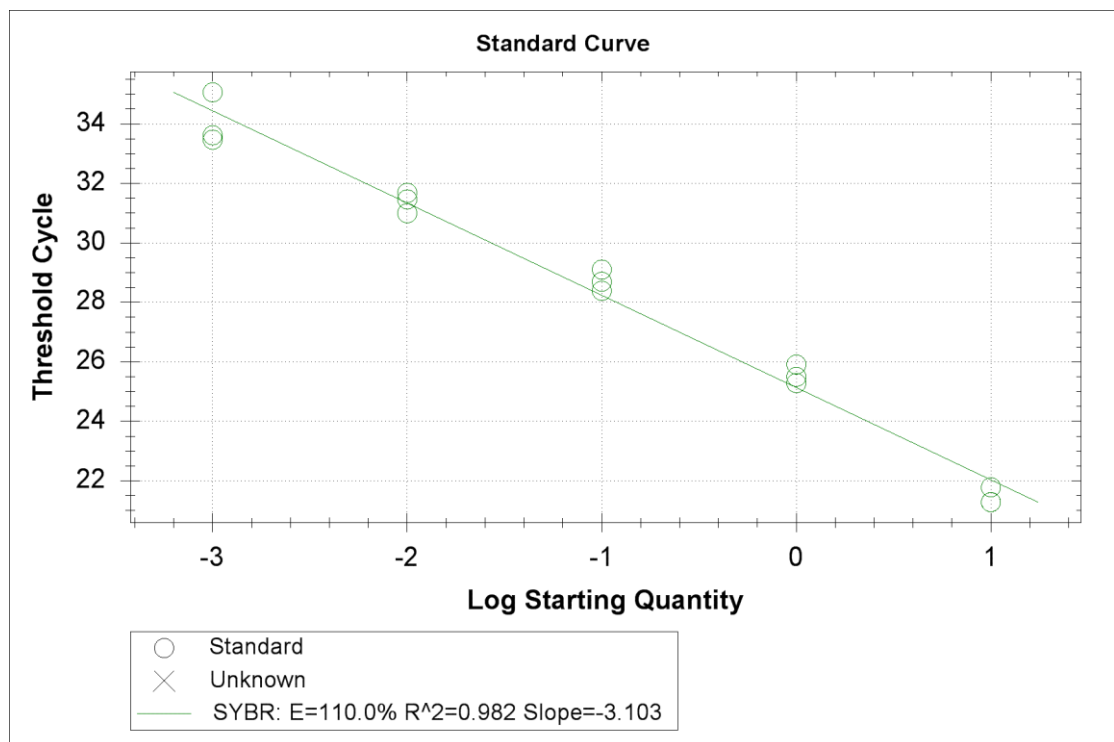


Figure 4.6: Standard curve generated for *bcl-xL* standards had an efficiency of 2.10.

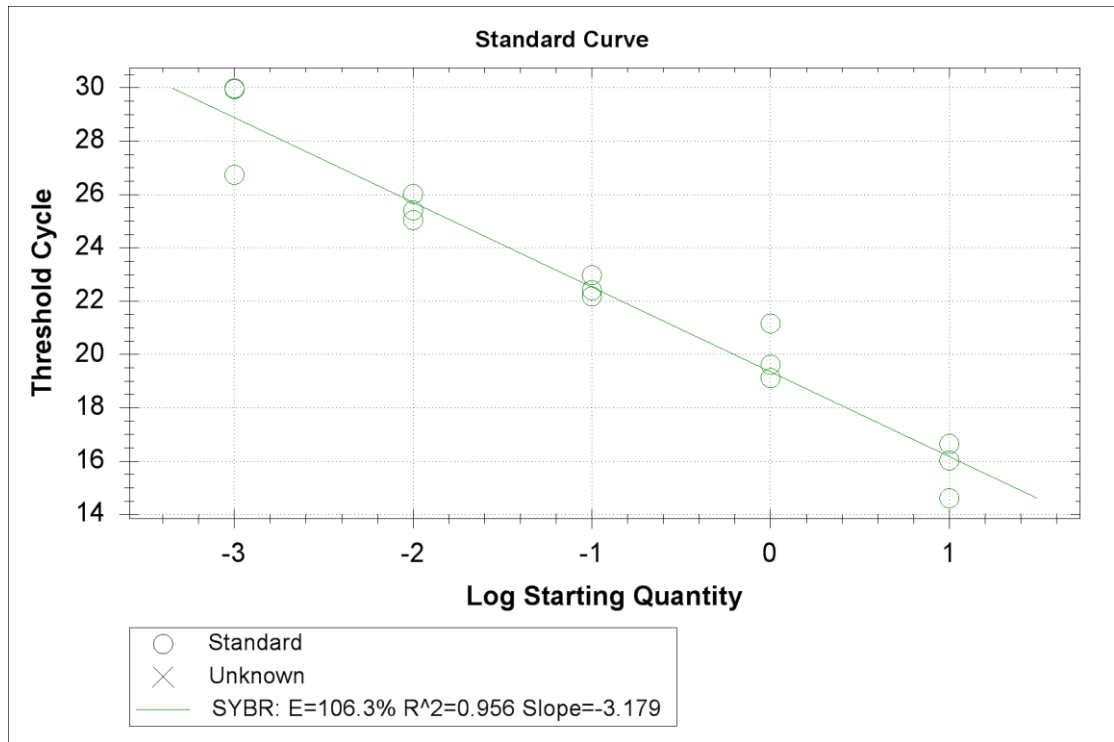


Figure 4.7: Standard curve generated for β -actin standards had an efficiency of 2.06.

4.1.4.2 Evaluation of *Bcl-xL* Gene Expression

After normalization to endogenous β -actin mRNA expression, the expression of *bcl-xL* in siRNA-transfected A549 cells were expressed in comparison to the levels observed in non-transfected cells. All experiments were carried out in triplicates and represented as \pm S.D. Results indicated that *bcl-xL* expression levels were lower for all siRNA transfected A549 cells in comparison to non-transfected cells (Figure 4.8). The fold change in the *bcl-xL* expression in siRNA-transfected and non-transfected cells was calculated using the Pfaffl method (Pfaffl, 2001):

$$\text{Fold change} = \frac{(\text{Efficiency}_{\text{Target}})^{\Delta\text{Ct Target}(\text{Control}-\text{Treated})}}{(\text{Efficiency}_{\text{Reference}})^{\Delta\text{Ct Reference}(\text{Control}-\text{Treated})}}$$

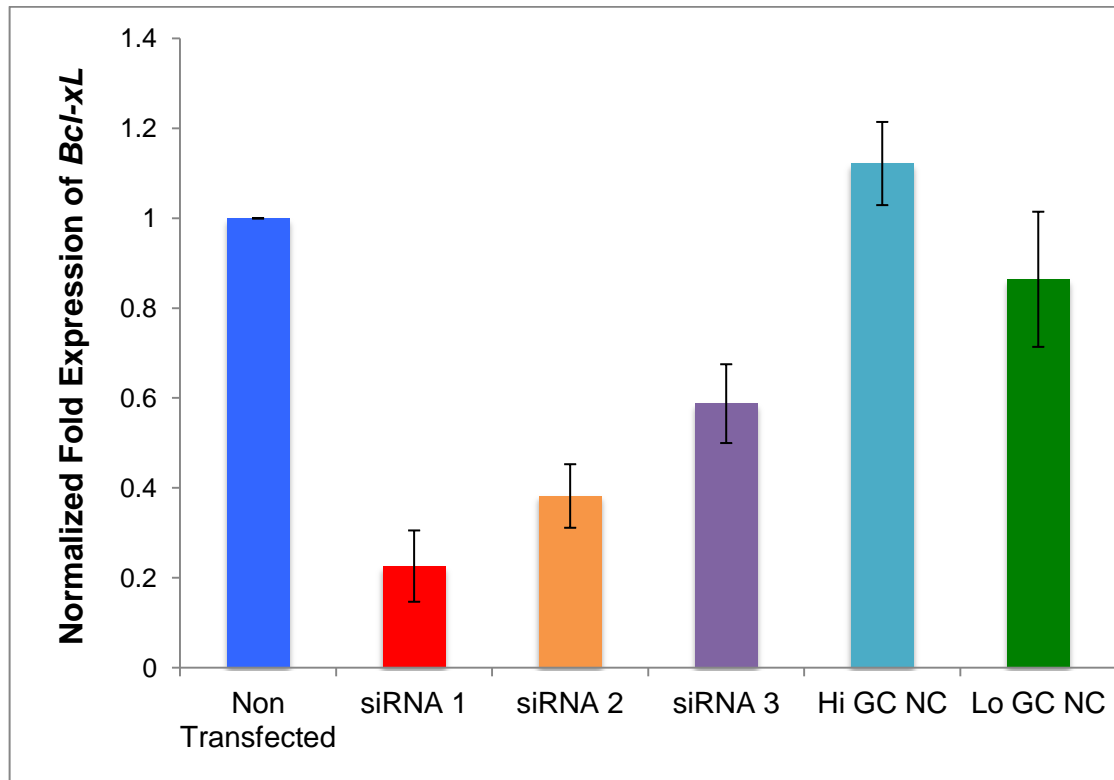


Figure 4.8: Quantitative real-time RT-PCR analysis of *bcl-xL* expression in siRNA-transfected and non-transfected A549 cells. All experiments were carried out in triplicates, and presented as mean \pm SD.

Table 4.4: Fold-change in *bcl-xL* gene expression in siRNA-transfected A549 cells as compared to non-transfected A549 cells ($p \leq 0.005$).

Sample	Fold Change* \pm SD	<i>p</i> -Value
siRNA 1	-4.42 \pm 0.079	0.009
siRNA 2	-2.62 \pm 0.071	0.003
siRNA 3	-1.70 \pm 0.088	0.013
Hi GC NC [†]	1.22 \pm 0.093	0.025
Lo GC NC [‡]	-1.16 \pm 0.150	0.013

*Positive values denote up-regulation while negative values denote downregulation.

[†] Hi GC NC denotes cells transfected with high GC content negative controls

[‡] Lo GC NC denotes cells transfected with low GC content negative controls

Table 4.5: Percentage of *Bcl-xL* gene knockdown in siRNA-transfected A549 cells as compared to non-transfected A549 cells.

Sample	% Knockdown \pm SD
siRNA 1	75.19 \pm 8.32
siRNA 2	55.52 \pm 4.32
siRNA 3	39.29 \pm 8.58
Hi GC NC [†]	-19.96 \pm 8.80
Lo GC NC [‡]	13.52 \pm 14.08

[†] Hi GC NC denotes cells transfected with high GC content negative controls

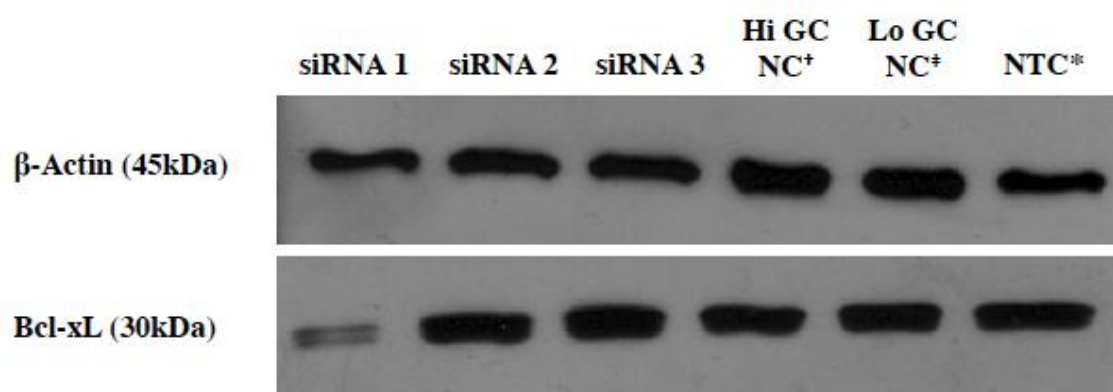
[‡] Lo GC NC denotes cells transfected with low GC content negative controls

As shown in Table 4.4, siRNA 1 had the highest negative fold induction at 4.42; followed by siRNA 2 and 3 with negative fold change of 2.62 and 1.70 respectively. The percentage of gene knockdown was also calculated (Table 4.5.) and results indicated that siRNA 1 had the greatest percentage of knockdown, with 75.19 \pm 8.32%, followed by siRNA 2 and 3 with a knockdown percentage of 55.52 \pm 4.23% and 39.29 \pm 8.58%, respectively. As siRNA 1 had the greatest *bcl-xL* gene knockdown, it was concluded that siRNA had the greatest silencing efficiency and was chosen to be used for further downstream work. As the SYBR Green dye was used to detect PCR product, the primer specificity was confirmed using a melting curve analysis as shown in Appendix 5.

4.1.5 Western Blot

Western blot was then carried out to further measure the total Bcl-xL protein levels following the transfection experiment. The relative level of Bcl-xL protein in siRNA-transfected and non-transfected A549 cells was quantified through densitometry, using the ImageJ Analyst software (National Institute of Mental Health, USA), with each band being normalized to β -actin. Figure 4.9 shows that the Bcl-xL protein level was significantly decreased in A549 cells transfected with siRNA set 1, in comparison

to the Bcl-xL protein levels in non-transfected A549 cells. Densitometry analysis of the bands illustrated that cells transfected with siRNA 1 had $28.33 \pm 6.79\%$ Bcl-xL protein level in comparison to the $100.00 \pm 0.48\%$ protein level in non-transfected cells. Bcl-xL protein levels in cells transfected with siRNA 2 and 3 had proteins levels of $82.01 \pm 1.56\%$ and $84.77 \pm 2.16\%$ respectively.



[†] Hi GC NC denotes cells transfected with high GC content negative controls

[‡] Lo GC NC denotes cells transfected with low GC content negative controls

^{*} NTC denotes non-transfected cells

Figure 4.9: Indication of significantly decreased Bcl-xL (30-kDa) protein levels in A549 cells transfected with siRNA 1. β-actin (45-kDa) was used as a normalization control to ensure equal protein concentrations across samples.

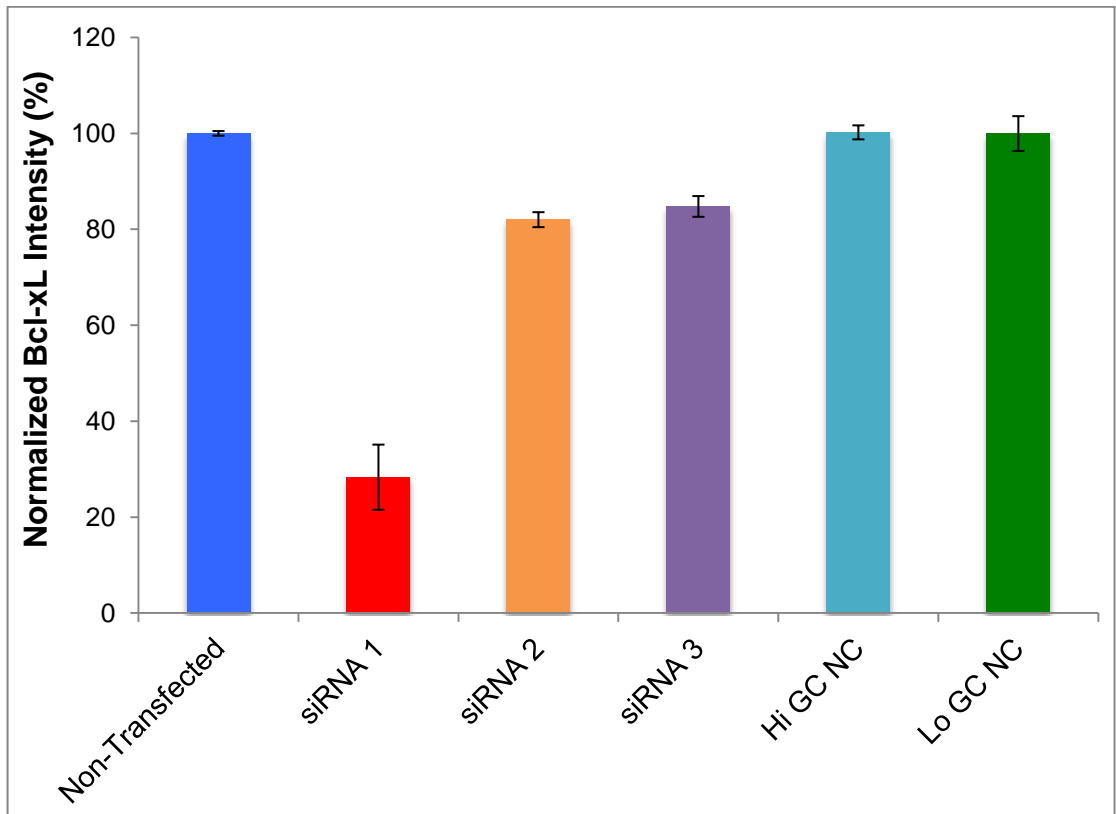


Figure 4.10. Densitometry analysis of the Western blots using the ImageJ Analyst software. The results were standardized against the levels of β -actin and are presented as normalized intensities. All experiments were carried out in triplicates, and presented as mean \pm SD.

Table 4.6: Densitometry analysis of the Western blots was carried out using the ImageJ Analyst software.

Sample	Bcl-xL Protein Level (%) \pm SD	<i>p</i> -Value
siRNA 1	28.33 \pm 6.79	0.0001
siRNA 2	82.01 \pm 1.56	0.0003
siRNA 3	84.77 \pm 2.16	0.0031
Hi GC NC [†]	99.96 \pm 1.46	0.4761
Lo GC NC [‡]	100.21 \pm 3.63	0.4687
NTC [*]	100.00 \pm 0.48	0.0001

[†] Hi GC NC denotes cells transfected with high GC content negative controls

[‡] Lo GC NC denotes cells transfected with low GC content negative controls

^{*} NTC denotes non-transfected cells

4.2 A549 Transfection With siRNA 1

Once it was determined that siRNA 1 had the greatest silencing efficiency in A549 cells amongst the three siRNAs used, A549 cells were once again transfected with siRNA in triplicates for use in miRNA microarray.

4.2.1 *Bcl-xL* Silencing Using siRNA 1

4.2.1.1 siRNA transfection efficiency in A459 cells

The percentage of transfection efficiency shown is a representative of mean values from independent triplicate experiments with mean \pm S.D. The complete transfection efficiency data for each transfection condition are shown in Appendix 4. As shown in Figures 4.11 – 4.13, all biological replicates had a transfection efficiency of 70% or higher, thus allowing for the experiment to proceed for confirmation of efficient silencing efficiency.

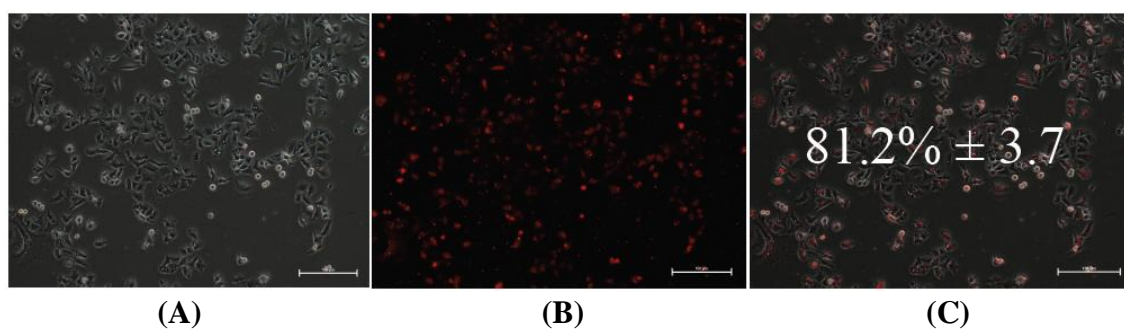


Figure 4.11: Determination of transfection efficiency in siRNA 1 biological replicate 1 transfected A549 cells. (A) Phase-contrast image of siRNA 1 biological replicate 1 A549 cells transfected with BLOCK-iT™ Alexa Fluor® Red Fluorescent Oligo. (B) Fluorescent image of siRNA 1 biological replicate 1 A549 cells transfected with BLOCK-iT™ Alexa Fluor® Red Fluorescent Oligo. (C) Merged image of siRNA 1 biological replicate 1 A549 cells transfected with BLOCK-iT™ Alexa Fluor® Red Fluorescent Oligo had a transfection efficiency of $81.2\% \pm 3.57\%$. Image shown are representative of triplicates independent experiments.

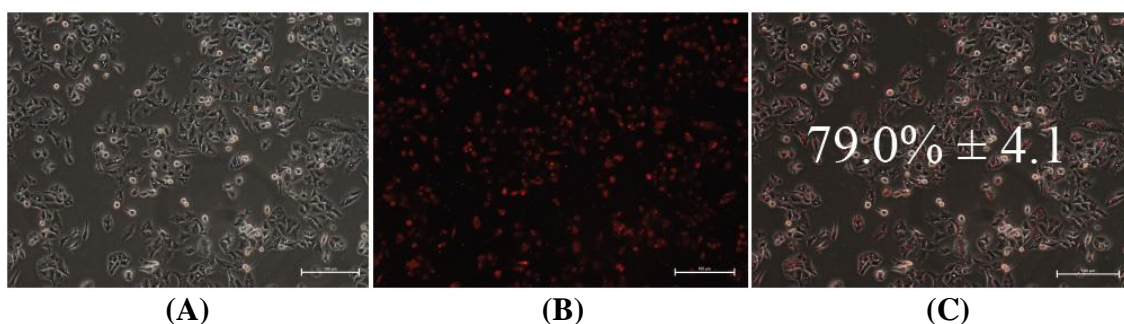


Figure 4.12: Determination of transfection efficiency in siRNA 1 biological replicate 2 transfected A549 cells. (A) Phase-contrast image of siRNA 1 biological replicate 2 A549 cells transfected with BLOCK-iT™ Alexa Fluor® Red Fluorescent Oligo. (B) Fluorescent image of siRNA 1 biological replicate 2 A549 cells transfected with BLOCK-iT™ Alexa Fluor® Red Fluorescent Oligo. (C) Merged image of siRNA 1 biological replicate 2 A549 cells transfected with BLOCK-iT™ Alexa Fluor® Red Fluorescent Oligo had a transfection efficiency of $79.0\% \pm 4.17\%$. Image shown are representative of triplicates independent experiments.

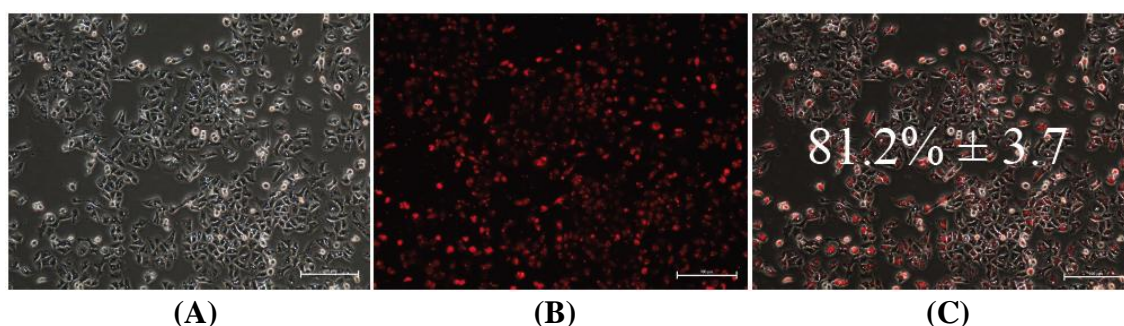


Figure 4.13: Determination of transfection efficiency in siRNA 1 biological replicate 3 transfected A549 cells. **(A)** Phase-contrast image of siRNA 1 biological replicate 3 A549 cells transfected with BLOCK-iT™ Alexa Fluor® Red Fluorescent Oligo. **(B)** Fluorescent image of siRNA 1 biological replicate 3 A549 cells transfected with BLOCK-iT™ Alexa Fluor® Red Fluorescent Oligo. **(C)** Merged image of siRNA 1 biological replicate 3 A549 cells transfected with BLOCK-iT™ Alexa Fluor® Red Fluorescent Oligo had a transfection efficiency of $81.2\% \pm 3.7\%$. Image shown are representative of triplicates independent experiments.

4.2.2 RNA Extraction

4.2.2.1 RNA Quantification Via NanoDrop

Table 4.7: Spectrophotometric quantification of total RNA extracted from siRNA 1 transfected and non-transfected cells.

Biological Replicate	Sample	Concentration (ng/ μ l)	A ₂₆₀	A ₂₈₀	A _{260/280}	A _{260/230}
1	siRNA	408.8	10.221	5.294	1.93	1.55
	Lo GC NC [†]	362.0	9.051	4.680	1.93	1.30
	NTC [‡]	442.2	11.054	5.749	1.92	1.85
2	siRNA	327.2	8.180	4.273	1.91	1.86
	Lo GC NC [†]	175.0	4.375	2.339	1.87	1.74
	NTC [‡]	181.2	4.529	2.391	1.89	3.60
3	siRNA	258.0	6.449	3.344	1.93	1.96
	Lo GC NC [†]	226.9	5.672	2.998	1.89	2.08
	NTC [‡]	490.9	12.272	6.339	1.94	2.16

[†] Lo GC NC denotes cells transfected with low GC content negative controls

[‡] NTC denotes non-transfected cells

4.2.2.2 Agarose Gel Electrophoresis

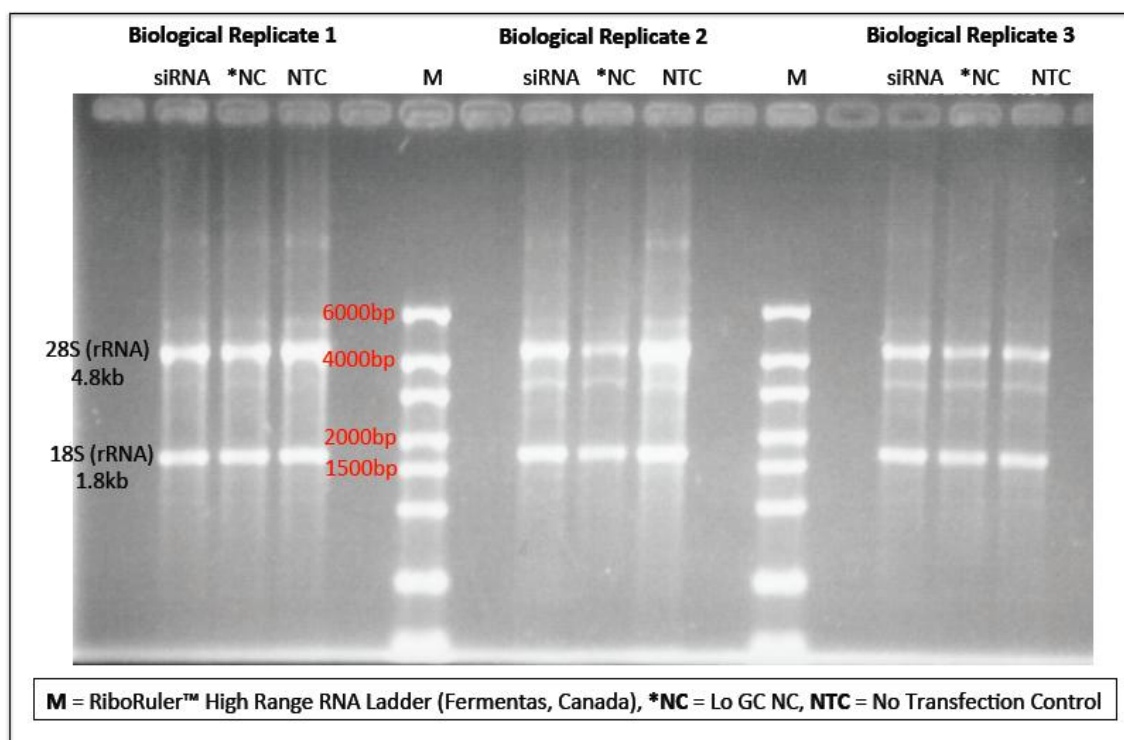


Figure 4.14: Agarose gel electrophoresis image for the total RNA extraction of siRNA 1 transfected and non-transfected A549 cells.

4.2.2.3 Quality Check Of Extracted Total RNA Using Agilent 2100 BioAnalyzer

The quality of the extracted total RNA samples were evaluated using the Agilent 2100 BioAnalyzer prior to running qRT-PCR and miRNA microarray. Analysis using the BioAnalyzer allows for an evaluation of the total RNA samples to ensure that all samples had acceptable levels of concentration, integrity and purity, in order to increase the accuracy of miRNA expression profiles in siRNA-transfected and non-transfected cells.

The RNA integrity number (RIN value) was also determined. The RIN software algorithm allows for the classification of total RNA based on a numbering system from 1 to 10, with 1 being the most degraded profile and 10 being the most intact. Figure

4.15 shows the nano gel image of total RNA samples, while the RIN, rRNA ratio and RNA concentration data of all replicates and samples types are summarized in Table 4.8. RIN of all samples were maintained between 9.0 and 10.0, where samples with RIN below 9.0 were discarded due to low RNA integrity levels (Table 4.8). All replicates were transfected and extracted independently of one another and at varying time points to ensure statistical significance.

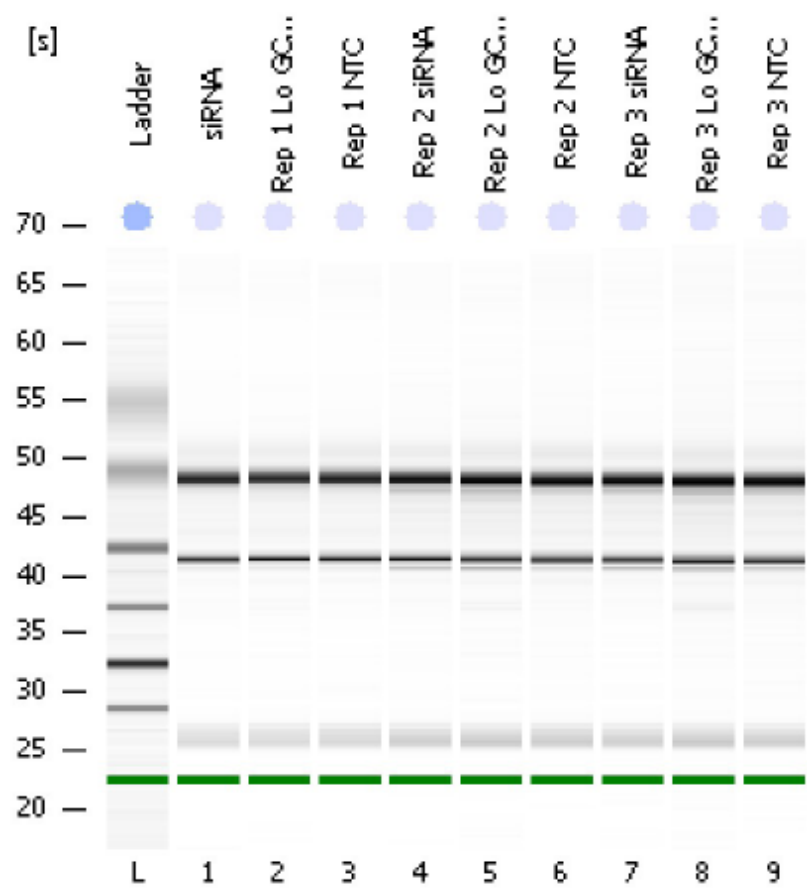


Figure 4.15: Total RNA Nano Agilent BioAnalyzer gel image of total RNA triplicate samples extracted from siRNA 1 transfected and non-transfected A549 cells.

Table 4.8: RNA integrity number (RIN value) was determined using the Agilent 2100 BioAnalyzer.

Biological Replicate	Sample	RNA Concentration (µg/µl)	RIN Value	rRNA Ratio [28s/18s]
1	siRNA	469.0	9.60	1.9
	Lo GC NC [†]	400.0	9.60	1.9
	NTC [‡]	660.0	9.60	1.8
2	siRNA	240.0	9.50	2.2
	Lo GC NC [†]	171.6	8.80	1.5
	NTC [‡]	193.9	9.50	2.2
3	siRNA	371.0	9.40	2.1
	Lo GC NC [†]	317.0	9.40	2.0
	NTC [‡]	306.4	9.60	2.1

[†] Lo GC NC denotes cells transfected with low GC content negative controls

[‡] NTC denotes non-transfected cells

4.2.3 Protein Extraction

4.2.3.1 Bradford Assay Protein Quantification

Table 4.9: Spectrophotometric quantification of protein using Bradford Assay.

Biological Replicate	Sample	Protein Concentration (µg/ml)	A ₅₉₅
1	siRNA	1945.000	0.172
	Lo GC NC [†]	1121.343	0.120
	NTC [‡]	1935.751	0.170
2	siRNA	1873.882	0.166
	Lo GC NC [†]	784.540	0.099
	NTC [‡]	1599.024	0.149
3	siRNA	1645.066	0.152
	Lo GC NC [†]	1604.805	0.149
	NTC [‡]	1542.621	0.146

[†] Lo GC NC denotes cells transfected with low GC content negative controls

[‡] NTC denotes non-transfected cells

4.2.4 Quantitative Real-Time Reverse Transcribe PCR (qRT-PCR)

4.2.4.1 Determination of PCR Amplification Efficiencies

Real-time PCR amplification efficiencies and linearity was determined through the generation of standard curves. The real-time PCR efficiencies were calculated from the given slopes in the Bio-Rad CFX Manager™ Software v1.6 (Bio-Rad Laboratories, USA). The corresponding real-time PCR (E) of one cycle in the exponential phase was calculated according to the equation: $E = 10^{-1/\text{slope}}$.

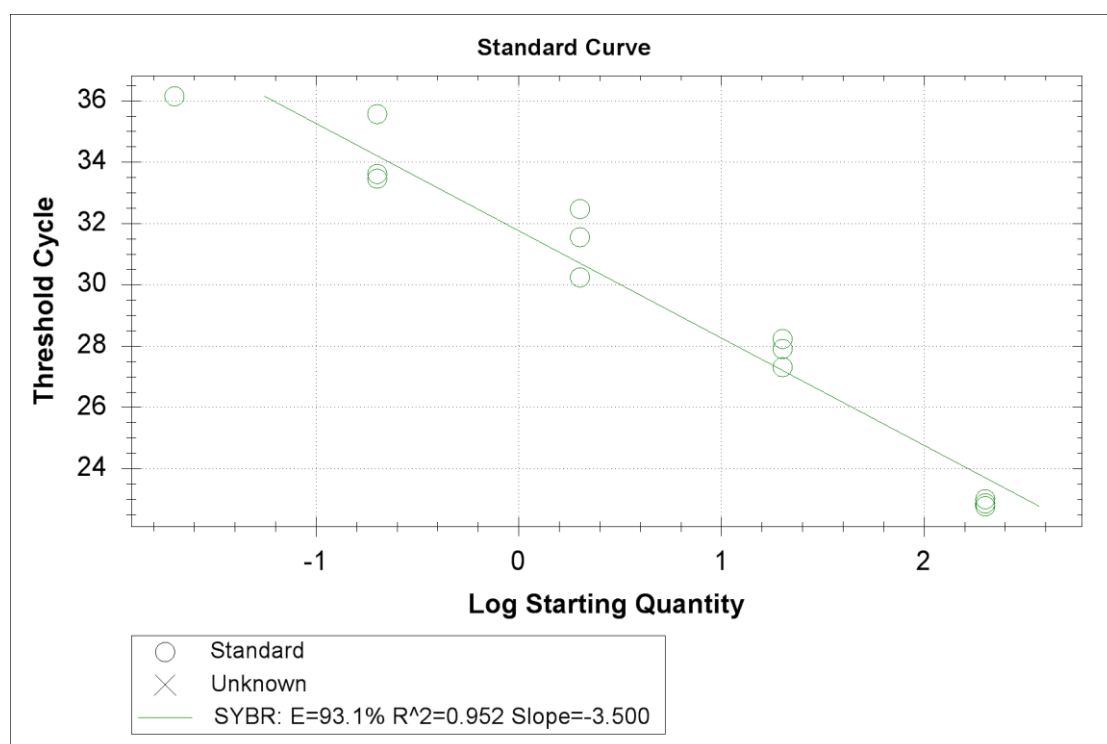


Figure 4.16: Standard curve generated for *bcl-xL* standards had an efficiency of 1.93.

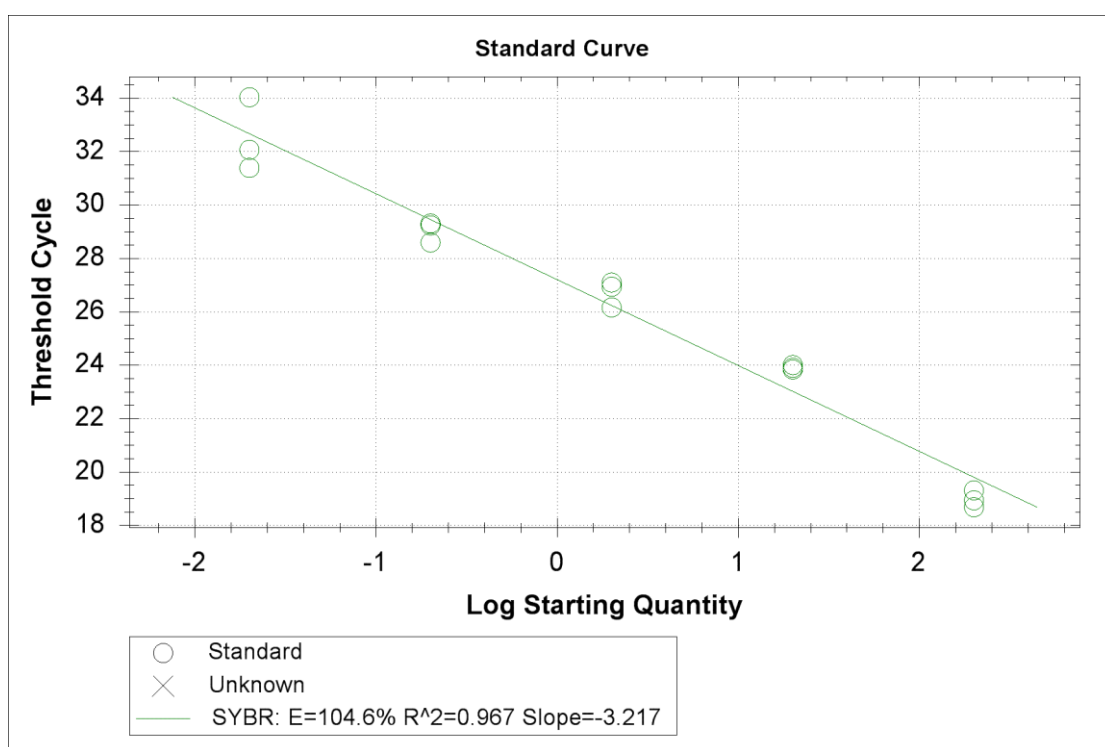


Figure 4.17: Standard curve generated for β -actin standards had an efficiency of 2.04.

4.2.4.2 Evaluation of *Bcl-xL* Gene Expression

After normalization to endogenous β -actin expression, the expression of *bcl-xL* in siRNA-transfected A549 cells was expressed in comparison to the levels observed in non-transfected cells. The *bcl-xL* gene expression levels were lower for siRNA-transfected A549 cells in comparison to the non-transfected cells. The fold change in the *bcl-xL* expression in transfected and non-transfected cells was calculated using the Pfaffl method.

As shown in Table 4.10, siRNA-transfected A549 cells had a significant negative fold induction of 6.15 ± 0.032 . The percentage of gene knockdown was also calculated (Table 4.11) and results indicated that siRNA-transfected A549 cells had a knockdown percentage of $79.90 \pm 3.67\%$. siRNA transfected A549 cells had significant knockdown of the *bcl-xL* gene allowing for the project to proceed to microRNA

microarray to determine the miRNA expression profile in siRNA-transfected and non-transfected A549 cells.

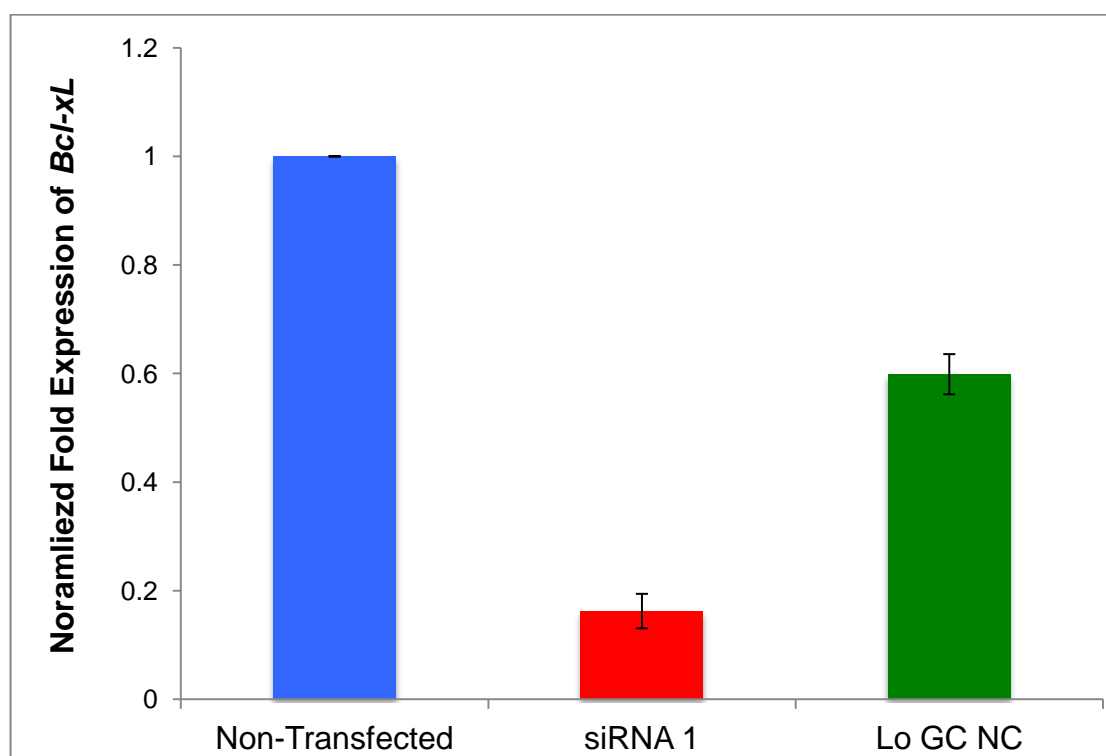


Figure 4.18: Quantitative real-time RT-PCR analysis for *Bcl-xL* expression in siRNA-transfected and non-transfected A549 cells. All experiments were carried out in triplicates, and presented as mean \pm SD.

Table 4.10: Fold-change in *bcl-xL* gene expression in siRNA-transfected A549 cells as compared to non-transfected A549 cells.

Sample	Fold Change [†] \pm SD	<i>p</i> -Value
siRNA	6.15 \pm 0.032	0.002
Lo GC NC [‡]	1.67 \pm 0.037	0.008

[†] Positive values denote up-regulation while negative values denote downregulation

[‡] Lo GC NC denotes cells transfected with low GC content negative controls

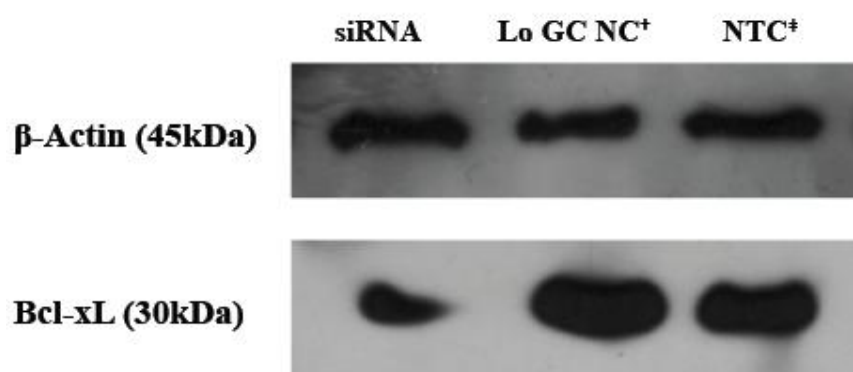
Table 4.11: Percentage of *Bcl-xL* gene knockdown in siRNA-transfected A549 cells as compared to non-transfected A549 cells.

Sample	% Knockdown \pm SD
siRNA	79.90 \pm 3.67
Lo GC NC [†]	22.00 \pm 4.32

[†] Lo GC NC denotes cells transfected with low GC content negative controls

4.2.5 Western Blot

Western blot was then carried out to further measure the total Bcl-xL protein levels following the transfection with siRNA 1. The relative level of Bcl-xL protein in siRNA-transfected and non-transfected A549 cells was quantified through densitometry, using the ImageJ Analyst software (National Institute of Mental Health), with each band being normalized to β -actin. Figure 4.19 shows that the Bcl-xL protein level was significantly decreased in A549 cells transfected with siRNA 1, in comparison to the Bcl-xL protein levels in non-transfected A549 cells. Densitometry analysis of the bands shows that cells transfected with siRNA 1 had $50.27 \pm 4.11\%$ Bcl-xL protein level in comparison to the $100.00 \pm 0.01\%$ protein level in non-transfected cells (Table 4.12).



[†] Lo GC NC denotes cells transfected with low GC content negative controls

[‡] NTC denotes non-transfected cells

Figure 4.19: Indication of significantly decreased Bcl-xL (30-kDa) protein levels in A549 cells transfected with siRNA 1. β -actin (45-kDa) was used as a normalization control to ensure equal protein concentrations across samples.

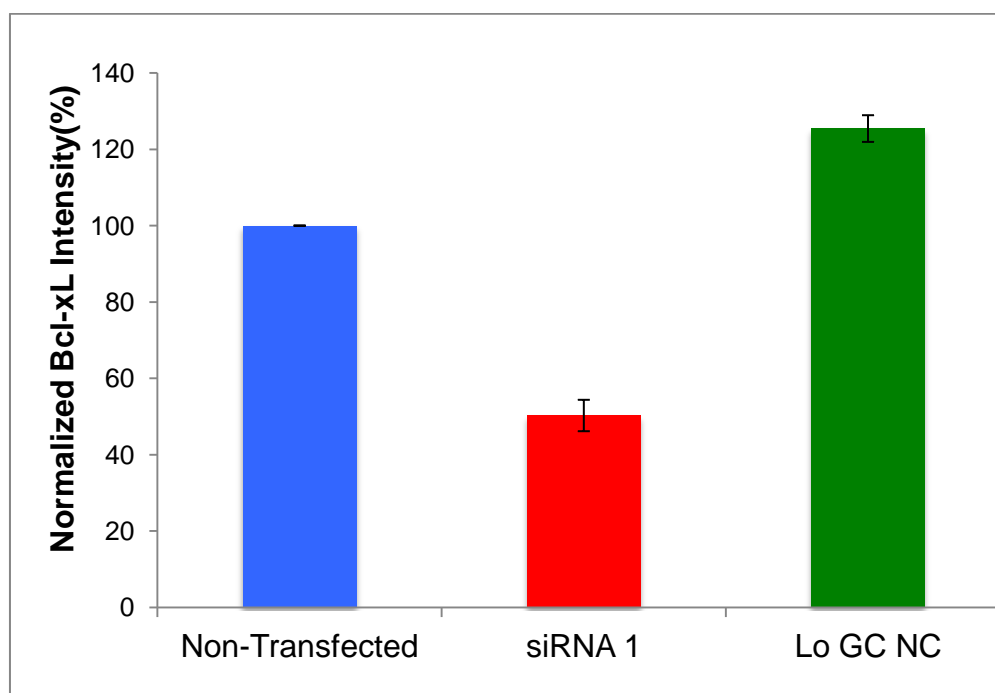


Figure 4.20: Densitometry analysis of the Western blots using the ImageJ Analyst software. The results were standardized against the levels of β -actin and are presented as normalized intensities. All experiments were carried out in triplicates, and presented as mean \pm SD.

Table 4.12: Densitometry analysis of the Western blots was carried out using the ImageJ Analyst software. Bcl-xL protein levels in cells transfected with siRNA 1 was $50.27 \pm 4.11\%$ in comparison to the $100.00 \pm 0.01\%$ protein levels in non-transfected cells.

Sample	Bcl-xL Protein Level (%) \pm SD	<i>p</i> -Value
siRNA 1	50.27 ± 4.11	0.0016
Lo GC NC [†]	125.44 ± 3.50	0.0023
NTC [‡]	100.00 ± 0.01	0.0001

[†] Lo GC NC denotes cells transfected with low GC content negative controls

[‡] NTC denotes non-transfected cells

4.3 MTT Cell Viability Assay

The MTT assay is a colormetric assay that was used to assess the viability of A549 cells in response to siRNA-based silencing of the *bcl-xL* gene. Figure 4.21 indicated that a knockdown of *bcl-xL* gene expression resulted in a reduction in cell viability after 48 hours post-transfection compared to non-transfected A549 cells. After 48 hours of transfection, A549 cells transfected with siRNA had a $69.8 \pm 2.2\%$ cell viability compared to the $98.2 \pm 2.2\%$ seen in non-transfected A549 cells (Table 4.13). Results also indicated that NP-69 normal cells were not negatively affected by the knockdown of *bcl-xL* gene expression (Figure 4.21 and Table 4.13).

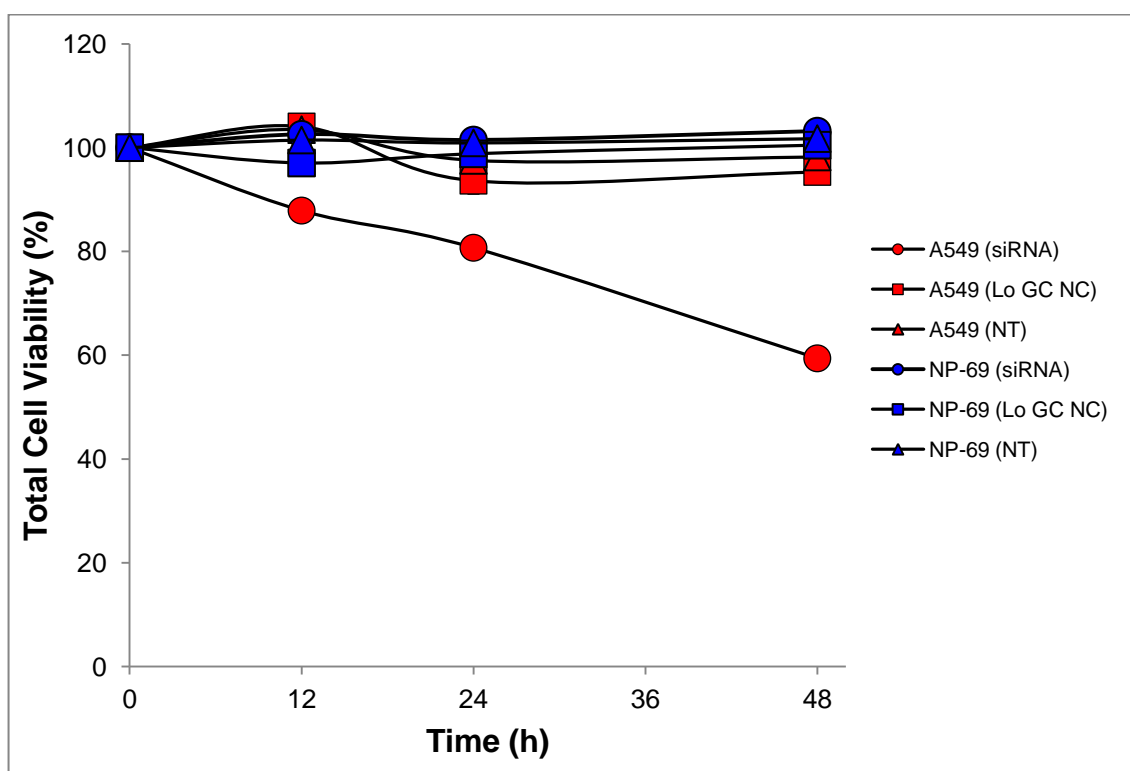


Figure 4.21: Comparison of total viable cell count on NP-69 normal cell control and A549 lung adenocarcinoma cells after siRNA transfection over 48 hours.

Table 4.13: Table comparing total cell viability levels (%) as obtained from MTT assays at 12 hours, 24 hours and 48 hours in NP-69 and A549 cell lines.

Cell Lines	Treatment (100nM)	Time (h)	Cell Viability \pm SD (%)
NP-69	NTC [†]	12	101.47 \pm 3.4
		24	100.92 \pm 1.0
		48	101.75 \pm 2.9
	siRNA	12	102.58 \pm 6.3
		24	101.48 \pm 3.7
		48	103.19 \pm 3.2
	Lo GC NC [‡]	12	97.04 \pm 1.6
		24	98.81 \pm 3.4
		48	100.48 \pm 1.4
A549	NT [†]	12	103.5 \pm 2.3
		24	97.5 \pm 4.7
		48	98.2 \pm 3.2
	siRNA	12	87.9 \pm 1.6
		24	80.7 \pm 1.0
		48	59.8 \pm 1.7
	Lo GC NC [‡]	12	104.1 \pm 2.2
		24	93.7 \pm 4.4
		48	95.3 \pm 2.1

[†] NTC denotes non-transfected cells

[‡] Lo GC NC denotes cells transfected with low GC content negative controls

4.4 MiRNA Microarray

4.4.1 MiRNA Microarray Analysis

Once it was determined that the *bcl-xL* gene was successfully silenced in A549 cells and subsequently decreased cell viability, to investigate which miRNA expressions was mediated by the presence of *bcl-xL*, a global miRNA expression profile in siRNA-transfected and non-transfected A549 cells was performed using miRNA microarray analysis. This allowed for the elucidation of which miRNAs aid in enhancing the anti-apoptotic ability of A549 cells in conjunction with Bcl-xL overexpression. Evaluation on miRNA expression changes following siRNA-based *bcl-xL* silencing was carried out in triplicates independently.

Total RNA from siRNA-transfected A549 and non-transfected A549 cells were labeled and hybridized onto the Affymetrix GeneChip[®] miRNA Arrays. The use of this array was coupled with the employment of the GeneChip[®] miRNA 2.0 Array (Affymetrix Inc., USA), which provides the most sensitive, accurate and complete measurement of small non-coding RNA transcripts involved in gene regulation. This chip has 100% miRBase v15 coverage of all 131 organisms, consisting of 15,644 probe sets, as well as 2,344 snoRNAs and scaRNAs, and 2,202 probe sets unique to pre-miRNA hairpins.

Using the GeneSpring[®] GX and Partek[®] Genomics Suite[™] software, raw microarray images were analyzed and the average values of the replicate spots of each miRNA were background subtracted, normalized and subjected to further analysis. The microarray raw data were normalized using per chip median normalization method and the summarization algorithm Robust Multichip Average (RMA). The differentially expressed miRNAs were then filtered with *p*-value of ≤ 0.05 and fold change difference of more than 1.5. Both software identified 10 miRNAs that were differentially expressed between the siRNA-transfected A549 cells and the non-transfected A549 cells. Of these, 7 miRNAs were down-regulated while 3 were up-regulated (Figure 4.22 and Table 4.14).

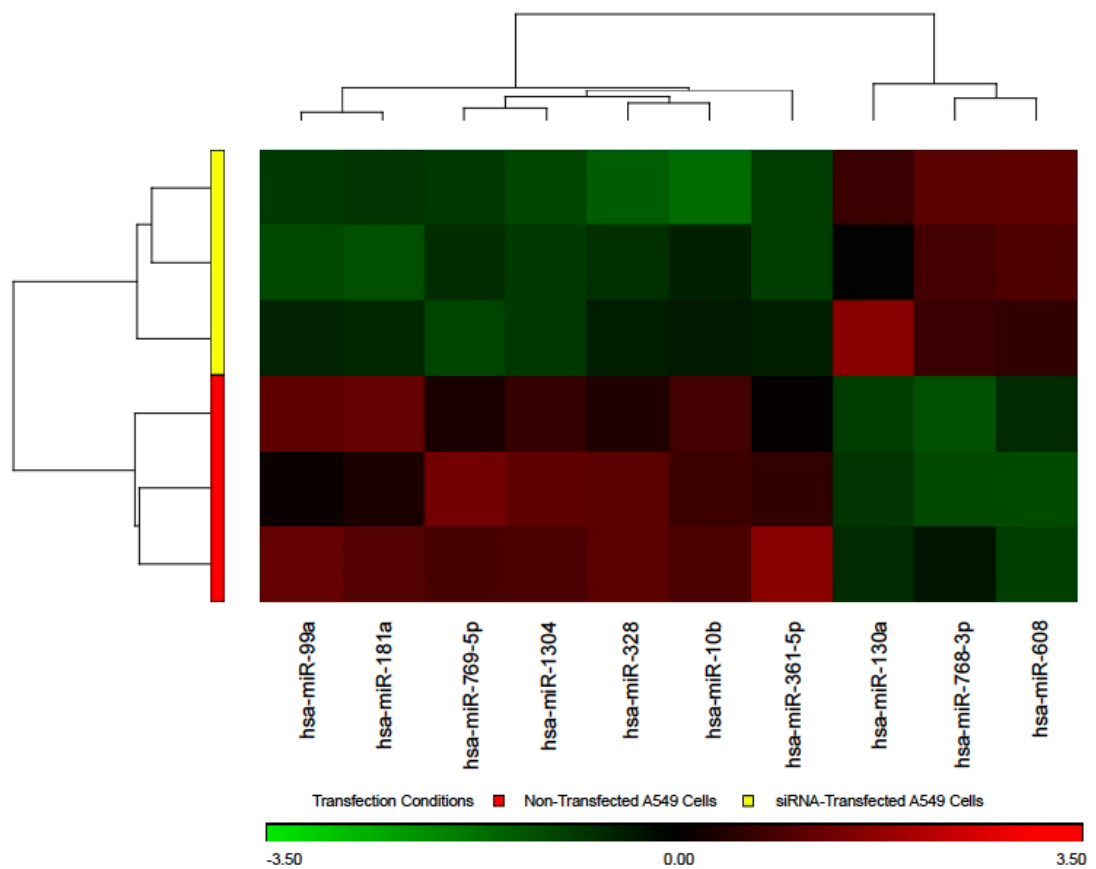


Figure 4.22: Hierarchical clustering heat map of 10 differentially expressed miRNAs in siRNA-transfected A549 cells versus non-transfected A549 cells. Up-regulated miRNAs are represented with red, while down-regulated miRNAs are represented with green.

Table 4.14: List of differentially expressed miRNAs filtered with at least a 1.5-fold change in expression and $p \leq 0.05$ using the GeneSpring[®] GX and Partek[®] Genomics Suite[™] Software.

MicroRNA	Partek [®] Fold- Change [†]	Partek [®] <i>p</i> -value	GeneSpring [®] Fold- Change [†]	GeneSpring [®] <i>p</i> -value
hsa-mir-181a	-3.37 ± 1.85	0.006	-3.39 ± 1.88	0.006
hsa-mir-769-5p	-2.42 ± 0.91	0.007	-2.41 ± 0.95	0.008
hsa-mir-10b	-1.76 ± 0.51	0.015	-1.75 ± 0.50	0.017
hsa-mir-361-5p	-1.55 ± 0.42	0.036	-1.54 ± 0.42	0.036
hsa-mir-1304	-1.53 ± 0.10	0.000	-1.53 ± 0.11	0.000
hsa-mir-328	-1.52 ± 0.24	0.011	-1.53 ± 0.29	0.010
hsa-mir-99a	-1.50 ± 0.31	0.013	-1.50 ± 0.31	0.014
hsa-mir-130a	1.87 ± 0.66	0.034	1.85 ± 0.63	0.032
hsa-mir-768-3p	2.02 ± 0.27	0.005	2.02 ± 0.26	0.005
hsa-mir-608	2.38 ± 0.31	0.001	2.38 ± 0.38	0.002

[†] Positive values denote up-regulation while negative values denote downregulation.

4.4.2 MiRNA Microarray Validation

4.4.2.1 Quantitative Real-Time Reverse Transcribe PCR (qRT-PCR)

Five representative differentially expressed miRNAs (hsa-miR-181a, hsa-miR-769-5p, hsa-miR-361-5p, hsa-miR-1304, and hsa-miR-608) between siRNA-transfected and non-transfected A549 cells were then selected based upon fold-change and preliminary target prediction, and validated using qRT-PCR.

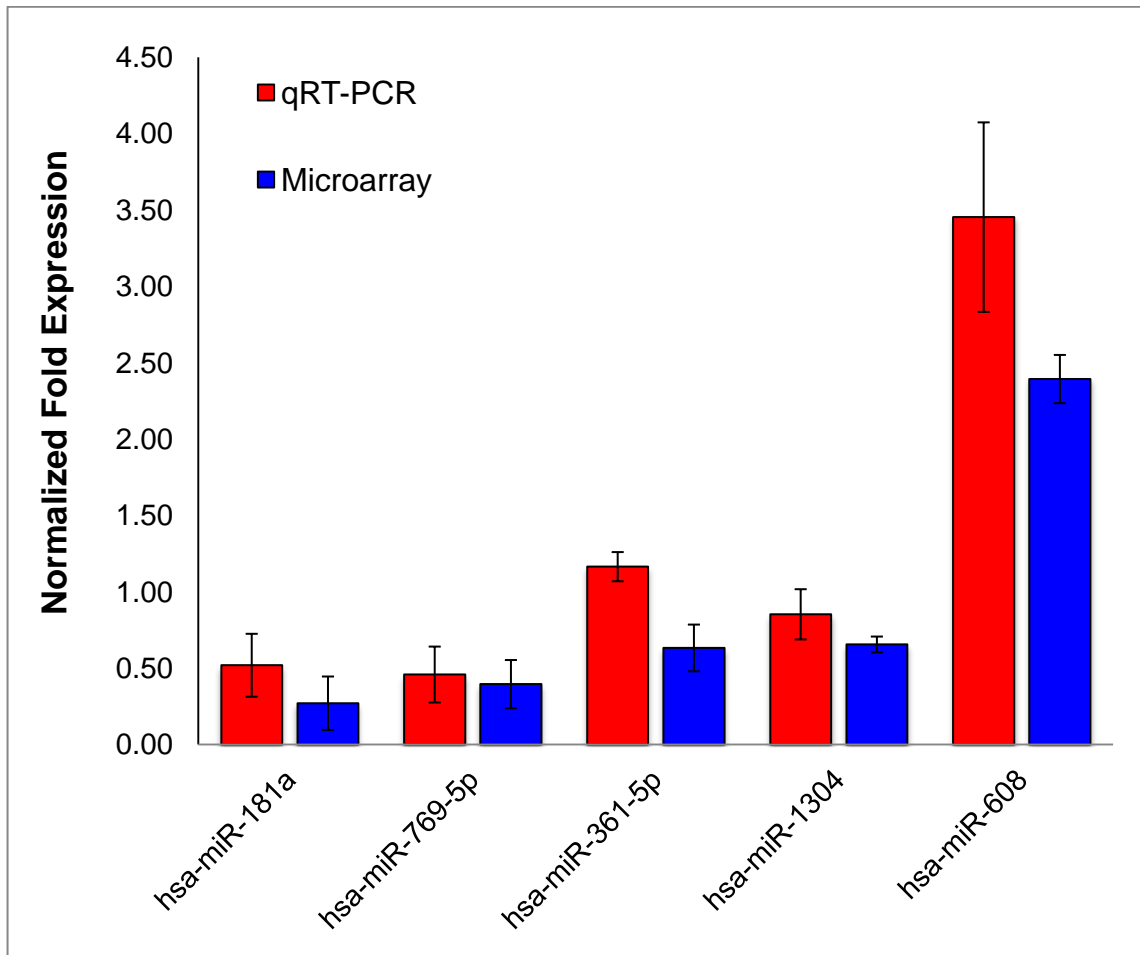


Figure 4.23: Quantitative real-time RT-PCR validation of five representative miRNAs. After normalization to the endogenous control (RNU6), the expression of miRNAs in siRNA-transfected A549 cells was expressed in comparison to the levels observed in non-transfected A549 cells. (n=3).

Table 4.15: Fold-change of miRNA expression in siRNA-transfected A549 cells as compared to non-transfected A549 cells ($p \leq 0.05$).

MicroRNA	Fold-Change [†]	<i>p</i> -Value
hsa-miR-181a	-2.17 ± 0.21	0.051
hsa-miR-769-5p	-2.43 ± 0.18	0.035
hsa-miR-361-5p	-1.16 ± 0.10	0.041
hsa-miR-1304	-1.49 ± 0.16	0.057
hsa-miR-608	3.45 ± 0.62	0.003

[†] Positive values denote up-regulation while negative values denote downregulation.

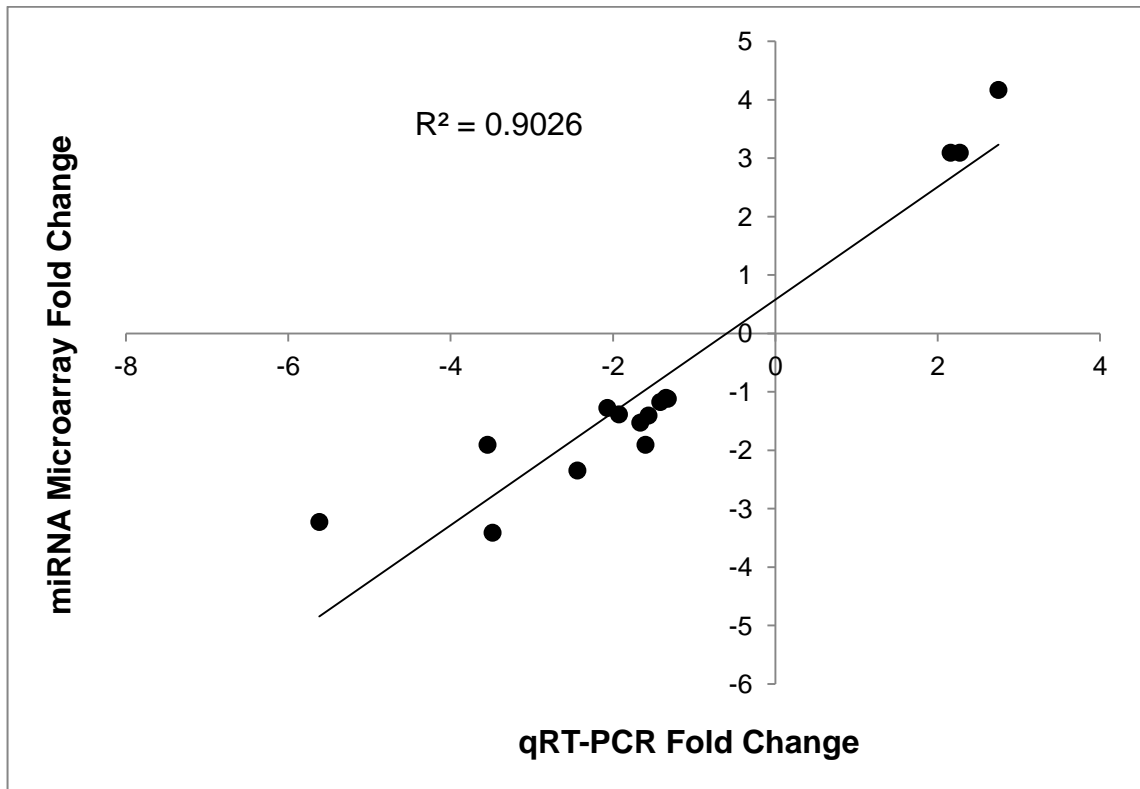


Figure 4.24: Pearson correlation scatter plot between two variables, miRNA microarray fold-change and qRT-PCR fold-change, produced a correlation coefficient value of $r = 0.950$ with an $r^2 = 0.903$, indicating a strong positive association between both sets of data.

4.4.3 MiRNA Putative Target

To understand the roles that the five representative miRNAs played in the anti-apoptotic ability of A549 cells, the TargetScan Human v5.2 software was used to identify the putative miRNA targets of the miRNAs and predicted targets with total context score of <0 were then selected for gene-annotation enrichment analysis using DAVID v6.7. The putative miRNA targets were filtered based on the genes related to apoptosis, proliferation and angiogenesis. The list of putative target genes is summarized in Table 4.16.

Table 4.16: Summary of miRNA apoptosis-, proliferation- and angiogenesis-related putative gene targets.

Gene Symbol	Gene Description	TargetScan Total Context Score				
		hsa-miR-181a	hsa-miR-769-5p	hsa-miR-361-5p	hsa-miR-1304	hsa-miR-608
AKT2	v-akt murine thymoma viral oncogene homolog 2	-0.21	-0.02	N/A	N/A	-0.17
AKT3	v-akt murine thymoma viral oncogene homolog 3	-0.25	-0.42	N/A	N/A	N/A
APC2	adenomatosis polyposis coli 2	N/A	0.05	N/A	-0.03	-0.33
BCL2	B-cell CLL/lymphoma 2	N/A	N/A	N/A	-0.15	N/A
BCL2L	BCL2-like 1	N/A	N/A	N/A	N/A	-0.59
BCL2L11	BCL2-like 11	-0.36	N/A	N/A	N/A	N/A
BCR	breakpoint cluster region	-0.05	-0.05	N/A	-0.14	-0.16
BMF	Bcl2 modifying factor	-0.07	N/A	N/A	N/A	N/A
CASP3	caspase 3, apoptosis-related cysteine peptidase	N/A	N/A	N/A	-0.12	N/A
CASP9	caspase 9, apoptosis-related cysteine peptidase	N/A	N/A	N/A	-0.21	-0.12
CCDC6	coiled-coil domain containing 6	-0.2	N/A	-0.06	N/A	-0.14
CCND1	cyclin D1	N/A	N/A	-0.12	N/A	-0.31
CCND2	cyclin D2	N/A	N/A	-0.11	N/A	N/A
CDK6	cyclin-dependent kinase 6	-0.04	N/A	N/A	-0.11	-0.16
COL4A1	collagen, type IV, alpha 1	-0.25	N/A	N/A		
COL4A2	collagen, type IV, alpha 2	N/A	N/A	-0.11		-0.08
COL4A4	collagen, type IV, alpha 4	N/A	N/A	-0.38	-0.17	
CREBBP	CREB binding protein	N/A	N/A	-0.32	N/A	-0.18
CYCS	cytochrome c, somatic	N/A	-0.07	N/A	-0.16	N/A
DAPK1	death-associated protein kinase 1	N/A	N/A	-0.17	N/A	N/A
DAPK2	death-associated protein kinase 2	N/A	N/A	N/A	-0.41	N/A
DVL3	dishevelled, dsh homolog 3	N/A	0.03	N/A	N/A	-0.51
E2F2	E2F transcription factor 2	-0.03	0.06	N/A	N/A	-0.13
EGFR	epidermal growth factor receptor	N/A	N/A	N/A	N/A	-0.56
FADD	Fas (TNFRSF6)-associated via death domain	N/A	N/A	-0.44	N/A	N/A

Table 4.16, continued

FAS	Fas (TNF receptor superfamily, member 6)	-0.44	N/A	-0.32	-0.08	-0.19
FASLG	Fas ligand (TNF superfamily, member 6)	-0.16	N/A	N/A	N/A	N/A
FGF1	fibroblast growth factor 1	N/A	N/A	-0.4	N/A	N/A
FGF11	fibroblast growth factor 11	N/A	N/A	N/A	N/A	-0.07
FGF12	fibroblast growth factor 12	N/A	N/A	N/A	-0.03	N/A
FGF17	fibroblast growth factor 17	N/A	N/A	N/A	-0.07	-0.21
FGF23	fibroblast growth factor 23	N/A	-0.08	N/A	N/A	N/A
FGF5	fibroblast growth factor 5	N/A	0.01	-0.45	N/A	-0.21
FGF7	fibroblast growth factor 7	-0.19	N/A	-0.5	-0.18	N/A
FGFR3	fibroblast growth factor receptor 3	N/A	0.04	N/A	N/A	-0.06
FLT3	fms-related tyrosine kinase 3	N/A	N/A	-0.14	N/A	N/A
FOS	v-fos FBJ murine osteosarcoma viral oncogene homolog	-0.16	N/A	N/A	-0.11	N/A
FOXO1	forkhead box O1	N/A	N/A	-0.05	N/A	N/A
FZD1	frizzled homolog 1	N/A	N/A	N/A	-0.15	N/A
FZD10	frizzled homolog 10	N/A	N/A	N/A	N/A	-0.12
FZD3	frizzled homolog 3	N/A	N/A	-0.55	N/A	N/A
FZD4	frizzled homolog 4	N/A	N/A	-0.07	-0.04	-0.38
FZD5	frizzled homolog 5	N/A	-0.17	N/A	N/A	-0.13
FZD7	frizzled homolog 7 (Drosophila)	N/A	N/A	N/A	N/A	-0.25
FZD8	frizzled homolog 8	N/A	N/A	N/A	N/A	-0.46
HGF	hepatocyte growth factor (hepapoietin A; scatter factor)	N/A	N/A	N/A	-0.19	N/A
ITGA2	integrin, alpha 2 (CD49B, alpha 2 subunit of VLA-2 receptor)	N/A	N/A	N/A	N/A	-0.11
ITGA3	integrin, alpha 3 (antigen CD49C, alpha 3 subunit of VLA-3 receptor)	-0.28	N/A	N/A	N/A	-0.33
ITGA6	integrin, alpha 6	-0.17	N/A	N/A	N/A	-0.24
JAK1	Janus kinase 1	N/A	-0.23	N/A	-0.15	N/A
JAK2	Janus kinase 2	-0.15	N/A	N/A	N/A	N/A
KIT	Proto-oncogene tyrosine-protein kinase Kit (c-kit) (CD117 antigen)	N/A	N/A	N/A	N/A	-0.06
KITLG	KIT ligand	-0.42	-0.28	N/A	-0.03	
LAMC3	laminin, gamma 3	N/A	-0.18	N/A	N/A	N/A
LEF1	lymphoid enhancer-binding factor 1	N/A	N/A	N/A	N/A	-0.08

Table 4.16, continued

MAP2K1	mitogen-activated protein kinase kinase 1	-0.42	N/A	N/A	N/A	N/A
MAP2K2	mitogen-activated protein kinase kinase 2	N/A	-0.03	N/A	N/A	N/A
MAPK1	mitogen-activated protein kinase 1	N/A	-0.26	-0.15	0.03	N/A
MAX	MYC associated factor X	N/A	N/A	-0.09	N/A	-0.18
MDM2	Mdm2 p53 binding protein homolog	N/A	N/A	N/A	-0.29	N/A
MET	met proto-oncogene (hepatocyte growth factor receptor)	-0.19	N/A	-0.61	N/A	-0.1
MMP1	matrix metalloproteinase 1 (interstitial collagenase)	-0.16	N/A	N/A	N/A	N/A
MMP2	matrix metalloproteinase 2 (gelatinase A, 72kDa gelatinase, 72kDa type IV collagenase)	N/A	N/A	N/A	N/A	-0.22
MYC	v-myc myelocytomatosis viral oncogene homolog	N/A	N/A	N/A	-0.46	N/A
NFKB2	nuclear factor of kappa light polypeptide gene enhancer in B-cells 2 (p49/p100)	N/A	N/A	N/A	N/A	-0.35
NRAS	neuroblastoma RAS viral (v-ras) oncogene homolog	-0.22	N/A	-0.2	-0.21	-0.29
PDGFA	platelet-derived growth factor alpha polypeptide	N/A	-0.21	N/A	N/A	N/A
PDGFB	platelet-derived growth factor beta polypeptide	N/A	-0.1	N/A	N/A	-0.18
PDGFRA	platelet-derived growth factor receptor, alpha polypeptide	N/A	N/A	-0.11	N/A	N/A
PIK3R1	phosphoinositide-3-kinase, regulatory subunit 1 (alpha)	-0.08	-0.04	-0.27	-0.05	-0.22
PIK3R2	phosphoinositide-3-kinase, regulatory subunit 2 (beta)	N/A	N/A	N/A	N/A	-0.34
PIK3R3	phosphoinositide-3-kinase, regulatory subunit 3 (gamma)	-0.5	N/A	N/A	N/A	N/A
PIK3R5	phosphoinositide-3-kinase, regulatory subunit 5	N/A	N/A	N/A	N/A	-0.1

Table 4.16, continued

PPARD	peroxisome proliferator-activated receptor delta	N/A	0.08	N/A	N/A	-0.15
PRKCA	protein kinase C, alpha	-0.04	-0.01	N/A	-0.18	-0.17
PTGS2	prostaglandin-endoperoxide synthase 2 (prostaglandin G/H synthase and cyclooxygenase)	-0.29	N/A	N/A	N/A	N/A
RAC1	ras-related C3 botulinum toxin substrate 1 (rho family, small GTP binding protein Rac1)	N/A	N/A	-0.42	N/A	N/A
RB1	retinoblastoma 1	-0.1	N/A	-0.35	N/A	N/A
RET	ret proto-oncogene	N/A	N/A	-0.18	N/A	N/A
SMAD2	SMAD family member 2	-0.26	-0.38	-0.44	N/A	N/A
SMAD3	SMAD family member 3	-0.24	-0.21	N/A	N/A	N/A
SMAD4	SMAD family member 4	N/A	N/A	-0.14	N/A	N/A
SOS1	son of sevenless homolog 1	-0.28	N/A	N/A	N/A	N/A
SOS2	son of sevenless homolog 2	N/A	N/A	N/A	N/A	-0.17
STAT3	signal transducer and activator of transcription 3 (acute-phase response factor)	-0.16	-0.01	-0.2	N/A	-0.13
STAT5B	signal transducer and activator of transcription 5B	N/A	N/A	N/A	-0.94	-0.27
TCF7	transcription factor 7 (T-cell specific, HMG-box)	N/A	-0.06	N/A	-0.18	N/A
TCF7L2	transcription factor 7-like 2 (T-cell specific, HMG-box)	N/A	N/A	N/A	N/A	-0.15
TGFA	transforming growth factor, alpha	-0.01	N/A	-0.01	-0.18	N/A
TGFBR1	transforming growth factor, beta receptor 1	N/A	-0.15	-0.21	N/A	N/A
TGFBR2	transforming growth factor, beta receptor II (70/80kDa)	N/A	-0.47	N/A	N/A	N/A
TP53	tumor protein p53	N/A	-0.15	N/A	N/A	-0.28
TRAF2	TNF receptor-associated factor 2	N/A	-0.03	N/A	N/A	N/A

Table 4.16, continued

TRAF3	TNF receptor-associated factor 3	N/A	N/A	-0.3	N/A	N/A
TRAF5	TNF receptor-associated factor 5	-0.17	N/A	-0.26	N/A	N/A
TRAF6	TNF receptor-associated factor 6	N/A	N/A	N/A	N/A	-0.16
VEGFA	vascular endothelial growth factor A	N/A	N/A	-0.49	N/A	N/A
VEGFB	vascular endothelial growth factor B	N/A	N/A	-0.09	N/A	N/A
WNT1	wingless-type MMTV integration site family, member 1	N/A	N/A	N/A	0.00	N/A
WNT10B	wingless-type MMTV integration site family, member 10B	N/A	N/A	N/A	N/A	-0.12
WNT16	wingless-type MMTV integration site family, member 16	-0.26	N/A	N/A	N/A	N/A
WNT3	wingless-type MMTV integration site family, member 3	N/A	N/A	-0.12	N/A	N/A
WNT3A	wingless-type MMTV integration site family, member 3A	N/A	-0.03	N/A	-0.39	-0.16
WNT4	wingless-type MMTV integration site family, member 4	N/A	-0.05	N/A	N/A	-0.35
WNT5A	wingless-type MMTV integration site family, member 5A	N/A	N/A	N/A	-0.17	N/A
WNT5B	wingless-type MMTV integration site family, member 5B	N/A	N/A	N/A	N/A	-0.09
WNT7A	wingless-type MMTV integration site family, member 7A	N/A	N/A	-0.6	N/A	N/A
XIAP	X-linked inhibitor of apoptosis	-0.24	N/A	N/A	N/A	N/A

TargetScan Total Context Score: N/A: (Not applicable) indicates that the gene is not a putative target of the miRNA.

4.4.3.1 Hypothetical Pathway Analysis

The predicted targets of the five validated miRNAs were found to be associated with various signaling pathways; mainly the intrinsic and extrinsic apoptotic pathways, PI3K/AKT pathway, WNT pathway, TGF- β pathway and the MAPK pathway. The miRNAs were organized into a hypothetical pathway model (Figure 4.25) to illustrate the effects these miRNAs play on apoptosis as well as cell proliferation and angiogenesis.

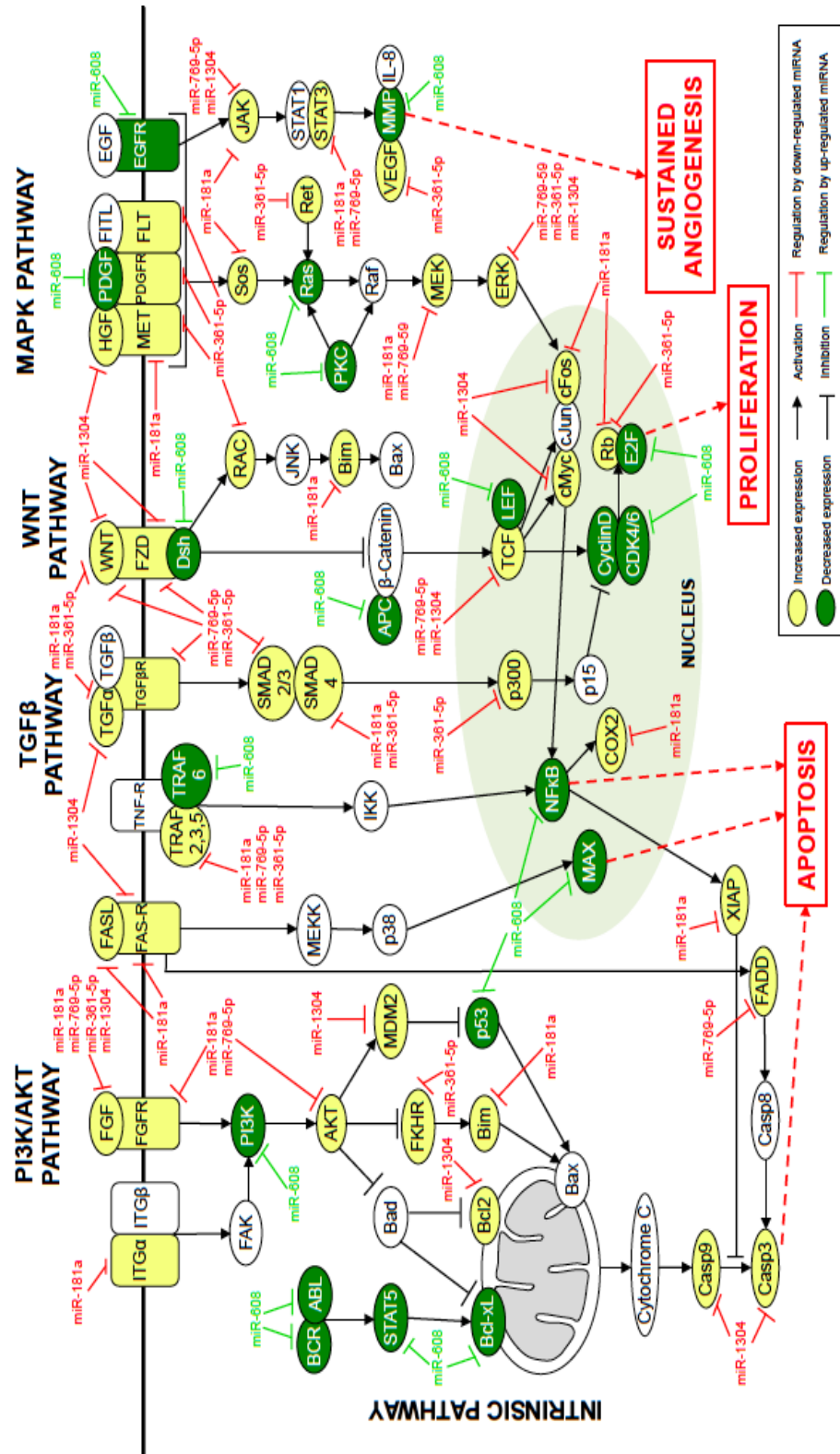


Figure 4.25: Hypothetical pathway model illustrating the effects the five selected miRNAs play on apoptosis as well as cell proliferation and angiogenesis in *bcl-xL* silenced A549 cells.

CHAPTER 5: DISCUSSION

5.1 Transient siRNA Based *Bcl-xL* Silencing in Lung Adenocarcinoma Cells (A549)

The anti-apoptotic proteins Bcl-2 and Bcl-xL are significantly expressed in solid tumors, including lung cancer, where they play a major role in cell survival (Gottschalk *et al.*, 1994; Simonian *et al.*, 1997). Expression of Bcl-2 is prominent in SCLC and in some squamous carcinomas, but is absent or lacks significant expression in lung adenocarcinomas (Dosaka-Akita *et al.*, 1999; Jiang *et al.*, 1995). Instead, lung adenocarcinomas have been found to express high levels of Bcl-xL (Reeve *et al.*, 1996). In studies where Bcl-xL antisense treatment was carried out, a strong apoptotic response was induced in lung adenocarcinoma cells that lack the significant expression of Bcl-2 (Leech *et al.*, 2000). However, SCLC cells did not undergo apoptosis following Bcl-xL downregulation, most probably due to the protection of high levels of Bcl-2 present in these cells (Leech *et al.*, 2000). These findings suggest that Bcl-xL is a more critical apoptosis repressor protein in lung adenocarcinoma cells than in SCLC cells (Leech *et al.*, 2000; Reeve *et al.*, 1996). This has led to studies to determine the effectiveness of use of antisense oligonucleotides inhibiting Bcl-xL expression as a means of therapy in various hyperproliferative diseases, including cancer (Ziegler *et al.*, 1997).

5.1.1 siRNA Transfection in A549 Cells

To determine which of the three was the most efficient in silencing *bcl-xL*, A549 cells were transfected with each siRNA independently. BLOCK-iTTM Alexa Fluor[®] Red Fluorescent Oligo is a highly stable, fluorescein-labeled, non-targeted dsRNA compound that was used for the visual monitoring of transfection efficiency. After 24 hours, transfection efficiency was assessed by visualizing uptake of BLOCK-iTTM Alexa Fluor[®] Red Fluorescent Oligo using fluorescence microscopy. Results indicated that for all three sets of siRNA had satisfactory transfection efficiency of 70% or above thus allowing for the silencing efficiency of the siRNAs to be determined using qRT-PCR.

After normalization to endogenous β -actin mRNA levels, the *bcl-xL* expression levels were lower for all siRNA-transfected A549 cells in comparison to the non-transfected cells. As shown in Table 4.4, siRNA 1 had the highest negative fold induction at 4.42; followed by siRNA 2 and 3 with negative fold change of 2.62 and positive fold change of 1.70 respectively. The percentage of knockdown was also determined and it was found that, out of the three siRNAs, siRNA 1 had the greatest percentage of gene knockdown, with $75.19 \pm 8.32\%$, followed by siRNA 2 and 3 with a knockdown percentage of $55.52 \pm 4.32\%$ and $39.29 \pm 8.58\%$, respectively (Table 4.5).

To further confirm that *bcl-xL* was successfully silenced, Western blot analysis was carried out. Results show that the Bcl-xL protein levels decreased in A549 cells transfected with siRNA in comparison to the non-transfected A549 cells. Densitometry analysis of the Western bands, confirmed that cells transfected with siRNA 1 had a Bcl-xL protein expression of $28.33 \pm 6.79\%$ compared to the $100.00 \pm 0.48\%$ protein expression seen in non-transfected cells (Figure 4.9). The Bcl-xL protein expression in siRNA 2 and 3 transfected A549 cells was $82.01 \pm 1.56\%$ and $84.77 \pm 2.16\%$ respectively (Figure 4.10). From our analysis, siRNA 1 was observed as the best

silencing among the siRNAs tested. Thus, siRNA 1 was chosen to be used for further downstream work.

siRNA 1 has a low G/C content, while siRNA 2 and 3 had a high GC content. Previous work has shown that siRNAs that contain a high G/C content at the 3' end of the antisense strand, and a lower G/C content at the 5' end of the antisense strand, will result in a significantly higher gene-silencing rate (Elbashir *et al.*, 2001; Holen *et al.*, 2002). In the cell, siRNAs unwind into 2 ssRNA strands, a passenger strand and a guide strand. The guide strand will be incorporated into the RISC and hybridize to the complementary target mRNA in the cell. The strand that is selected to be incorporated into RISC, is selected upon the basis of thermodynamic instability and weaker base pairing. siRNA strands with a high G/C content is more stable than an siRNA with a low G/C content, therefore, the siRNA with a lower G/C content at its 5' end is preferentially loaded into RISC (Elbashir *et al.*, 2001).

Theoretically, it can be assumed that siRNA 1 would have the greatest silencing efficiency, due to its low G/C content. However, as the company that provided the siRNA had only carried out *in silico* design and validation, it was necessary to perform a bench test to confirm which siRNA would provide the greatest silencing efficiency.

Once it was confirmed that siRNA 1 had the greatest silencing efficiency, MTT viability assay was carried out to determine the viability of A549 cells in response to siRNA-based silencing of the *bcl-xL* gene. Results indicated that after 48 hours post-transfection cell viability in siRNA-transfected cells was decreased to $69.8 \pm 2.2\%$ cell viability compared to the $98.2 \pm 2.2\%$ seen in non-transfected A549 cells (Table 4.13). This finding corresponds with the results of other Bcl-xL antisense treatments, as discussed previously, suggesting that Bcl-xL may be a critical apoptosis repressor protein in lung adenocarcinoma cell line A549.

5.2 MiRNAs Dysregulated in Response to *Bcl-xL* Silencing

Cancer cells have the ability to disrupt the balance between pro- and anti-apoptotic factors to promote cell survival under the conditions of environmental stress. In terms of molecular events occurring in tumors, evasion of apoptosis is an important hallmark of tumor progression. Cell survival or death is determined by the competitive action of death agonists, such as Bcl-2 and Bcl-xL (Leech *et al.*, 2000).

MiRNAs play a role in a wide range of biological processes including cell proliferation (Hayashita *et al.*, 2005), differentiation (Shivdasani, 2006), and apoptosis (Mott *et al.*, 2007). Bioinformatics data have shown that miRNAs have the potential to regulate at least 20-30% of all human genes. A single miRNA has the ability to control hundreds of mRNA gene targets (Lewis *et al.*, 2005). As miRNAs are an integral part of the regulatory networks in cells, a disturbed miRNA function or altered miRNA expression may disorganize cellular processes and eventually cause or contribute to diseases, including cancer (Weimer, 2007).

MiRNAs are critical apoptosis regulator in tumorigenesis, and cancer cells are able to manipulate miRNAs to regulate cell survival in oncogenesis. For example, miR-133 acts as a regulator of survival in cardiac cells by repressing caspase-9 expression at both the protein and mRNA levels (Xu *et al.*, 2007), while the miR-17-92 cluster, which is amplified in B cell lymphomas, is capable of evading apoptosis by negatively regulating the tumor suppressor PTEN and the pro-apoptotic protein Bim (Xiao *et al.*, 2008).

To date, no studies have been conducted to identify miRNAs that are regulated or affected by the expression of the *bcl-xL* gene. Therefore, the identification of miRNAs whose expression are dysregulated in response to the silencing of *Bcl-xL* in A549 cells is important, as it will allow for further insight into the biological functions of miRNAs as well as the roles they may play in the mechanisms of pathogenesis in lung adenocarcinoma cells.

5.2.1 MiRNA Microarray Analysis

A global miRNA expression profile was established using miRNA microarray, and compared between total RNA extracted from siRNA-transfected A549 cells and non-transfected cells to determine the miRNA expression changes that occur in response to *bcl-xL* gene silencing. Analysis of the microarray images using the GeneSpring[®] GX and Partek[®] Genomics Suite[™] software led to the identification of 10 miRNAs that were differentially expressed between the siRNA-transfected A549 cells and the non-transfected A549 cells. Of these, 7 miRNAs were down-regulated while 3 were up-regulated, when compared to non-transfected A549 cells (Table 4.14 and Figure 4.22).

Previously, studies have been carried out which have implicated a number of the 10 dysregulated miRNAs in a wide variety of cancers. For example, miR-181a is up-regulated in thyroid papillary carcinomas (He *et al.*, 2005), but down-regulated in glioblastomas (Shi *et al.*, 2008), and oral squamous cell carcinoma (OSCC) (Shin *et al.*, 2011). In a study conducted by Shi and colleagues, it was found that miR-181a in human glioma cells function as a tumor suppressor, with the ability to induce apoptosis and inhibit division (Shi *et al.*, 2008). Thus deregulation of miR-181a in glioma cells was found to play a critical role in the pathogenesis of gliomas (Shi *et al.*, 2008). miR-

181a was also found to elicit tumor suppressive activity in OSCC by down-regulating the K-ras oncogene (Shin *et al.*, 2011). Activation of K-ras either through mutation or overexpression is an important molecular event that is required for the development and progression of OSCC (Shin *et al.*, 2011). In non-small-cell-lung cancer cells, expression of miR-181a has been found to be down-regulated compared to normal lung cells. This downregulation was found to be negatively correlated with the survival time of the patients (Gao *et al.*, 2010). Furthermore, miR-181a has been found to be a chemosensitizer, enhancing the lethality of various chemotherapeutic agents, such as cisplatin, carboplatin, and oxaliplatin, in several NSCLC, by stimulating Bax oligomerization and activation of the pro-apoptotic caspases (Galluzi *et al.*, 2010).

In a study carried out by Pan and colleagues in 2009, it was found that the expression of miR-328 was inversely related to the ATP-binding cassette, subfamily G, member 2 (ABCG2) in human breast cancer cells. The breast cancer resistance protein BCRP/ABCG2 is an ATP-binding cassette member transporter that is expressed in humans, and controls absorption, distribution and clearance of various xenobiotics, including pharmaceutical agents, dietary carcinogens and conjugated metabolites (Mao and Unadkat, 2005; van Herwaarden and Schinkel, 2006; Vore and Leggas, 2008). Overexpression of this ABCG2 represents an important mechanism for multidrug resistance (Pan *et al.*, 2009). It has been found that miR-328 negatively regulates the expression of ABCG2, and thus significantly increases drug sensitivity in cancer cells (Pan *et al.*, 2009).

While many studies have been carried out linking the dysregulated miRNAs with various cancers, studies on association of these miRNAs with apoptosis in lung adenocarcinoma are still lacking. Therefore, this study is essential as it aims to develop a hypothetical pathway model that relates these miRNAs with the apoptotic pathways in the lung adenocarcinoma cell line.

5.2.2 qRT-PCR Validation

To warrant the accuracy of the microarray analysis, qRT-PCR validation with the same RNA preparations used in microarray analysis was carried out. Five representative miRNAs were selected to undergo qRT-PCR validation based upon the highest fold-change as well as preliminary putative cancer related targets identified using the TargetScan Human v5.2 database. These five miRNAs were miR-181a, miR-769-5p, miR-361-5p, miR-1304 and miR-608. cDNA was first prepared by miRNA specific primers and then real-time quantification RT-PCR for these miRNAs and an endogenous control (RNU6B) were performed on the BioRad CFX96[™] Real-Time PCR Detection System. RNU6B is a widely used endogenous reference RNA in miRNA quantification experiments because RNU6B is not affected under the experimental conditions and shows a constant level of expression and similar abundance to the target miRNA.

Results of the qRT-PCR indicated that miR-181a, miR-769-5p, miR-36105p were all down-regulated in siRNA-transfected A549 cells when compared to non-transfected A549 cells, while miR-608 was up-regulated. The Pearson correlation plot was used to determine how well the miRNA microarray results correlated with the qRT-PCR results. Pearson correlation coefficient measures the strength of the linear relationship between two random variables. The correlation coefficient takes on values between -1 and +1, ranging from being negatively correlation (-1) to uncorrelated (0) to positively correlated (+1) (Zuo *et al.*, 2003). These data from miRNA microarray and qRT-PCR had a correlation coefficient of +0.950 indicating that the two sets of data were strongly positively correlated

5.3 Hypothetical Pathway Analysis

A bioinformatics analysis was then carried out on the five selected dysregulated miRNAs to determine their interaction with their putative gene targets. TargetScan Human v5.2 was used and predicted targets with total context score of <0 were then selected for gene-annotation enrichment analysis using DAVID v6.7. These miRNAs were found to be involved in various signaling pathways; primarily the intrinsic and extrinsic pathway, the PI3K/AKT pathway, the WNT pathway, the TGF- β pathway and the MAPK pathway. Based on this, a hypothetical pathway illustrating the interactions between these miRNAs with their specific targets were generated describing the effects of *bcl-xL* silencing on initiation of apoptosis in A549 cells (Figure 4.25). If more than one miRNA targets a specific gene, the miRNA with the most favorable context score (the miRNA with the lowest number) was shown on the hypothetical pathway.

5.3.1 PI3K/Akt Pathway

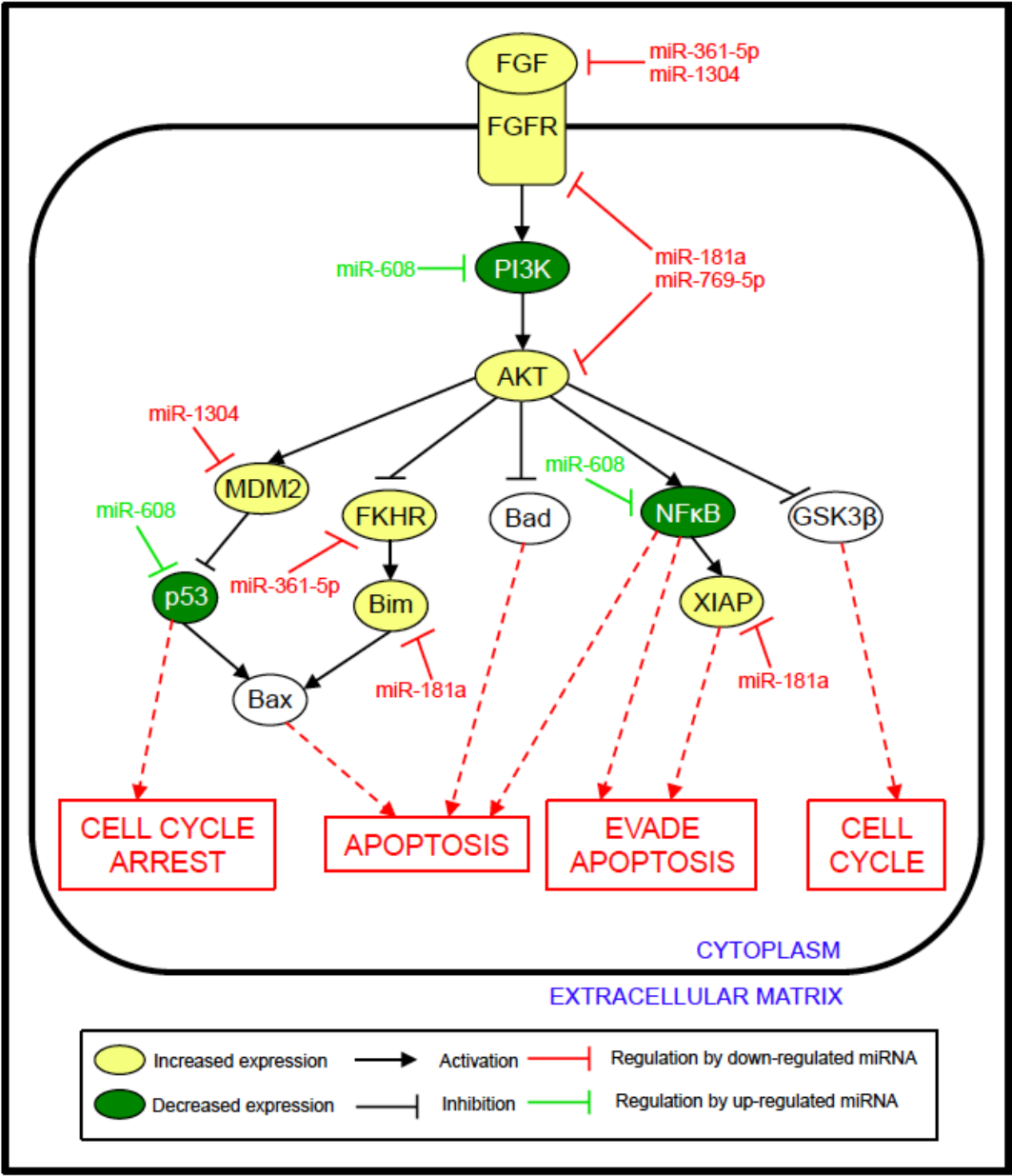


Figure 5.1: Hypothetical pathway model illustrating miRNA targets in the PI3K/Akt pathway.

The PI3K/Akt pathway is an important regulator of cell survival and proliferation in human cancers (Vivanco and Sawyers, 2002). An important target in this pathway is Akt, which plays a significant role in the activation of a number of processes critical for tumorigenesis including inhibition of apoptosis, aberrant cell proliferation, promotion of angiogenesis and tumor cell invasiveness (Testa and Bellacosa, 2001). Akt exerts its anti-apoptotic properties through phosphorylation of Bad or caspase 9 (Cardone *et al.*, 1998), which directly regulates the apoptotic machinery or substrates including the forkhead family members, or I κ B kinases (Datta *et al.*, 1997), which in turn can indirectly inhibit apoptosis (Kandasamy and Srivastava, 2002).

This study indicated that Akt was a target of two down-regulated miRNAs, hsa-miR-769-5p and hsa-miR-181a. As miRNAs are negative gene regulators, genes targeted by down-regulated miRNAs would therefore be expected to increase in expression. PI3K, which activates AKT through phosphorylation, on the other hand was a target of up-regulated hsa-miR-608, thereby negatively regulating its expression levels and indirectly reducing the activation of Akt. Previously, phosphorylated Akt (p-Akt) was found to be overexpressed in clinical specimens of NSCLC leading to continued cell survival and proliferation (Tang *et al.*, 2006). This increase in p-Akt expression was found to be significantly correlated with reduced patient survival (Tang *et al.*, 2006; David *et al.*, 2004). As Akt regulates the activity of various downstream transcription factors that control cell death genes (Brunet *et al.*, 1999), the withdrawal of this survival factor, due to a decrease in PI3K levels, will lead to an increase in apoptosis.

For example, a dephosphorylated forkhead transcription factor (FKHR) targeted by down-regulated hsa-miR-361-5p, will now be able to translocate into the nucleus and induce target genes such as pro-apoptotic proteins Bim and Fas ligand to trigger apoptosis (Brunet *et al.*, 1999). Similarly, dephosphorylation of murin double minute 2 (Mdm2), a target of hsa-miR-1304, will inhibit its translocation into the nucleus thereby preventing degradation of tumor-suppressor p53 proteins (Honda and Yasuda, 2000; Kubbutat *et al.*, 1997).

However, pathway analysis also revealed that p53, which directly activates the pro-apoptotic gene Bax, was a target of up-regulated hsa-miR-608. A decrease in p53 expression may affect the stabilization of the mitochondrial membrane (Amaral *et al.*, 2010). However, as the expression of other pro-apoptotic proteins such as Bak, were not found to be affected by miRNAs, cytochrome c can still be released leading to initiation of the caspase cascade (Cheng *et al.*, 2001).

5.3.2 Intrinsic and Extrinsic Pathway

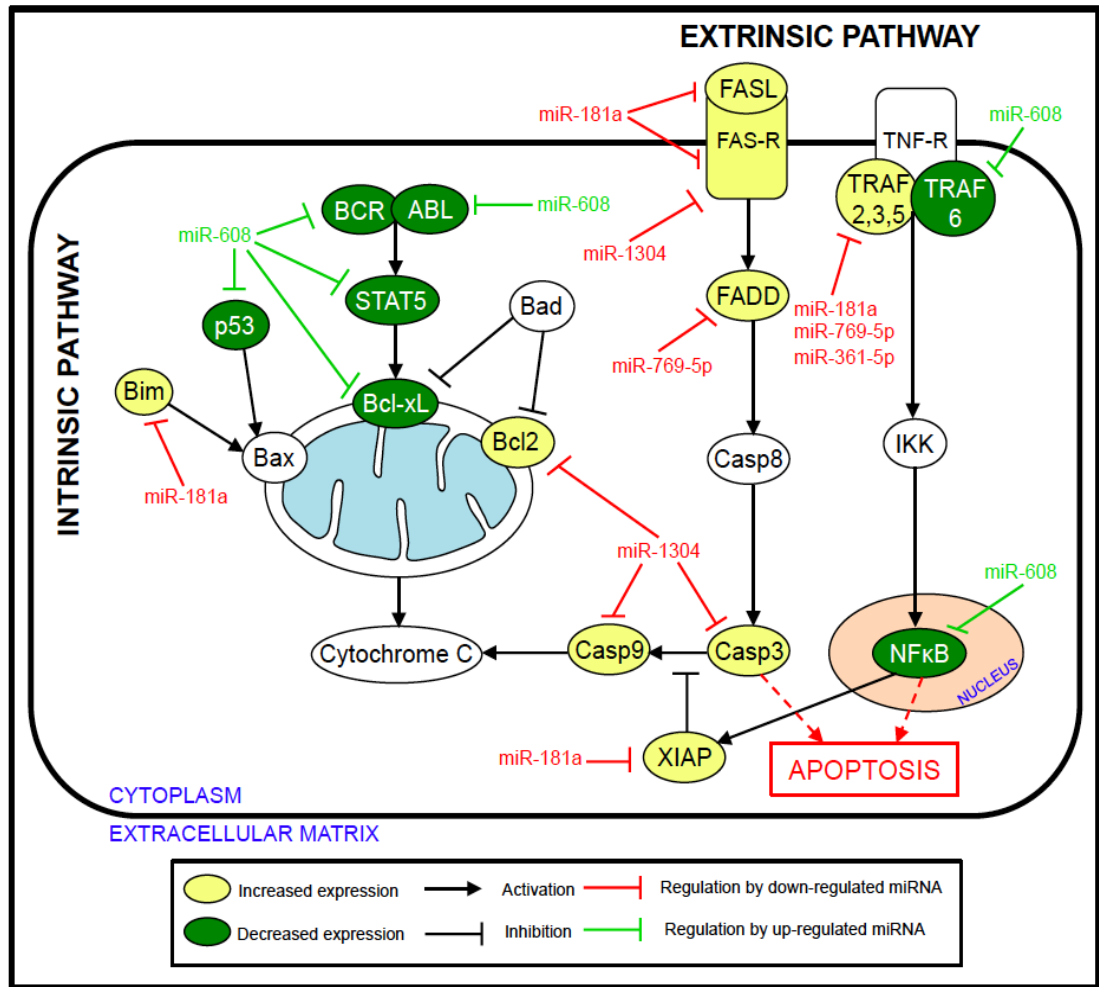


Figure 5.2: Hypothetical pathway model illustrating miRNA targets in the intrinsic and extrinsic apoptotic pathway.

The intrinsic apoptotic pathway, also termed mitochondrial pathway, is primarily regulated by the Bcl-2 family of proteins. The balance of expression of the various pro- and anti-apoptotic members of the Bcl-2 family is largely responsible for the apoptotic homeostasis in cells (Daniel and Smith, 2004). Previously, Bcl-xL overexpression in NSCLC was associated with an inhibition of apoptosis and poor prognosis in patients with this disease (Daniel and Smith, 2004; Soini *et al.*, 1999). Antisense treatment targeting Bcl-xL in NSCLC cell has resulted result in apoptosis,

thus validating Bcl-xL as a potent target in cancer (Leech *et al.*, 2000; Reeve *et al.*, 1996).

Figure 5.2 illustrates the hypothetical network between the miRNAs and their gene targets in the intrinsic and extrinsic apoptotic pathway. Pathway analysis indicates that breakpoint cluster region/Abelson (BCR/Abl), STAT5 and Bcl-xL were all targeted by the up-regulated hsa-miR-608. BCR/Abl is an oncogene that is able to activate STAT5, which has been found to be increased in lung cancer cell lines, and was speculated to control the process of apoptosis through the upregulation of the anti-apoptotic protein Bcl-xL (Gesbert and Griffin, 2000; Sánchez-Ceja *et al.*, 2006). Therefore an inhibition of BCR/Abl, STAT5 and Bcl-xL by hsa-miR-608 would hypothetically lead to the reinforcement of apoptosis in A549 cells, through the release of cytochrome c and the activation of caspase 3, the main apoptosis effector. Furthermore, dephosphorylation of Akt as a result of decreased PI3K levels, will allow pro-apoptotic Bad to be released from Akt inhibition allowing it to form a heterodimer with anti-apoptotic Bcl-xL and Bcl-2, thus further promoting apoptosis (Datta *et al.*, 1997).

In the extrinsic pathway, results reveal that all of the upstream genes that result in the activation of caspase 8 were exclusively targeted by down-regulated miRNAs (has-miR-181a and has-miR-79-5p), indicating an up-regulation in its expression. Active caspase-8 will result in downstream apoptotic processes that include the activation of pro-caspase-3 directly or amplification of its signal through Bid cleavage (Garrido *et al.*, 2006). Truncated Bid will translocate into the mitochondria where it will promote the release of cytochrome c (Garrido *et al.*, 2006), thus enabling an alternative pathway for apoptosis to occur in the A549 cells.

5.3.3 WNT Pathway

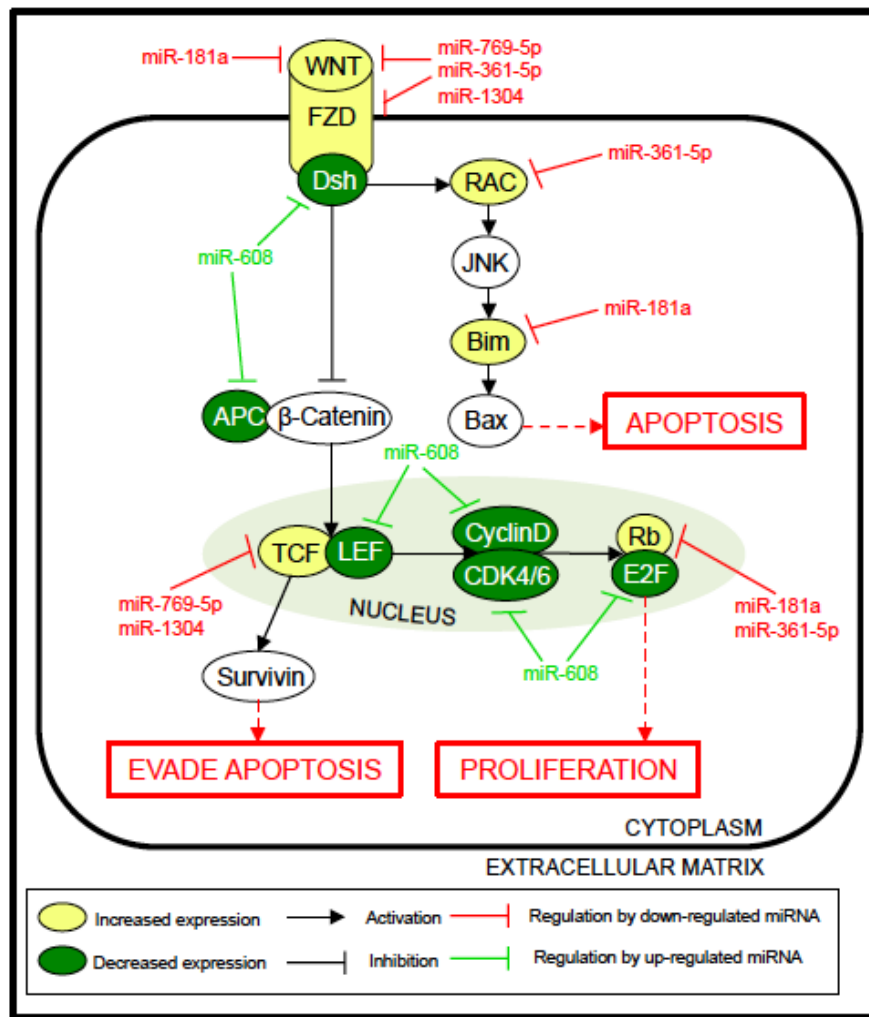


Figure 5.3: Hypothetical pathway model illustrating miRNA targets in the WNT pathway.

The WNT pathway mediates a variety of cellular processes including proliferation, differentiation, survival, apoptosis and cell motility (Willert and Jones, 2006). The loss of regulation of any of these processes can lead to tumorigenesis, and the WNT pathway has been implicated in the development of various cancers including leukemia (Mikesch *et al.*, 2007), colon (Jass *et al.*, 2003), breast (Turashvili *et al.*, 2006), thyroid, prostate (Yardy and Brewster, 2005) and lung (Tennis *et al.*, 2007).

Pathway analysis revealed that various members of the WNT pathway were also putative targets of the dysregulated miRNAs, including Wnt, frizzled (Fzd), dishevelled (Dsh) and adenomatous polyposis coli (APC) genes. Previously the overexpression of Dvl-3 has been found in NCLC tumors, leading to an activation of the WNT signaling in this disease (Uematsu *et al.*, 2003; Mazieries *et al.*, 2005; Tennis *et al.*, 2007). An increase in the Dsh concentration results in β -catenin stabilization and accumulation in the cytoplasm. Accumulated β -catenin will translocate into the nucleus where it will bind with members of the TCF transcription family (Young *et al.*, 1998), which will activate the transcription of various Wnt target genes including matrix metalloproteinases (MMP) (Tamamura *et al.*, 2005), cyclin D1 (Shtutman *et al.*, 1999), Cox-2 (Longo *et al.*, 2002), c-Myc (He *et al.*, 1998), c-Jun (Mann *et al.*, 1999), VEGF (Zhang *et al.*, 2001), and others. Thus, an increase in the β -catenin concentration will result in an increase in cell proliferation and growth, enhancing the tumorigenesis ability of the cell.

An inhibition of Dsh and APC by up-regulated hsa-miR-608 will result in the subsequent inhibition of the glycogen synthase-kinase-3-beta (GSK-3 β)/APC/Axin complex, which would prevent the phosphorylation of β -catenin and consequently decrease cell proliferation and cell growth in A549 cells. Inhibition of Dsh will also lead to the obstruction of survivin activation, via inhibition of T-cell factor/lymphoid enhancer factor (TCF/LEF), thus allowing for caspase activation to proceed, reinstating the cell's ability to carry out apoptosis (Uematsu *et al.*, 2003; Mazieries *et al.*, 2005; Tennis *et al.*, 2007). Other targets of up-regulated hsa-miR-608 include the LEF, CDK4/6 and cyclin D1, further inhibiting the cells ability to proliferate through cell cycle arrest.

5.3.4 TGF- β Pathway

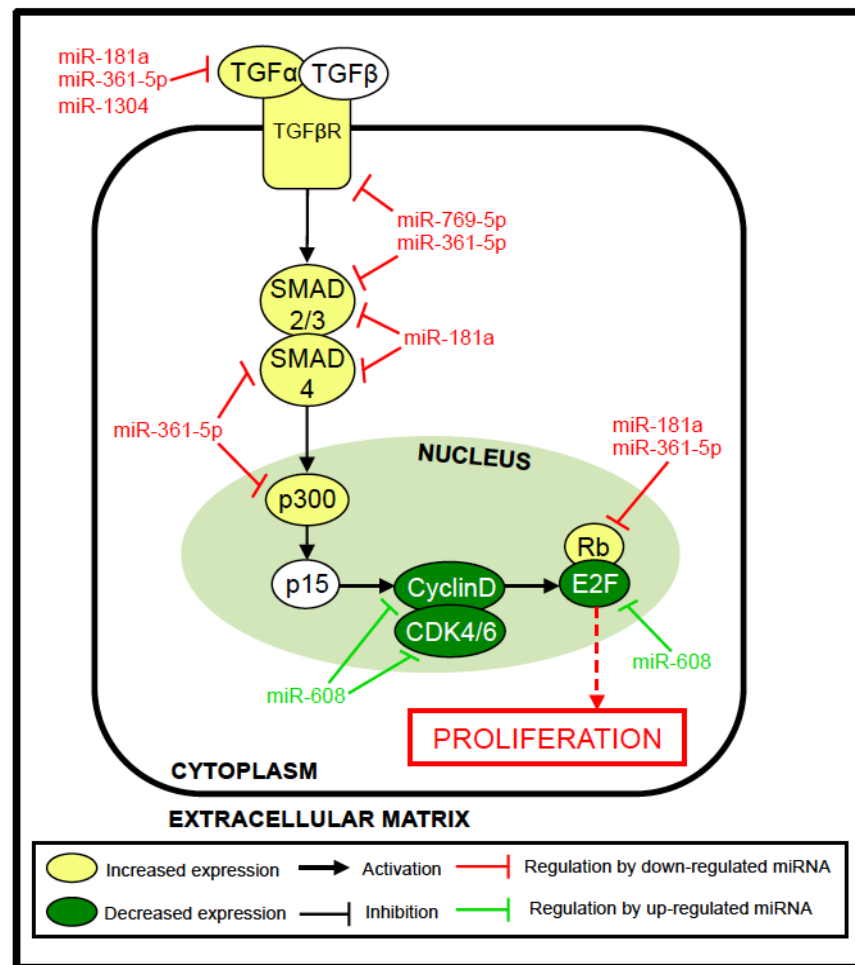


Figure 5.4: Hypothetical pathway model illustrating miRNA targets in the TGF- β pathway.

Alterations in the TGF- β signaling pathway have been linked to various human diseases including cancer. Studies have shown that the ligands along with its downstream elements, including its receptors and primary cytoplasmic signal transducers, as well as the Smad proteins are crucial for suppression of tumorigenesis in many tissue types (Markowitz and Roberts, 1996). In lung cancer studies, it has been found that TGF- β is frequently overexpressed, however the malignant transformation that occurs in lung cancer results in a loss of the tumor suppressor effects of TGF- β (Jeon and Jen, 2010). The loss of the tumor suppressor effects will promote cell

proliferation, tumor invasion and metastasis, and has therefore been strongly associated with tumor development or progression (Massagué 2008). Studies have also shown that in multiple lung cancer cell lines, in both small cell (Damstrup *et al.*, 1992) and non-small cell (Anumanthan *et al.*, 2005), the expression of TGFBR 2 is reduced (Toonkel *et al.*, 2010) allowing for the cancer cells to further circumvent the suppressive effects of TGF- β (Massagué, 2008).

Referring to Figure 5.4 it can be seen that TGFBR 1/2, Smad 2/3/4 are all targets of down-regulated miRNAs (hsa-miR-181a, hsa-miR-769-5p and hsa-miR-361-5p) indicating that gene expression was increased thus allowing them to carry out their tumor suppressive activities. Furthermore, with none of the p15 upstream proteins being inhibited by miRNAs, its presence will result in CDK inhibition and hypophosphorylated retinoblastoma protein (pRb) accumulation, which is associated with early G₁ phase arrest (Hannon and Beach, 1994; Reynisdottir *et al.*, 1995; Hanahan and Weinberg, 2000). Therefore this would presumably inhibit lung cancer cells' excessive proliferation and growth.

Cell proliferation and growth activity would be further decreased by the inhibition of cyclin D, CDK4/6 and E2F by the up-regulated hsa-miR-608. Cell proliferation is regulated by protein complexes that are made up of cyclins and cyclin-dependent kinases (CDKs) (Caputi *et al.*, 1999). Cyclin D1 assembles with CDK4, and alternatively with CDK6, and this complex will enter the nucleus to phosphorylate retinoblastoma (Rb) proteins which would in turn promote the release of E2F transcription factors (Caputi *et al.*, 1999; Kato *et al.*, 1994). Cyclin D1 is involved in the regulation of the G₁-to-S phase transition and is important for the restriction of cell growth (MacLachlan *et al.*, 1995). Studies have shown that cyclin D1 is frequently amplified in lung carcinomas (Yang *et al.*, 1996; Caputi *et al.*, 1999), therefore an inhibition of this gene is thought to play a role in the decrease of cell proliferation and

tumorigenesis of lung cancer.

5.3.5 MAPK Pathway

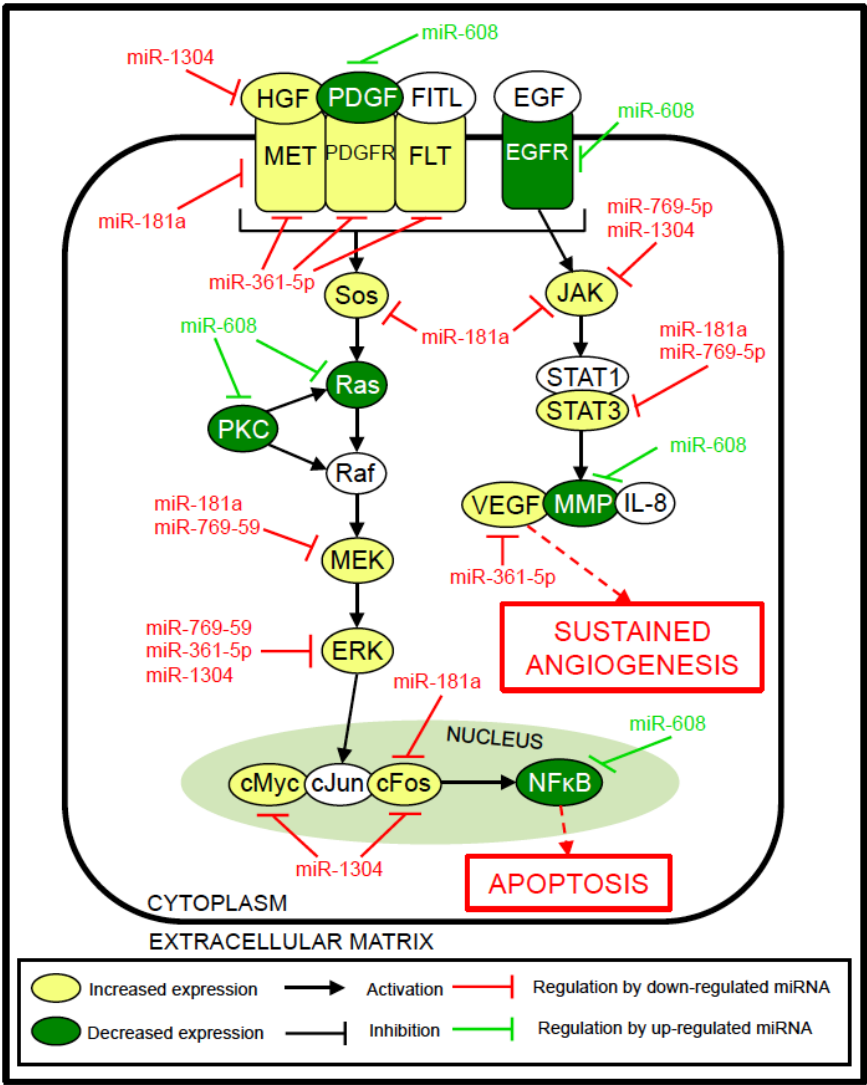


Figure 5.5: Hypothetical pathway model illustrating miRNA targets in the MAPK pathway.

The ERK signaling pathway has been shown to play a role in several steps of tumor development. Mutations associated with cancer have been found in components of the ERK signaling pathway, mainly in Ras and B-Raf (Dhillon *et al.*, 2007; Boutros *et al.*, 2008). Mutations of K-Ras frequently occur in colon and lung cancer, mainly in adenocarcinoma (Graziano *et al.*, 1999; Schubbert *et al.*, 2007). K-Ras activation will lead to stimulation of various pathways, primarily the Raf-MEK-ERK pathway and the PI3K pathway, that consequently results in tumor cell growth and proliferation, apoptosis, metastasis, invasion and angiogenesis (Aviel-Ronen *et al.*, 2006). Studies have shown that mutations in K-Ras have conferred poor prognosis and shorter overall survival in lung cancer patients (Slebos *et al.*, 1990).

K-Ras is activated when ligands bind to the receptor tyrosine kinases (RTKs) such as platelet-derived growth factor receptor (PDGFR), hepatocyte growth factor receptor (HGFR), and epidermal growth factor receptor (EGFR) (Molina and Adjei, 2006). Mutations in EGFR have also been found to frequently occur in lung cancer, and have been associated with a worse prognosis in patients with NSCLC (Hynes and MacDonald, 2009). Activation of the receptors upon binding of ligands will trigger the signaling pathways through the Ras-MAPK, and PI3K/Akt pathway (Paez *et al.*, 2004). Therefore a mutation in both EGFR and K-Ras will augment the tumorigenesis process in lung cancer cells.

Results indicate that both EGFR and Ras are targets of up-regulated hsa-miR-608. Inhibition of EGFR may lead to a slight decrease in the activation of Grb, however there are other receptors that may still provide stimulation for Grb. Nonetheless, an inhibition of Ras by hsa-miR-608 would lead to a break in the activation of the ERK pathway, by preventing Raf activation, which in turn prevents the phosphorylation of MEK and ERK1/2 leading to a decrease in cell growth and proliferation. Even though MEK and ERK are targets of down-regulated miRNAs (hsa-miR-181a, hsa-miR-769-5p,

hsa-miR-361-5p and hsa-miR-1304), and assuming that their expression increased or did not change, they would not be able to carry out their tumorigenic functions, as upstream proteins would not be able to phosphorylate and activate them. Inhibition of EGFR by has-miR-608 would also prevent the activation of JAK thus disrupting angiogenesis in the lung cancer cells as well.

To further support the linkage between MAPK and Bcl-xL miRNA interactions, recent studies have revealed new mechanisms by which ERK1/2 pathway can control the activity of Bcl-2 family proteins to promote cell survival (Balmanno and Cook, 2009). For example, ERK1/2 activation can repress the mRNA levels of the pro-apoptotic protein BIM (Fu and Tindall, 2008). Therefore, coupled with repression of Ras, it can be assumed that the downstream proteins will no longer be activated, thus Bim degradation would be avoided, allowing it to carry out its functions which would hypothetically lead to the occurrence of apoptosis.

5.4 Future Prospects

MiRNAs are strongly associated with cancer development and progression and a deregulation of miRNA expression are often seen in cancer. Experimental studies have shown that targeting miRNA expression can modify cancer phenotypes, thus miRNAs have become targets of novel anticancer gene therapy. As the miRNA field continues to evolve and develop it is important to gain a better understanding of miRNA biogenesis and function, as it will certainly affect the development of these miRNA-based therapies. While miRNAs as a target for cancer treatment has great potential, there are many challenges that must still be overcome. Major challenges for developing miRNA-based therapeutics may include issues of delivery, potential off-target effects as well as long-term safety concerns in humans (Garzon *et al.*, 2010). The chemical design of the

antisense and miRNA mimics must be improved as well as developing new delivery methods to overcome issues such as cellular uptake of the synthetic oligonucleotides to achieve target inhibition. Pharmacokinetic and pharmacodynamics studies will also have to be carried out to ensure that the desired miRNA concentrations are achieved in tissues and that targets are down-regulated (Garzon *et al.*, 2010). Generally, the idea of targeting miRNAs to reprogramme miRNA networks in cancer has a strong potential and chance for success.

In summary, this study describes the successful determination of miRNAs dysregulated in response to *bcl-xL* silencing in A549 adenocarcinoma NSCLC cells, with the aim to elucidate the hypothetical pathway these dysregulated miRNAs may be involved in to affect the induction of apoptosis. The identification of 10 significantly dysregulated miRNAs were linked to several apoptotic signaling pathways, using the TargetScan software, including the PI3K/AKT, intrinsic and extrinsic, WNT, TGF- β , and ERK pathway, and were all implicated as those directly affected by *bcl-xL* levels. However as many drawbacks exist in using only one target prediction software, in the future a comparison should be carried out using other miRNA targeting softwares such as PicTar and miRANDA. Furthermore, studies should also be carried out in other types of lung adenocarcinoma cell lines to investigate the similarity in the pattern of expression of dysregulated miRNAs when *bcl-xL* expression has been ectopically suppressed.

With further studies carried out to determine the specific functions of these dysregulated miRNAs, this study has provided a platform for antisense treatment whereby miRNA expression can be exploited to increase the apoptotic properties in lung adenocarcinoma cells.

CHAPTER 6: CONCLUSION

The main purpose of this entire study was to determine miRNAs dysregulated in response to *bcl-xL* silencing in A549 cells, with the aim to elucidate the hypothetical pathway these dysregulated miRNAs may be involved in to affect the apoptotic properties in lung adenocarcinoma. siRNA transfection in A549 cells decreased the *bcl-xL* expression at both the gene and protein levels and miRNA microarray analysis determined the differential miRNA expression profile between *bcl-xL* silenced and non-silenced cells, with the identification of ten significantly dysregulated miRNAs (hsa-miR-181a, hsa-miR-769-5p, hsa-miR-10b, hsa-miR-361-5p, hsa-miR-1304, hsa-miR-328, hsa-miR-99a, hsa-miR-130a, hsa-miR-768-3p, and hsa-miR-608). These ten dysregulated miRNAs were linked to several apoptotic signaling pathways including the PI3K/AKT, intrinsic and extrinsic, WNT, TGF- β , and ERK, and all were implicated as those directly affected by *bcl-xL* levels. It was therefore concluded that these miRNAs may play a significant role in inducing apoptosis in lung adenocarcinoma cells and may potentially be used as an antisense treatment in lung adenocarcinomas.

REFERENCES

- Akao, Y., Nakagawa, Y. and Naoe, T. (2006). *Let-7* microRNA functions as a potential growth suppressor in human colon cancer cells. *Biological and Pharmaceutical Bulletin* **29**: 903-906.
- Alexandrow, M.G. and Moses, H.L. (1995). Transforming growth factor β and cell cycle regulation. *Cancer Research* **55**: 1452-1457.
- Alnemri, E.S., Livingston, D.J., Nicholson, D.W., Salvesen, G., Thornberry, N.A., Wong, W.W. and Yuan J. (1996). Human ICE/CED-3 protease nomenclature. *Cell* **87**: 171.
- Amaral, J.D., Xavier, J.M., Steer, C.J. and Rodrigues, C.M. (2010). The role of p53 in apoptosis. *Discovery Medicine* **45**: 145-152.
- Anumanthan, G., Halder, S.K., Osada, H., Takahashi, T., Massion, P.P., Carbone, D.P. and Datta, P.K. Restoration of TGF-beta signaling reduces tumorigenicity in human lung cancer cells. *British Journal of Cancer* **10**: 1157-1167.
- Aplin, A.E., Howe, A., Alahari, S.K. and Juliano, R.L. (1998). Signal transduction and signal modulation by cell adhesion receptors: the role of integrins, cadherins, immunoglobulin-cell adhesion molecules, and selectins. *Pharmacological Reviews* **50**: 197-263.
- Aviel-Ronen, S., Blackhall, F.H., Shepherd, F.A. and Tsao, M.S. (2006). K-ras mutations in non-small-cell lung carcinoma: a review. *Clinical Lung Cancer* **1**: 30-38.
- Baffy, G., Miyashita, T., Williamson, J.R. and Reed, J.C. (1993). Apoptosis induced by withdrawal of interleukin-3 (IL-3) from an IL-3-dependent hematopoietic cell line is associated with repartitioning of intracellular calcium and is blocked by enforced Bcl-2 oncoprotein production. *Journal of Biological Chemistry* **268**: 6511-6519.
- Bakshi, A., Jensen, J.P., Goldman, P., Wright, J.J., McBride, O.W., Epstein, A.L. and Korsmeyer, S.J. (1985) Cloning the chromosomal breakpoint of t(14;18) human lymphomas: clustering around JH on chromosome 14 and near a transcriptional unit on 18. *Cell* **41**: 899-906.
- Balmano, K. and Cook, S.J. (2009). Tumour cell survival signaling by the ERK1/2 pathway. *Cell Death & Differentiation* **3**: 368-377.
- Bartel, D.P. (2004). MicroRNAs: genomics, biogenesis, mechanism and function. *Cell* **116**: 281-297.
- Bellacosa, A., de Feo, D., Godwin, A.K., Bell, D.W., Cheng, J.Q., Altomare, D.A., Wan, M., Dubeau, L., Scambia, G., Masciullo, V., Ferrandina, G., Benedetti Panici, P., Mancuso, S., Neri, G. and Testa, J.R. (1995). Molecular alterations of the AKT2 oncogene in ovarian and breast carcinomas. *International Journal of Cancer* **64**: 280-285.

- Bendotti, C., Bao Cutrona, M., Cheroni, C., Grignaschi, G., Lo Coco, D., Peviani, M., Tortarolo, M., Veglianese, P. and Zennaro, E. (2005). Inter- and intracellular signaling in amyotrophic lateral sclerosis: role of p38 mitogen-activated protein kinase. *Neurodegenerative Diseases* **2**: 128-134.
- Blenkiron, C. and Miska, E.A. (2007). miRNAs in cancer: approaches, aetiology, diagnostics and therapy. *Human Molecular Genetics* **16**: 106-113.
- Bonci, D., Coppola, V., Musumeci, M., Addario, A., Giuffrida, R., Memeo, L., D'Urso, L., Pagliuca, A., Biffoni, M., Labbaye, C., Bartucci, M., Muto, G., Peschle, C. and De Maria, R. (2008). The miR-15a-miR-16-1 cluster controls prostate cancer by targeting multiple oncogenic activities. *Nature Medicine* **14**: 1271-1277.
- Bouck, N., Stellmach, V. and Hsu, S.C. (1996). How tumors become angiogenic. *Advances in Cancer Research* **69**: 135-174.
- Boutros, T., Chevet, E. and Metrakos, P. (2008). Mitogen-activated protein (MAP) kinase/MAP kinase phosphatase regulation: roles in cell growth, death and cancer. *Pharmacological Reviews*. **60**: 261-310.
- Bradley, J.R. and Pober, J.S. (2001). Tumor necrosis factor receptor-associated factors (TRAFs). *Oncogene* **20**: 6482-6491.
- Brognard, J., Clark, A.S., Ni, Y. and Dennis, P.A. (2001) Akt/protein kinase B is constitutively active in non-small cell lung cancer cells and promotes cellular survival and resistance to chemotherapy and radiation. *Cancer Research* **61**: 3986-3997.
- Brunet, A., Bonni, A., Zigmond, M.J., Lin, M.Z., Juo, P., Hu, L.S., Anderson, M.J., Arden, K.C., Blenis, J. and Greenberg, M.E. (1999). Akt promotes cell survival by phosphorylating and inhibiting a Forkhead transcription factor. *Cell* **6**: 857-868.
- Buendia, B., Santa-Maria, A. and Courvalin, J.C. Caspase-dependent proteolysis of integral and peripheral proteins of nuclear membranes and nuclear pore complex proteins during apoptosis. *Journal of Cell Science* **112**: 1743-1753.
- Bull, H.A., Brickell, P.M. and Dowd, P.M. (1994) Src-related protein tyrosine kinases are physically associated with the surface antigen CD36 in human dermal microvascular endothelial cells. *FEBS Letters* **351**: 41-44.
- Calin, G.A., Dumitru, C.D., Shimizu, M., Bichi, S., Zupo, E., Noch, H., Aldler, S., Rattan, S., Keating, M., Rai, K., Rassenti, L., Kipps, T., Negrini, M., Bullrich, F. and Croce, C.M. (2002). Frequent deletions and downregulation of micro-RNA genes miR15 and miR16b at 13q14 in chronic lymphocytic leukemia. *Proceedings of the National Academy of Sciences of the United States of America* **99**: 15524-15529.

- Calin, G.A., Sevignani, C., Dumitru, C.D., Hyslop, T., Noch, E., Yendamuri, S., Shimizu, M., Rattan, S., Bullrich, F., Negrini, M. and Croce, C.M. (2004). Human microRNA genes are frequently located at fragile sites and genomic regions involved in cancers. *Proceedings of the National Academy of Sciences* **101**: 2999-3004.
- Calvo, R., West, J., Franklin, W., Erickson, P., Bemis, L., Li, E., Helfrich, B., Bunn, P., Roche, J., Brambilla, E., Rosell, R., Gemmill, R.M. and Drabkin, H.A. (2000). Altered HOX and WNT7A expression in human lung cancer. *Proceedings of the National Academy of Sciences of the United States of America* **97**: 12776-12781.
- Cano E. and Mahadevan, L.C. (1995). Parallel signal processing among mammalian MAPKs. *Trends in Biochemical Sciences* **20**: 117-122.
- Cano, E., Hazzalin, C.A. and Mahadevan, L.V. (1994). Anisomycin-activated protein kinases p45 and p55 but not mitogen-activated kinases ERK-1 and -2 are implicated in the induction of c-fos and c-jun. *Molecular and Cellular Biology* **14**: 7352-7362
- Caputi, M., Groeger, A.M., Esposito, V., Dean, C., De Luca, A., Pacilio, C., Muller, M.R., Giordano, G.G., Baldi, F., Wolner, E. and Giordano, A. (1999). Prognostic role of cyclin D1 in lung cancer. Relationship to proliferating cell nuclear antigen. *American Journal of Respiratory Cell and Molecular Biology* **4**: 746-750.
- Cardone, M.H., Roy, N., Stennicke, H.R., Salvesen, G.S., Franke, T.F., Stanbridge, E., Frisch, S. and Reed, J.C. (1998). Regulation of cell death protease caspase-9 by phosphorylation. *Science* **282**: 1318-1321.
- Chen, Z., Gibson, T.B., Robinson, F., Silvestro, L., Pearson, G. Xu, B.E., Wright, A., Vanderbilt, C. and Cobb, M.H. (2001). MAP kinases. *Chemical Reviews* **101**: 2449-2476.
- Cheng, H.L. and Feldman, F.L. (1998). Bidirectional regulation of p38 kinase and c-Jun N-terminal protein kinase by insulin-like growth factor-1. *Journal of Biological Chemistry* **273**: 14560-14565.
- Cheng, E.H., Wei, M.C., Weiler, S., Flavel, R.A., Mak, T.W., Lindsten, T. and Korsmeyer, S.J. (2001). BCL-2, BCL-X(L) sequester BH3 domain-only molecules preventing BAX- and BAK-mediated mitochondrial apoptosis. *Molecular Cell*. **8**: 705-711.
- Cheng, J.Q., Ruggeri, B., Klein, W.M, Sonoda, G., Altomare, D.A., Watson, D.K. and Testa, J.R. (1996). *Proceedings of the National Academy of Sciences of the United States of America* **93**: 3636-3641.
- Cimmino, A., Calin, G.A., Fabbri, M., Iorio, M.V., Ferracin, M., Shimizu, M., Wojcik, S.E., Aqeilan, R.I., Zupo, S., Dono, M., Rassenti, L., Alder, H., Volinia, S., Liu, CG., Kipps, T.J., Negrini, M. and Croce, CM. (2005). *miR-15* and *miR-16* induce apoptosis by targeting BCL2. *Proceedings of the National Academy of Sciences of the United States of America* **102**: 13944-13949.

- Cleary, M.L., Smith, S.D. and Sklar, J. (1986). Cloning and structural analysis of cDNA for *bcl-2* and a hybrid *bcl-2*/immunoglobulin transcript resulting from the t(14;18) translocation. *Cell* **47**: 19-28.
- Cohen, J.J., Duke, R.C., Fadok, V.A. and Sellins, K.S. (1992). Apoptosis and programmed cell death in immunity. *Annual Review of Immunology* **10**: 267-293.
- Collins, L.G., Haines, C., Perkel, R. and Enck, R.E. (2007). Lung cancer: diagnosis and management. *American Family Physician* **75**: 56-63.
- Croce, C.M. (2008). Oncogenes and cancer. *New England Journal of Medicine* **358**: 502-511.
- Dai, T., Rubie, E., Franklin, C.C., Kraft, A., Gillespie, D.A. Avruch, J., Kyriakis, J.M. and Woodgett, J.R. (1995). Stress activated protein kinases bind directly to the delta domain of c-Jun in resting cells: implications for repression of c-Jun function. *Oncogene* **10**: 849-855.
- Damstrup, L., Rygarrrd, K., Spang-Thomsen, M. and Poulsen, H.S. (1992). Expression of the epidermal growth factor receptor in human small cell lung cancer cell lines. *Cancer Research* **52**: 3089-3093.
- Daniel, J.C. and Smith, R. (2004). The role of Bcl-2 family members in nonsmall cell lung cancer. *Seminars in Thoracic and Cardiovascular Surgery* **16**: 19-27.
- Datta, S.R., Dudek, H., Tao, X., Masters, S., Fu, H., Gotoh, Y. and Greenberg, M.E. (1997). Akt phosphorylation of BAD couples survival signals to the cell-intrinsic death machinery. *Cell* **91**: 231-241.
- Davis, R.J. (1994). MAPKs: new JNK expands the ground. *Trends in Biochemical Sciences* **19**: 470-473.
- Davis, R.J. (2000). Signal transduction by the JNK Group of MAP kinases. *Cell* **103**: 239-252.
- Debatin, K.M. (2004) Apoptosis pathways in cancer and cancer therapy. *Cancer Immunology, Immunotherapy* **53**: 153–159.
- Dewson, G. and Kluck, R.M. (2010). Bcl-2 family-regulated apoptosis in health and disease. *Cell Health and Cytoskeleton* **2**: 9-22.
- Dhanasekaran, D.N. and Reddy, E.P. (2008). JNK signaling in apoptosis. *Oncogene* **27**: 6245-6251.
- Dhillon, A.S., Hagan, S., Rath, O. and Kolch, W. (2007). MAP kinase signaling pathways in cancer. *Oncogene* **26**: 3279-3290.
- Diehl, J.A., Cheng, M., Roussel, M.F. and Sherr, C.J. (1998). Glycogen synthase kinase-3B regulates cyclin D1 proteolysis and subcellular localization. *Genes & Development* **12**: 3499-3511.

- Dosaka-Akita, H., Katabami, M., Hommura, H., Fujiko, Y., Katoh, H., Kawakami, Y. (1999). Bcl-2 expression in non-small cell lung cancers: higher frequency of expression in squamous cell carcinomas with earlier pT status. *Oncology* **3**: 259-264.
- Elbashir, S.M, Martinez, J., Patkaniowska, A., Lendeckel, W. and Tuschl, T. (2001). Functional anatomy of siRNAs for mediating efficient RNAi in *Drosophila melanogaster* embryo lysate. *EMBO Journal* **23**: 6877-6888.
- Engel, T. and Henshall, D.C (2009). Apoptosis, Bcl-2 family proteins and caspases: the ABCs of seizure damage and epileptogenesis? *International Journal of Physiology, Pathophysiology and Pharmacology* **1**: 97-115.
- Fan, M. and Chambers, T.C. (2001). Role of mitogen-activated protein kinases in the response of tumor cells to chemotherapy. *Drug Resistance Updates* **4**: 253-267.
- Filipowicz, W. (2005). RNAi: the nuts and bolts of the RISC machine. *Cell* **122**: 17-20.
- Fisher, T.C., Milner, A.E., Gregory, C.D., Jackman, A.L., Aherne, G.W., Hartley, J.A., Dive, C. and Hickman, J.A. (1993). Bcl-2 modulation of apoptosis induced by anticancer drugs: resistance to thymidylate stress is independent of classical resistance pathways. *Cancer Research* **53**: 3321-3326.
- Fong, K.M., Yoshitaka, S. and John, D.M. (1999). Molecular pathogenesis of lung cancer. *Journal of Thoracic and Cardiovascular Surgery* **118**: 1136-1152.
- Fu, Z. and Tindall, D.J. (2008). FOXOs, cancer and regulation of apoptosis. *Oncogene* **16**: 2312-2319.
- Galluzzi, L., Morselli, E., Vitale, I., Kepp, O., Senovilla, L., Criollo, A., Servant, N., Paccard, C., Hupe, P., Robert, T., Ripoche, H., Lazar, V., Harel-Bellan, A., Dessen, P., Barillot, E. and Kroemer, G. (2010). miR-181a and miR-630 regulate cisplatin-induced cancer cell death. *Cancer Research* **5**: 1793-1803.
- Garrido, C., Galluzzi, L., Brunet, M., Puig, P.E, Didelot, C. and Kroemer, G. (2006). Mechanisms of cytochrome c release from mitochondria. *Cell Death and Differentiation* **9**: 1423-1433.
- Garzon, R., Marcucci, G. and Croce, C.M. (2010). Targeting microRNAs in cancer: rationale, strategies and challenges. *Nature Reviews Drug Discovery* **9**: 775-789.
- Ge, B., Gram, H., Di Padova, F., Huang, B., New, L., Ulevitch, R.J., Luo, Y. and Han, J. (2002). MAPKK-independent activation of p38alpha mediated by TAB1-dependent autophosphorylation of p38alpha. *Science* **295**: 1291-1294.
- Gesbert, E. and Griffin, J.D. (2000). Bcr/Abl activates transcription of the Bcl-X gene through STAT5. *Blood* **6**: 2269-2276.
- Giard, D.J., Aaronson, S.A., Todaro, G.J., Arnstein, P., Kersey, J.H., Dosik, H. and Parks, W.P. (1972). In vitro cultivation of human tumors: establishment of cell lines derived from a series of solid tumors. *Journal of the National Cancer Institute* **51**: 1417-1423.

- Gille, H., Sharrocks, A.D. and Shaw, P.E. (1992). Phosphorylation of transcription factor p62TCF by MAP kinase stimulates ternary complex formation at cfos promoter. *Nature* **358**: 414-417.
- Gills, J.J., Castillo, S.S., Zhang, C., Petukhov, P.A., Memmott, R.M., Hollingshead, M., Warfel, N., Han, J., Kozikowski, A.P. and Dennis, P.A. (2007). Phosphatidylinositol ether analogues that inhibit AKT also independently activate the stress kinase, p38alpha through MKK3/6-independent and – dependent mechanisms. *Journal of Biological Chemistry* **282**: 27020-27029.
- GLOBOCAN 2008 Fast Stats. 2008. International Agency for Research on Cancer. 14 March 2009. <http://globocan.iarc.fr/factsheets/populations/factsheet.asp?uno=900>
- Gottlieb, E., Vander Heiden, M.G. and Thompson, C.G. (2000). Bcl-xL prevents the initial decrease in mitochondrial membrane potential and subsequent reactive oxygen species production during tumor necrosis factor alpha-induced apoptosis. *Molecular and Cellular Biology* **20**: 5680-5689.
- Gottschalk, A.R., Boise, L.H., Thompson, C.B. and Quintanos, J. (1994). Identification of immunosuppressant-induced apoptosis in a murine B-cell line and its prevention by bcl-x but not bcl-2. *Proceedings of the National Academy of Sciences USA* **15**: 7350-7354.
- Grad, J.M., Zeng, X.R. and Boise, J.H. (2000). Regulation of Bcl-xL: a little bit of this and a little bit of STAT. *Current Opinion in Oncology* **12**: 543-549.
- Graziano, S.L., Gamble, G.P., Newman, N.B., Abbott, L.Z., Rooney, M., Mookherjee, S., Lamb, M.L., Kohman, L.J. and Poiesz, B.J. (1999). Prognostic significance of K-ras codon 12 mutations in patients with resected stage I and II non-small-cell lung cancer. *Journal of Clinical Oncology* **2**: 668-675.
- Green, D.R. and Kroemer, G. (2004). The pathophysiology of mitochondrial cell death. *Science* **305**: 626-629).
- Greenberg, A.K., Basu, S., Hu, J., Yie, T.A., Tchou-Wong, K.M., Rom, W.N. and Lee, T.C. (2002). Selective p38 activation in human non-small cell lung cancer. *American Journal of Respiratory Cell and Molecular Biology* **26**: 558-564.
- Greenblatt, M.S., Bennet, W.P., Hollstein, M. and Harris, C.C. (1994). Mutations in the p53 tumor suppressor gene: clues to cancer etiology and molecular pathogenesis. *Cancer Research* **54**: 4855-4878.
- Groeger, A.M., Esposito, V., De Luca, A., Cassandro, R., Tonini, G., Ambrogi, V., Baldi, F., Goldfarb, R., Mineo, T.C., Baldi, A. and Wolner E. (2004). Prognostic value of immunohistochemical expression of p53, bax, Bcl-xL in resected non-small-cell lung cancers. *Histopathology* **44**: 54 – 63.
- Haeusgen, W., Boehm, R. Zhao, Y., Herdegen, T. and Waetzig, V. (2009). Specific activities of individual c-Jun N-terminal kinases in the brain. *Neuroscience* **161**: 951-959.

- Han, J., Goldstein, L.A., Gastman, B.R. and Rabinowich, H. (2006). Interrelated roles for Mcl-2 and BIM in regulation of TRAIL-mediated mitochondrial apoptosis. *The Journal of Biological Chemistry* **281**: 10153-10163.
- Han, J., Lee, Y., Yeom, K.H., Kim, Y.K., Jin, H. and Kim, V.N. (2004). The Drosha-DGCR8 complex in primary microRNA processing. *Genes & Development* **18**: 3016-3027.
- Han, S.W., Hwang, P.G., Chung, D.H., Kim, D.W., Im, S.A., Kim, Y.T., Kim, T.Y., Heo, D.S., Bang, Y.J. and Kim, N.K. (2005). Epidermal growth factor receptor (EGFR) downstream molecules as response predictive markers for gefitinib (Iressa ZD1839) in chemotherapy-resistant non-small cell lung cancer. *International Journal of Cancer* **113**: 109-115.
- Hanahan, D. and Folkman, J. (1996) Patterns and emerging mechanisms of the angiogenic switch during tumorigenesis. *Cell* **86**: 353-364.
- Hanahan, D. and Weinberg, R.A. (2000). The hallmarks of cancer. *Cell* **100**: 57-60.
- Hanahan, D. and Weinberg, R.A. (2011). Hallmarks of cancer: the next generation. *Cell* **144**: 646-674.
- Hannon, G.J. and Beach, D. (1994). P15^{INK4B} is a potential effector of TGF- β -induced cell cycle arrest. *Nature* **371**: 257-261.
- Harrington, K.J. (2007). Biology of cancer. *Medicine* **36**: 1-4.
- Hart, I.R. (2004) Biology of cancer. *Medicine* **32**: 1-5.
- Hayashita, Y., Osada, H., Tatematsu, Y., Yamada, H., Yanagisawa, K., Tomida, S., Yatabe, Y., Kawahara, K., Sekido, Y. and Takahashi, T. (2005). A polycistronic microRNA cluster, miR-17-92, is overexpressed in human lung cancers and enhances cell proliferation. *Cancer Research* **65**: 9628-9632.
- He, B., You, L., Uematsu, K., Xu, Z., Lee, A.Y., Matsangou, M., McCormick, F. and Jablons, D.M. (2004). A monoclonal antibody against Wnt-1 induces apoptosis in human cancers. *Neoplasia* **6**: 7-14.
- He, L., He, X., Lim, L.P., de Stanchina, E., Xuan, Z., Liang, Y., Xue, W., Zender, L., Magnus, J., Ridzon, D., Jackson, A.I., Linsley, P.S., Chen, C., Lowe, S.W., Cleary, M.A. and Hannon, G.J. (2007). A microRNA component of the p53 tumour suppressor network. *Nature* **447**: 1130-1134.
- He, L., Thomson, J.M., Hemann, M.T., Hernandez-Monge, E., Mu, D., Goodson, S., Powers, S., Cordon-Cardo, C., Lowe, S.W., Hannon, G.J. and Hammond, S.M. (2005). A microRNA polycistron as a potential human oncogene. *Nature* **435**: 828-833.
- He, T.C., Sparks, A.B., Rago, C., Hermeking, H., Zawel, L., da Costa, L.T., Morin, P.J., Vogelstein, B. and Kinzler, K.W. (1998). Identification of c-MYC as a target of the APC pathway. *Science* **281**: 1509-1512.

- Hecht, S.S. (1999). Tobacco smoke carcinogens and lung cancer. *Journal of the National Cancer Institute* **91**: 1194-1210.
- Hengartner, M.O. (2000). The biochemistry of apoptosis. *Nature* **407**: 770-776.
- Hibi, M., Lin, A., Smeal, T., Minden, A. and Karin, M. (1993). Identification of an oncoprotein and UV-responsive protein kinase that binds and potentiates the c-Jun activation domain. *Genes & Development* **7**: 2135-2148.
- Hill, M.M. and Hemmings, B.A. (2002). Inhibition of protein kinase B/Akt. Implications for cancer therapy. *Pharmacology Therapeutics* **93**: 243-251.
- Hockenbery, D.M., Zutter, M., Hickey, W., Nahm, M. and Korsmeyer, S.J. (1991). BCL2 protein is topographically restricted in tissues characterized by apoptotic cell death. *Proceedings of the National Academy of Sciences of the United States of America* **88**: 6961-6965.
- Holen, T., Amarzguoui, M., Wiiger, M.T., Babaie, E. and Prydz, H. (2002). Positional effects of short interfering RNAs targeting the human coagulation trigger Tissue Factor. *Nucleic Acids Research* **8**: 1757-1766.
- Hommura, F., Furuuchi, K., Yamazaki, K., Ogura, S., Kinoshita, I., Shimizu, M., Moriuchi, T., Katoh, H., Nishimura, M. and Dosaka-Akita, H. (2002). Increased expression of β -catenin predicts better prognosis in nonsmall cell lung carcinomas. *Cancer* **94**: 752-758.
- Honda, R. and Yasuda, H. (2000). Activity of MDM2, a ubiquitin ligase, toward p53 or itself is dependent on the RING finger domain of the ligase. *Oncogene* **11**: 1473-1478.
- Huang, D.W., Sherman, B.T. and Lempicki, R.A. (2009). Systematic and integrative analysis of large gene lists using DAVID Bioinformatic Resources *Nature Protocols* **4**: 44-57.
- Huang, G., Shi, L.Z. and Chi, H. (2009). Regulation of JNK and p38 MAPK in the immune system: signal integration, propagation and termination. *Cytokine* **48**: 161-169.
- Hynes, N.E. and MacDonald, G. (2009). ErbB receptors and signaling pathways in cancer. *Current Opinion in Cell Biology* **2**: 177-184.
- Iavarone, A. and Massagué, J. (1997). Repression of the CDK activation Cdc25A and cell-cycle arrest by cytokine TGF- β in cells lacking the CDK inhibitor p15. *Nature* **387**: 417-422.
- Janmaat, M.L., Kruij, F.A., Rodriguez, J.A. and Giaccone, G. (2003). Response to epidermal growth factor receptor inhibitors in non-small cell lung cancer cells: limited antiproliferative effects and absence of apoptosis associated with persistent activity of extracellular signal-regulated kinase or Akt kinase pathways. *Clinical Cancer Research* **9**: 2316-2326.

- Jass, J.R., Barker, M., Fraser, L., Walsh, M.D., Whitehall, V.L., Gabrielli, B., Young, J. and Leggett, B.A. (2003). *Journal of Clinical Pathology* **1**: 69-73.
- Jemal, A., Bray, F., Center, M.M., Ferlay, J., Ward, E. and Forman, D. (2011). Global Cancer Statistics. *CA: A Cancer Journal for Clinicians* **16**: 69-90.
- Jeon, H.S. and Jen, J. (2010). TGF- β signaling and the role of inhibitory Smads in non-small cell lung cancer. *Journal of Thoracic Oncology* **5**: 417-419.
- Jeong, S.Y., Gaume, B., Lee, Y.J., Hsu, Y.T., Ryu, S.W., Yoon, S.H. and Youle, R.J. (2004). Bcl-x(L) sequesters its C-terminal membrane anchor in soluble, cytosolic homodimers. *The European Molecular Biology Organization Journal*. **23**: 2146-2155.
- Jiang, S.X., Sato, Y., Kuwao, S. and Kameya, T. (1995). Expression of bcl-2 oncogene protein is prevalent in small cell lung carcinomas. *The Journal of Pathology* **2**: 135-139.
- Johnson, G.L. and Nakamura, K. (2007). The c-Jun kinase/stress-activated pathway: regulation, function and role in human disease. *Biochimica et Biophysica Acta* **1773**: 1341-1348.
- Kamesaki, S., Kamesaki, H., Jorgensen, T.J., Tanizawa, A., Pommier, Y. and Crossman, J. (1993). Bcl-2 protein inhibits etoposide-induced apoptosis through its effects on events subsequent to topoisomerase II-induced DNA strand breaks and their repair. *Cancer Research* **53**: 4251-4256.
- Kandasamy, K. and Srivastava, R.K. (2002). Role of the phosphatidylinositol 3'-kinase/PTEN/Akt kinase pathway in tumor necrosis factor-related apoptosis-inducing ligand-induced apoptosis in non-small cell lung cancer cells. *Cancer Research* **17**: 4929-4937.
- Kato, M., Sasaki, T., Imazumi, K., Takahashi, K., Araki, K., Shirataki, H., Matsuura, Y., Ishida, A., Fujisawa, H. and Takai, Y. (1994). Phosphorylation of Rabphilin-3A by calmodulin-dependent protein kinase II. *Biochemical and Biophysical Research Communications* **3**: 1776-1784.
- Kazutsugu, U., Biao, H., Liang, Y., Zhidong, X., McCormick, F., and Jablons, D.M. (2003). Activation of the Wnt pathway in non small cell lung cancer: evidence of disheveled overexpression. *Oncogene* **22**: 7218-7221.
- Kerr, J.F., Wyllie, A.H. and Currie, A.R. (1972). Apoptosis: a basic biological phenomenon with wide-ranging implications in tissue kinetics. *British Journal of Kinetics* **26**: 239-257.
- Khosravi-Far, R. and Esposti, M.D. Death receptor signals to mitochondria. *Cancer Biology & Therapy* **3**: 1051-1057.
- Kim, E.K. and Choi, E.J. (2010). Pathological role of MAPK signaling pathways in human diseases. *Biochimica et Biophysica Acta* **1802**: 396-405

- Kim, S.J., Im, Y.H., Markowitz, S.D. and Bang, Y.J. (2000). Molecular mechanisms of inactivation of TGF-beta receptors during carcinogenesis. *Cytokine & Growth Factor Reviews* **11**: 159-168.
- Kim, V.N. and Nam, J.W. (2006). Genomics of microRNA. *Trends in Genetics* **14**: 165-173.
- Kota, J., Chivukula, R.R., O'Donnell, K.A., Wentzel, E.A., Montgomery, C.L., Hwang, H.W., Chang, T.C., Vivekanandan, P., Torbenson, M., Clark, R., Mendell, J.R. and Mendell, J.T. (2009). Therapeutic microRNA delivery suppresses tumorigenesis in a murine liver cancer model. *Cell* **137**: 1005-1017.
- Kubbutat, M.H., Jones, S.N. and Vousden, K.H. (1997). Regulation of p53 stability by Mdm2. *Nature* **6630**: 299-303.
- Kyriakis, J.M. and Avruch, J. (2001). Mammalian mitogen-activated protein kinase signal transduction pathways activated by stress and inflammation. *Physiological Reviews* **81**: 807-869.
- Lagos-Quintana, M., Rauhut, R., Meyer, J., Borkhardt, A. and Tuschl, T. (2003). New microRNAs from mouse and human. *RNA* **9**: 175-179.
- Lagos-Quintana, M., Rauhut, R., Lendeckel, W. and Tuschl, T. (2001). Identification of novel genes coding for small expressed RNAs. *Science* **294**: 853-858.
- Lee, R.C., Feinbaum, R.L. and Ambros, V. (1993). The *C. elegans* heterochronic gene *lin-4* encodes small RNAs with antisense complementarity to *lin-14*. *Cell* **75**: 843-854.
- Leech, S.H., Olie, R.A., Gautschi, O., Simoes-Wust, A.P., Tschopp, S., Haner, R., Hall, J., Stahel, R.A. and Zangemeister-Wittke, U. (2000). Induction of apoptosis in lung-cancer cells following bcl-xL anti-sense treatment. *International Journal of Cancer* **4**: 570-576.
- Levy, O.A., Malagelada, C. and Greene, L.A. (2009). Cell death pathways in Parkinson's disease: proximal triggers, distal effectors, and final steps. *Apoptosis* **14**: 478-500.
- Lewis, B.P., Burge, C.B. and Bartel, B.P. (2005). Conserved seed pairing, often flanked by adenosines, indicates that thousands of human genes are microRNA targets. *Cell* **120**: 15-20.
- Lewis, T.S., Shapiro, P.S. and Ahn, N.G. (1998). Signal transduction through MAP kinase cascades. *Advances in Cancer Research* **74**: 49-139.
- Liam C.K, Pang Y.K, Leow C.H, Poosparajah S. and Menon A (2006) Changes in the distribution of lung cancer cell types and patient demography in a developing multiracial Asian country: Experience of a university teaching hospital. *Lung Cancer* **53**: 23-30.

- Lieber, M., Smith, B., Szakal, A., Nelson-Rees, W. and Todaro, G. (1976). A continuous tumor-cell line from a human lung carcinoma with properties of type II alveolar epithelial cells. *International Journal of Cancer* **17**: 62-70.
- Loffler, D., Brocke-Heidrich, K., Pfeifer, G., Stocsits, C., Hackermuller, J., Kretschmar, A.K., Burger, R., Gramatzki, M., Blumert, C., Bauer, D., Cvijic, H., Ullmann, A.K., Stadler, P.F. and Horn, F. (2007). Interleukin-6 dependent survival of multiple myeloma cells involves the Stat3-mediated induction of microRNA-21 through a highly conserved enhancer. *Blood* **110**: 1330-1333.
- Longo, K.A., Kennel, J.A., Ochocinska, M.J., Ross, S.E., Wright, W.S. and MacDougald, O.A. (2002). Wnt signaling protects 3T3-L1 preadipocytes from apoptosis through induction of insulin-like growth factors. *Journal of Biological Chemistry* **277**: 38239-38244.
- Lu, J., Getz, G., Miska, E.A., Alvarez-Saavedra, E., Lamb, J., Peck, D., Sweet-Cordero, A., Ebert, B.L., Mak, R.H., Ferrando, A.A., Downing, J.R., Jacks, T., Horvitz, H.R. and Golub, T.R. (2005). MicroRNA expression profiles classify human cancers. *Nature* **435**: 834-838.
- Lund, E., Guttinger, S., Calado, A., Dahlberg, J.E. and Kutay, U. (2004). Nuclear export of microRNA precursors. *Science* **303**: 95-98.
- Lung Carcinoma. 2009. The Merck Manuals Online Medical Library. 1 March 2009. <http://www.merck.com/mmpe/sec05/ch062/ch062b.html#sec05-ch062-ch062b-1405>
- Ma, X. and Yu, H. (2006). Cancer epidemiology: Global burden of cancer. *Yale Journal of Biology and Medicine* **79**: 85-94.
- MacLachlan, T.K., Sang, N. and Giordano, A. (1995). Cyclins, cyclin-dependent kinases and cdk inhibitors: implications in cell cycle control and cancer. *Critical Reviews in Eukaryotic Gene Expression* **2**: 127-158.
- Malumbres, M. and Barbacid, M. (2003). RAS oncogenes: the first 30 years. *Nature Reviews of Cancer* **3**: 459-465.
- Mann, B., Gelos, M., Siedow, A., Hanski, M.L., Gratchev, A., Ilyas, M., Bodmer, W.F., Moyer, M.P., Riecken, E.O. and Buhr, H.J. (1999). Target genes of betacatenin-T cell-factor/lymphoid-enhancer factor signaling in human colorectal carcinomas. *Proceedings of the National Academy of Sciences of the United States of America* **96**: 1603-1608.
- Mao, Q. and Unadkat, J.D. (2005). Role of the breast cancer resistance protein (ABCG2) in drug transport. *The AAPS Journal* **1**: 118-133.
- Markowitz, S.D. and Roberts, A.B. (1996). Tumor suppressor activity of the TGF-beta pathway in human cancers. *Cytokine and Growth Factor Reviews* **1**: 93-102.
- Massagué, J. (1998). TGF- β signal transduction. *Annual Review of Biochemistry* **67**: 753-791.

- Massagué, J. and Wotton, D. (2000). Transcriptional control by the TGF- β /Smad signaling system. *The European Molecular Biology Organization Journal* **19**: 1745-1754.
- Matranga, C., Tomari, Y. and Shin, C. (2005). Passenger-strand cleavage facilitates assembly of siRNA into Ago2-containing RNAi enzyme complexes. *Cell* **123**: 607-620.
- Mayo, L.D. and Donner, D.B. (2001). A phosphatidylinositol 3-kinase/Akt pathway promotes translocation of Mdm2 from the cytoplasm to the nucleus. *Proceedings of the National Academy of Sciences of the United States of America* **98**: 11598-11603.
- Mazieries, J., He, B., You, L., Xu, Z. and Jablons, D.M. (2005). Wnt signaling in lung cancer. *Cancer Letters* **222**: 1-10.
- Menon, M.A., and Saw, H.S. (1979). Lung cancer in Malaysia. *Thorax* **34**: 269-273.
- Mercer, B.A. and D'Armiento, J.M. (2006). Emerging role of MAPkinase pathways as therapeutic targets in COPD. *International Journal of COPD* **2**: 137-150.
- Mikesch, J.H., Steffen, B., Berdel, W.E., Serve, H. and Muller-Tidow, C. (2007). The emerging role of Wnt signaling in the pathogenesis of acute myeloid leukemia. *Leukemia* **8**: 1638-1647.
- Miller, Y.E. (2005) Pathogenesis of lung cancer – 100 year report. *American Journal of Respiratory Cell and Molecular Biology* **33**: 216-223.
- Milne, D.M., Campbell, D.G., Caudwell, F.B. and Meek, D.W. (1994). Phosphorylation of the tumor suppressor protein p53 by mitogen-activated protein kinases. *The Journal of Biological Chemistry* **269**: 9253-9260.
- Miyashita, T. and Reed, J.C. (1993). Bcl-2 oncoprotein blocks chemotherapy-induced apoptosis in human leukemia cell line. *Blood* **81**: 151-157.
- Molina, J.R. and Adjei, A.A. (2006). The Ras/Raf/MAPK pathway. *Journal of Thoracic Oncology* **1**: 7-9.
- Morton, S., Davis, R.J., McLaren, A. and Cohen, P. (2003). A reinvestigation of the multisite phosphorylation of the transcription factor c-Jun. *The European Molecular Biology Organization Journal* **22**: 3876-3886.
- Mott, J.L., Kobayahi, S., Bronk, S.F. and Gores, G.J. (2007). miR-29 regulates Mcl-1 protein expression and apoptosis. *Oncogene* **26**: 6133-6140.
- Murphy, L.O., Smith, S., Chen, R.H., Fingar, D.C. and Blenis, J. (2002). Molecular interpretation of ERK signal duration by immediate early gene products. *Nature Cell Biology* **4**: 556-564.
- Nana-Sinkan, S.P. and Croce, C.M. (2011). MicroRNAs as therapeutic targets in cancer. *Translational Research* **157**: 216-225.

- Noordermeer, J., Klingensmith, J., Perrimon, N. and Nusse, R. (1994). Dishevelled and armadillo act in the wingless signaling pathway in *Drosophila*. *Nature* **367**: 80-83.
- Paez, J.G., Janne, P.A., Lee, J.C., Tracy, S., Greulich, H., Gabriel, S., Herman, P., Kaye, F.J., Lindeman, N., Boggon, T.J., Naoki, K., Sasaki, H., Fujii, Y., Eck, M.J., Sellers, W.R., Johnson, B.E. and Meyerson, M. (2004). EGFR mutations in lung cancer: correlation with clinical response to gefitinib therapy. *Science* **5676**: 1497-1500.
- Parkin, D.M., Ehelan, S.L., Ferlay, J., Raymond, L. and Young, J. (1996) Cancer incidence in five continents. *International Agency for Research on Cancer* 143.
- Pasquinelli, A.E., Reinhart, B.J. and Slack, F. (2000). Conservation of the sequence and temporal expression of let-7 heterochronic regulatory RNA. *Nature* **408**: 86-89.
- Perez, M., Moran, M.A., Ferrer, I., Avila, J. and Gomez-Ramos, P. (2008). Phosphorylated tau in neuritic plaques of APP (sw)/Tau (vlw) transgenic mice and Alzheimer disease. *Acta Neuropathologica* **116**: 409-418.
- Pfaffl, M.W. (2001). A new mathematical model for relative quantification in real-time RT-PCR. *Nucleic Acids Research* **29**: 2002-2007.
- Plotnikov, A., Zehorai, E., Procaccia, S. and Seger, R. (2011). The MAPK cascades: signaling components, nuclear roles, and mechanisms of nuclear translocation. *Biochimica et Biophysica Acta* **1813**: 1619-1633
- Pyne N.J. and Pyne, S. (1997). Platelet-derived growth factor activates a mammalian Ste20 coupled mitogen-activated protein kinase in airway smooth muscles. *Cell Signal* **3-4**: 311-317.
- Rachwal, W.J., Bongiorno, P.F., Orringer, M.B., Whyte, R.I., Ethier, S.P. and Beer, D.G. (1995). Expression and activation of erb-2 and epidermal growth factor receptor in lung adenocarcinomas. *British Journal of Cancer* **72**: 56-64.
- Raman, M., Chen, W. and Cobb, M.H. (2007) Differential regulation and properties of MAPK. *Oncogene* **26**: 3100-3112.
- Rand, T.A., Petersen, S., Du., F. and Wang, X. (2005). Argonaute2 cleaves the antitarget strand of siRNA during RISC activation. *Cell* **123**: 621-629.
- Rao, L., Perez, D. and White, E. (1996). Lamin proteolysis facilitates nuclear events during apoptosis. *Journal of Cell Biology* **135**: 1441-1445.
- Reeve, J.G., Xiong, J., Morgan, J. and Bleehen, N.M. (1996). Expression of apoptosis-regulatory genes in lung tumour cell lines: relationship to p53 expression and relevance to acquired drug resistance. *British Journal of Cancer* **10**: 1193-1200.
- Reinhart, B.J., Slack, F.J., Basson, M., Pasquinelli, A.E., Bettinger, J.C., Rougvie, A.E., Horvitz, H.R. and Ruvkun, G. (2000). The 21-nucleotide let-7 RNA regulates developmental timing in *Caenorhabditis elegans*. *Nature* **403**: 901-906.

- Reynisdottir, I., Polvak, K., Iavarone, A. and Massague, J. (1995). Kip/Cip and Ink4 Cdk inhibitors cooperate to induce cell cycle arrest in response to TGF-beta. *Genes & Development* **15**: 1832-1845.
- Richardson, G.E. and Johnson, B.E. (1993). The biology of lung cancer. *Seminars in Oncology* **20**: 105-127.
- Rincon, M. and Davis, R.J. (2009). Regulation of the immune response by stress-activated protein kinases. *Immunological Reviews* **228**: 212-224.
- Roberts, A.B. and Wakefield L.M. (2003). The two faces of transforming growth factor beta in carcinogenesis. *Proceedings of the National Academy of Sciences of the United States of America* **100**: 8621-8623.
- Rodriguez, A., Griffiths-Jones, S., Ashurst, J.L. and Bradley, A. (2004). Identification of mammalian microRNA host genes and transcription units. *Genome Research*. **14**: 1902-19020.
- Rosell, R., Pifarre, A., Monzo, M., Astudillo, J., Lopez-Cabrerizo, M.P., Calvo, R., Moreno, I., Sanchez-Cespedes, M., Font, A. and Navas-Palacios, J.J. (1997). Reduced survival in patients with stage-I non-small-cell lung cancer associated with DNA-replication errors. *International Journal of Cancer* **74**: 330-334.
- Rousseau, S., Houle, F., Landry, J. and Huot, J. (1997). P38 MAP kinase activation by vascular endothelial growth factor mediates actin reorganization and cell migration in human endothelial cells. *Oncogene* **18**: 2169-2177.
- Ruan, K., Fang, X. and Ouyang, G. (2009). MicroRNAs: Novel regulators in the hallmarks of human cancer. *Cancer Letters* **28**: 116-126
- Ruano-Ravina, A., Figueiras, A. and Barros-Dios, J.M. (2003). Lung cancer and related risk factors: an update of the literature. *Journal of The Royal Institute of Public Health* **17**: 149-156.
- Sanchez-Ceja, S.G., Reyes-Maldonado, E., Vazquez-Manriquez, M.E., Lopez-Luna, J.J., Belmont, A. and Gutierrez-Castellanos, S. (2006). Differential expression of STAT5 and Bcl-xL, and high expression of Neu and STAT3 in non-small-cell lung carcinoma. *Lung Cancer* **2**: 163-168.
- Sassen, S., Miska, E.A. and Caldas, C. (2008). MicroRNA- implications for cancer. *Virchows Arch* **452**: 1-10.
- Schubbert, S., Shannon, K. and Bollag, G. (2007). Hyperactive Ras in developmental disorders and cancer. *Nature Reviews of Cancer* **7**: 295-308.
- Sebolt-Leopold, J.S., Dudley, D.T., Herrera, R., Becelaere, K.V., Wiland, A., Gowan, R.C., Tecle, H., Barrett, S.D., Bridges, A., Przybranowski, S., Leopold, W.R. and Saltiel, A.R. (1999). Blockade of the MAP kinase pathway suppresses growth of colon tumors in vivo. *Nature Medicine* **5**: 810-816.
- Second Report of the National Cancer Registry, Cancer Incidence in Malaysia. (2008). National Cancer Registry, Malaysia. 20 April 2009. <http://www.crc.gov.my/ncr>

- Sekido, Y., Fong, K.M. and Minna, J.D. (1998). Progress in understanding the molecular pathogenesis of human lung cancer. *Biochimica et Biophysica Acta* **1378**: 21-59.
- Shaul, Y.D. and Seger, R. (2007). The MEK/ERK cascade: From signaling specificity to diverse functions. *Biochimica et Biophysica Acta* **1773**: 1213-1226.
- Shi, L., Cheng, Z., Zhang, J., Li, R., Zhao, P., Fu, Z. and You, Y. (2008). Hsa-miR-181a and hsa-miR-181b function as tumor suppressors in human glioma cells. *Brain Research* **1236**: 185-193.
- Shivdasani, R.A. (2006). MicroRNAs: regulators of gene expression and cell differentiation. *Blood* **108**: 3646-3653.
- Shtutman, M., Zhurinsky, J., Simcha, I., Albanese, C., D'Amico, M., Pestell, R. and Ben-Ze'ey, A. (1999). The cyclin D1 gene is a target of the beta-catenin/LEF-1 pathway. *Proceedings of the National Academy of Sciences of the United States of America* **96**: 5522-5527.
- Singh, N. (2007). Apoptosis in health and disease and modulation of apoptosis therapy: An overview. *Journal of Clinical Biochemistry* **22**: 6-16.
- Singh, N. and Anand, S. (1994). Cell death by apoptosis. *Indian Journal of Experimental Biology* **1644**: 169-177.
- Slebos, R.J.C., Kibbelaar, R.E., Dalesio, O., Kooistra, A., Stam, J., Meijer, C.J.L.M., Wagenaar, S.S., Vanderschueren, R.G.J.R.A., van Zandwijk, N., Mooi, W.J., Bos, J.L. and Rodenhuis, S. (1990). K-ras oncogene activation as a prognostic marker in adenocarcinoma of the lung. *The New England Journal of Medicine* **323**: 561-565.
- Sluss, H.K., Barrett, T., Derijard, B. and Davis, R.J. (1994). Signal transduction by tumor necrosis factor mediated by JNK protein kinases. *Molecular and Cellular Biology* **14**: 8376-8384.
- Sohn, S.J., Thompson, J. and Winoto, A. (2007). Apoptosis during negative selection of autoreactive thymocytes. *Current Opinion in Immunology* **19**: 510-515.
- Soini, Y., Kinnula, V., Wiik-Kaarteenaho, R., Kurtilla, E., Linnainmaa, K. and Paakko, P. (1999) Apoptosis and expression of apoptosis regulating proteins bcl-2, mcl-1, bcl-x and bax in malignant mesothelioma. *Clinical Cancer Research* **5**: 3508-3515.
- Sontheimer, E.J. (2005). Assembly and function of RNA silencing complexes. *Nature Reviews Molecular Cell Biology* **6**: 127-138.
- Sorenson CM (2004) Bcl-2 family members and disease. *Biochimica et Biophysica Acta* **1644**: 169-177.

- Staal, S.P. (1987) Molecular cloning of the akt oncogene and its human homologues AKT1 and AKT2: amplification of AKT1 in a primary human gastric adenocarcinoma. *Proceedings of the National Academy of Sciences of the United States of America* **84**: 5034-5037.
- Strasser, A., Jost, P.J. and Nagata, S. (2009). The many roles of FAS receptor signaling in the immune system. *Immunity* **30**: 180-192.
- Sunaga, N., Kohno, T., Kolligs, F.T., Fearon, E.R., Saito, R. and Yokota, J. (2001). Constitutive activation of the Wnt signaling pathway by *CTNNB1* (β -catenin) mutations in a subset of human lung adenocarcinoma. *Genes, Chromosomes and Cancer* **30**: 316-321.
- Takamizawa, J., Konishi, H., Yanagisawa, K., Tomida, S., Osada, H., Endoh, H., Harano, T., Yatabe, Y., Nagino, M., Nimura, Y., Mitsudomi, T. and Takahashi, T. (2004). Reduced expression of the let-7 microRNAs in human lung cancers in association with shortened postoperative survival. *Cancer Research*. **64**: 3753-3756.
- Tamamura, Y., Otani, T., Kanatani, N., Koyama, E., Kitagaki, J., Komori, T., Yamada, Y., Costantini, F., Wakisaka, S., Pacifici, M., Iwamoto, M. and Enomoto-Iwamoto, M. (2005). Developmental regulation of Wnt/betacatenin signals is required for growth plate assembly, cartilage integrity, and endochondral ossification. *Journal of Biological Chemistry* **280**: 19185-19195.
- Tang, C., Willingham, M.C., Reed, J.C., Miyashita, T., Ray, S., Ponnathpur, V., Huang, Y., Mahoney, M.F., Bullock, G. and Bhalla, K. (1994). High levels of p26BCL-2 oncoprotein retard taxol-induced apoptosis in human pre-B leukemia cells. *Leukemia* **8**: 1960-1969.
- Tang, J.M., He, Q.Y., Guo, R.X. and Chang, X.J. (2006). Phosphorylated Akt overexpression and loss of PTEN expression in non-small cell lung cancer confers poor prognosis. *Lung Cancer* **51**: 181-191.
- Tateishi, M., Ishida, T., Mitsudomi, T., Kaneko, S. and Sugimachi, K. (1990). Immunohistochemical evidence of autocrine growth factors in adenocarcinoma of the human lung. *Cancer Research* **50**: 7077-7080.
- Taylor, R.C., Cullen, S.P. and Martin, S.J. (2008). Apoptosis: controlled demolition at the cellular level. *Nature Reviews Molecular Cell Biology*. **9**: 231-241.
- Tennis, M., Van Scoyk, M. and Winn, R.A. (2007). Role of the Wnt signaling pathway and lung cancer. *Journal of Thoracic Oncology* **2**: 889-892.
- Tetsu, O. and McCormick, F. (1999). Beta-catenin regulates expression of cyclin D1 in colon carcinoma cells. *Nature* **398**: 422-426.
- Testa, J.R. and Bellacosa, A. (2001). AKT plays a central role in tumorigenesis. *Proceedings of the National Academy of Sciences of the United States of America* **98**: 10983-10985.

- Thornton, T.M. and Rincon, M. (2009). Non-classical p38 map kinase functions: cell cycle checkpoints and survival. *International Journal of Biological Sciences* **5**: 44-51.
- Toonkel, R.L., Borczuk, A.C. and Powell, C.A. (2010). Tgf-beta signaling pathway in lung adenocarcinoma invasion. *Journal of Thoracic Oncology* **2**: 153-157.
- Tricoli, J.V. and Jacobson, J.W. (2007). MicroRNA: Potential for cancer detection, diagnosis, and prognosis. *Cancer Research* **67**: 4553-4555.
- Tsang, W.P. and Kwok, T.T. (2008). Let-7a microRNA suppressed therapeutics-induced cancer cell death by targeting caspase-3. *Apoptosis* **13**: 1215-1222.
- Tsujimoto, Y., Cossman, J., Jaffe, E. and Croce, C. M. (1985). Involvement of the *bcl-2* gene in human follicular lymphoma. *Science* **228**, 1440–1443.
- Turashvili, G., Bouchal, J., Burkadze, G. and Kolar, Z. (2006). Wnt signaling pathway in mammary gland development and carcinogenesis. *Pathobiology* **5**: 213-223.
- Uematsu, K., He, B., You, L., Xu, Z., McCormick, F. and Jablons, D.M. (2003). Activation of the Wnt pathway in non small cell lung cancer: evidence of disheveled overexpression. *Oncogene* **46**: 7218-7221.
- Van Herwaarden, A.E. and Schinkel, A.H. (2006). The function of breast cancer resistance protein in epithelial barriers, stem cells and milk secretion of drugs and xenotoxins. *Trends in Pharmacological Sciences* **1**: 10-16.
- Vincent, S., Garayoa, M., Lopez-Picazo, J.M., Lozano, M.D., Toledo G., Thunnissen, F.B.J.M., Manzano, R.G. and Montuenga, L.M. (2004). Mitogen-activated protein kinase phosphatase-1 is overexpressed in non-small cell lung cancer and is an independent predictor of outcome in patients. *Clinical Cancer Research* **10**: 3639-3649.
- Vivanco, I. and Sawyers, C.L. (2002). The phosphatidylinositol 3-kinase-AKT pathway in human cancer. *Nature Reviews: Cancer* **2**: 489-501
- Volinia, S., Calin, G.A., Liu, C.G., Ambs, S., Cimmino, A., Petrocca, F., Visone, R., Iorio, M., Roldo, C., Ferracin, M., Prueitt, R.L., Yanaihara, N., Lanza, G., Scarpa, A., Vecchione, A., Negrini, M., Harris, C.C. and Croce, C.M. (2006). A microRNA expression signature of human solid tumors defines cancer gene targets. *Proceedings of the National Academy of Sciences of the United States of America* **103**: 2257-2261.
- Vore, M. and Leggas, M. (2006). Progesterone acts via progesterone receptors A and B to regulate breast cancer resistance protein expression. *Molecular Pharmacology* **3**: 613-615.
- Walker, J.C. and Harland, R.M. (2009). MicroRNA-24a is required to repress apoptosis in the developing neural retina. *Genes & Development* **23**: 1046-1051.

- Walton, M.I., Whyson, D., O'Connor, P.M., Hockenbery, D., Korsmeyer, S.J. and Kohn, K.W. (1993). Constitutive expression of human Bcl-2 modulates nitrogen mustard and camptothecin induced apoptosis. *Cancer Research* **53**: 1853-1861.
- Wang, J.Z. and Liu, F. (2008). Microtubule-associated protein tau in development, degeneration and protection of neurons. *Progress in Neurobiology*. **85**: 148-175.
- Weber, M.J. (2005). New human and mouse microRNA genes found by homology search. *The FEBS Journal* **272**: 59-73
- Weimer, EAC. (2007). The role of microRNAs in cancer: No small matter. *European Journal of Cancer* **43**: 1529-1544.
- Weiner, D.B., Nordber, J., Robinson, R., Nowell, P.C., Gazdar, A., Green, M.I., Williams, W.V., Cohen, J.A. and Kern, J.A. (1990). Expression of the *neu* gene-encoded protein (P185*neu*) in human non-small cell carcinomas of the lung. *Cancer Research* **50**: 421-425.
- Westwick, J.K., Weitzel, C., Minden, A., Karin, M. and Brenner, D.A. (1994). Tumor necrosis factor alpha stimulates AP-1 activity through prolonged activation of the c-Jun kinase. *The Journal of Biological Chemistry* **269**: 26396-26401.
- Whitmarsh, A.J. and Davis, R.J. (2007). Role of mitogen-activated protein kinase kinase 4 in cancer. *Oncogene* **26**: 3172-3184.
- Wightman, B., Ha, I. and Ruvkun, G. (1993). Posttranscriptional regulation of the heterochronic gene *lin-14* by *lin-4* mediates temporal pattern formation in *C. elegans*. *Cell* **75**: 855-862.
- Willert, K. and Jones, K.A. (2006). Wnt signaling: is the party in the nucleus. *Genes & Development* **11**: 1394-1404.
- Winn, R.A., Bremnes, R.M, Bemis, L., Franklin, W.A., Miller, Y.E., Cool, C. and Heasley, L.E. (2002). gamma-Catenin expression is reduced or absent in a subset of human lung cancers and re-expression inhibits transformed cell growth. *Oncogene* **21**: 7497-7506.
- Witschi, H. (2001). A short history of lung cancer. *Toxicological Sciences* **64**: 4-6.
- Woods, K., Thomson, J.M. and Hammond, S.M. (2007). Direct regulation of an oncogenic micro-RNA cluster by E2F transcription factors. *Journal of Biological Chemistry* **282**: 2130-2134.
- Xiao, C., Srinivasan, L., Calado, D.P, Patterson, H.C., Zhang, B., Wang, J., Henderson, J.M., Kutok, J.L. and Rajewsky, K. (2008). Lymphoproliferative disease and autoimmunity in mice with increased miR-17-92 expression in lymphocytes. *Nature Immunology* **9**: 405-414.
- Xu, C., Lu, Y., Pan, Z., Chu, W., Luo, X., Lin, H., Xiao, J., Shan, H., Wang, Z. and Yang, B. (2007). The muscle-specific microRNAs miR-1 and miR-133 produce opposing effects on apoptosis by targeting HSP60, HSP70 and caspase-9 in cardiomyocytes. *Journal of Cell Science* **120**: 3045-3052.

- Yanagisawa, K., Osada, H., Masuda, A., Kondo, M., Saito, T., Yatabe, Y., Takagi, K., Takahashi, T. and Takahashi, T. (1998). Induction of apoptosis by Smad3 and downregulation of Smad3 expression in response to TGF-beta in human normal lung epithelial cells. *Oncogene* **17**: 1743-1747.
- Yanaihara, N., Caplen, N., Bowman, E., Seike, M., Kumamoto, K., Yi, M., Stephens, R.M., Okamoto, A., Yokota, J., Tanaka, T., Calin, G.A., Liu, C.G., Croce, C.M. and Harris, C.C. (2006). Unique microRNA molecular profiles in lung cancer diagnosis and prognosis. *Cancer Cell* **9**: 189-198.
- Yang, B.S., Hauser, C.A., Henkel, G., Colman, M.S., Van Beveren, C., Stacey, K.J., Hume, D.A., Maki, R.A. and Ostrowski, M.C. (1996). Ras-mediated phosphorylation of a conserved threonine-residue enhances the transactivation activities of c-Ets1 and c-Ets2. *Molecular and Cellular Biology*. **16**: 538-547.
- Yardy, G.W. and Brewster, S.F. (2005). Wnt signaling and prostate cancer. *Prostate Cancer and Prostatic Diseases* **2**: 119-126.
- Yi, R., Qin, Y., Macara, I.G. and Cullen, B.R. (2003). Exportin-5 mediates the nuclear export of pre-microRNAs and short hairpin RNAs. *Gene & Development*. **17**: 3011-3016.
- You, L., He, B., Xu, Z., Uematsu, K., Mazieres, J., Mikami, I., Reguart, N., Wood, T.W., Kitajewski, J., McCormick, F. and Jablons, D.M. (2004). Inhibition of Wnt-2-mediated signaling induces programmed cell death in non-small-cell lung cancer cell. *Oncogene* **23**: 6170-6174.
- Youle, R.J. and Strasser A. (2008). The Bcl-2 protein family: opposing activities that mediate cell death. *Nature Reviews: Molecular Cell Biology* **9**: 47-59.
- Yu, D., Wang, S.S., Dulski, K.M., Tsai, C.M., Nicolson, G.L. and Hung, M.C. (1994). c-erbB-2/*neu* overexpression enhances metastatic potential of human lung cancer cells by induction of metastasis-associated properties. *Cancer Research* **54**: 3260-3266.
- Zainal, A.O. and Nor Saleha, I.T. (2011). National Cancer Registry Report : Malaysia Cancer Statistics – Data and Figure 2007. National Cancer Registry, Ministry of Health Malaysia.
- Zha, J., Harada, H., Yang, E., Jockel, J. and Korsmeyer, S.J. (1996). Serine phosphorylation of death agonist BAD in response to survival factor results in binding to 14-3-3 not Bcl-XL. *Cell* **87**: 619-628.
- Zhang, B., Pan, X., Cobb, G.P. and Anderson, T.A. (2007). MicroRNAs as oncogenes and tumor suppressors. *Developmental Biology* **302**: 1-12.
- Zhang, X., Gaspard, J.P. and Chung, D.C. (2001). Regulation of vascular endothelial growth factor by the Wnt and K-ras pathways in colonic neoplasia. *Cancer Research* **61**: 6050-6054.

Zhou, B.P., Liao, Y., Xia, W., Zou, Y. Spohn, B. and Hung, M.C. (2001). HER-2/neu induces p53 ubiquitination via Akt-mediated MDM2 phosphorylation. *Nature Cell Biol.* **3**: 973-982.

APPENDICES

Appendix 1: Solutions and Formulations

i) Roswell Park Memorial Institute 1640 (RPMI 1640)

To prepare 250ml of Roswell Park Memorial Institute 1640 (RPMI 1640) culture media supplemented with heat inactivated 10% (v/v) fetal bovine serum (FBS), 25mL of FBS was added into a sterile autoclaved bottle and mixed with 225ml of sterile RPMI 1640, and stored at 4°C.

ii) 1×Phosphate-Buffered Saline (PBS)

To prepare 1 liter of 1×PBS solution (pH 7.4), 100ml of premixed 10× calcium- and magnesium-free (CMF) PBS (Mediatech, USA) was added to a sterile autoclaved bottle and topped up with distilled water to 1 liter. The 1×PBS was then autoclaved at 121°C, 15psi for 45 minutes and then stored at room temperature.

iii) 0.1% (v/v) Trypsin-0.53mM EDTA

98mg of ethylenediaminetetracetic acid (EDTA) (GibcoBRL, USA) was dissolved in 500ml of 1×PBS to prepare 1×PBS-0.53mM EDTA. The solution was then autoclaved at 121°C, 15psi for 45 minutes and stored at room temperature. 100ml of 0.1% (v/v) of trypsin solution was prepared by mixing 4ml of 2.5% (v/v) trypsin (Sigma-Aldrich, USA) with 96ml of sterile 1×PBS-0.53mM EDTA, and then stored at room temperature.

iv) Diethyl pyrocarbonate (DEPC)-treated water

1L of 0.1% (v/v) DEPC-treated water was prepared by adding 1ml of DEPC (Merck, Germany) to 1 liter of distilled water. The solution was mixed well by shaking and left at room temperature overnight prior to being autoclaved at 121°C, 15psi for 45 minutes, and then stored at room temperature.

v) 1×Tris/Borate/EDTA (TBE) electrophoresis buffer

1L of 1×TBE was prepared by mixing 100ml of 10×Tris/Boric Acid/EDTA (Bio-Rad, USA) with 900ml of DEPC-treated water and was then stored at room temperature.

vi) 1% (w/v) agarose gel

A 1% (w/v) agarose gel was prepared by dissolving 400mg of agarose powder (Fisher Scientific, USA) in 40ml of 1×TBE electrophoresis buffer. The solution was boiled to allow for the solution to be completely dissolved. The molten gel was poured into a casting tray with a comb and left at room temperature to allow for complete polymerization.

vii) Ethidium bromide (EtBr) solution

10mg/ml of stored EtBr (Sigma-Aldrich, USA) was diluted to 0.5µg/ml in DEPC-treated water, and stored at room temperature.

viii) 2.0% (w/v) Bis-acrylamide

2 grams of bisacrylamide powder (Promega, USA) was added to a sterile autoclaved bottle and topped up to 100ml with ultra-pure water.

ix) 0.5M Tris-HCl, pH 6.8

200ml of 0.5M Tris-HCl was prepared by dissolving 12.1 grams of Tris Base powder (Promega, USA) in 100ml of ultra-pure water. The pH of the solution was adjusted to 6.8 with hydrogen chloride (HCl) and the total volume brought up to 200ml.

x) 1.5M Tris-HCl, pH 8.8

200ml of 1.5M Tris-HCl was prepared by dissolving 36.6 grams of Tris Base powder in 100ml of Ultra-pure water. The pH of the solution was adjusted to 8.8 with HCl and the total volume brought up to 200ml.

xi) 10% (w/v) Sodium Dodecyl Sulfate (SDS)

10 grams of SDS powder (Promega, USA) was added to a sterile autoclaved bottle and topped up to 100ml with ultra-pure water, and then stored at room temperature.

xii) 10% (w/v) Ammonium Persulfate (APS)

10% APS was prepared fresh each time in a microcentrifuge tube. 10mg APS (Pierce, USA) was dissolved in 100 μ l of distilled water. The solution was mixed well using a vortex.

xiii) Transfer buffer (1 \times TGS + 10% MeOH (v/v))

500ml of transfer buffer was prepared by mixing 100ml of methanol (Merck, Germany) with 40ml of premixed 10 \times TGS buffer (Merck, Germany) and topped up to 500ml with distilled H₂O.

xiv) 1 \times Tris/Glycine/SDS (TGS) buffer

1L of 1 \times TGS buffer was prepared by diluting 100ml of premixed 10 \times TGS buffer (Merck, Germany) with 900ml of distilled water.

xv) Blocking buffer

Blocking buffer for phosphorylated protein (blocking buffer A) consisted of 5.0% (w/v) non-fat skim milk powder (Merck, Germany), 0.05% (v/v) Tween20 (Promega, USA) in 1 \times TBS. Blocking buffer for non-phosphorylated proteins (blocking buffer B) consisted of 5.0% Bovine Serum Albumin (BSA) (Calbiochem, USA), 0.05% Tween 20 and 1 \times TBS.

xvi) 1×Tris-buffered saline-0.05% (v/v) Tween20 (TBST) buffer

To prepare 1L of 10×TBST buffer the following were mixed together: 12.11g of Tris Base powder, 87.66g of sodium chloride (NaCl) (Merck, Germany), 5.0ml of Tween20, and 800ml of distilled water. The solution was adjusted with 1N of HCl (Merck, Germany) to pH7.6 and then topped up with distilled water to 1L. 100ml of 10×TBST was diluted with 900ml of distilled water to prepare 1L of 1×TBST.

xvii) 1×Tris-buffered saline (TBS) buffer

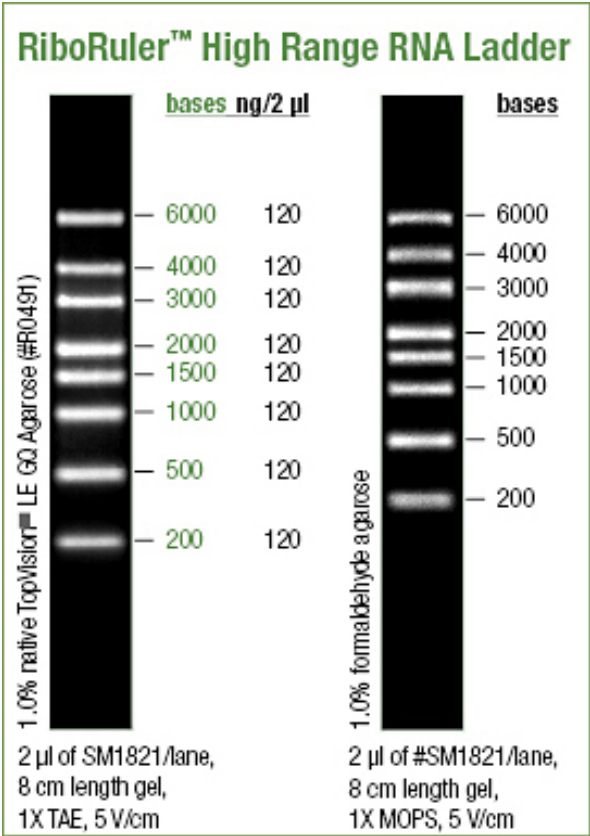
To prepare 1L of 10×TBS buffer the following were mixed together: 12.11g of Tris Base powder, 87.66g of NaCl, and 800ml of distilled water. The solution was adjusted with 1N of HCl to pH 7.6, and then topped up with distilled water to 1L. 100ml of 10×TBS was diluted with 900ml of distilled water to prepare 1L of 1×TBS.

xviii) MTT reagent

MTT reagent was prepared by adding 50.0mg of MTT (Calbiochem, USA) to 10.0ml of 1× CMF-PBS. The reagent was shaken vigorously and vortexed to ensure that the MTT granules were completely dissolved. MTT working solutions were stored in the dark at room temperature (25°C), and the MTT stock was stored in the dark at 4°C. The final concentration of MTT working solution in the MTT cell viability assay was 5mg/ml.

Appendix 2: Molecular Markers

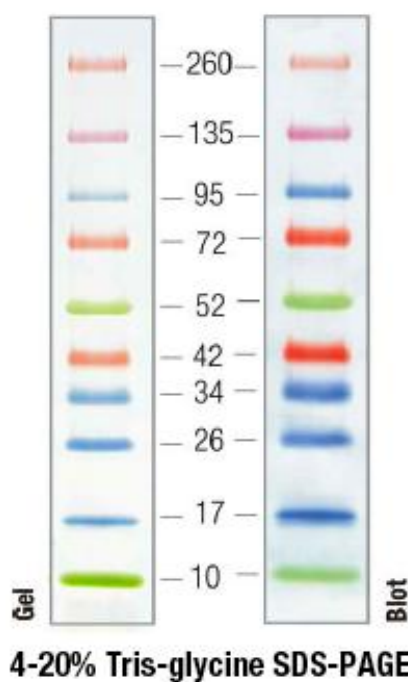
- i) **RNA Molecular Weight Marker** - RiboRuler™ High Range RNA Ladder with 200-6000 bases as reference sizes



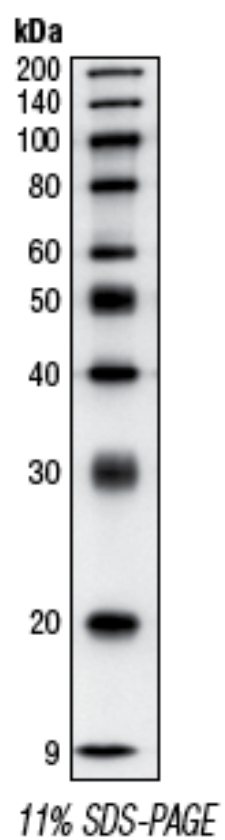
ii) Protein Ladder

Spectra™ Multicolor Broad Range Protein Ladder consisted of ten pre-stained sized recombinant proteins molecular weight 260, 135, 95, 72, 52, 42, 34, 26, 17 and 10kDa.

Representative lot of Spectra™ Multicolor Broad Range Protein Ladder, apparent MW, kDa



The Biotinylated Protein Ladder (Cell Signaling Technology, USA) consisted of 10 proteins ranging in apparent molecular weights from 9 to 200kDa.



Appendix 3: siRNA Binding Site

siRNA binding sites on Homo sapiens *Bcl-xL*, nuclear gene encoding mitochondrial protein, transcript variant 1, mRNA. The sequence identity of all three siRNAs to the *bcl-xL* mRNA was 100%.

```

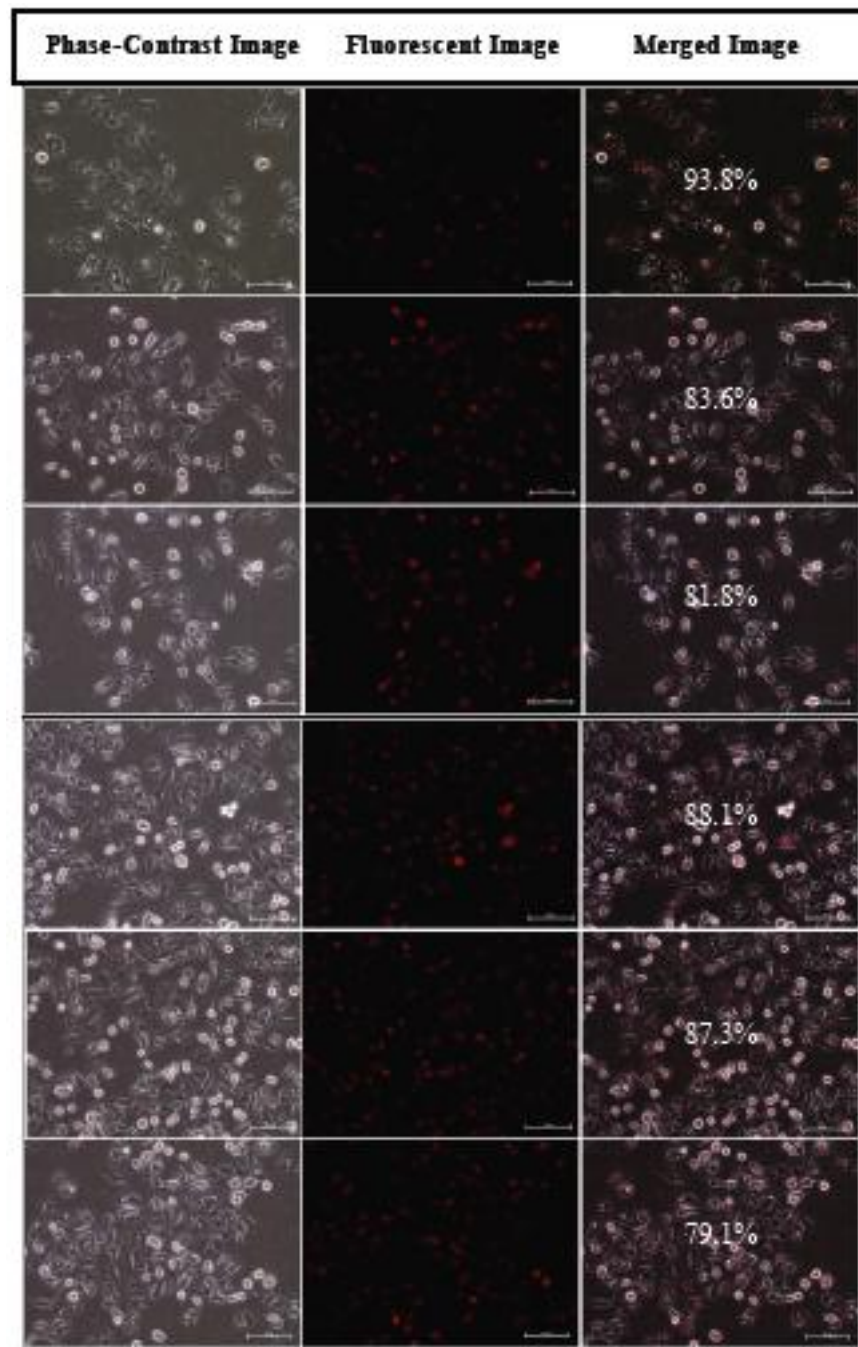
1  ggaggaggaa gcaagcgagg gggctggttc ctgagcttcg caattcctgt gtcgccttct
61  gggctcccag cctgccgggt cgcgatgatcc ctccggcccg agctggtttt ttgcccagcc
121 accgcgaggc cggctgagtt accggcatcc ccgcagccac ctccctctccc gacctgtgat
181 acaaaagatc ttccgggggc tgcacctgcc tgccctttgcc taaggcggat ttgaatctct
241 ttctctccct tcagaatctt atcttggctt tggatcttag aagagaatca ctaaccagag
301 acgagactca gtgagtgagc aggtgttttg gacaatggac tggttgagcc catccctatt
361 ataaaaatgt ctcagagcaa ccgggagctg gtggttgact ttctctocta caagctttcc
421 cagaaaggat acagctggag tcagtttagt gatgtggaag agaacaggac tgaggcccca
481 gaagggactg aatcggagat ggagaccgcc agtgccatca atggcaaccc atcctggcac
541 ctggcagaca gccccgcggt gaatggagcc actggccaca gcaacagttt ggatgcccgc
601 gaggtgatcc ccatggcagc agtaaaagcaa gcgctgaggg aggcaggcga cgagtttgaa
661 ctgcggtacc ggcgggcatt cagtgcctg acatcccagc tccacatcac cccagggaca
721 gcatatcaga gctttgaaca ggtagtgaat gaactcttcc gggatggggg aaactggggg
781 cgcatgtgtg cctttttctc cttcggcggt gcaactgtgc tggaaagcgt agacaaggag
841 atgcaggtat tggtagtgct gatcgcagct tggatggcca cttacctgaa tgaccacctc
901 gagccttgga tccaggagaa cgcgggctgg gatacttttg tggaactcta tgggaacaat
961 gcagcagcgg agagccgaaa gggccaggaa cgcttcaacc gctggttcct gacgggcatg
1021 actgtggccg gcgtggttct gctgggctca ctcttcagtc ggaaatgaccagacactgac
1081 catccactct accctcccac cccttctct gctccaccac atcctccgtccagccgccat
1141 tgccaccagg agaaccacta catgcagccc atgcccacct gcccatcacagggttgggccc
1201 cagatctggt cccttgacgc tagttttcta gaatttatca cacttctgtgagacccccac
1261 acctcagttc ccttggcctc agaattcaca aaatttccac aaaatctgtccaaaggaggc
1321 tggcaggtat ggaagggttt gtggctgggg gcaggagggc cctacctgattggtgcaacc
1381 cttaccctct agcctccctg aaaatgtttt tctgcccagg agcttgaaagttttcagaac
1441 gtcctccaga agcctctggc tagattgcct ttgttttgat gtttgggctcagaaattga
1501 tcattttccc cccactctcc ccacactaac ctgggttccc tttccttccatccctacccc
1561 ctaagagcca tttaggggcc acttttgact agggattcag gctgcttgggataaagatgc
1621 aaggaccagg actccctcct cacctctgga ctggctagag tcctcactcccagtcacaaat
1681 gtcctccaga agcctctggc tagaggccag cccaccccag gagggaggggctatagcta
1741 caggaagcac cccatgccaa agctagggtg gcccttgca gttcagcaccaccctagtccc
1801 ttcccctccc tggctcccat gaccatactg agggaccaac tgggcccagacagatgccc
1861 cagagctggt tatggectca gctgectcac ttcctacaag agcagcctgtggcatctttg
1921 ccttgggctg ctccctcatg tgggttcagg ggactcagcc ctgaggtgaaaggagctat
1981 caggaacagc tatgggagcc ccagggtctt ccctacctca ggcaggaagggcaggaagga
2041 gagcctgtct catggggtgg ggtagggtct actagaaggg ccagtcctgcctggccaggc
2101 agatctgtgc cccatgcctg tccagcctgg gcagccaggc tgccaaggccagagtggcct
2161 gcccaggagc tcttcaggcc tccctctctc ttctgtctca ccttggcctgtctcatccc
2221 cagggttccc agccaccccg ggctctctgc tgtacatatt tgagactagtttttattcct
2281 tgtgaagatg atatactatt tttgttaagc gtgtctgtat ttatgtgtgaggagctgctg
2341 gcttgacagt cgcgtgcacg tggagagctg gtgcccggag attggacggcctgatgctcc
2401 ctcccctgcc ctgggtccag gaagctggcc gagggtcctg gctcctgaggggcatctgcc
2461 cctcccccaa cccccacccc acactgttcc cagctctttg aaatagtctgtgtgaaggtg
2521 aaagtgcagt tcagtaataa actgtgttta ctcagtgaat aaaaaaaaaa aaaaa

```

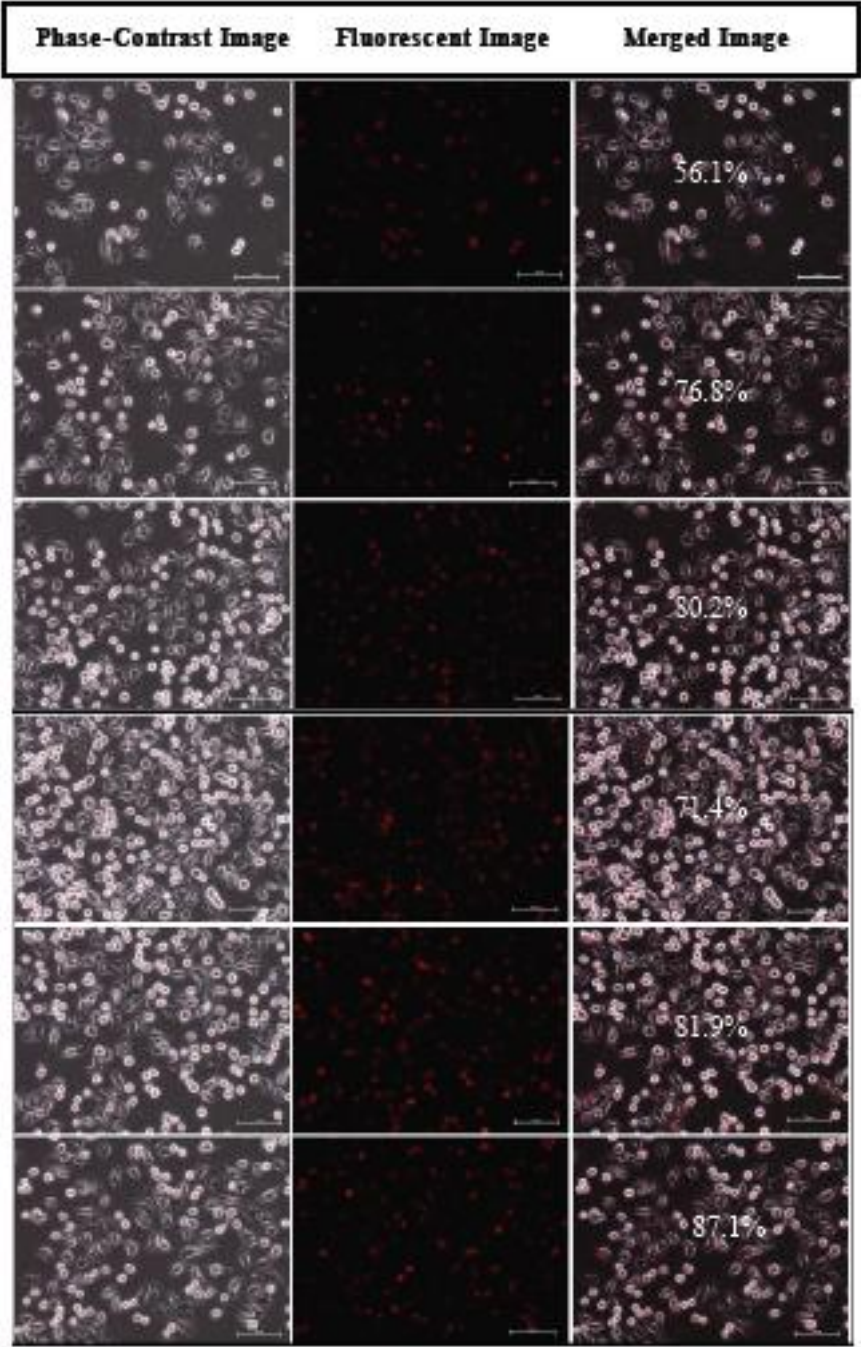
	siRNA 1 – HSS141361		siRNA 2 – HSS141362		siRNA 3 – HSS141363
--	---------------------	--	---------------------	--	---------------------

Appendix 4: siRNA Transfection Efficiency



















i) siRNA 1 transfection efficiency



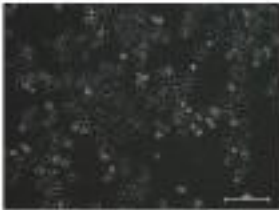
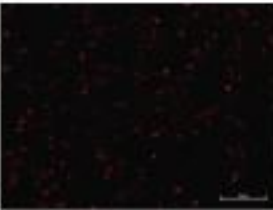
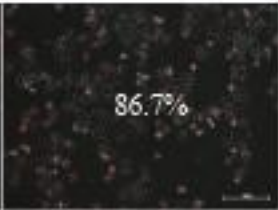

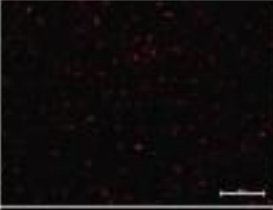













ii) siRNA 2 transfection efficiency




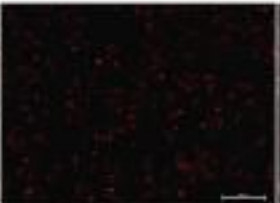


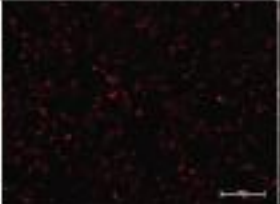





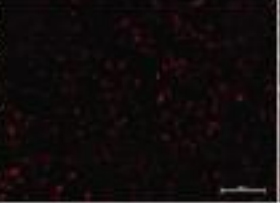


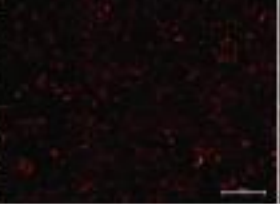


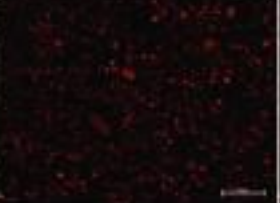

iii) siRNA 3 transfection efficiency

Phase-Contrast Image	Fluorescent Image	Merged Image
		 84.5%
		 90.4%
		 79.8%
		 84.0%
		 83.2%
		 87.6%


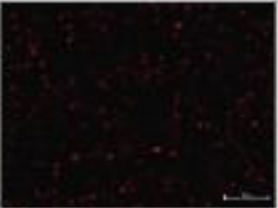


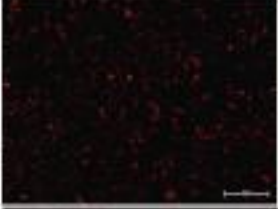





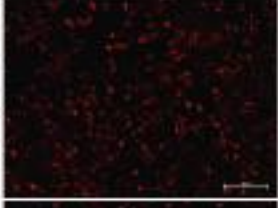


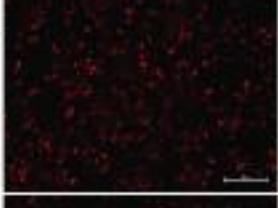




iv) siRNA 1 biological replicate 1 transfection efficiency

Phase-Contrast Image	Fluorescent Image	Merged Image
		 86.7%
		 78.6%
		 75.8%
		 82.5%
		 81.5%
		 81.9%

v) siRNA 1 biological replicate 2 transfection efficiency

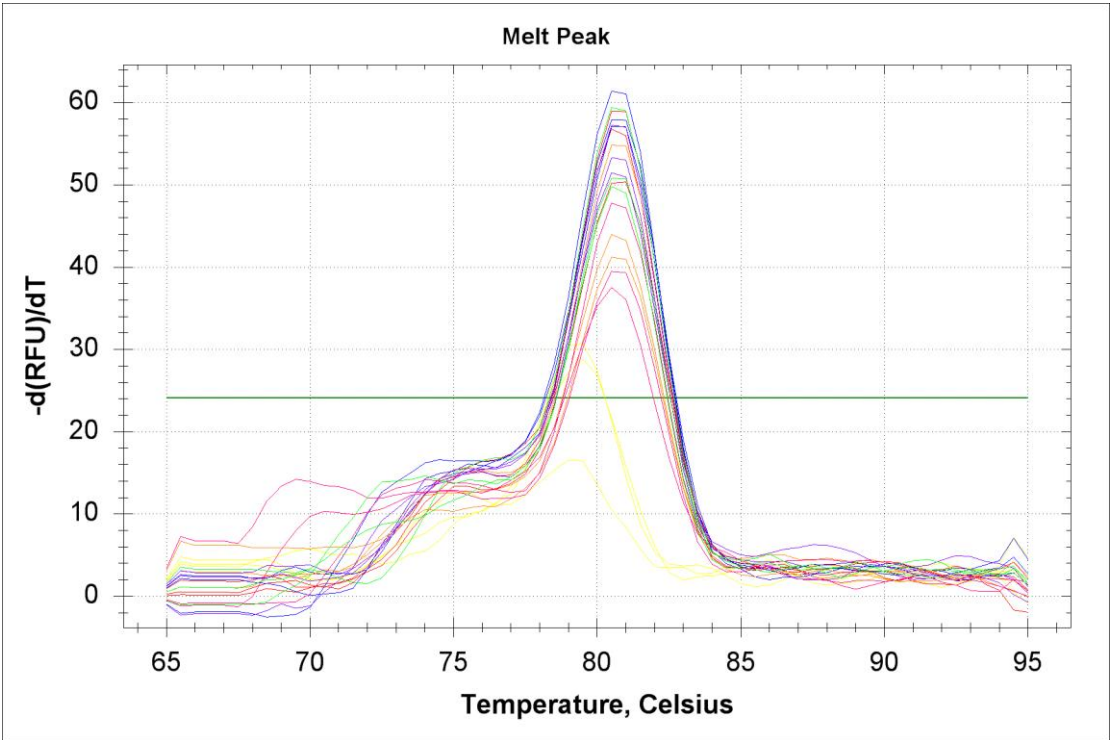
Phase-Contrast Image	Fluorescent Image	Merged Image
		 79.7%
		 72.3%
		 83.3%
		 79.1%
		 76.4%
		 82.9%

vi) siRNA 1 biological replicate 3 transfection efficiency

Phase-Contrast Image	Fluorescent Image	Merged Image
		
		
		
		
		
		

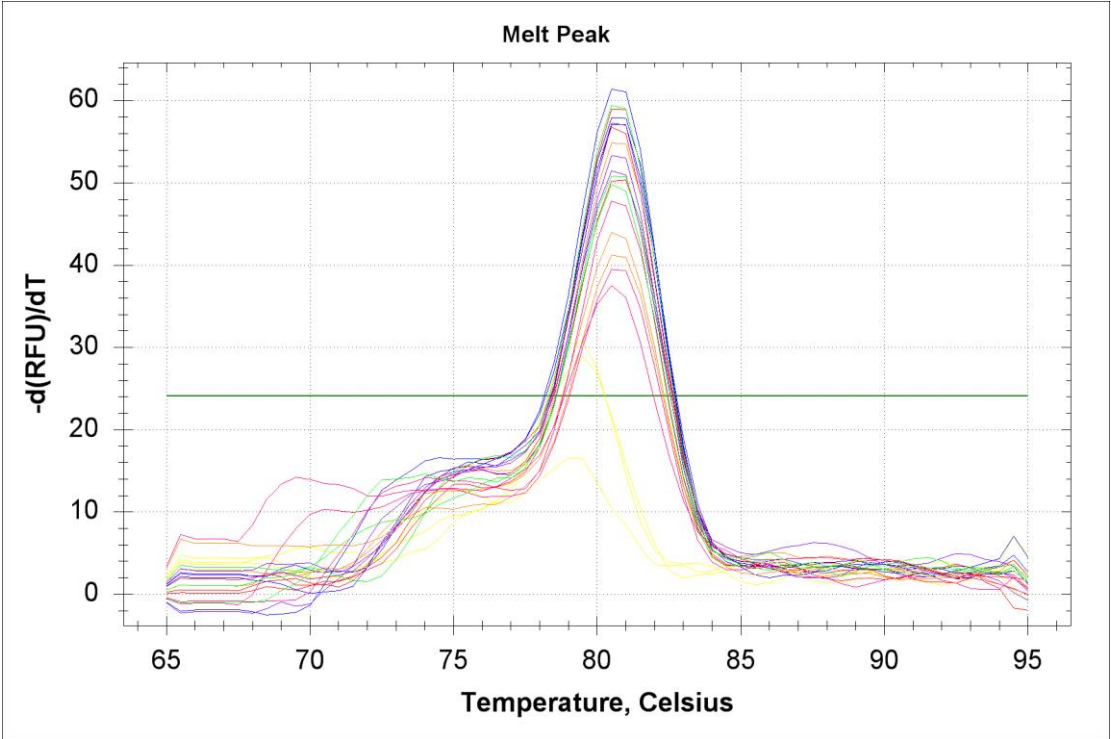
Appendix 5: qRT-PCR Melting Curve Analysis

i) Melting curve analysis for target gene, *bcl-xL*, samples siRNA 1-3



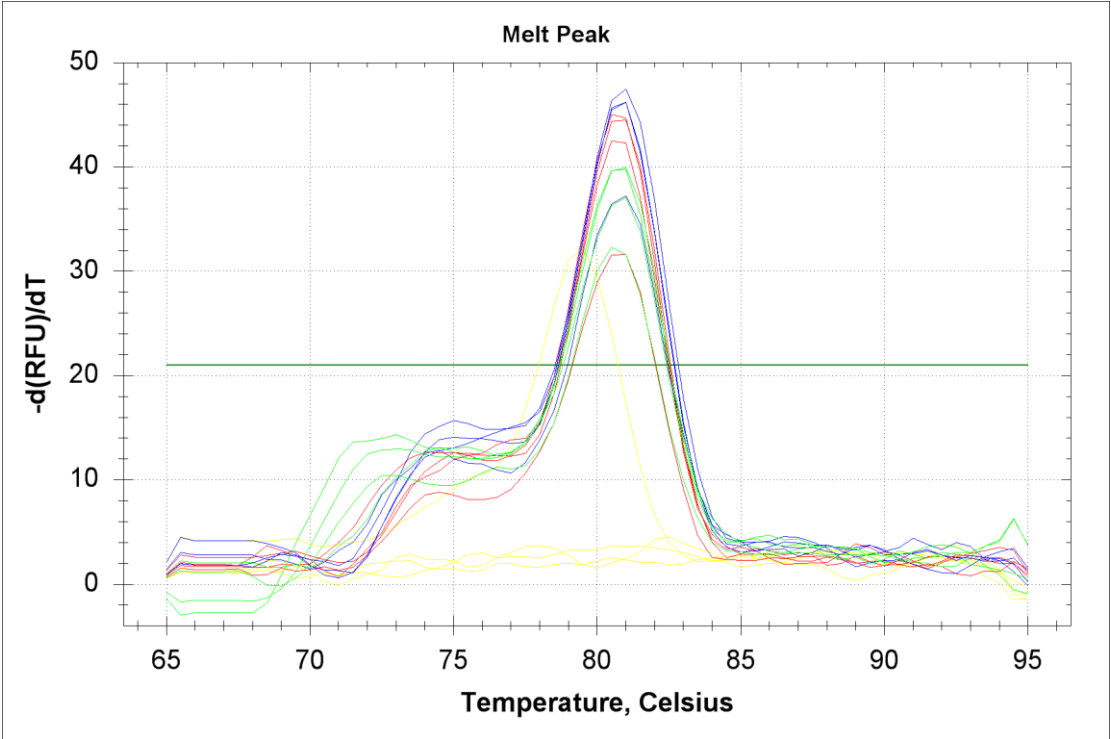
	No Transfection
	Hi GC NC
	Lo GC NC
	siRNA 1
	siRNA 2
	siRNA 3
	No Template

ii) Melting curve analysis for normalizer gene, *β-actin*, samples siRNA 1-3.



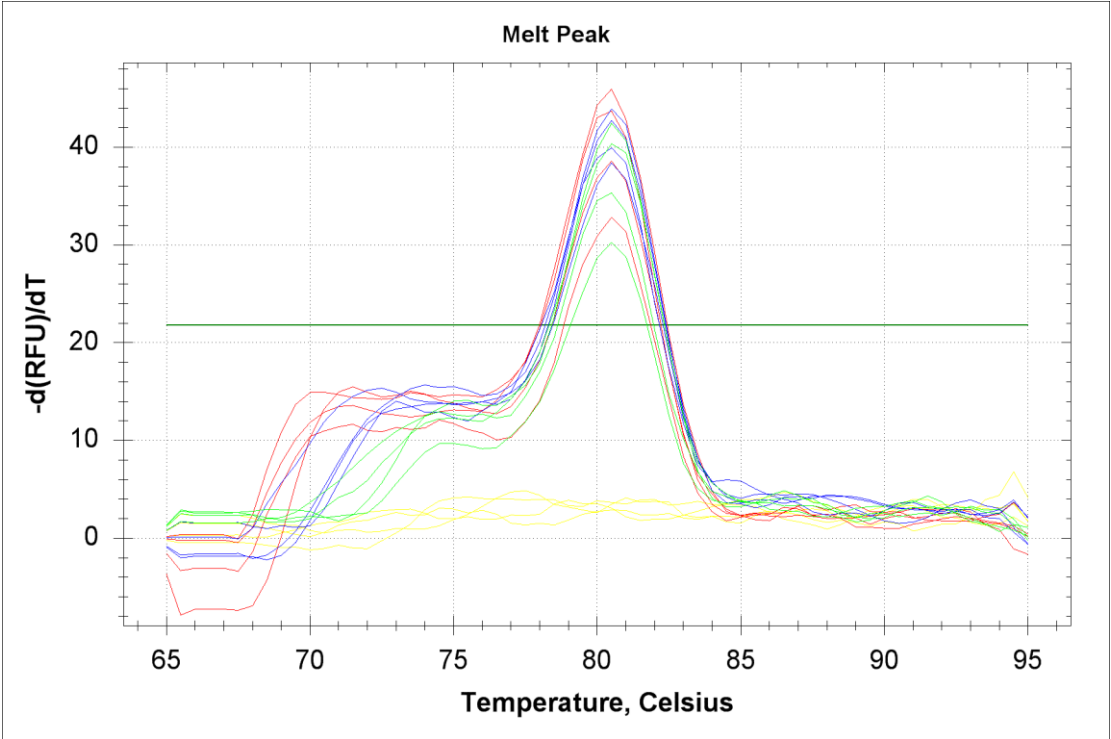
	No Transfection
	Hi GC NC
	Lo GC NC
	siRNA 1
	siRNA 2
	siRNA 3
	No Template

iii) Melting curve analysis for target gene, *bcl-xL*, sample siRNA 1



	No Transfection
	Lo GC NC
	siRNA
	No Template

iv) Melting curve analysis for normalizer gene, *β-actin*, samples siRNA 1



	No Transfection
	Lo GC NC
	siRNA
	No Template

Appendix 6: qRT-PCR Quantification Data

i) qRT-PCR quantification data for siRNA 1-3

	Replicate	Experimental (<i>Bcl-xL</i>) C_T^\dagger	Endogenous (<i>β-actin</i>) C_T^\dagger
NTC	1	22.4	16.82
	2	22.11	16.91
	3	21.48	16.52
siRNA 1	1	24.17	17.01
	2	23.97	16.72
	3	23.48	15.95
siRNA 2	1	22.4	15.73
	2	22.4	15.86
	3	23.24	17.19
siRNA 3	1	22.82	16.69
	2	22.77	16.61
	3	22.25	16.61
Hi GC NC	1	21.89	16.68
	2	21.44	16.4
	3	21.37	16.66
Lo GC NC	1	22.06	16.4
	2	21.65	16.37
	3	21.56	16.09

$^\dagger C_T$ = Cycle Threshold

ii) qRT-PCR quantification data for siRNA 1, replicates 1-3

	Replicate	Experimental (<i>Bcl-xL</i>) C_T^\dagger	Endogenous (<i>β-actin</i>) C_T^\dagger
NTC	1	24.14	18.99
	2	24.06	18.79
	3	24.04	18.6
siRNA	1	21.45	13.8
	2	21.58	14.27
	3	21.44	13.55
Lo GC NC	1	19.91	14.32
	2	19.95	14.4
	3	19.66	13.86

$^\dagger C_T$ = Cycle Threshold

iii) qRT-PCR quantification data for validated miRNAs

MicroRNA	Sample	Replicate	Experimental (MicroRNA) C _T [†]	Endogenous (U6) C _T [†]
Hsa-miR-181a	siRNA- Transfected	1	30.03	32.36
		2	30.45	32.50
		3	30.21	32.25
	Non- Transfected	1	29.15	33.17
		2	29.55	32.53
		3	30.21	32.72
Hsa-miR769-5p	siRNA- Transfected	1	31.46	32.25
		2	31.63	32.36
		3	31.14	32.50
	Non- Transfected	1	31.13	32.53
		2	30.22	32.72
		3	30.58	33.17
Hsa-miR-361-5p	siRNA- Transfected	1	32.01	30.96
		2	31.63	30.40
		3	31.54	30.38
	Non- Transfected	1	31.33	30.42
		2	31.27	30.39
		3	31.23	30.23
Hsa-miR1304	siRNA- Transfected	1	35.64	30.96
		2	35.56	30.38
		3	35.26	30.40
	Non- Transfected	1	34.87	30.42
		2	34.64	30.39
		3	34.6	30.23
Hsa-miR-608	siRNA- Transfected	1	34.53	30.96
		2	34.28	30.40
		3	34.05	30.38
	Non- Transfected	1	36.05	30.42
		2	35.90	30.39
		3	35.53	30.23

[†] C_T = Cycle Threshold